



symmetry

Chiral Auxiliaries and Chirogenesis

Edited by

Victor Borovkov

Printed Edition of the Special Issue Published in *Symmetry*

Chiral Auxiliaries and Chirogenesis

Chiral Auxiliaries and Chirogenesis

Editor

Victor Borovkov

MDPI • Basel • Beijing • Wuhan • Barcelona • Belgrade • Manchester • Tokyo • Cluj • Tianjin



Editor

Victor Borovkov
South-Central University for Nationalities
China

Editorial Office

MDPI
St. Alban-Anlage 66
4052 Basel, Switzerland

This is a reprint of articles from the Special Issue published online in the open access journal *Symmetry* (ISSN 2073-8994) (available at: <https://www.mdpi.com/journal/symmetry/special-issues/chirogenesis>).

For citation purposes, cite each article independently as indicated on the article page online and as indicated below:

| |
|--|
| LastName, A.A.; LastName, B.B.; LastName, C.C. Article Title. <i>Journal Name</i> Year , Volume Number, Page Range. |
|--|

ISBN 978-3-0365-1016-3 (Hbk)

ISBN 978-3-0365-1017-0 (PDF)

Cover image courtesy of pixabay.com user Buddy_Nath.

© 2021 by the authors. Articles in this book are Open Access and distributed under the Creative Commons Attribution (CC BY) license, which allows users to download, copy and build upon published articles, as long as the author and publisher are properly credited, which ensures maximum dissemination and a wider impact of our publications.

The book as a whole is distributed by MDPI under the terms and conditions of the Creative Commons license CC BY-NC-ND.

Contents

| | |
|--|------------|
| About the Editor | vii |
| Preface to “Chiral Auxiliaries and Chirogenesis” | ix |
| Riina Aav and Kamini A. Mishra The Breaking of Symmetry Leads to Chirality in Cucurbituril-Type Hosts Reprinted from: <i>Symmetry</i> 2018 , <i>10</i> , 98, doi:10.3390/sym10040098 | 1 |
| Vaibhav N. Khose, Marina E. John, Anita D. Pandey, Victor Borovkov and Anil V. Karnik Chiral Heterocycle-Based Receptors for Enantioselective Recognition Reprinted from: <i>Symmetry</i> 2018 , <i>10</i> , 34, doi:10.3390/sym10020034 | 27 |
| Mohammed Hasan and Victor Borovkov Helicene-Based Chiral Auxiliaries and Chirogenesis Reprinted from: <i>Symmetry</i> 2017 , <i>10</i> , 10, doi:10.3390/sym10010010 | 103 |
| Kuppusamy Kanagaraj, Kangjie Lin, Wanhua Wu, Guowei Gao, Zhihui Zhong, Dan Su and Cheng Yang Chiral Buckybowl Molecules Reprinted from: <i>Symmetry</i> 2017 , <i>9</i> , 174, doi:10.3390/sym9090174 | 151 |
| Keiji Hirose, Masaya Ukimi, Shota Ueda, Chie Onoda, Ryohei Kano, Kyosuke Tsuda, Y uko Hinohara and Yoshito Tobe The Asymmetry is Derived from Mechanical Interlocking of Achiral Axle and Achiral Ring Components –Syntheses and Properties of Optically Pure [2]Rotaxanes– Reprinted from: <i>Symmetry</i> 2018 , <i>10</i> , 20, doi:10.3390/sym10010020 | 177 |

About the Editor

Victor Borovkov received a Ph.D. degree from Moscow Institute of Fine Chemical Technology (Russia) in 1988. Following a postdoctoral period at Osaka University, he worked at different research organizations in Japan for over 20 years. He also worked at Tallinn University of Technology (Estonia) as a senior research scientist and at South-Central University for Nationalities (China) as a full professor. He is a member of the editorial board of several scientific journals and serves as an external peer-reviewer of various international journals and scientific foundations. He is an author of more than 140 publications including research papers, reviews, and books, with an h-index of 29 (WOS and Scopus) and 30 (Google Scholar), and he has produced 10 patents. He has headed and participated in different international and industrial collaboration projects and attended numerous international and national conferences as an invited speaker and a member of advisory committees. His current research interests include chemistry of porphyrins and related macrocycles, supramolecular chemistry, nanotechnology, chirality science, functional chiral materials, and asymmetric catalysis.

Preface to “Chiral Auxiliaries and Chirogenesis”

Chirality, the ability of any object to exist as a pair of non-superimposable mirror images or a unidirectional action (such as motion), is one of the most fundamental properties of nature. This phenomenon is widely seen and plays a key role in various biological structures, such as saccharides, proteins, enzymes, membranes, and DNA/RNA [1–3]. Furthermore, chirality is important for different branches of modern science, technology, and medicine. Essentially, all aspects of chirality dynamics including asymmetry generation, transfer, amplification, modulation, memorizing, and others relate to chiral auxiliaries and chirogenic processes, which are cutting-edge scientific activities [4–10]. Investigation of these effects is a rapidly growing area of research and directly connects with numerous natural processes, artificial systems, and modern industries. In addition, this research field has important practical implications in novel materials, enantioselective catalysis, chiral sensors, optical resolution, asymmetric synthesis, nanotechnology, medicine, pharmacology, biomimetic studies, and others. Many types of chemical molecules and supramolecular systems including various porphyrinoids have been well studied, as summarized in several comprehensive reviews published so far [6,11–16].

The aim of this Special Issue consisting of four review articles and one research paper was to highlight and overview all aspects of chiral auxiliary and chirogenesis in different natural/physical sciences and in modern technologies. In particular, some newly emerging classes of molecules used for these purposes have been overviewed.

Thus, in their review, Aav and Mishra [17] described chirogenic processes in cucurbituril (CB)-type hosts, which are oligomeric compounds, based on cyclic urea monomers, which are connected through methylene bridges. Indeed, while CB molecules are essentially symmetric, the following three major pathways to induce chirality in or by CB-type hosts were highlighted: first, through the incorporation of stereogenic elements into host molecules; second, through complexation with achiral guests, which leads to axial supramolecular chirality and helical structures; and third, through the formation of complexes with chiral guests in multimolecule complexes and induction of supramolecular chirality. This review is of particular importance due to the emergence of new supramolecular systems, whose selectivity can be directed by external stimuli and that can be applied for chirality sensing and enantioselective applications. Indeed, the first example of supramolecular chirogenesis in porphyrins generated by chiral CB was recently published [18].

Chiral heterocycle-based receptors as another type of chemical compound used for enantioselective recognition were comprehensively analyzed by Khose et al. in a review article [19]. Different structural motifs, intermolecular interactions, and analytical techniques employed for detecting the difference between corresponding enantiomers were found to be major components of the chiral recognition process. It is essentially important since there exists a huge global market for chiral separation technology for qualitative and quantitative estimations of chiral analytes.

In [20], Hasan and Borovkov reviewed helicene-based chiral auxiliaries as prospective chirogenic systems. Helicenes are unique helical chromophores possessing advanced and well-controlled spectral and chemical properties owing to their diverse functionalization and defined structures. Essentially, these distinct structural features of helicenes, the different synthetic and supramolecular approaches responsible for their efficient chirality control, and their employment in the chirogenic systems have been thoroughly analyzed. Moreover, the limitations, scope, and future prospects of helicene chromophores in chiral chemistry have been highlighted.

Buckybowls are polynuclear aromatic hydrocarbons that have a curved aromatic surface and are considered fragments of buckminsterfullerenes. The curved aromatic surface leads to the loss of planar symmetry of the normal aromatic plane and may cause unique inherent chirality, so-called bowl chirality, which it is possible to thermally racemize through a bowl-to-bowl inversion process. The studies concerning the special field of bowl chirality, focusing on recent practical aspects of attaining diastereo/enantioenriched chiral buckybowls through asymmetric synthesis, chiral optical resolution, selective chiral metal complexation, and chiral assembly formation have been summarized by Kanagaraj et al. in a review article [21]. While the study of chiral buckybowls is still immature yet highly promising, further investigation will provide more insight into this particular area and lead to applications in various fields such as materials, electronics, and photonics.

In the last research paper of this Special Issue [22], Hirose et al. described the syntheses and properties of optically pure [2]rotaxanes. Rotaxanes consisting of achiral axle and achiral ring components can possess supramolecular chirality due to their unique geometrical architectures. However, it is difficult to synthesize such rotaxanes as optically pure forms. To synthesize such chiral rotaxanes, a prerotaxane method based on aminolysis of a metacyclophane-type prerotaxane that had planar chirality, which is composed of an achiral stopper unit and a crown ether type ring component, was successfully applied. It was found that the rotaxane with mechanical chirality had a complexation ability against enantiopure phenylglycinol, with high enough enantioselectivity to be applied as a chiral selector of the chiral stationary phase for chiral chromatography.

Based on citations and access statistics of the published articles, this Special Issue has had a high scientific impact and attracted the considerable attention of the research community. Therefore, it was decided to launch the second Special Issue "Chiral Auxiliaries and Chirogenesis II" on the same subject in 2020, which will be completed in 2021 and then summarized in another Reprint Book.

References

1. Voet, D.; Voet, J.G. *Biochemistry*, 2nd ed.; John Wiley & Sons, Inc.: New York, NY, USA, 1995.
2. Saenger, W. *Principles of Nucleic Acid Structure*; Springer: New York, NY, USA, 1984.
3. Kyte, J. *Structure in Protein Chemistry*; Garland Publishing, Inc.: New York, NY, USA, 1995.
4. Escarcega-Bobadilla, M.V.; Kleij, A.W. Artificial chirogenesis: A gateway to new opportunities in material science and catalysis. *Chem. Sci.* **2012**, *3*, 2421–2428
5. Lee, J.; Zhang, W. Chiroptical switches: Applications in sensing and catalysis. *Molecules* **2012**, *17*, 1247–1277.
6. Hembury, G.A.; Borovkov, V.V.; Inoue, Y. Chirality sensing supramolecular systems. *Chem. Rev.* **2008**, *108*, 1–73.
7. Berova, N.; Di Bari, L.; Pescitelli, G. Application of electronic circular dichroism in configurational and conformational analysis of organic compounds. *Chem. Soc. Rev.* **2007**, *36*, 914–931.
8. Miyake, H.; Tsukube, H. Helix architecture and helicity switching via dynamic metal coordination chemistry. *Supramol. Chem.* **2005**, *17*, 53–59.
9. Peng, X.; Komatsu, N.; Bhattacharya, S.; Shimawaki, T.; Aonuma, S.; Kimura, T.; Osuka, A. Optically active single-walled carbon nanotubes. *Nat. Nanotechnol.* **2007**, *2*, 361–365.
10. Allenmark, S. Induced circular dichroism by chiral molecular interaction. *Chirality* **2003**, *15*, 409–422.

11. Borovkov, V. Effective supramolecular chirogenesis in ethane-bridged bis-porphyrinoids. *Symmetry* **2010**, *2*, 184–200.
12. Borovkov, V. Supramolecular chirality in porphyrin chemistry. *Symmetry* **2014**, *6*, 256–294.
13. Borovkov, V.; Inoue, Y. A versatile bisporphyrinoid motif for supramolecular chirogenesis. *Eur. J. Org. Chem.* **2009**, *2009*, 189–197.
14. Mamardashvili, N.Z.; Borovkov, V.V.; Mamardashvili, G.M.; Inoue, Y.; Koifman, O.I. Complexation of porphyrins with ions and organic molecules. In *Chemical Processes with Participation of Biological and Related Compounds. Biophysical and Chemical Aspects of Porphyrins, Pigments, Drugs, Biodegradable Polymers and Nanofibers*; Lomova, T.N., Zaikov, G.E., Eds.; Koninklijke Brill: Leiden, The Netherlands, 2008; pp. 117–168.
15. Borovkov, V.V.; Mamardashvili, N.Z.; Inoue, Y. Optically active supramolecular systems on the basis of porphyrins. *Russ. Chem. Rev.* **2006**, *75*, 820–832.
16. Borovkov, V.V.; Inoue, Y. Supramolecular chirogenesis in host-guest systems containing porphyrinoids. *Top. Curr. Chem.* **2006**, *265*, 89–146.
17. Aav, R.; Mishra, K.A. The breaking of symmetry leads to chirality in cucurbituril-type hosts. *Symmetry* **2018**, *10*, 98.
18. Ustrnul, L.; Kaabel, S.; Burankova, T.; Martõnova, J.; Adamson, J.; Konrad, N.; Burk, P.; Borovkov, V.; Aav, R. Supramolecular chirogenesis in zinc porphyrins by enantiopure hemicucurbit[n]urils (n = 6, 8). *Chem. Commun.* **2019**, *55*, 14434–14437.
19. Khose, V.N.; John, M.E.; Pandey, A.D.; Borovkov, V.; Karnik, A.V. Chiral heterocycle-based receptors for enantioselective recognition. *Symmetry* **2018**, *10*, 34.
20. Hasan, M.; Borovkov, V. Helicene-based chiral auxiliaries and chirogenesis. *Symmetry* **2018**, *10*, 10.
21. Kanagaraj, K.; Lin, K.; Wu, W.; Gao, G.; Zhong, Z.; Su, D.; Yang, C. Chiral buckybowl molecules. *Symmetry* **2017**, *9*, 174.
22. Hirose, K.; Ukimi, M.; Ueda, S.; Onoda, C.; Kano, R.; Tsuda, K.; Hinohara, Y.; Tobe, Y. The asymmetry is derived from mechanical interlocking of achiral axle and achiral ring components –syntheses and properties of optically pure [2]rotaxanes–. *Symmetry* **2018**, *10*, 20.

Victor Borovkov
Editor

Review

The Breaking of Symmetry Leads to Chirality in Cucurbituril-Type Hosts

Riina Aav * and Kamini A. Mishra

Department of Chemistry and Biotechnology, School of Science, Tallinn University of Technology, Akadeemia tee 15, 12618 Tallinn, Estonia; kamish@ttu.ee

* Correspondence: riina.aav@ttu.ee; Tel.: +372-620-4365

Received: 2 February 2018; Accepted: 30 March 2018; Published: 5 April 2018

Abstract: Cucurbituril-type hosts are highly symmetric, but there are means to break their symmetry. This review will present examples from three directions of induction of chirality in or by cucurbituril-type hosts: first, through the incorporation of stereogenic elements into host molecules; second, through complexation with achiral guests, which leads to axial supramolecular chirality and helical structures; third, through the formation of complexes with chiral guests in multi-molecule complexes and induction of supramolecular chirality. In addition, a list of chiral guests used in binding studies with cucurbiturils is collected. We would envision that encouraged by the outlined examples of outstanding applications of chiral cucurbituril-supramolecular systems, the boundaries of chiral applications of cucurbiturils would be widened.

Keywords: cucurbiturils; hemicucurbiturils; chirality; supramolecular chirality; symmetry breaking; helices

1. Introduction

Cucurbituril (CB)-type hosts are oligomeric compounds, where cyclic urea monomers are connected through methylene bridges. Core CBs are double-bridged macrocycles, which are made from glycoluril and formaldehyde [1–4]. Further on, the family has enlarged [5–7]. One can divide CBs into two main branches: the double-bridged and single-bridged CBs (Figure 1). All CBs have hydrophobic cavities, but electronic binding properties are different for single- and double-bridged CBs. Double-bridged CBs bind cations at the portals and single-bridged CBs anions in their cavity. All single-bridged CBs can be viewed as derivatives of hemicucurbiturils (HCs). HCs are formed in condensation of ethylene urea and formaldehyde, and cyclohexano-HC, bambusurils and biotinuril all contain linked ethylene urea moieties in their structures.

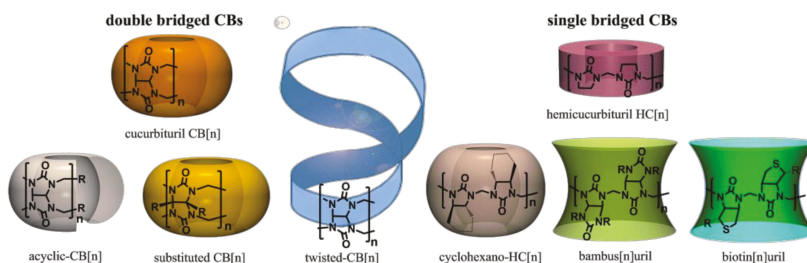


Figure 1. Cucurbituril-type hosts. CB, cucurbituril; HC, hemicucurbituril.

CB chemistry has been reviewed from various aspects [5–28], though so far, only one focused on the chirality of CBs [29]. CB-type hosts are very symmetric, but there are means to break this symmetry. This review will present examples from three directions of inducing chirality in CB chemistry: first, through the incorporation of stereogenic elements into the structure of CBs, through stereogenic atoms and helices; second, through complexation with achiral guests, which leads to axial supramolecular chirality in the helical structures; third, through the formation of complexes with chiral guests in multi-molecule complexes and induction of supramolecular chirality. In addition, a list of chiral guests that have been used in studies with CB-type hosts is collected.

2. Chiral Cucurbituril-Type Hosts

In general, the structures of core cucurbiturils are very symmetric. The CB[6] has seven planes of symmetry, as shown in Figure 2. Three vertical planes of symmetry pass through urea oxygens and three vertical planes through methylene bridges; additionally, one horizontal plane goes through the equator of the macrocycle.

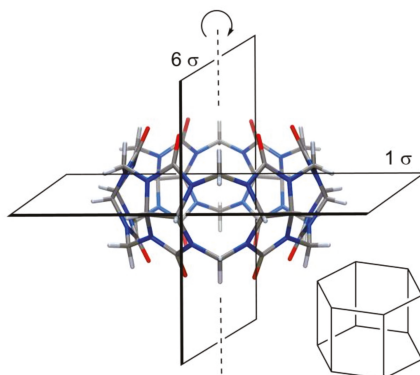


Figure 2. CB[6] and its planes of symmetry.

Because of these symmetry planes, neither substitution at a single methylene bridge nor at hydrogens of monomers by achiral groups will lead to chirality in the CB. To induce chirality, one must make changes at least at two methylene bridges in a way that disrupts all symmetry planes. In (\pm)-bis-*nor-seco*-CB[6] (Figure 3A), two methylene bridges are missing and trimeric glycolurils are connected in a diagonal fashion. Because of this, all glycoluril CH carbons become stereogenic, and as there are no symmetry planes, the macrocycle is chiral. Of course, if such a compound is formed in an achiral medium, then equal amounts of enantiomers are produced [30].

Isaacs et al. investigated the formation of host–guest complexes of (\pm)-bis-*nor-seco*-CB[6] in D₂O with a number of chiral compounds (Figure 3B) [30]. Intriguingly, differences in NMR signals were noted while complexes were formed from enantiopure or racemic guests with (\pm)-bis-*nor-seco*-CB. This observation is clear evidence of the formation of different supramolecular complexes. In a simple system, when one host enantiomer forms a complex with an enantiomerically pure guest, a single enantiomerically pure complex is formed. If an enantiomerically pure guest complexes with the chiral racemic host, then a mixture of two diastereomeric and enantiomerically pure complexes will be formed. By ¹H-NMR spectroscopy, one can distinguish diastereomers, and therefore, two sets of signals can appear. Now, if both chiral compounds would be mixed as racemates, then the same two diastereomeric complexes will be formed, just racemic complexes. By a simple NMR measurement, one cannot see the difference between enantiomerically pure and racemic complexes; therefore, the NMR spectra are expected to be the same. The situation with (\pm)-bis-*nor-seco*-CB[6] is not that simple. Isaacs et al. noted that the ratio of diastereomeric host–guest complexes is influenced by the guest stereoisomeric

purity. The reasons for these observations were not disclosed, but the aggregation of one or both chiral entities used in the study might have influenced the NMR signals [31,32]. Binding dynamics were dependent on the structure of the guest, as NMR spectra of (\pm)-bis-nor-seco-CB[6] showed increased complexity and multiplicity in the presence of an aromatic chiral guest, referring to binding where guests are not exchanged on the NMR timescale. On the other hand, NMR peaks became very broad upon complexation with aliphatic guests, referring to association-dissociation during the measurement at room temperature.

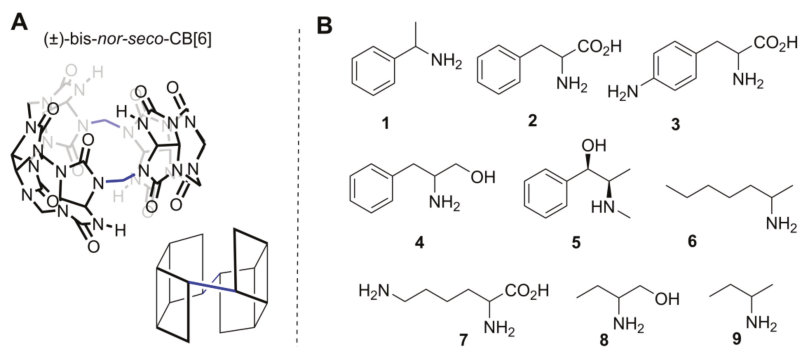


Figure 3. (A) One enantiomer of (\pm)-bis-nor-seco-CB[6]; (B) chiral guest whose binding was studied with (\pm)-bis-nor-seco-CB[6].

According to our knowledge, only a few chiral compounds have been isolated to date from the condensation reaction between glycoluril and formaldehyde, the abovementioned (\pm)-bis-nor-seco-CB[6] and acyclic 10-membered oligomer [33] (Figure 4), which have stereogenic atoms and twisted-CBs [34–36], which possess axial chirality (Figure 6). In the acyclic 10-membered oligomer, two pentamers are connected to each other through a single bond with no plane of symmetry.

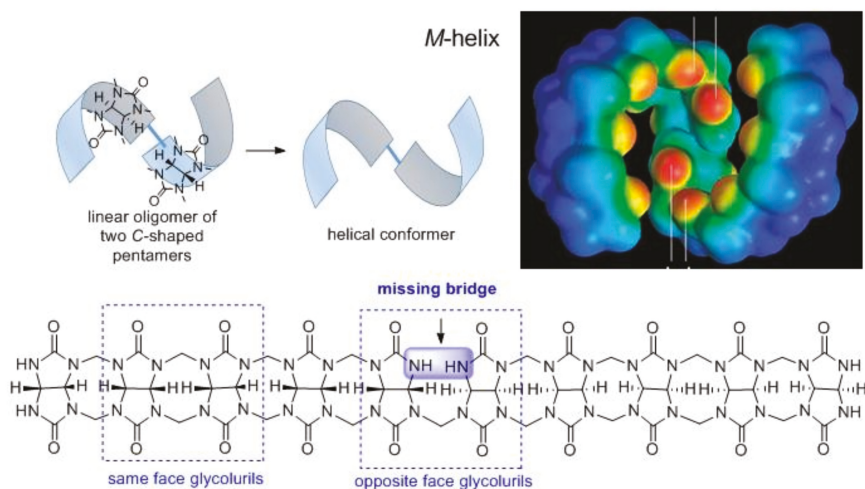


Figure 4. Map of electronic potential of a single enantiomer of the (\pm)-glycoluril decamer in the shape of an *M*-helix (adopted with permission from [33]) and its structure.

It is remarkable how a very small change in the structure of the oligomer, like the single turn of the face of the glycoluril and disconnection of one methylene bridge, can affect the geometry of the molecule. Oligomers, where same face glycolurils are linked, have a C-letter-shaped conformation, and they are achiral and can form a macrocycle. Absence of one methylene bridge in (\pm)-glycoluril decamer turns all glycoluril CH carbon atoms stereogenic, which induced its crystallization in a helical conformation. As this compound was formed in an achiral medium, two opposite-handed helices were formed in a ratio of 1:1 [33]. Binding with chiral guests was not probed with (\pm)-glycoluril decamer.

C-letter-shaped conformation of glycoluril oligomers and their ability to bind guest through electrostatic interactions with glycoluril carbonyl groups encouraged Isaacs to develop a new branch type of CB-type molecules, the acyclic CBs. To enrich oligomer structure with sites for additional functionalization and to add UV-active properties, Isaacs used substituted aromatic groups at the terminus of acyclic CBs. The structures of chiral and enantiopure acyclic CBs are shown in Figure 5A [37].

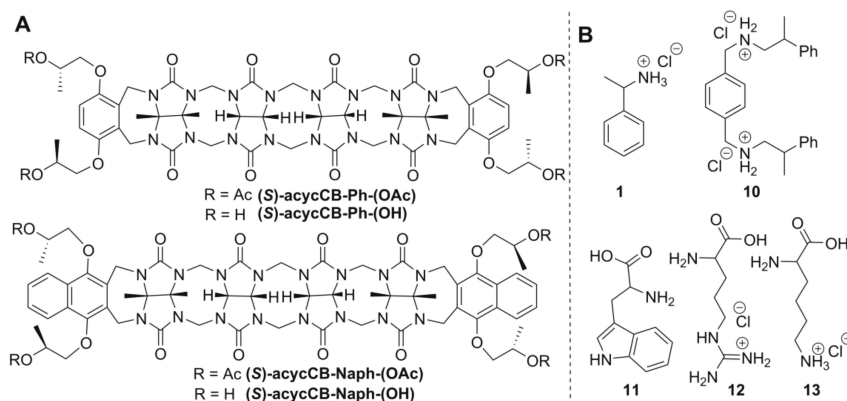


Figure 5. (A) Chiral acyclic CBs; (B) chiral guests, whose binding was studied with acyclic CBs [37].

Chiral acyclic CBs showed binding with ammonium-functionalized guest (Figure 5B) in acetic acid buffer at pH 5.5, and association constants were found to be in range of 10^3 – 10^6 M⁻¹. Small enantioselectivity in the binding of opposite enantiomers was also detected. The ratio of association constants for binding the (*S*)-1 over (*R*)-1 the $K_{(S)}/K_{(R)}$ was 1.3 for binding with (*S*)-acycCB-Ph-(OAc). Unfortunately, the binding of guest 1 to host (*S*)-acycCB-Ph-(OH) and guest 10 to both chiral acyclic CBs (*S*)-acycCB-Ph-(OAc) and (*S*)-acycCB-Ph-(OH) gave very close $K_{(S)}$ and $K_{(R)}$ values, and as the differences in measured K values were in the range of the measurement uncertainty, one can conclude that enantiodiscrimination is either absent or very small. The hosts (*S*)-acycCB-Naph-(OAc) and (*S*)-acycCB-Naph-(OH) were also able to bind cationic guests, but association constants could not be determined.

Isaacs has also developed a synthesis of functionalized CBs through macrocyclization of glycoluril hexamer and substituted glycoluril. By this strategy, amino acids and biotin were linked covalently to CBs, and efficient uptake of Oxaliplatin by cancer cells was achieved [38]. Recently, a polymeric biomaterial was prepared from glucose-based polymer: dextran and covalently-bound acyclic CB. This sugar-based chiral polymer was used for encapsulation of antitumor drugs, and its chiral properties were not investigated [39].

Apart from the listed CBs, which incorporate stereogenic centers in their structure, there is a special sub-class of CBs, which do not have stereocenters, but are still chiral. These are twisted CBs with axial chirality. The crystal structure of CB[14] revealed helical conformations of this CB, and therefore, the name *twisted*-CB[14] [34,35] was given (Figure 6). Currently there are three known CBs with 13,

14 and 15 glycolurils in their structures that have a helical conformation (Figure 6). Twisted CBs have a 360° turn in their oligomer belt, and the direction of this turn defines the stereochemistry of the macrocycle. Helical conformation is locked into the macrocyclic structure. One should mention that, in *twisted*-CB[13–15]s [34,36], the belt is formed so that all glycoluril monomers have the same faces linked next to each other, so these are not Möbius band [40]. Curiously, in aqueous solution, without any guests, *twisted*-CB[14] looks like normal cucurbituril, having only three signals in its $^1\text{H-NMR}$. Despite that, complexation studies of *twisted*-CB[14] in solution showed binding of a 1,8-octyldiammonium in a 1:1 stoichiometry, similarly to CB[8], with a K_a of $7.9 \times 10^6 \text{ M}^{-1}$, and smaller 1,4-butyldiammonium guest binds in a 1:2 ratio, with K_a values of $1.9 \times 10^8 \text{ M}^{-1}$ and $2.9 \times 10^6 \text{ M}^{-1}$, indicating clearly that *twisted*-CB[14] has two separate binding compartments and that these compartments are adaptable [41].

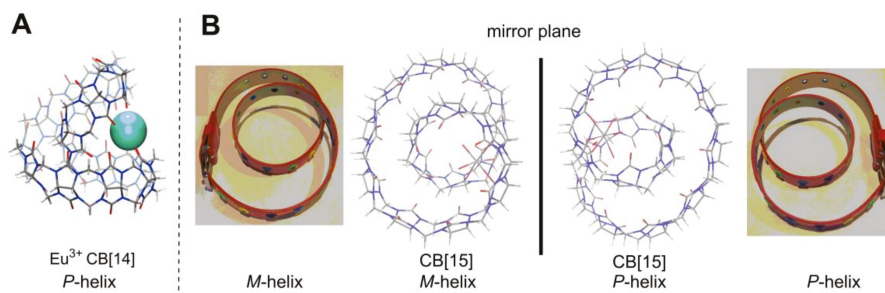


Figure 6. (A) Eu^{3+} -CB[14] side view of *P*-helix [34]; (B) top view of Cd^{2+} -CB[15] in *M*- and *P*-helical conformations formed in the same crystal [36] and illustration of these helix configurations with a belt.

Single-bridged CB-type macrocycles (Figure 1), the hemicucurbiturils [6,42] (HC), also have high symmetry like most CBs. The structure of an unsubstituted six-membered HC is shown in Figure 7. The monomers of HC are positioned in a “zig-zag” manner; therefore, HCs have fewer planes of symmetry in their structure than the parent CBs. Six-membered unsubstituted HC (Figure 7) and substituted HCs, which are formed from achiral monomers (Figure 8A), have three planes of symmetry.

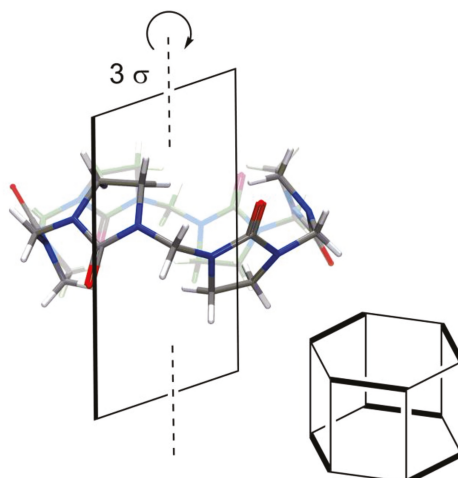


Figure 7. Hemicucurbit[6]uril [42] and its planes of symmetry.

Bambusurils [22,43] are a sub-class of single-bridged CBs that are made of achiral monomers (Figure 8B). One can see that nonequivalent R-substituents at glycolurils would lead to desymmetrization and creation of stereogenic centers at carbons of fused cycles. In this way, the formation of chiral bambusurils would be feasible.

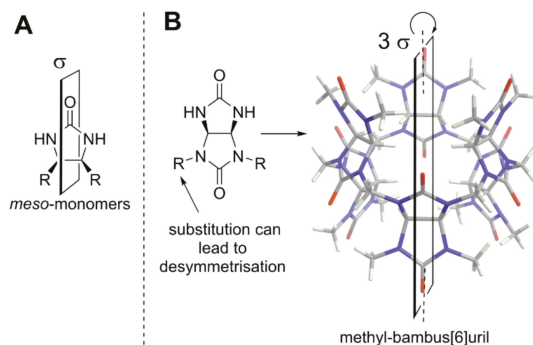


Figure 8. (A) The general structure of achiral substituted ethylene urea; (B) crystal structure of achiral methyl-bambus[6]uril [43] and its monomer.

Very interesting desymmetrization was achieved in azabambusuril [23,44] (Figure 9): substitution of a sulfur atom in symmetric thiobambusurils with an alkylimine moiety leads to the loss of all symmetry planes in this macrocycle.

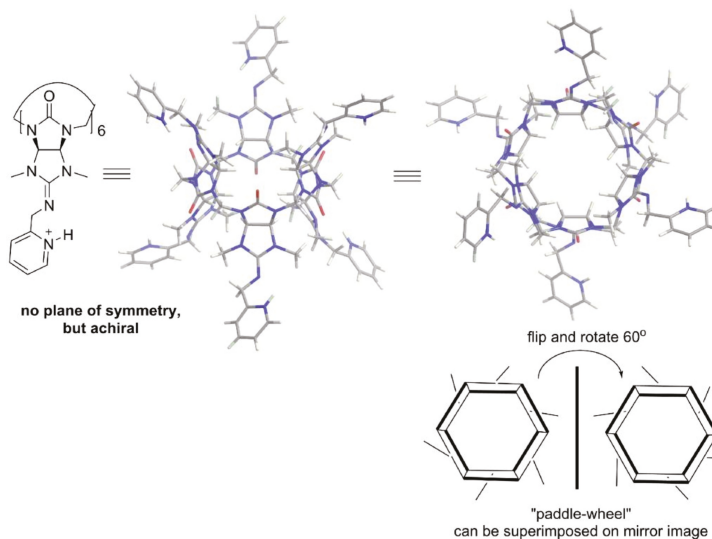


Figure 9. Drawing and crystal structure of protonated picolyl-azabambusuril [44] and cartoon of its "paddle-wheel" configuration.

The alkyl-azabambusuril crystal structure [44] revealed its "paddle-wheel"-like configuration. The unidirectional orientation of the imine double bonds in azabambusuril (Figure 9, right side), reflects high diastereoselectivity during their formation. Curiously, in spite of the desymmetrization

of bambusuril monomer, alkyl-azabambusuril is achiral, as its mirror image can be superimposed by flipping and rotating this “paddle-wheel” (Figure 9). Nevertheless, in the future chiral bambusurils could be made from nonuniformly substituted monomers.

As one can see, HCs have many options for the incorporation of stereogenic atoms into their structure, and several of them have been prepared in enantiopure form with high yield and in a single macrocyclization step [45–47]. Chiral (*S,S*)- or (*R,R*)-cyclohexano-hemicucurbit[6,8]urils (cycHC) are derived from enantiopure cyclohexa-1,2-diylurea [45,47] (Figure 10A), and biotin[6]juril from the vitamin biotin [46] (Figure 11).

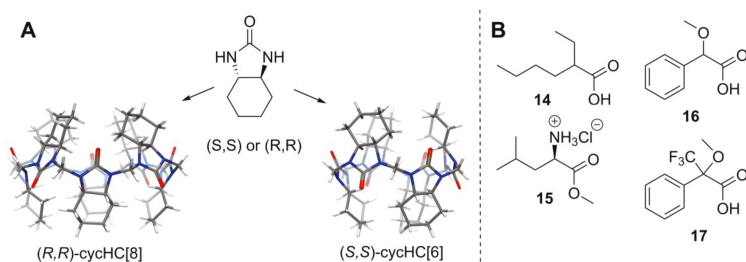


Figure 10. (A) Structure of cyclohexa-1,2-diylurea and crystal structure of chiral cycHCs [45,47]; (B) chiral guests whose binding was studied with cycHCs [47].

Enantiopure (*S,S*)-cycHC[6] binding ability has been tested on some chiral compounds shown in Figure 10B. Association constants determined by DOSY NMR in CDCl_3 were quite low and remained in the range 10^1 – 10^2 M^{-1} . The (*R,R*)-cycHC[6] [45] showed a preference for binding of (*R*)-**16** and (*R,R*)-cycHC[8] [47] for (*S*)-**16**, with a $K_{(R)}/K_{(S)}$ value of 1.4 and $K_{(S)}/K_{(R)}$ of 2.0, respectively. Interestingly, the guest **17**, whose acidity and also association constant was higher than those of **16**, bound to (*R,R*)-cycHC[8] nonstereoselectively. No crystal structures of these complexes were obtained; therefore, the position of the guests is not fully disclosed.

Nevertheless, a tentative binding mode of guests to cycHCs was proposed based on ion-mobility MS of cycHC[6] complexes with Na^+ and anions, accompanied by DFT calculations of neutral molecules and anions [48]. Anions form inclusion complexes with cycHCs, and undissociated carboxylic acids form external complexes through hydrogen bonding with the urea carbonyl group. (Figure 11A).

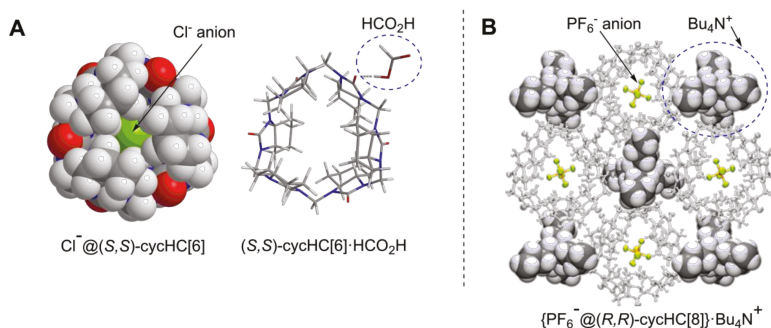


Figure 11. (A) Minimum energy geometry of inclusion complex of Cl^- @(*S,S*)-cycHC[6] and external complex of (*S,S*)-cycHC[6]· HCO_2H [48]; (B) crystal structure of $(\text{PF}_6^-$ @(*R,R*)-cycHC[8])· Bu_4N^+ [49]. Published by The Royal Society of Chemistry.

The crystal structure of the tetrabutylammonium hexafluorophosphate complex with (*R,R*)-cycHC[8] (Figure 11B) [49] confirmed the previous hypotheses that an anion can be encapsulated and that the cation forms an external complex with this host.

Another enantiopure member of single-bridged CBs is biotin[6]uril [46] (Figure 12), but so far, only its binding to achiral anions has been studied [50,51], and no reports on its stereoselective applications have been presented yet.

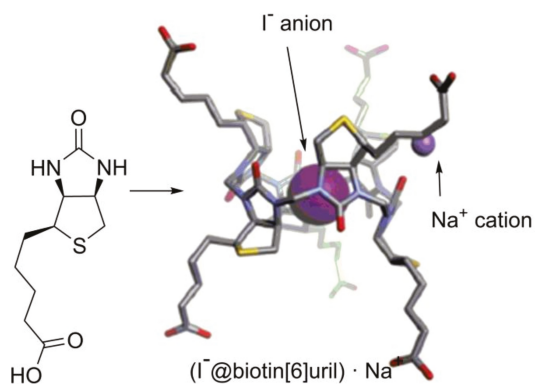


Figure 12. Biotin structure and crystal structure of the $(\text{I}^-@ \text{biotin}[6] \text{uril}) \cdot \text{Na}^+$ complex [46].

Noteworthy is the diastereoselectivity of biotin[6]uril formation. Biotin is the most unsymmetrical urea monomer that has been used for making CB-type macrocycles. It does not have any symmetry elements in its structure, and therefore, the possibility of the formation of nine diastereomeric six-membered HCs exists. In spite of that, only a single diastereomer was formed during biotin condensation with formaldehyde [46]. This is the result of the dynamic formation of methylene bridges, which drives equilibrium toward the formation of the thermodynamically most favorable macrocycle.

From the examples above, one can see that several chiral hosts are known in the CB family, though their chiral recognition properties are barely studied, and their applications are awaiting.

3. Breaking Symmetry through Complex Formation with Achiral Compounds

The symmetry of achiral CBs might also be broken through complexation. The majority of studies in the field of CB chemistry are associated with binding affinity and their applications. Here, just some references to reviews are given [24,25]. Depending on the application, different non-covalent interactions become important. In the solid state [26,27,52], some examples exist, where achiral ligands can cause spontaneous resolution during crystallization and right- or left-handed chiral crystals are produced with equal probability. Examples where chiral helices have been formed with CB complexes are presented in this section.

The first helical structure formed upon complexation of the achiral ligand with CB was reported by Kim et al. [53]. A helix was constructed based on ammonium cation-dipole interaction between a guest and CB and silver cation-dipole interaction between pseudorotaxanes. A polyrotaxane chain was formed from CB[6], *N,N'*-bis(3-pyridylmethyl)-1,5-diaminopentane and AgNO_3 . The crystal structure had an equal number of right- and left-handed helices, so it was racemic. (Figure 13, on the left). Later, along with several achiral polyrotaxanes, another helical racemic polyrotaxane was reported by Kim's group [54]. In that, a silver ion was exchanged with a cadmium ion, and as a result, a longer helical pitch was formed (Figure 13, on the right).

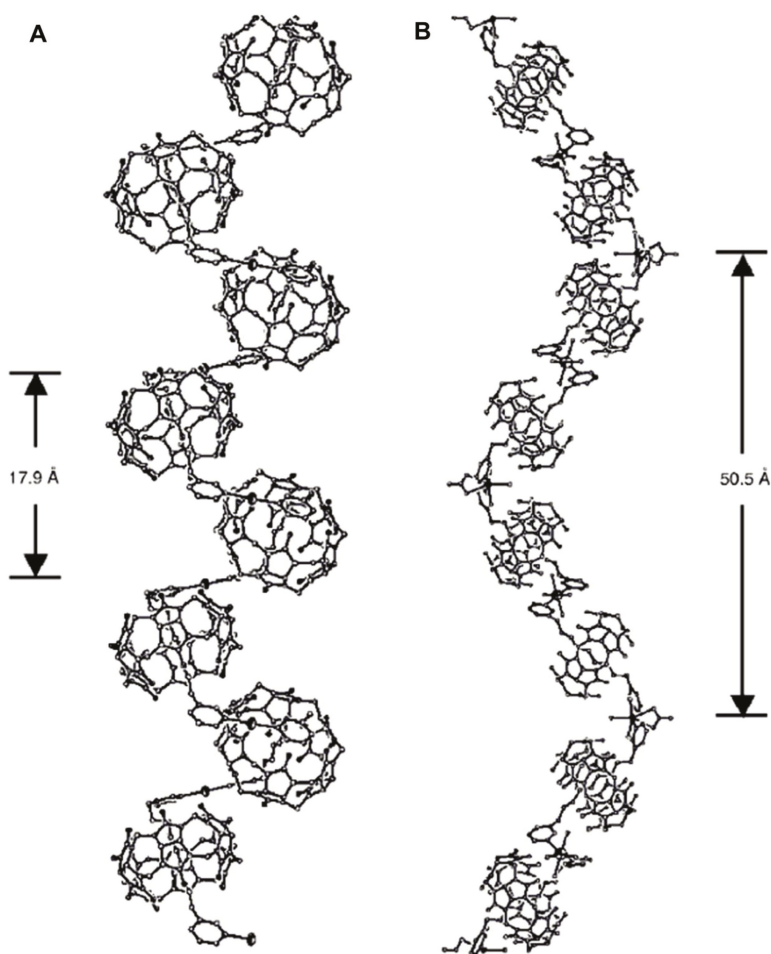


Figure 13. CB[6] polyrotaxane formed from CB[6] (A) *N,N'*-bis(3-pyridylmethyl)-1,5-diaminopentane and AgNO_3 [53] (B) or $\text{Cd}(\text{NO}_3)_2$ [54]; reproduced from [54].

Solid phase complexes with both handed helical networks of polyrotaxane were also shown by Xue and Liu et al., upon complex formation from *N,N'*-bis(2-pyridylmethyl)-1,6-hexanediamine, tetramethyl-CB[6] and AgNO_3 . In the reported structure, CBs are aligned, as the dumbbell of rotaxane, which is constructed from substituted hexanediamine, taking a helical conformation. The authors state that the source of conformational chirality is the linkage of two 2-pyridylmethyl moieties with the silver ion [55].

Helical solid-state structures might be constructed also without pseudorotaxane formation. The network of CBs in Figure 14 is built through cation-dipole interaction and halogen bonding. CB[6] sodium cationic units are connected with copper(II) anionic complexes, the $[\text{Cu}(3,5\text{-diiodosalicylate})(8\text{-hydroxyquinoline-5-sulfonate})]^{2-}$ [56] (Figure 14A). Right- and left-handed helices were both incorporated into a racemic crystal structure. Further, Chen, Liu, Yamauchi et al. [56] noted that upon exchange of iodo-ligand $[\text{Cu}(3\text{-iodobenzoate})(8\text{-hydroxyquinoline-5-sulfonate})\text{Cl}]^{2-}$ was formed, which had all CB-chains organized into homochiral helix (Figure 14B).

The research group of Tao and Liu [57] reported the formation of a pair of homochiral 1-D-helical coordination polymers of CB[5] with Dy^{3+} upon crystallization in the presence of achiral hydroquinone (Figure 15). The interaction between hydroquinone and CB through π -H-C and π - π stacking might direct the formation of a chiral helix.

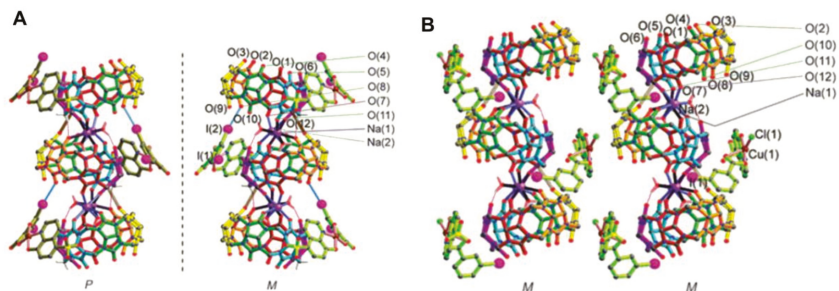


Figure 14. (A) Racemic $[CB[6]Na_2 \cdot Cu(3,5\text{-diiodosalicylate})(8\text{-hydroxyquinoline-5-sulfonate})]$; (B) homochiral $[CB[6]Na_2 \cdot Cu(3\text{-iodobenzoate})(8\text{-hydroxyquinoline-5-sulfonate})Cl]$. Reproduced from [56].

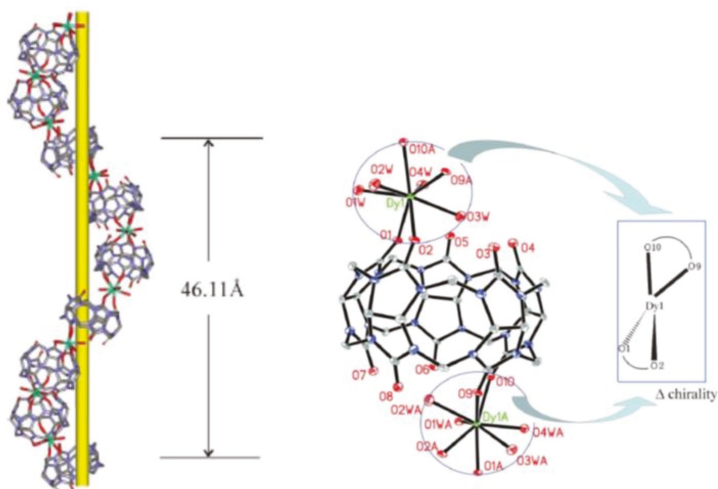


Figure 15. Right-handed *P*-helix and network structure of $(CB[5]Dy(H_2O)_4CB[5])^{3+}$ and hydroquinone, crystallized in space group $P6_1$ [57], reproduced from [57] with permission from The Royal Society of Chemistry.

In the crystal structure with a *P*-helix, two carbonyl groups of CB[5] are coordinated to Dy^{3+} and as every Dy^{3+} is connected with two CB[5] molecules; also, Dy^{3+} is chiral and has the Δ -configuration. The authors attempted also a measurement of circular dichroism (CD) of single crystal, but unfortunately could not detect a reliable CD signal. The absolute configuration was assigned by single crystal diffraction analysis through the Flack parameter. Intriguingly, randomly performed crystallizations showed that two clusters crystallized in the space group $P6_5$, whereas the other six clusters crystallized in the space group $P6_1$. In other words, the sample in the present case had undergone spontaneous resolution with an enantiomeric excess value of 50% [57]. Formation

of similar helical networks has also been observed with heavy lanthanides like Er^{3+} , Yb^{3+} or Lu^{3+} , but not with light lanthanides [58].

The given examples of helical polyrotaxanes show that upon understanding the supramolecular interactions of CBs with guests and with the suitable interplay between participating species, one can obtain chiral material. On the other hand, helical networks with CBs are relatively rare, compared with solid-state structures of coordination polymers made by the incorporation of various CBs. Therefore, one could state that induction of chirality in the solid state with CBs has been the result of good luck, and further research is required to develop an understanding for directed design.

In addition to the formation of helices from CB units, one can utilize larger homologues of CBs as a confined space, in which the helix can be fitted. Tao et al. [59] have shown that CB[8] is large enough to fold a long-hydrocarbon guest into a helix conformation within its cavity (Figure 16). The asymmetric unit of CB[8] pseudorotaxanes contained both the right- and left-handed helical guests in equal occupancy in its structure.

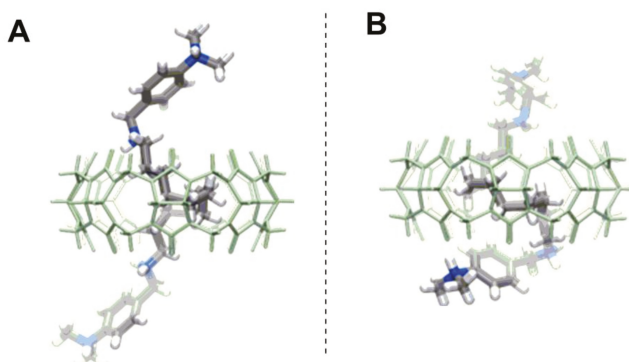


Figure 16. *N,N'*-bis(4-dimethylaminobenzyl)-dodecane-1,12-diamine folded inside of the CB[8] (A) into a right-handed helix; (B) into a left-handed helix [59].

One can see that CBs can be involved in the formation of chiral helical structures, but so far, stereoselectivity of this process has not been directed. Hopefully, future methods for homochiral and stereoselective helix formation will be developed, for example through seeding or by some chiral stimulus.

4. Breaking Symmetry through Complex Formation with Chiral Compounds

It is clear that upon complexation with an enantiomerically pure guest, the entire host-guest complex becomes chiral. The situation becomes more intriguing if such a supramolecular complex can be applied in further chirogenesis or enantiodiscrimination [60,61].

One of the most reliable methods to detect chirality is CD. Cucurbiturils' carbonyl-group UV-absorbance is below 250 nm and coincides with the cut-off region of the many organic solvents, therefore the signal of a chiral guest is often used for interaction studies. One of the parameters that reflects chirality, the concentration independent value of the *g*-factor, is a good measure of chirality sensing. Inoue and Kim et al. [62] have shown that the *g*-factor of chiral charge transfer dyad **18** can be affected by complexation with CB[8] (Figure 17).

One step further from the creation of a chiral complex of CB through binding with a chiral guest is the compilation of a ternary system that can show stereoselectivity. The very first and very comprehensive study in this direction was done by the group of Inoue and Kim [63]. They investigated a number of ternary systems and found that the CB[6] complex with (*R*)-2-methylpiperazine is especially selective toward complexation with (*S*)-2-methylbutylamine ($K = 15,000 \pm 3000 \text{ M}^{-1}$)

if compared with the complex between (S)-2-methylpiperazine with (S)-2-methylbutylamine ($K = 800 \pm 100 \text{ M}^{-1}$) (Figure 18). A matched enantiomer is bound with 19-times greater affinity than the mismatched enantiomer. It was claimed to be the highest enantioselectivity ever reported for a supramolecular system derived from an achiral host. To explain such a selectivity, an analogy to the commander–sergeant–soldier [64] system was exploited. Binding to CBs is governed by the hydrophobic effect related to the guest’s ability to enter the CBs’ cavity. Double-charged methylpiperazine is designated as a soldier, and it is weakly bound to CB at portals; it cannot enter the cavity, but can attract two CBs, causing aggregation of the CB-methylpiperazine complex. Aggregation can be minimized at a concentration below 0.3 mM. CB is designated as the sergeant, and its role is to mediate the formation of diastereomeric complexes between two ammonium compounds. 2-Methylbutylamine is the commander, as its binding controls the formation of the final complex. The mismatching enantiomer of 2-methylbutylamine induces an unfavorable change of enthalpy, leading to an endothermic reaction, which is explained by the geometry of the bound methylpiperazine. The matching enantiomer of 2-methylbutylamine, on the other hand, does not disturb the complex between CB and bound methylpiperazine and is therefore overall strongly favored, and its binding leads eventually to disaggregation of the CB complex. In addition, in this work, selectivity toward diastereomeric dipeptides was shown [63].

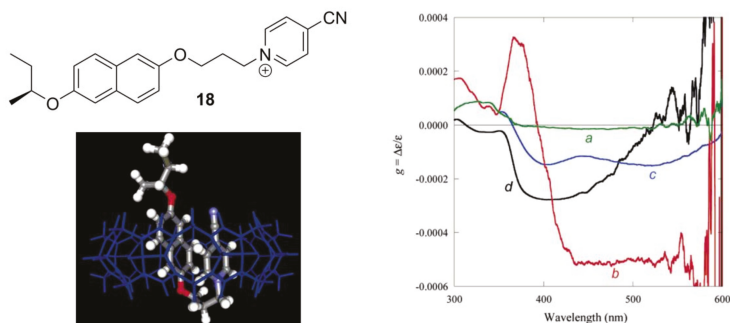


Figure 17. Structure of the charge-transfer dyad **18**; **18**@CB[8] complex 3D model and g-factor graph for: (a) the folded monomer in acetonitrile at 25 °C; (b) the head-to-tail dimer of **18** in CH_2Cl_2 at -95 °C; (c) the folded conformation in CB[8] in D_2O at 25 °C; (d) the inclusion complex with α -CD in H_2O at 25 °C. Reprinted from [62].

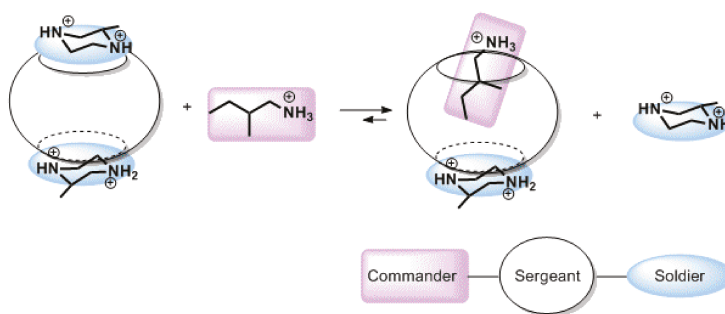


Figure 18. Representation of the complexation pathway in a ternary supramolecular system of CB[6], (S)-2-methylpiperazine and 2-methylbutylamine, with outstanding chiral selectivity [63].

The most recent study on a ternary system with two chiral compounds and CB[7] was published by Day et al. [65]. They observed that chiroptical properties of chiral organic salts can be affected by the formation of CB complexes. The most illustrative example of the effect of CB[7] is the change in the CD signal of diastereomeric pairs of chiral (*S*)-ammonium-2-benzyloxycyclopentane (*R*- or *S*-ABC⁺) salts with hydrogen tartrate (*L*- or *D*-HT⁻) (Figure 15). The additional absorption band is induced in the signal of one diastereomer (*S*-ABC@CB7·*D*-HT, the positive CD signal), as the other diastereomer signal retains the same λ_{\max} (*S*-ABC@CB7·*L*-HT, negative CD band) (Figure 19A). CB[7] has the same influence with respect to enantiomeric ammonium tartrate salts, and the sign of the Cotton effect is dictated by the chiral salt itself and is opposite for the signal for the enantiomeric pairs (Figure 19B).

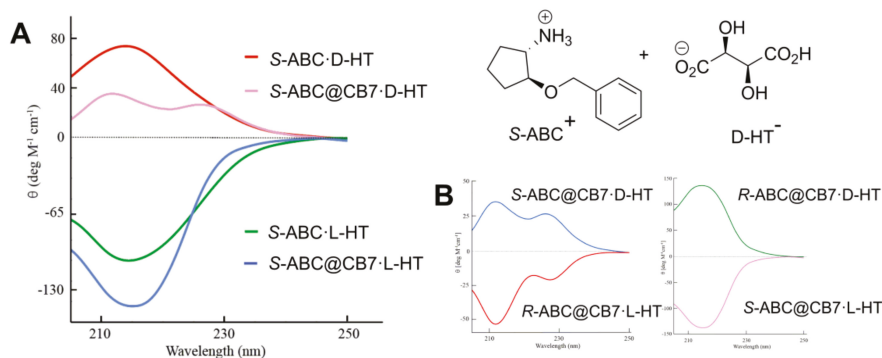


Figure 19. (A) CD signals for (*S*)-ammonium-2-benzyloxycyclopentane salt with *D*- and *L*-hydrogen tartrate and with and without CB[7]; (B) CD signal of two enantiomeric pairs of ternary complexes [65]. HT, hydrogen tartrate; (*S*)-ammonium-2-benzyloxycyclopentane (*S*-ABC⁺).

Based on the phenomena that chiral compounds can induce CD signal upon complexation with achiral molecules and that CB[8] forms a complex with two aromatic guests, Biedermann and Nau [66,67] developed a wonderful analytical method for the detection of chiral amino acids, peptides, proteins and aromatic drugs (Figure 20). Some examples of the application of this method are outlined in Figure 20B. One can follow the formation of some particular chiral product that chemoselectively forms a complex with a CB[8] sensor. In this sensor CB[8] acts as a host and fluorescent dye, for instance dimethyldiazaperopyrenium (MDPP), serves as a signaling unit. For example, during enzymatic hydrolysis of racemic glycyl-phenylalanine dipeptide (Gly-*D*/*L*-Phe), only one enantiomer is digested, and *L*-phenylalanine (*L*-Phe) is formed, while the Gly-*D*-Phe dipeptide remains intact. The binding constant of *L*-Phe ($450 \times 10^3 \text{ M}^{-1}$) to supramolecular sensor MDPP@CB[8] is much higher, compared with binding of Gly-*D*-Phe ($7 \times 10^3 \text{ M}^{-1}$) dipeptide; therefore, the [L-Phe-MDPP@CB[8]] complex is mainly formed, and *L*-Phe can be sensed through the CD signal of the ternary complex (Figure 20B, top). It is also remarkable that the kinetics of the enzyme reaction can be monitored by following the formation of a single enantiomer. Hippuryl-phenylalanine dipeptide hydrolysis kinetics, which was determined through the CD signal of the CB[8]-sensor system, coincides with conventionally measured UV-outcome, but in the first method, one can directly monitor enantioselectivity of the reaction and assign absolute configuration of the product.

In addition to chiral sensing applications, CBs have also been engaged in enantioselective supramolecular catalysis. Scherman and Herrmann et al. [68] showed that the CB[8] complex with a copper salt of a chiral amino acid can function as a chiral nanoreactor (Figure 21). The Diels-Alder reaction in the presence of CB[8], *L*-tryptophan and Cu²⁺ gave cycloaddition product in enantiomeric excess (*ee*) of 73% compared with *ee* 31% from the reaction without CB. A catalytic system utilizing *N*- α -methyl-*L*-tryptophan as a chiral inducer gave the product in the presence of CB[8] in an *ee* of 92%

and without CB[8] in an *ee* of 72%. As a result, for the first time, it was shown that CB can increase enantioselectivity in the catalysis.

There are also fascinating examples of diastereoselective photocycloaddition reactions catalyzed by complexation with CBs, but as this topic has just been recently reviewed, it is not covered herein [28].

The presented examples show that there are outstanding approaches already proven to be possible, and noteworthy input has been made by studying complexation of chiral compounds with CBs. In addition to the examples described above, in Tables 1–4 is outlined a collection of chiral guests, whose complexation with CBs has been studied.

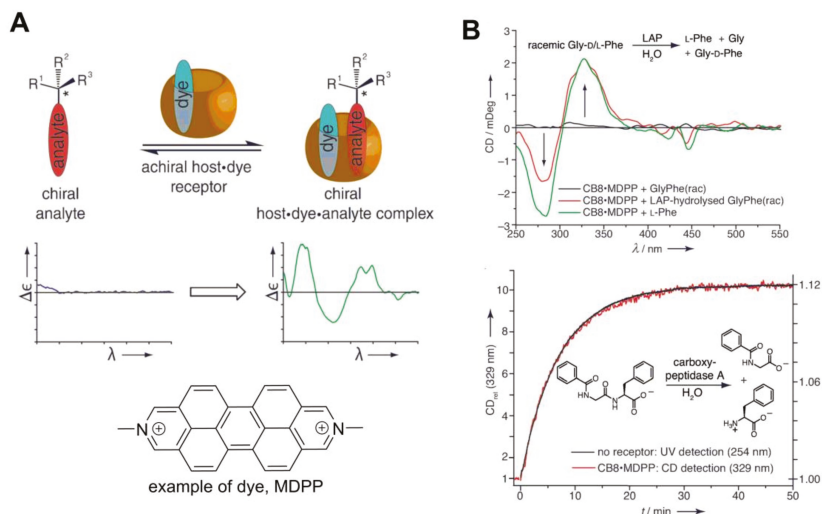


Figure 20. (A) Principle of the supramolecular chirality sensing system with CB[8]; (B) examples of the application of this sensing system: (top) CD spectra of CB[8]·MDPP (20 mm) in the presence of racemic Gly-D/L-Phe, before and after its enzymatic hydrolysis by leucine aminopeptidase (LAP) at pH 7.8; (bottom) kinetic trace for the hydrolysis of hippuryl-Phe (160 mm) by carboxypeptidase A at pH 7.8. The reaction progress was monitored by CD (329 nm) in the presence of MDPP@CB8 (20 mm, red line) and, as a control, directly by UV-Vis spectroscopy (254 nm, black line). Reprinted with permission from [66]. MDPP, dimethyldiazaperopyrenium.

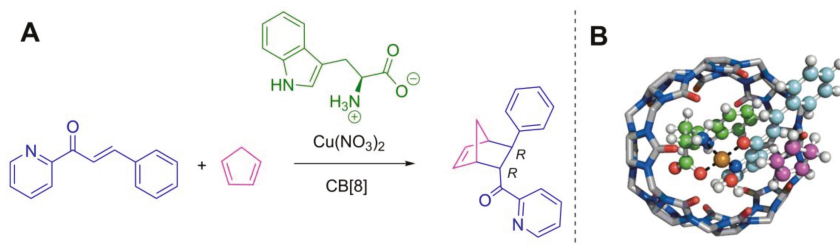


Figure 21. (A) Diels-Alder reaction catalyzed in a CB-nanoreactor; (B) lowest energy geometry of the complex of Cu^{2+} , H_2O , tryptophan, azachalcone and CB[8] with cyclopentadiene approaching in the endo direction [68].

Table 1. Carbohydrates as guests for CBs (G, guest; H, Host; Ref, reference).

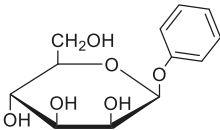
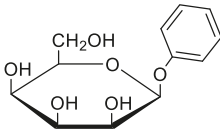
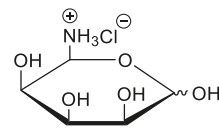
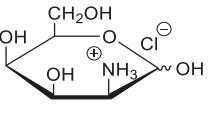
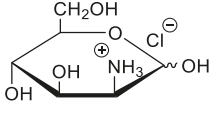
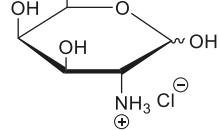
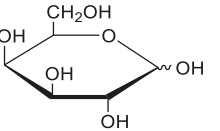
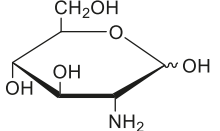
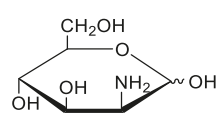
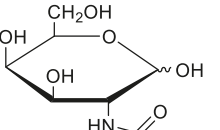
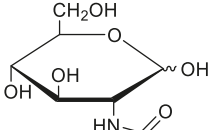
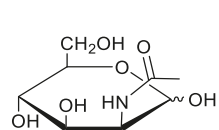
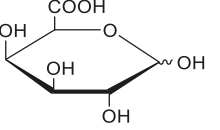
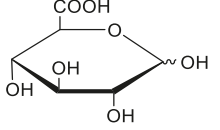
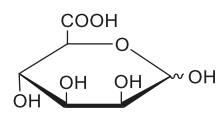
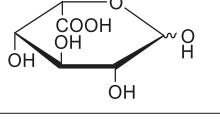
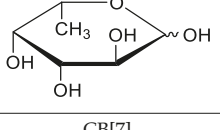
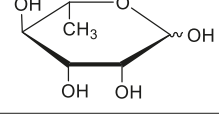
| Legend | Structure of Guest, Name of Host and Reference Number | | |
|--------|---|---|--|
| G |  |  |  |
| H | CB[8] | CB[8] | CB[7] |
| Ref. | [66] | [66] | [69] |
| G |  |  |  |
| H | | CB[7] | |
| Ref. | | [69] | |
| G |  |  |  |
| H | | CB[7] | |
| Ref. | | [70] | |
| G |  |  |  |
| H | | CB[7] | |
| Ref. | | [70] | |
| G |  |  |  |
| H | | CB[7] | |
| Ref. | | 70 | |
| G |  |  |  |
| H | | CB[7] | |
| Ref. | | [70] | |

Table 2. Pharmaceuticals as guests for CBs.

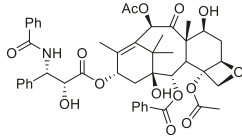
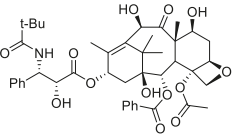
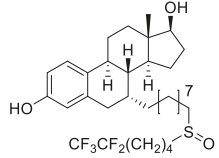
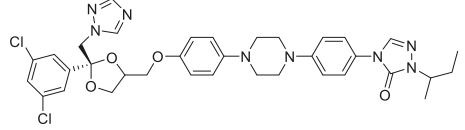
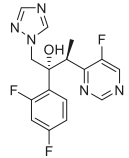
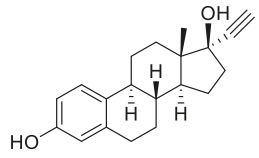
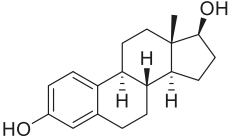
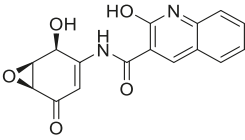
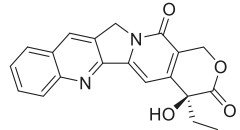
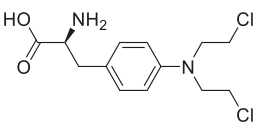
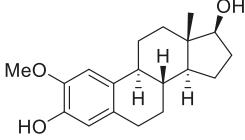
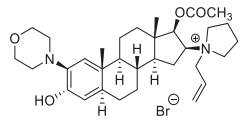
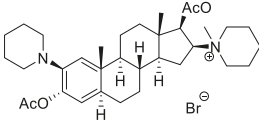
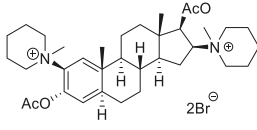
| Legend | Structure of Guest, Name of Host and Reference Number | | |
|--------|---|---|--|
| G |  |  |  |
| | Paclitaxel | Docetaxel | Fulvestrant |
| H | Acyclic CB | | |
| Ref. | [71] | | |
| G |  |  | |
| | Itraconazole | Voriconazole | |
| H | Acyclic CB | | |
| Ref. | [71] | | |
| G |  |  |  |
| | α -ethynylestradiol | Estradiol | PBS 1086 |
| H | Acyclic CB | | |
| Ref. | [71–73] | | |
| G |  |  |  |
| | S-camptothecin | Melphalan | 2-methoxyestradiol |
| H | Acyclic CB, CB[7], CB[8] | Acyclic CB | Acyclic CB |
| Ref. | [71–77] | [71–73] | [73] |
| G |  |  |  |
| | Rocuronium | Vecuronium | Pancuronium |
| H | Acyclic CB | | |
| Ref. | [78] | | |

Table 2. Cont.

| Legend | Structure of Guest, Name of Host and Reference Number | | |
|--------|---|----------------------|---------------------------|
| G | | | |
| | Cisatracurium | Tubocurarine | |
| H | Acyclic CB | | |
| Ref. | [78] | | |
| G | | | |
| | Labetalol | Phenylephrine | |
| H | CB[7] | CB[6], Acyclic CB | |
| Ref. | [79] | [80] | |
| G | | | |
| | Pseudoephedrine | Adrenaline | Amphetamine hydrochloride |
| H | CB[6], Acyclic CB | CB[6] | CB[7] |
| Ref. | [80] | [81] | [82] |
| G | | | |
| | Methamphetamine hydrochloride | Prilocaine | Sodium ascorbate |
| H | CB[7] | CB[7] | CB[6] |
| Ref. | [82] | [83] | [84] |
| G | | | |
| | Pilocarpine | 6-monoacetylmorphine | Noroxycodone |

Table 2. Cont.

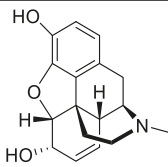
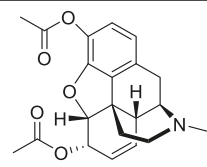
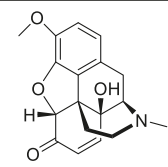
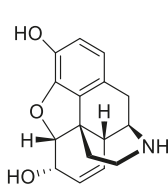
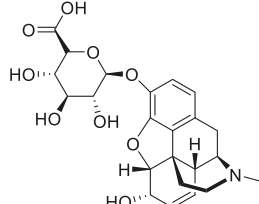
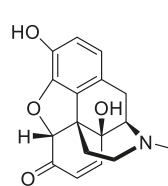
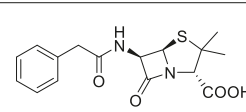
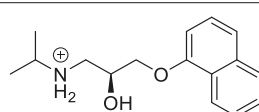
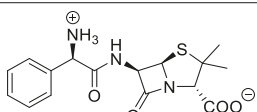
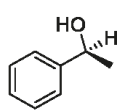
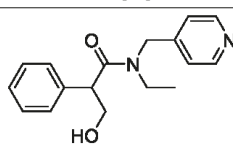
| Legend | Structure of Guest, Name of Host and Reference Number | | |
|--------|---|---|---|
| H | CB[7] | Acyclic CB | Acyclic CB |
| Ref. | [85] | [86] | [86] |
| G |  |  |  |
| | Morphine | Heroin | Oxycodone |
| H | Acyclic CB | | |
| Ref. | [86] | | |
| G |  |  |  |
| | Normorphine | Morphine-6-glucuronide | Oxymorphone |
| H | Acyclic CB | | |
| Ref. | [86] | | |
| G |  |  |  |
| | Penicillin G | (S)-propranolol | Ampicillin |
| H | CB[8] | | |
| Ref. | [66] | | |
| G |  |  | |
| | (S)-1-phenylethanol | Tropicamide | |
| H | CB[8] | CB[7], CB[8] | |
| Ref. | [66] | [87] | |

Table 3. Amino acids, amino derivatives and peptides as guests for CBs.

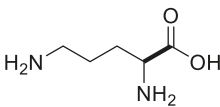
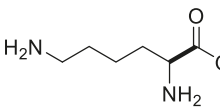
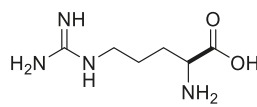
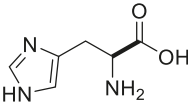
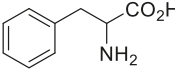
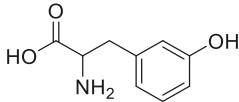
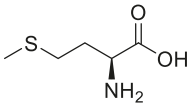
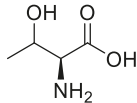
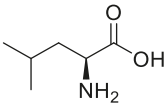
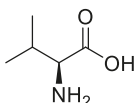
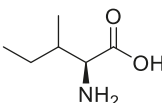
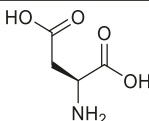
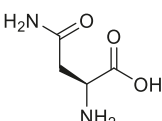
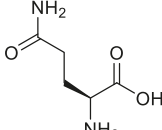
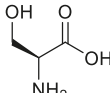
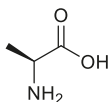
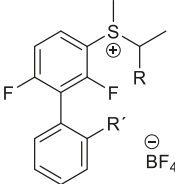
| Legend | Structure of Guest, Name of Host and Reference Number | | |
|--------|---|---|---|
| G |  |  |  |
| H | CB[6], Acyclic CB | CB[6], Acyclic, CB[7], iCB[7] | CB[6], Acyclic, CB[7], iCB[7] |
| Ref. | [88] | [82,89–92] | [82,89–92] |
| G |  |  |  |
| H | CB[6], CB[7], CB[8], iCB[7] | CB[6], CB[7], CB[8], iCB[7] | CB[6], CB[7], CB[8], iCB[7] |
| Ref. | [82,89,91,93,94] | [89,91–96] | [89,92–94] |
| G |  |  |  |
| H | iCB[7], CB[6] | iCB[7] | iCB[7] |
| Ref. | [91,97] | [91] | [91] |
| G |  |  |  |
| H | iCB[7], CB[7] | iCB[7], CB[7] | CB[7] |
| Ref. | [91,92] | [91,92] | [92] |
| G |  |  |  |
| H | | CB[7] | |
| Ref. | | [92] | |
| G |  |  | R = H, CH ₃ ; R' = CH ₃ , Cl |
| H | CB[7] | CB[8] | |
| Ref. | [92] | [98] | |

Table 3. Cont.

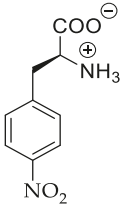
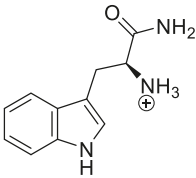
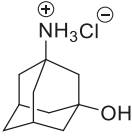
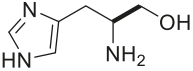
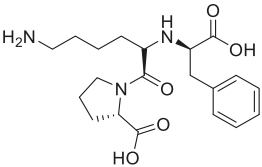
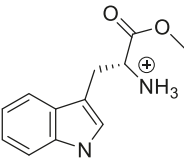
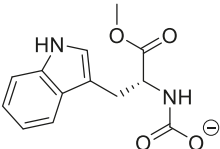
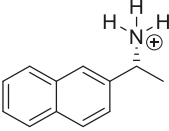
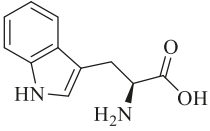
| Legend | Structure of Guest, Name of Host and Reference Number | | |
|--------|---|---|---|
| G |  |  |  |
| H | CB[7] | | |
| Ref. | [66] | | |
| G |  |  |  |
| H | CB[6], Acyclic CB | CB[6], Acyclic CB | CB[8] |
| Ref. | [88] | [88] | [94] |
| G |  |  |  |
| H | CB[8] | CB[7], CB[6] | CB[6], CB[8], iCB[7] |
| Ref. | [94] | [99] | [91,94,100,101] |
| G | Phe-Gly Phe-Ala Phe-Val Gly-Ala Asp-Phe Hippuryl-Phe | TrpPro Trp-OMe NAc-Trp Aspartame NAcTrp-NH2 Trp(Pro)6-NH2 Trp(Gly)6-NH2 | Trp(Ala)6-NH2 Trp(Val)6-NH2 Trp(Leu)6-NH2 Trp(Asp)6-NH2 Trp(Glu)6-NH2 5-F-Trp(Gly)6-NH2 5-F-Trp(Asn)6-NH2 |
| H | CB[8] | | |
| Ref. | [66] | | |
| G | Phe-Gly-Gly Gly-Phe-Gly Gly-Gly-Phe Gly-Gly-Trp-Gly-Gly | His-Gly-Gly Gly-His-Gly Gly-Gly-His Gly-Gly-Tyr Tyr-Gly-Gly | Gly-Tyr Gly-Trp Gly-Gly |
| H | CB[8] | CB[8] | CB[6] |
| Ref. | [102] | [102] | [103] |
| G | Gly-Tyr-Gly | Trp-Gly-Gly | Gly-Gly-Trp |
| H | CB[8] | CB[8] | CB[8] |
| Ref. | [102,104] | [94,102,104] | [94,102] |

Table 3. Cont.

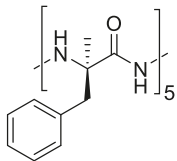
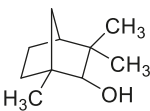
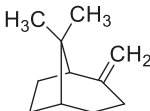
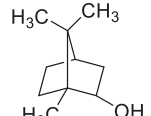
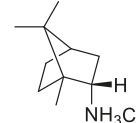
| Legend | Structure of Guest, Name of Host and Reference Number | | |
|--------|---|--|--|
| G |  | Thr-Gly-Ala-Phe-Met Thr-Gly-Ala-AMPhe-Met | Phe-Leu Phe-Met-NH ₂ Phe-Leu-NH ₂ Thr-Gly-Ala-Phe-Leu Thr-Gly-Ala-Phe-Met-NH ₂ Thr-Gly-Ala-Phe-Leu-NH ₂ Thr-Gly-Ser-Phe-Met-NH ₂ Thr-Gly-Gly-Phe-Met-NH ₂ Thr-Gly-DAla-Phe-Met-NH ₂ |
| H | CB[8] | CB[7] | CB[7] |
| Ref. | [105] | [106] | [96] |
| G | Gly-Phe | | |
| H | CB[8], CB[6] | | |
| Ref. | [51,88] | | |

Table 4. Terpenes as guests for CBs.

| Legend | Structure of Guest, Name of Host and Reference Number | | | |
|--------|---|---|---|--|
| G |  |  |  |  |
| H | CB[7], CB[8] | CB[7] | CB[7] | CB[7] |
| Ref. | [74,107] | [107] | [107] | [108] |

5. Conclusions

Cucurbituril chemistry has undergone remarkable growth in recent years. Applications of CB-type hosts have gained considerable attention due to CBs' outstanding binding ability and influence on the optical signal of dyes. However, studies on chiral sensing have emerged just recently, even though the first results in studies on the influence of CBs on supramolecular chirality appeared more than a decade ago. One can see that CB-type hosts are rich in means of symmetry breaking, which leads to induction of chirality. In addition, the synthesis of some chiral and enantiopure CB-type hosts have been developed, though the utilization of the created chiral systems is still obscure. Outstanding examples for the induction of supramolecular chirality from achiral building blocks and for the formation of helices in the solid state have been shown. Further on, the first elegant applications of the phenomena that CBs do form complexes with chiral guests and can induce specific chiroptical and catalytic properties are available. In addition, there are examples of stereoselective binding between diastereomers and cis–trans isomers, the selectivity of which is driven by the confined space inside the cucurbiturils. Based on that, the foundation for the emergence of new supramolecular systems, whose selectivity can be directed by external stimuli and that can be applied for chirality sensing and enantioselective applications, exists and should be encouraged.

Acknowledgments: The authors thank Sandra Kaabel for fruitful discussion and illustrations. The writing of this paper was supported by the Estonian Ministry of Education and Research through Grant PUT692.

Author Contributions: Both authors contributed substantially to the work reported.

Conflicts of Interest: The authors declare no conflict of interest.

References

- Freeman, W.A.; Mock, W.L.; Shih, N.Y. Cucurbituril. *J. Am. Chem. Soc.* **1981**, *103*, 7367–7368. [[CrossRef](#)]
- Flinn, A.; Hough, G.C.; Stoddart, J.F.; Williams, D.J. Decamethylcucurbit[5]uril. *Angew. Chem. Int. Ed.* **1992**, *31*, 1475–1477. [[CrossRef](#)]
- Kim, J.; Jung, I.-S.; Kim, S.-Y.; Lee, E.; Kang, J.-K.; Sakamoto, S.; Yamaguchi, K.; Kim, K. New Cucurbituril Homologues: Syntheses, Isolation, Characterization, and X-ray Crystal Structures of Cucurbit[*n*]uril (*n* = 5, 7, and 8). *J. Am. Chem. Soc.* **2000**, *122*, 540–541. [[CrossRef](#)]
- Day, A.; Arnold, A.P.; Blanch, R.J.; Snushall, B. Controlling Factors in the Synthesis of Cucurbituril and Its Homologues. *J. Org. Chem.* **2001**, *66*, 8094–8100. [[CrossRef](#)] [[PubMed](#)]
- Aav, R.; Kaabel, S.; Fomitšenko, M. Cucurbiturils: Synthesis, Structures, Formation Mechanisms, and Nomenclature. In *Comprehensive Supramolecular Chemistry II*; Atwood, J.L., Ed.; Elsevier: Oxford, UK, 2017; Volume 3, pp. 203–220, ISBN 978-0-12-803199-5.
- Lisbjerg, M.; Pittelkow, M. Hemicucurbit[*n*]urils. In *Comprehensive Supramolecular Chemistry II*; Atwood, J.L., Ed.; Elsevier: Oxford, UK, 2017; Volume 3, pp. 221–236, ISBN 978-0-12-803199-5.
- Ganapati, S.; Isaacs, L. Acyclic Cucurbit[*n*]uril-type Receptors: Preparation, Molecular Recognition Properties and Biological Applications. *Isr. J. Chem.* **2018**, in print. [[CrossRef](#)]
- Andersen, N.N.; Lisbjerg, M.; Eriksen, K.; Pittelkow, M. Hemicucurbit[*n*]urils and Their Derivatives—Synthesis and Applications. *Isr. J. Chem.* **2018**, in print. [[CrossRef](#)]
- Masson, E.; Raeisi, M.; Kotturi, K. Kinetics Inside, Outside and Through Cucurbiturils. *Isr. J. Chem.* **2018**, in print. [[CrossRef](#)]
- Ouari, O.; Bardelang, D. Nitroxide Radicals with Cucurbit[*n*]urils and Other Cavitands. *Isr. J. Chem.* **2018**, in print. [[CrossRef](#)]
- Shen, J.; Dearden, D.V. Recent Progress in Gas Phase Cucurbit[*n*]uril Chemistry. *Isr. J. Chem.* **2018**, in print. [[CrossRef](#)]
- Kaifer, A.E. Portal Effects on the Stability of Cucurbituril Complexes. *Isr. J. Chem.* **2018**, in print. [[CrossRef](#)]
- Hou, C.; Zeng, X.; Gao, Y.; Qiao, S.; Zhang, X.; Xu, J.; Liu, J. Cucurbituril As A Versatile Tool to Tune the Functions of Proteins. *Isr. J. Chem.* **2018**, in print. [[CrossRef](#)]
- Kaabel, S.; Aav, R. Templating Effects in the Dynamic Chemistry of Cucurbiturils and Hemicucurbiturils. *Isr. J. Chem.* **2018**, in print. [[CrossRef](#)]
- Wiemann, M.; Jonkheijm, P. Stimuli-Responsive Cucurbit[*n*]uril-Mediated Host-Guest Complexes on Surfaces. *Isr. J. Chem.* **2018**, in print. [[CrossRef](#)]
- Vícha, R.; Jelínková, K.; Rouchal, M. Cucurbit[*n*]urils-related Multitopic Supramolecular Components: Design, Properties, and Perspectives. *Isr. J. Chem.* **2018**, in print. [[CrossRef](#)]
- Koc, A.; Tuncel, D. Supramolecular Assemblies of Cucurbiturils with Photoactive, π -conjugated Chromophores. *Isr. J. Chem.* **2018**, in print. [[CrossRef](#)]
- Robinson-Duggon, J.; Pérez-Mora, F.; Dibona-Villanueva, L.; Fuentealba, D. Potential Applications of Cucurbit[*n*]urils Inclusion Complexes in Photodynamic Therapy. *Isr. J. Chem.* **2018**, in print. [[CrossRef](#)]
- Barooah, N.; Khurana, R.; Bhasikuttan, A.C.; Mohanty, J. Stimuli-responsive Supra-biomolecular Nanoassemblies of Cucurbit[7]uril with Bovine Serum Albumin: Drug Delivery and Sensor Applications. *Isr. J. Chem.* **2018**. [[CrossRef](#)]
- Macartney, D.H. Cucurbit[*n*]uril Host-Guest Complexes of Acids, Photoacids, and Super Photoacids. *Isr. J. Chem.* **2018**. [[CrossRef](#)]
- Masson, E.; Ling, X.; Joseph, R.; Kyeremeh-Mensah, L.; Lu, X. Cucurbituril chemistry: A tale of supramolecular success. *RSC Adv.* **2012**, *2*, 1213–1247. [[CrossRef](#)]
- Tomas, L.; Vladimír, S. Bambusuril Anion Receptors. *Isr. J. Chem.* **2018**, in print. [[CrossRef](#)]
- Reany, O.; Amar, M.; Ehud, K. Hetero-Bambusurils. *Isr. J. Chem.* **2018**, in print. [[CrossRef](#)]
- Barrow, S.J.; Kasera, S.; Rowland, M.J.; del Barrio, J.; Scherman, O.A. Cucurbituril-Based Molecular Recognition. *Chem. Rev.* **2015**, *115*, 12320–12406. [[CrossRef](#)] [[PubMed](#)]
- Sinn, S.; Biedermann, F. Chemical Sensors Based on Cucurbit[*n*]uril Macrocycles. *Isr. J. Chem.* **2018**, *58*. [[CrossRef](#)]
- Ni, X.-L.; Xiao, X.; Cong, H.; Liang, L.-L.; Cheng, K.; Cheng, X.-J.; Ji, N.-N.; Zhu, Q.-J.; Xue, S.-F.; Tao, Z. Cucurbit[*n*]uril-based coordination chemistry: From simple coordination complexes to novel poly-dimensional coordination polymers. *Chem. Soc. Rev.* **2013**, *42*, 9480–9508. [[CrossRef](#)] [[PubMed](#)]

27. Ni, X.-L.; Xiao, X.; Cong, H.; Zhu, Q.-J.; Xue, S.-F.; Tao, Z. Self-Assemblies Based on the “Outer-Surface Interactions” of Cucurbit[n]urils: New Opportunities for Supramolecular Architectures and Materials. *Acc. Chem. Res.* **2014**, *47*, 1386–1395. [[CrossRef](#)] [[PubMed](#)]
28. Pattabiraman, M.; Sivaguru, J.; Ramamurthy, V. Cucurbiturils as Reaction Containers for Photocycloaddition of Olefins. *Isr. J. Chem.* **2017**, *57*, in print. [[CrossRef](#)]
29. Mandadapu, V.; Day, A.I.; Ghanem, A. Cucurbituril: Chiral Applications. *Chirality* **2014**, *26*, 712–723. [[CrossRef](#)] [[PubMed](#)]
30. Huang, W.-H.; Zavalij, P.Y.; Isaacs, L. Chiral Recognition inside a Chiral Cucurbituril. *Angew. Chem. Int. Ed.* **2007**, *46*, 7425–7427. [[CrossRef](#)] [[PubMed](#)]
31. Kozerski, L.; Hansen, P.E. Aggregation of amphiphilic molecules in water. I. α -phenylethylamine: ^1H and ^{13}C NMR study. *J. Phys. Org. Chem.* **1991**, *4*, 58–66. [[CrossRef](#)]
32. Parve, O.; Reile, I.; Parve, J.; Kasvandik, S.; Kudrjašova, M.; Tamp, S.; Metsala, A.; Villo, L.; Pehk, T.; Jarvet, J.; et al. An NMR and MD Modeling Insight into Nucleation of 1,2-Alkanediols: Selective Crystallization of Lipase-Catalytically Resolved Enantiomers from the Reaction Mixtures. *J. Org. Chem.* **2013**, *78*, 12795–12801. [[CrossRef](#)] [[PubMed](#)]
33. Huang, W.-H.; Zavalij, P.Y.; Isaacs, L. Metal-Ion-Induced Folding and Dimerization of a Glycoluril Decamer in Water. *Org. Lett.* **2009**, *11*, 3918–3921. [[CrossRef](#)] [[PubMed](#)]
34. Cheng, X.-J.; Liang, L.-L.; Chen, K.; Ji, N.-N.; Xiao, X.; Zhang, J.-X.; Zhang, Y.-Q.; Xue, S.-F.; Zhu, Q.-J.; Ni, X.-L.; et al. Twisted Cucurbit[14]uril. *Angew. Chem. Int. Ed.* **2013**, *52*, 7252–7255. [[CrossRef](#)] [[PubMed](#)]
35. Qiu, S.-C.; Chen, K.; Wang, Y.; Hua, Z.; Li, F.; Huang, Y.; Tao, Z.; Zhang, Y.; Wei, G. Crystal structure analysis of twisted cucurbit [14]uril conformations. *Inorg. Chem. Commun.* **2017**, *86*, 49–53. [[CrossRef](#)]
36. Li, Q.; Qiu, S.-C.; Zhang, J.; Chen, K.; Huang, Y.; Xiao, X.; Zhang, Y.; Li, F.; Zhang, Y.-Q.; Xue, S.-F.; et al. Twisted Cucurbit[n]urils. *Org. Lett.* **2016**, *18*, 4020–4023. [[CrossRef](#)] [[PubMed](#)]
37. Lu, X.; Isaacs, L. Synthesis and Recognition Properties of Enantiomerically Pure Acyclic Cucurbit[n]uril-Type Molecular Containers. *Org. Lett.* **2015**, *17*, 4038–4041. [[CrossRef](#)] [[PubMed](#)]
38. Cao, L.; Hettiarachchi, G.; Briken, V.; Isaacs, L. Cucurbit[7]uril Containers for Targeted Delivery of Oxaliplatin to Cancer Cells. *Angew. Chem. Int. Ed.* **2013**, *52*, 12033–12037. [[CrossRef](#)] [[PubMed](#)]
39. Chen, J.; Liu, Y.; Mao, D.; Ma, D. Acyclic cucurbit[n]uril conjugated dextran for drug encapsulation and bioimaging. *Chem. Commun.* **2017**, *53*, 8739–8742. [[CrossRef](#)] [[PubMed](#)]
40. Herges, R. Topology in Chemistry: Designing Möbius Molecules. *Chem. Rev.* **2006**, *106*, 4820–4842. [[CrossRef](#)] [[PubMed](#)]
41. Li, Q.; Qiu, S.-C.; Chen, K.; Zhang, Y.; Wang, R.; Huang, Y.; Tao, Z.; Zhu, Q.-J.; Liu, J.-X. Encapsulation of alkylidiammonium ions within two different cavities of twisted cucurbit[14]uril. *Chem. Commun.* **2016**, *52*, 2589–2592. [[CrossRef](#)] [[PubMed](#)]
42. Miyahara, Y.; Goto, K.; Oka, M.; Inazu, T. Remarkably Facile Ring-Size Control in Macrocyclization: Synthesis of Hemicucurbit[6]uril and Hemicucurbit[12]uril. *Angew. Chem. Int. Ed.* **2004**, *43*, 5019–5022. [[CrossRef](#)] [[PubMed](#)]
43. Svec, J.; Necas, M.; Sindelar, V. Bambus[6]uril. *Angew. Chem. Int. Ed.* **2010**, *49*, 2378–2381. [[CrossRef](#)] [[PubMed](#)]
44. Singh, M.; Solel, E.; Keinan, E.; Reany, O. Aza-Bambusurils En Route to Anion Transporters. *Chem. Eur. J.* **2016**, *22*, 8848–8854. [[CrossRef](#)] [[PubMed](#)]
45. Aav, R.; Shmatova, E.; Reile, I.; Borissova, M.; Topić, F.; Rissanen, K. New Chiral Cyclohexylhemicucurbit[6]uril. *Org. Lett.* **2013**, *15*, 3786–3789. [[CrossRef](#)] [[PubMed](#)]
46. Lisbjerg, M.; Jessen, B.M.; Rasmussen, B.; Nielsen, B.E.; Madsen, A.Ø.; Pittelkow, M. Discovery of a cyclic 6 + 6 hexamer of D-biotin and formaldehyde. *Chem. Sci.* **2014**, *5*, 2647–2650. [[CrossRef](#)]
47. Prigorchenko, E.; Öeren, M.; Kaabel, S.; Fomitšenko, M.; Reile, I.; Järving, I.; Tamm, T.; Topić, F.; Rissanen, K.; Aav, R. Template-controlled synthesis of chiral cyclohexylhemicucurbit[8]uril. *Chem. Commun.* **2015**, *51*, 10921–10924. [[CrossRef](#)] [[PubMed](#)]
48. Öeren, M.; Shmatova, E.; Tamm, T.; Aav, R. Computational and ion mobility MS study of (all-*S*)-cyclohexylhemicucurbit[6]uril structure and complexes. *Phys. Chem. Chem. Phys.* **2014**, *16*, 19198–19205. [[CrossRef](#)] [[PubMed](#)]
49. Kaabel, S.; Adamson, J.; Topić, F.; Kiesilä, A.; Kalenius, E.; Öeren, M.; Reimund, M.; Prigorchenko, E.; Löökene, A.; Reich, H.J.; et al. Chiral hemicucurbit[8]uril as an anion receptor: Selectivity to size, shape and charge distribution. *Chem. Sci.* **2017**, *8*, 2184–2190. [[CrossRef](#)] [[PubMed](#)]

50. Lisbjerg, M.; Nielsen, B.E.; Milhøj, B.O.; Sauer, S.P.A.; Pittelkow, M. Anion binding by biotin[6]juril in water. *Org. Biomol. Chem.* **2014**, *13*, 369–373. [CrossRef] [PubMed]
51. Lisbjerg, M.; Valkenier, H.; Jessen, B.M.; Al-Kerdi, H.; Davis, A.P.; Pittelkow, M. Biotin[6]juril Esters: Chloride-Selective Transmembrane Anion Carriers Employing C–H⋯Anion Interactions. *J. Am. Chem. Soc.* **2015**, *137*, 4948–4951. [CrossRef] [PubMed]
52. Leong, W.L.; Vittal, J.J. One-Dimensional Coordination Polymers: Complexity and Diversity in Structures, Properties, and Applications. *Chem. Rev.* **2011**, *111*, 688–764. [CrossRef] [PubMed]
53. Whang, D.; Kim, K. Helical polyrotaxane: Cucurbituril ‘beads’ threaded onto a helical one-dimensional coordination polymer. *Chem. Commun.* **1997**, 2361–2362. [CrossRef]
54. Park, K.-M.; Whang, D.; Lee, E.; Heo, J.; Kim, K. Transition Metal Ion Directed Supramolecular Assembly of One- and Two-Dimensional Polyrotaxanes Incorporating Cucurbituril. *Chem. Eur. J.* **2002**, *8*, 498–508. [CrossRef]
55. Zeng, J.-P.; Cong, H.; Chen, K.; Xue, S.-F.; Zhang, Y.-Q.; Zhu, Q.-J.; Liu, J.-X.; Tao, Z. A Novel Strategy to Assemble Achiral Ligands to Chiral Helical Polyrotaxane Structures. *Inorg. Chem.* **2011**, *50*, 6521–6525. [CrossRef] [PubMed]
56. Zhang, F.; Yajima, T.; Li, Y.-Z.; Xu, G.-Z.; Chen, H.-L.; Liu, Q.-T.; Yamauchi, O. Iodine-Assisted Assembly of Helical Coordination Polymers of Cucurbituril and Asymmetric Copper(II) Complexes. *Angew. Chem. Int. Ed.* **2005**, *44*, 3402–3407. [CrossRef] [PubMed]
57. Chen, K.; Hu, Y.-F.; Xiao, X.; Xue, S.-F.; Tao, Z.; Zhang, Y.-Q.; Zhu, Q.-J.; Liu, J.-X. Homochiral 1D-helical coordination polymers from achiral cucurbit[5]juril: Hydroquinone-induced spontaneous resolution. *RSC Adv.* **2012**, *2*, 3217–3220. [CrossRef]
58. Chen, K.; Liang, L.-L.; Liu, H.-J.; Zhang, Y.-Q.; Xue, S.-F.; Tao, Z.; Xiao, X.; Zhu, Q.-J.; Lindoy, L.F.; Wei, G. Hydroquinone-assisted assembly of coordination polymers from lanthanides and cucurbit[5]juril. *CrystEngComm* **2012**, *14*, 7994–7999. [CrossRef]
59. Xiao, X.; Liu, J.-X.; Fan, Z.-F.; Chen, K.; Zhu, Q.-J.; Xue, S.-F.; Tao, Z. Chirality from achiral components: *N,N'*-bis(4-dimethylaminobenzyl)dodecane-1,12-diammonium in cucurbit[8]juril. *Chem. Commun.* **2010**, *46*, 3741–3743. [CrossRef] [PubMed]
60. Hembury, G.A.; Borovkov, V.V.; Inoue, Y. Chirality-Sensing Supramolecular Systems. *Chem. Rev.* **2008**, *108*, 1–73. [CrossRef] [PubMed]
61. Liu, M.; Zhang, L.; Wang, T. Supramolecular Chirality in Self-Assembled Systems. *Chem. Rev.* **2015**, *115*, 7304–7397. [CrossRef] [PubMed]
62. Mori, T.; Ko, Y.H.; Kim, K.; Inoue, Y. Circular Dichroism of Intra- and Intermolecular Charge-Transfer Complexes. Enhancement of Anisotropy Factors by Dimer Formation and by Confinement. *J. Org. Chem.* **2006**, *71*, 3232–3247. [CrossRef] [PubMed]
63. Rekharsky, M.V.; Yamamura, H.; Inoue, C.; Kawai, M.; Osaka, I.; Arakawa, R.; Shiba, K.; Sato, A.; Ko, Y.H.; Selvapalam, N.; et al. Chiral Recognition in Cucurbituril Cavities. *J. Am. Chem. Soc.* **2006**, *128*, 14871–14880. [CrossRef] [PubMed]
64. Green, M.M.; Reidy, M.P.; Johnson, R.D.; Darling, G.; O’Leary, D.J.; Willson, G. Macromolecular stereochemistry: The out-of-proportion influence of optically active comonomers on the conformational characteristics of polyisocyanates. The sergeants and soldiers experiment. *J. Am. Chem. Soc.* **1989**, *111*, 6452–6454. [CrossRef]
65. Wu, W.; Cronin, M.P.; Wallace, L.; Day, A.I. An Exploration of Induced Supramolecular Chirality Through Association of Chiral Ammonium Ions and Tartrates with the Achiral Host Cucurbit[7]juril. *Isr. J. Chem.* **2018**, *58*, in print. [CrossRef]
66. Biedermann, F.; Nau, W.M. Noncovalent Chirality Sensing Ensembles for the Detection and Reaction Monitoring of Amino Acids, Peptides, Proteins, and Aromatic Drugs. *Angew. Chem. Int. Ed.* **2014**, *53*, 5694–5699. [CrossRef] [PubMed]
67. Nau, W.; Biedermann, F. A Method for Detecting a Chiral Analyte. Patent DE102013021899A1, 2015. Available online: <https://patents.google.com/patent/DE102013021899A1/en> (accessed on 2 February 2018).
68. Zheng, L.; Sonzini, S.; Ambarwati, M.; Rosta, E.; Scherman, O.A.; Herrmann, A. Turning Cucurbit[8]juril into a Supramolecular Nanoreactor for Asymmetric Catalysis. *Angew. Chem. Int. Ed.* **2015**, *54*, 13007–13011. [CrossRef] [PubMed]

69. Jang, Y.; Natarajan, R.; Ko, Y.H.; Kim, K. Cucurbit[7]uril: A High-Affinity Host for Encapsulation of Amino Saccharides and Supramolecular Stabilization of Their α -Anomers in Water. *Angew. Chem. Int. Ed.* **2014**, *53*, 1003–1007. [[CrossRef](#)] [[PubMed](#)]
70. Lee, H.H.L.; Kim, H.I. Supramolecular Analysis of Monosaccharide Derivatives Using Cucurbit[7]uril and Electrospray Ionization Tandem Mass Spectrometry. *Isr. J. Chem.* **2018**, in print. [[CrossRef](#)]
71. Zhang, B.; Isaacs, L. Acyclic Cucurbit[*n*]uril-type Molecular Containers: Influence of Aromatic Walls on their Function as Solubilizing Excipients for Insoluble Drugs. *J. Med. Chem.* **2014**, *57*, 9554–9563. [[CrossRef](#)] [[PubMed](#)]
72. Gilberg, L.; Zhang, B.; Zavalij, P.Y.; Sindelar, V.; Isaacs, L. Acyclic cucurbit[*n*]uril-type molecular containers: Influence of glycoluril oligomer length on their function as solubilizing agents. *Org. Biomol. Chem.* **2015**, *13*, 4041–4050. [[CrossRef](#)] [[PubMed](#)]
73. Sigwalt, D.; Moncelet, D.; Falcinelli, S.; Mandadapu, V.; Zavalij, P.Y.; Day, A.; Briken, V.; Isaacs, L. Acyclic Cucurbit[*n*]uril-Type Molecular Containers: Influence of Linker Length on Their Function as Solubilizing Agents. *ChemMedChem* **2016**, *11*, 980–989. [[CrossRef](#)] [[PubMed](#)]
74. Romero, M.A.; González-Delgado, J.A.; Mendoza, J.; Arteaga, J.F.; Basilio, N.; Pischel, U. Terpenes Show Nanomolar Affinity and Selective Binding with Cucurbit[8]uril. *Isr. J. Chem.* **2018**, in print. [[CrossRef](#)]
75. Gavvala, K.; Sengupta, A.; Hazra, P. Modulation of Photophysics and pKa Shift of the Anti-cancer Drug Camptothecin in the Nanocavities of Supramolecular Hosts. *ChemPhysChem* **2013**, *14*, 532–542. [[CrossRef](#)] [[PubMed](#)]
76. Dong, N.; Xue, S.-F.; Zhu, Q.-J.; Tao, Z.; Zhao, Y.; Yang, L.-X. Cucurbit[*n*]urils ($n = 7, 8$) binding of camptothecin and the effects on solubility and reactivity of the anticancer drug. *Supramol. Chem.* **2008**, *20*, 663–671. [[CrossRef](#)]
77. Yang, X.; Wang, Z.; Niu, Y.; Chen, X.; Lee, S.M.Y.; Wang, R. Influence of supramolecular encapsulation of camptothecin by cucurbit[7]uril: Reduced toxicity and preserved anti-cancer activity. *Med. Chem. Comm.* **2016**, *7*, 1392–1397. [[CrossRef](#)]
78. Ma, D.; Zhang, B.; Hoffmann, U.; Sundrup, M.G.; Eikermann, M.; Isaacs, L. Acyclic Cucurbit[*n*]uril-Type Molecular Containers Bind Neuromuscular Blocking Agents In Vitro and Reverse Neuromuscular Block In Vivo. *Angew. Chem. Int. Ed.* **2012**, *51*, 11358–11362. [[CrossRef](#)] [[PubMed](#)]
79. Li, C.; Feng, J.; Ju, H. Supramolecular interaction of labetalol with cucurbit[7]uril for its sensitive fluorescence detection. *Analyst* **2014**, *140*, 230–235. [[CrossRef](#)] [[PubMed](#)]
80. Minami, T.; Esipenko, N.A.; Akdeniz, A.; Zhang, B.; Isaacs, L.; Anzenbacher, P. Multianalyte Sensing of Addictive Over-the-Counter (OTC) Drugs. *J. Am. Chem. Soc.* **2013**, *135*, 15238–15243. [[CrossRef](#)] [[PubMed](#)]
81. Danylyuk, O.; Fedin, V.P.; Sashuk, V. Kinetic trapping of the host–guest association intermediate and its transformation into a thermodynamic inclusion complex. *Chem. Commun.* **2013**, *49*, 1859–1861. [[CrossRef](#)] [[PubMed](#)]
82. Jang, Y.; Jang, M.; Kim, H.; Lee, S.J.; Jin, E.; Koo, J.Y.; Hwang, I.-C.; Kim, Y.; Ko, Y.H.; Hwang, I.; et al. Point-of-Use Detection of Amphetamine-Type Stimulants with Host-Molecule-Functionalized Organic Transistors. *Chem* **2017**, *3*, 641–651. [[CrossRef](#)]
83. Wyman, I.W.; Macartney, D.H. Host–guest complexations of local anaesthetics by cucurbit[7]uril in aqueous solution. *Org. Biomol. Chem.* **2010**, *8*, 247–252. [[CrossRef](#)] [[PubMed](#)]
84. Pandey, S.; Soni, V.K.; Choudhary, G.; Sharma, P.R.; Sharma, R.K. Understanding behaviour of vitamin-C guest binding with the cucurbit[6]uril host. *Supramol. Chem.* **2017**, *29*, 387–394. [[CrossRef](#)]
85. Saleh, N.; Al-Handawi, M.B.; Al-Kaabi, L.; Ali, L.; Salman Ashraf, S.; Thiemann, T.; al-Hindawi, B.; Meetani, M. Intermolecular interactions between cucurbit[7]uril and pilocarpine. *Int. J. Pharm.* **2014**, *460*, 53–62. [[CrossRef](#)] [[PubMed](#)]
86. Shcherbakova, E.G.; Zhang, B.; Gozem, S.; Minami, T.; Zavalij, P.Y.; Pushina, M.; Isaacs, L.D.; Anzenbacher, P. Supramolecular Sensors for Opiates and Their Metabolites. *J. Am. Chem. Soc.* **2017**, *139*, 14954–14960. [[CrossRef](#)] [[PubMed](#)]
87. Saleh, N.; Meetani, M.A.; Al-Kaabi, L.; Ghosh, I.; Nau, W.M. Effect of cucurbit[*n*]urils on tropicamide and potential application in ocular drug delivery. *Supramol. Chem.* **2011**, *23*, 650–656. [[CrossRef](#)]
88. Minami, T.; Esipenko, N.A.; Zhang, B.; Isaacs, L.; Anzenbacher, P. “Turn-on” fluorescent sensor array for basic amino acids in water. *Chem. Commun.* **2014**, *50*, 61–63. [[CrossRef](#)] [[PubMed](#)]
89. Lee, J.W.; Lee, H.H.L.; Ko, Y.H.; Kim, K.; Kim, H.I. Deciphering the Specific High-Affinity Binding of Cucurbit[7]uril to Amino Acids in Water. *J. Phys. Chem. B* **2015**, *119*, 4628–4636. [[CrossRef](#)] [[PubMed](#)]

90. Bailey, D.M.; Hennig, A.; Uzunova, V.D.; Nau, W.M. Supramolecular Tandem Enzyme Assays for Multiparameter Sensor Arrays and Enantiomeric Excess Determination of Amino Acids. *Chem. Eur. J.* **2008**, *14*, 6069–6077. [CrossRef] [PubMed]
91. Gao, Z.-Z.; Kan, J.-L.; Chen, L.-X.; Bai, D.; Wang, H.-Y.; Tao, Z.; Xiao, X. Binding and Selectivity of Essential Amino Acid Guests to the Inverted Cucurbit[7]uril Host. *ACS Omega* **2017**, *2*, 5633–5640. [CrossRef]
92. Kovalenko, E.; Vilaseca, M.; Díaz-Lobo, M.; Masliy, A.N.; Vicent, C.; Fedin, V.P. Supramolecular Adducts of Cucurbit[7]uril and Amino Acids in the Gas Phase. *J. Am. Soc. Mass Spectrom.* **2016**, *27*, 265–276. [CrossRef] [PubMed]
93. Hang, C.; Tau, L.-L.; Yu, Y.-H.; Yang, F.; Du, Y.; Xue, S.-F.; Tao, Z. Molecular Recognition of Amino acid by Cucurbiturils. *Acta Chim. Sin.* **2006**, *64*, 989–996.
94. Bush, M.E.; Bouley, N.D.; Urbach, A.R. Charge-Mediated Recognition of N-Terminal Tryptophan in Aqueous Solution by a Synthetic Host. *J. Am. Chem. Soc.* **2005**, *127*, 14511–14517. [CrossRef] [PubMed]
95. Liu, S.; Ruspic, C.; Mukhopadhyay, P.; Chakrabarti, S.; Zavalij, P.Y.; Isaacs, L. The Cucurbit[n]uril Family: Prime Components for Self-Sorting Systems. *J. Am. Chem. Soc.* **2005**, *127*, 15959–15967. [CrossRef] [PubMed]
96. Ghale, G.; Ramalingam, V.; Urbach, A.R.; Nau, W.M. Determining Protease Substrate Selectivity and Inhibition by Label-Free Supramolecular Tandem Enzyme Assays. *J. Am. Chem. Soc.* **2011**, *133*, 7528–7535. [CrossRef] [PubMed]
97. Thuéry, P. Supramolecular assemblies built from lanthanide ammoniocarboxylates and cucurbit[6]uril. *CrystEngComm* **2012**, *14*, 8128–8136. [CrossRef]
98. Joseph, R.; Masson, E. Cucurbit[8]uril recognition of rapidly interconverting diastereomers. *Supramol. Chem.* **2014**, *26*, 632–641. [CrossRef]
99. Tang, H.; Fuentealba, D.; Ko, Y.H.; Selvapalam, N.; Kim, K.; Bohne, C. Guest Binding Dynamics with Cucurbit[7]uril in the Presence of Cations. *J. Am. Chem. Soc.* **2011**, *133*, 20623–20633. [CrossRef] [PubMed]
100. Danylyuk, O.; Fedin, V.P. Solid-State Supramolecular Assemblies of Tryptophan and Tryptamine with Cucurbit[6]uril. *Cryst. Growth Des.* **2012**, *12*, 550–555. [CrossRef]
101. Ling, Y.; Wang, W.; Kaifer, A.E. A new cucurbit[8]uril-based fluorescent receptor for indole derivatives. *Chem. Commun.* **2007**, 610–612. [CrossRef] [PubMed]
102. Heitmann, L.M.; Taylor, A.B.; Hart, P.J.; Urbach, A.R. Sequence-specific recognition and cooperative dimerization of n-terminal aromatic peptides in aqueous solution by a synthetic host. *J. Am. Chem. Soc.* **2006**, *128*, 12574–12581. [CrossRef] [PubMed]
103. Danylyuk, O. Exploring cucurbit[6]uril–peptide interactions in the solid state: Crystal structure of cucurbit[6]uril complexes with glycyl-containing dipeptides. *CrystEngComm* **2017**, *19*, 3892–3897. [CrossRef]
104. Biedermann, F.; Rauwald, U.; Cziferszky, M.; Williams, K.A.; Gann, L.D.; Guo, B.Y.; Urbach, A.R.; Bielawski, C.W.; Scherman, O.A. Benzobis(imidazolium)–Cucurbit[8]uril Complexes for Binding and Sensing Aromatic Compounds in Aqueous Solution. *Chem. Eur. J.* **2010**, *16*, 13716–13722. [CrossRef] [PubMed]
105. Sonzini, S.; Ryan, S.T.J.; Scherman, O.A. Supramolecular dimerisation of middle-chain Phe pentapeptides via CB[8] host–guest homoternary complex formation. *Chem. Commun.* **2013**, *49*, 8779–8781. [CrossRef] [PubMed]
106. Logsdon, L.A.; Urbach, A.R. Sequence-Specific Inhibition of a Nonspecific Protease. *J. Am. Chem. Soc.* **2013**, *135*, 11414–11416. [CrossRef] [PubMed]
107. Romero, M.A.; Basílio, N.; Moro, A.J.; Domingues, M.; González-Delgado, J.A.; Arteaga, J.F.; Pischel, U. Photocaged Competitor Guests: A General Approach Toward Light-Activated Cargo Release from Cucurbiturils. *Chem. Eur. J.* **2017**, *23*, 13105–13111. [CrossRef] [PubMed]
108. Cao, L.; Isaacs, L. Absolute and relative binding affinity of cucurbit[7]uril towards a series of cationic guests. *Supramol. Chem.* **2014**, *26*, 251–258. [CrossRef]



© 2018 by the authors. Licensee MDPI, Basel, Switzerland. This article is an open access article distributed under the terms and conditions of the Creative Commons Attribution (CC BY) license (<http://creativecommons.org/licenses/by/4.0/>).

Review

Chiral Heterocycle-Based Receptors for Enantioselective Recognition

Vaibhav N. Khose¹, Marina E. John¹, Anita D. Pandey¹, Victor Borovkov^{2,*}
and Anil V. Karnik^{1,*}

¹ Department of Chemistry, University of Mumbai, Vidyanagari, Mumbai 400 098, India; vnkhose@gmail.com (V.N.K.); marinajohn126@gmail.com (M.E.J.); anitadpandey@gmail.com (A.D.P.)

² Department of Chemistry and Biochemistry, Tallinn University of Technology, Akadeemia tee 15, 12618 Tallinn, Estonia

* Correspondence: victor.borovkov@ttu.ee (V.B.); avkarnik@chem.mu.ac.in (A.V.K.); Tel.: +91-022-26526091 (A.V.K.)

Received: 27 December 2017; Accepted: 12 January 2018; Published: 24 January 2018

Abstract: The majority of biomolecules found in living beings are chiral, therefore chiral molecular recognition in living systems is crucial to life. Following Cram's seminal work on the crown-based chiral recognition, prominent research groups have reported innumerable chiral receptors with distinctly different geometrical features and asymmetry elements. Main applications of such chiral receptors are found in chiral chromatography, as for analytical purposes and for bulk separation of racemates. Incorporation of heterocyclic rings in these recognition systems added a new dimension to the existing group of receptors. Heterocycles have additional features such as availability of unshared electron pairs, pronounced conformational features, introduction of hydrogen bonding and presence of permanent dipoles as well as specific spectral properties in certain cases. These features are found to enhance binding properties of the receptors and the selectivity factors between opposite enantiomers, allowing them to be effectively separated. The review presents the synthetic approaches towards these heterocyclic receptors and their distinctly different behavior vis-à-vis carbocyclic receptors.

Keywords: heterocycle; receptors; enantioselective recognition; hydrogen bonding; conformational rigidity; configuration; diastereomeric interactions; macrocycle size; pyridine; dipolar interactions

1. Introduction

Chiral Analytical techniques have become indispensable tools in pharmaceutical and fragrance industries. Qualitative and quantitative analyses of the enantiomerically pure or enriched compounds used in these industries are essential in the view of criteria set by regulating authorities [1,2]. Most of these techniques are based on the non-bonded diastereomeric interactions between a host and enantiomeric guests. Such diastereomeric interactions are the genesis of the chiral manifestations in natural and man-made systems.

Indeed, chiral molecular recognition remains one of the most expanding research fields in organic chemistry [3]. Various biological phenomena such as enzyme-substrate, antibody-antigen and drug-biomolecule interactions are a manifestation of the importance of enantiospecific supramolecular processes in living organisms [4]. The importance of chirality in the fields of medicine [5,6], asymmetric synthesis, [7,8] catalysis [9], flavor [10], fragrances [11], biochemistry [12] and material science chemistry [13] has already been well established. While the area of asymmetric synthesis has witnessed a tremendous growth, the practicality of preparing homochiral compounds still remains a challenge. Thus, the stimulus for interest in the separation of racemic mixtures exploiting host-guest chemistry has gained popularity over the years.

The earliest studies on enantiomeric recognition of chiral organic ammonium salts by chiral crown ethers were carried out by Cram and coworkers [14]. Since then, the importance of furnishing chiral macrocyclic ligands has been realized. Some of these ligands include amino acid units [15], sugar molecules [16], diaza-crown moieties [17], and crown ethers containing a pyridine sub-cyclic fragment [18]. In the last few decades, strategies and methods for synthesizing simpler organic compounds that mimic the biological receptors have been the prime focus in this research area [19–21]. Thus, the artificial receptors having diverse chiral backbones with different elements of chirality [22–25], incorporating aromatic/heteroaromatic alicyclic rings [26–28] in the core structural motif with multiple functionalities [29] have been reported. The receptors containing heteroaromatic ring/heteroalicyclic rings have attracted widespread interest due to their excellent chiral discriminating ability [30]. The receptors with five/six membered heterocycles offer additional advantages while binding the chiral guests through several non-covalent interactions such as hydrogen bonding, electrostatic interactions, hydrophobic binding, cation- π interactions, π - π stacking, steric complementarity, etc. in the enantioselective recognition processes [31]. Analytical techniques such as NMR, UV-Vis, circular dichroism, and fluorescence spectroscopy are commonly used to study chiral recognition, among which the fluorescence approach provides the highest sensitivity and real-time measurement.

Till date, there is no comprehensive review emphasizing heterocycle-based chiral receptors in enantioselective processes. The present review article presents a detailed account of the recent developments in the design and synthesis of various chiral receptors with heterocyclic motif such as pyridine [18], chromene [32,33], imidazole [34], benzimidazole [35,36], furan [37], thiophene [38], oxazole [22–25] etc. and its application in the enantioselective recognition of different classes of chiral analytes [39,40].

2. Components of Chiral Molecular Recognition

2.1. Different Types of Forces

Various non-covalent and covalent interactions are the key elementary factors involved in the host-guest molecular recognition phenomena. Much effort in recent years have moved to more keen understanding for the basis of molecular recognition and the physical principles governing this phenomenon have been the focus of many researchers for centuries. Besides, a wide range of the controlled separation and chemical transformation processes in the drug design, scientific and engineering fields relies on the host-guest chemistry. This section comprehensively addresses the different types of interaction forces in detail.

2.2. Non-Covalent Interactions

Non-bonded interactions are susceptible to thermal fluctuations and other external factors unlike covalent linkages. Weak forces by themselves are able to form strong intra and intermolecular significant interactions only upon working together or in combination with a covalent binding. They are most ubiquitous in nature and are crucial in determining the three-dimensional structures adopted by proteins and nucleic bases.

Depending upon the origin, non-covalent interactions are divided into the following sub classes; Electrostatic Interactions, Hydrogen Bonding, π -electronic effects, Van der Waals forces and Hydrophobic binding, which are summarized briefly below.

2.2.1. Electrostatic Interactions

Electrostatic or Ionic interactions [41] are strong coulombic attractive forces between opposite charges, observed in the case of several receptors, such as cations and anions, binding effectively to the corresponding guest in place. This type of interaction is non-directional, whilst for the ion-dipole interactions the dipole must be suitably aligned for optimal binding efficiency. The high strength of electrostatic interactions has made them an invaluable tool amongst supramolecular chemists for

achieving strong binding. Ionic interactions are basically of two types; the classic ionic bond which is a non-directional attractive force, for example between a positively charged metal ion and negatively charged non-metal, and the salt bridge wherein there is a balance of the electrostatic forces between three or more atoms with partial charges. Such strong attractive interactions stabilize the host-guest complex extensively.

Hydrogen Bonding Interaction

Hydrogen bonding [41,42] is attractive electrostatic interaction between the hydrogen atom, bearing a partial positive charge, covalently attached to an electronegative atom and another electronegative atom which has a partial negative charge developed on it. Hydrogen bonding is the most widely employed dipole-dipole interaction in the field of supramolecular chiral discrimination. Most receptors have electronegative heteroatoms such as Nitrogen, Oxygen as binding sites involved in hydrogen bonding.

2.2.2. π -Electronic Interactions

π - π Interaction

π - π Interactions [43] are rather weak bindings occurring in the face-to-face or edge-to-face or edge-to-edge manners, which play a major role in many aspects of biological, solid-state and host-guest supramolecular chemistry. The quadrupole-quadrupole forces are responsible for the π - π stacking of aromatic rings. Aromatic rings such as benzene, naphthalene, pyridine, imidazole, triazole, indole etc. are often incorporated into the chiral macrocycle for increasing the capacity for chiral recognition to a greater extent owing to the π - π stacking interaction of the host and guest systems.

Cation- π Interaction

The interaction between a cation and delocalized π -electron cloud of the aromatic system exemplifies the cation- π interaction [44]. The simplest view of this non-bonding interaction is in the gas phase. In this case, there is no solvent and stabilization of the system is entirely dependent on the cation and π system of interest. The cation- π interactions between the hydrogen-bonded ammonium ion and the aromatic ring of host, exemplify the chiral recognition of organic ammonium ions by various chiral receptors.

2.2.3. Van der Waals Forces

Van der Waals forces [45] are an attractive noncovalent type of interactions between the fixed dipole in one molecule and induced instantaneous oscillating dipole in another molecule via the corresponding distortion of electron clouds. These forces though underappreciated, are of immense importance to the supramolecular properties of all molecules. However, it is difficult to rationally design the receptors specifically, as this type of interactions is very common to most molecules. The binding of guest into the hydrophobic cavity of host is driven by an enthalpy stabilization. Therefore, even small molecules can make a large number of the Van der Waals contacts and each of them add in a synergistic manner.

Additionally, there is one specific subclass in this category called the "London dispersion forces" and attributed to two induced dipoles.

2.2.4. Hydrophobic Interactions

Hydrophobic interactions [46] are a result of the nonpolar side chains (aromatic rings and hydrocarbon groups) holding tightly in polar solvents, especially water. In this case, there is no sharing of electrons between any groups, therefore it does not produce a true bond. The hydrophobicity of receptors can be manipulated by introducing long side chains. On binding of a guest, the water molecules around a polar surface of the hydrophobic cavity of the host are released into the bulk solvent,

which in turn leads to enhancement of its hydrogen bonding capabilities simultaneously increasing the entropy of the system. The hydrophobic interactions are comparatively stronger than Van der Waals forces or Hydrogen bonding. For example, cyclophanes and cyclodextrins being macrocyclic itself possess inbuilt hydrophobicity contributing to the host-guest affinity and are well-designed to encapsulate guest molecules from an aqueous solution.

3. Analytical Tool for Chiral Recognition

For efficient enantioselective discrimination, the chiral host-guest interactions should result in certain chemical-physical changes that can be read out by various analytical techniques. Depending on spectral properties of the host-guest complexes, analytical techniques such as fluorescence, UV-visible absorption, circular dichroism, NMR, HPLC, electrochemistry, IR, and mass spectrometry could be used as effective tools to measure the chiral recognition phenomenon. The detailed description of each technique is presented below.

3.1. Fluorescence

Fluorescence spectroscopic technique received considerable attention because it is able to provide special advantages which include simplicity, low cost, high sensitivity, adaptation to automation and real-time analysis, diverse signal output modes and small quantity of host and guest. This technique allows multiple detection modes such as emission, excitation and lifetime measurements.

For chiral analysis/recognition fluorophores (fluorescent chromophoric systems) should be either intrinsically chiral or made chiral by attaching an enantiopure moiety. The corresponding diastereomeric interactions with the concerned chiral analyte give different fluorescence responses; i.e., the recognition. Such sensors generally respond via the fluorescence enhancement or quenching. The fluorescence quenching is observed due to loss of the energy of the excited state by a non-radiative decay. Such systems are commonly studied by the Stern-Volmer equation [47] (see below).

$$F_0/F = 1 + K_{sv} [Q]$$

where

F_0 = Initial emission intensity of the host

F = Intensity of the host after addition of analyte (Guest)

K_{sv} = Stern-Volmer constant/Stability constant for the complex

$[Q]$ = Concentration of the analyte (Guest)

The Stern-Volmer plot of fluorescence intensity ratio, F_0/F vs. $[Q]$, concentration of guest enantiomers would exhibit the linear relationship with host and from the graph, Stern-Volmer constant can be calculated.

However, when complexation results in the enhancement of fluorescence, the system is studied by using the Benesi-Hildebrand equation [48] (see below).

$$I_0/(I - I_0) = [b/(a - b)] [1/(K[M]) + 1]$$

where

I_0 = Initial emission intensity of the host

I = Intensity of the host after addition of analyte (Guest)

K = Stability constant for the complex

a, b = Constants terms

$[M]$ = Concentration of the analyte (Guest)

The $[b/(a - b)]$ can be found out by plotting the $I_0/(I - I_0)$ against the inverse of the concentration of analyte, M^{-1} .

The Benesi-Hildebrand equation is similar to equation for straight line, $y = mx + C$. The intercept of the graph gives the $[b/(a - b)]$; the I_0 and I are found out experimentally and hence K can then be calculated.

3.2. UV-Vis Absorption

UV-vis spectroscopy is one of the widely used methods for chiral recognition as it provides high sensitivity and simplicity to the host-guest binding study. In this case, the host molecule should contain a chromophoric system with the absorption band in the UV-Vis range, while the host-guest complex generally has a different absorption band. The difference in the absorbance of host and corresponding host-guest complex is used for determination of the extent and strength of binding in a quantitative manner.

The association constants related to binding process of the opposite guest enantiomers with the chiral host can be calculated by using the modified Benesi–Hildebrand equation [35] as follows.

$$[H]_0[G]_0 = \frac{1}{K_a \Delta \epsilon} + \frac{[G]_0}{\Delta \epsilon}$$

Further modified equation, where a double reciprocal plot can be made with $1/\Delta A$ as a function of $1/[G]_0$. {where $[G]_0 \gg [H]_0$ }.

$$\frac{1}{\Delta A} = \frac{1}{K_a \Delta \epsilon [H]_0 [G]_0} + \frac{1}{\Delta \epsilon [G]_0}$$

where,

$[H]_0$ and $[G]_0$ are total concentrations of host and guest, respectively,

$\Delta \epsilon$ is the change of molar extinction coefficient between the free and complexed host,

ΔA represents the absorption change of host upon the addition of opposite guest enantiomers.

The plots of $1/\Delta A$ against $1/[G]_0$ values, usually give an excellent linear relationship, indicating the corresponding binding process between the host and guest enantiomers. The $\Delta \epsilon$ value can be derived from the intercept, while K_a (association constant) can be calculated from the slope. The binding constants, $K(R)$ or $K(S)$ and associated free energy change (ΔG_0) for the host molecule upon the complexation are obtained by the curve fitting analysis of observed absorbance changes.

3.3. Circular Dichroism (CD)

Circular dichroism (CD) spectroscopic technique responds to the spatial asymmetry change in conformation and/or configuration, and hence is effectively used for investigating the chiroptical properties of chiral hosts and their complexes with enantiomeric guests. It enables probing the discrimination efficiency of supramolecular hosts and determination of complex stoichiometry and stability.

In general, two or more electronic transitions of the chromophoric units around a chiral center excitonically couple with each other generating bisignate CD signals. It allows the reliable determination of enantiomeric preference by comparing the corresponding amplitudes of exciton couplets from exciton-coupled circular dichroism (ECCD) spectra of the resulting complexes. The sign of the Cotton effect can be used to assign the absolute configuration or relative conformation [3].

3.4. Nuclear Magnetic Resonance (NMR) Analysis

Enantioselective recognition can be readily studied by using NMR spectroscopy as the diastereomeric interaction between a chiral host and enantiopure guest that is usually accompanied by significant chemical shift changes. This technique is useful for both liquid and solid compounds, while only milligram quantities of samples are required. The recognition process via NMR can be carried out by two main approaches: the use of chiral solvating agents (CSA) and enantiopure

chiral derivatizing agents (CDA). In the case of CSA [49] based on non-covalent interactions, the corresponding diastereomeric complexes are formed between a solute and chiral solvent and the resultant NMR signals deduce the chirality of molecule of interest. A sub-class of CSA is chiral shift reagents (CSR), where a paramagnetic metal ligated to chiral ligands. In the case of CDA [50], the covalent bonded diastereomeric derivatives are formed and their NMR pattern helps in assignment of the configuration of the target compound. Determination of the enantiomeric purity of the samples with certain enantiomeric excess is also possible by using NMR [51]. Furthermore, the variable-temperature ^1H NMR measurements are useful in estimating a kinetically more stable complex and exhibit the enantiomeric recognition effect.

Presence of aromatic moieties in the host as well as in the guest generally gives better results due to the magnetic anisotropic effect. It is expected that the protons present in the vicinity of chiral center are affected by the shielding or deshielding effect during the formation of diastereomeric complexes. It results in better separation of the peaks for these protons in both the diastereomers; hence enhancing the chiral recognition.

3.5. High Performance Liquid Chromatography (HPLC)

Chiral HPLC [52] serves as the most extensively used analytical method for resolving enantiomers of the chiral samples. A stationary phase of the chiral HPLC columns contains an enantiomeric form of the chiral materials such as cellulose or cyclodextrin. Two opposite enantiomers of the analyte are distinct in affinity to the chiral stationary phase (CSP), and therefore show different retention times.

The chiral compounds synthesized in laboratory in a racemic form or enantio-enriched form via asymmetric synthesis are commonly analyzed by chiral HPLC. The separation of enantiomers on chiral HPLC column is based on the diastereomeric binding via three point interactions with a chiral coating present in the column. The difference in the retention time of enantiomers is an example of chiral molecular recognition between the chiral column packing materials and the enantiomers. The most popular chiral columns are Chiralcel OD and Chiralpak AD. Chiralcel OD has the tris(3,5-dimethylphenyl carbamate)s derivative of cellulose as CSP, whereas Chiralpak AD has the same derivative but of amylose (Figure 1). These polysaccharide-based chiral columns are nearly universal with the capability to resolve chiral compounds being almost 80–90% as reported so far using hexane-alcohol as eluents. Most commercially available chiral HPLC columns are carbohydrate-based such as Chiralcel OD and Chiralpak AD, crown ether-based column includes crown pack CR, crown pack CR (+), crown pack CR (–) etc. Thus, re-emphasizing the role of heterocycles in chiral supramolecular chemistry.

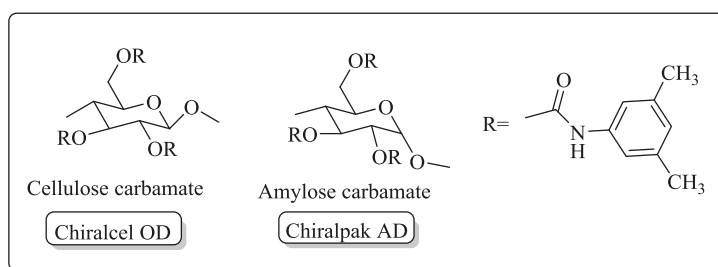


Figure 1. Chiral column packing materials, of cellulose carbamate and amylose carbamate.

3.6. Mass Spectrometry

Mass spectrometry [23,53] is the ubiquitous powerful analytical tool for the chiral molecular recognition. The chiral recognition using fast atom bombardment mass spectrometry (FAB-MS) and electrospray ionization mass spectrometry (ESI-MS) are the most significant ways to quantify the

recognition phenomena. The methodology working on the basis of isotopic labeling of one of the guest (G^+) enantiomers is carried out followed by comparing the peak intensities of 1:1 mixture of the unlabeled (G_R^+) and labeled enantiomer guests (G_{S-dn}^+). Chiral recognition of the given host is simply measured by using the following equation.

'IRIS' value was defined to be peak intensity ratio, $I[(H + G_R^+)]/I[(H + G_{S-dn}^+)] = I_R/I_{S-dn}IRIS$, of two diastereomeric host-guest complex, exhibited in the n mass unit difference in the mass spectrum.

There are three possible cases of *IRIS*.

- (1) $IRIS > 1.0$ means that the given chiral host binds more strongly (*R*)-enantiomer of the guest, hence indicating the (*R*)-enantiomer preference; the larger I_R/I_{S-dn} value corresponds to the higher degree of chiral recognition of the host.
- (2) In contrast, $IRIS < 1.0$ means that the given chiral host binds more strongly (*S*)-enantiomer of the guest, indicating the (*S*)-enantiomer preference with the opposite tendency for the I_R/I_{S-dn} value.
- (3) $IRIS = 1.0 \pm 0.05$ means that the given chiral host cannot differentiate the chirality of the guest.

3.7. Electrochemical Methods

Electrochemical methods have attracted much attention due to their high sensitivity, operational simplicity, and cost efficiency.

Electrochemical methods such as ion-selective electrodes (ISEs) for pH and cyclic voltammetry (CV) enable the qualitative as well as quantitative determination of the target analyte along with the elucidation of thermodynamics and kinetics of the electron transfer reactions. These techniques convert the chemical and/or physical information of analyte into the electrical signal of either potential or current or both, which is then processed to reveal the accurate chemical information.

The chemical or physical change may be induced directly by the target analyte interacting with the electrode, thereby generating the electric signals monitored as a potential, or current change, or both. Detection based on each of these signals is termed *potentiometry*, *amperometry* (including *coulometry*), and *voltammetry*, respectively.

Electrochemical detection has been applied mainly to the redox-active targets that are charged, that are, ions, and/or capable of undergoing the redox reactions on an electrode leading to either oxidation or reduction of the target.

Cyclic Voltammetry

Simultaneous recording and analyzing the potential and current variations with time are the merits of voltammetry [54]. In particular, to make the control and analysis easier, the change of potential can be made linear against five times. The corresponding voltammetry is called *linearsweep voltammetry*. Further, the potential can be linearly increased and then decreased in a cyclic manner, and such a method is called *cyclic voltammetry*. Upon combining with the three-electrode cell it becomes the widely used electrochemical technique for either fundamental studies or detection applications. The most important result from such a measurement is the cyclic *voltammogram*, or simply CV, which plots the variation of current against the linearly changing electrode potential E .

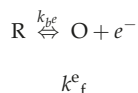
CV is nowadays conventionally performed on a computer-controlled potentiostat as commercially supplied. The user needs to input at least three parameters into the potentiostat: the initial and final potentials E_i and E_f of the potential scan, and the potential scan rate dE/dt . The equations below describe the relationships between these parameters:

$$dE/dt = (E_f - E_i)/(t_f - t_i)$$

$$E = E_i + t \times dE/dt$$

where t is the variable time. In this equation, the start (t_i) and final (t_f) times of potential scan are used here to explain the relationship, but are not independent because they are determined by E_i , E_f , and dE/dt . Also, it is of note that the scan rate dE/dt is positive when $E_f > E_i$ and negative when $E_f < E_i$.

The electrode reaction potential and kinetics of redox active molecule are well reflected by the peak potentials and the shape of CV. In general, for a one-electron reaction that converts a molecule in the reduced state R to the oxidized state O, the reaction proceeds as follows:



where k_f^e and k_b^e are the rate constants for the forward and backward electron transfer reactions, respectively. If $k_f^e \approx k_b^e$ and both are sufficiently large, the reaction represents a reversible electrode process. If $k_f^e \gg k_b^e$, the reaction is electrochemically irreversible, even though it may be chemically reversed given a sufficiently long time. Between these two-edged points, the reaction is regarded as quasi-reversible. These situations can be mathematically processed, giving rise to useful conclusions in relation to CVs, particularly for electrochemical detection.

4. Special Features of Heterocyclic Receptors for Enantioselective Recognition

Chiral molecular recognition is dependent on several parameters. To facilitate and exploit these parameters, the design of chiral receptors is the most crucial factor. The research community continuously broadens the scope of chiral receptors containing the aromatic/heteroaromatic/aliphatic rings. The present review covers a variety of hosts containing one or more heterocyclic rings as a vital part for enantiodiscrimination. Thus, these heterocyclic rings can be of different sizes and structure, for example aromatic rings such as imidazole, benzimidazole, furan, thiophene, pyrrole, triazole, pyridine, quinoline, isoquinoline, etc. or aliphatic rings such as pyrrolidine, tetrahydrofuran, tetrahydrothiophene, imidazolidine, oxazolidine, etc. A plethora of the heterocyclic receptors synthesized so far has different elements of chirality and possesses special characteristic features to influence the stability of host-guest complex and enantioselective sensing. The key features of these hosts are summarized as follows:

1. Heterocycles have unshared electron pairs present on the heteroatoms useful for the three points hydrogen bond formation, especially when chiral ammonium cations are studied, with the chiral guest molecule.
2. Heterocycles possess a permanent dipole responsible for the charge-dipole electrostatic interactions.
3. The aromatic heterocycles have π electrons to facilitate the corresponding π - π stacking interaction and cation- π binding with a chiral aromatic guest molecule.
4. The conformational rigidity is increased by the presence of heterocyclic ring, which imparts a good deal of preorganization of the chiral host suiting a guest molecule.
5. The aliphatic heterocyclic ring system may assist the hydrophobic interaction with a chiral guest molecule.
6. The heterocyclic ring may additionally influence the steric interaction responsible for chiral discrimination.

5. Chiral Hosts with Six Member Heterocycle/s

Six-membered cyclic structures are most abundant in nature. One of the primary reasons being conformational and hence such structures are thermodynamically stable. Aromatic rings have advantage of presence of ring current which very strongly influence the NMR signals of the analyte. Pyridine ring has found wide-spread use in the reported receptors so far.

5.1. Nitrogen Containing Six Member Heterocycle/s

Pyridine Ring

Pyridine is one of the six membered aromatic heterocycles which has been extensively used in chiral organocatalysis [55], chiral metal-based catalysis [56], chiral resolving agents [57,58] etc. Reports reveal that inclusion of symmetrical, 2,6-disubstituted pyridine motifs in the host architecture, offers enhanced binding properties to it. The strikingly common unit found in pyridine containing hosts are the presence of one or more 2,6-disubstituted pyridines, with pyridine nitrogen pointing inwardly, in the structural construct of the macrocycle or the molecular cleft. (Chart 1, part A). Another class of pyridine containing receptors include one or more 4,4'-bipyridine motif giving rise to rigid molecular clefts or cyclophanes (Chart 1, part B).

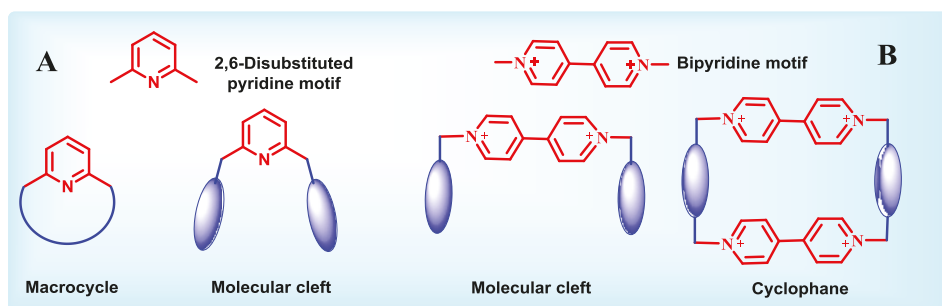


Chart 1. 2,6-disubstituted pyridine (A) and 4,4'-Bipyridine (B) containing hosts.

Incorporation of a pyridine unit provides proton acceptors at the pyridyl nitrogens which are important for the tripod hydrogen bonding, while the aromatic system contributes via π - π stacking interaction, along with imparting increased rigidity to form thermodynamically stable complexes with guest molecules. Owing to the aforementioned special features of the pyridine ring, Izatt and group have designed various macrocyclic hosts, particularly chiral crown ethers containing pyridine units [18], which enable these hosts to recognize specific guests such as chiral organic ammonium salts. It was one of the first extensive recognition studies using chiral macrocycles (Figure 2) and enantiopure alkylammonium salts. Several experimental techniques such as temperature-dependent ^1H NMR spectroscopy, titration calorimetry, Fourier transform ion cyclotron resonance mass spectrometry, and selective crystallization have been employed to establish the corresponding host-guest chiral recognition in the given systems and to report the K , ΔH , and ΔS values for the interactions, thus quantitating the binding processes. Additionally, the X-ray crystallographic results provided a structural basis for the recognition.

The parameters and supramolecular interactions that are involved in these chiral systems have been studied exhaustively and several [18,59,60] reviews on this and similar works have been summarized by the group. Their systematic investigations revealed the effect of substituents on the crown ether, guest type and solvent on the extent of enantiomeric recognition.

In continuation of the research on chiral recognition, the authors [61] have developed a gas-phase ion-molecule host-guest system, based on (*S,S*)-dimethyldiketopyridino-18-crown-6 (*S,S*-8) macrocycle for the enantioselective recognition of *R* and *S* enantiomers of α -(1-naphthyl)ethylammonium (NapEt^+) cation (Figure 3) using mass spectrometry (Reaction 1). It was demonstrated that the *S,S*-8-*R*- NapEt^+ complex was more stable than the *S,S*-8-*S*- NapEt^+ complex with the equilibrium constant K obtained for *S*- NapEt^+ being larger than that for *R*- NapEt^+ by a factor of 4. These results confirmed considerable recognition, which was measured by using the FT-ICR/MS techniques. However, no recognition was observed for the same host-guest interaction in the solution phase, indicating that the stabilization of

the complex formed is entirely dependent on the cation- π interactions between the hydrogen-bonded ammonium ion and aromatic ring of the host.

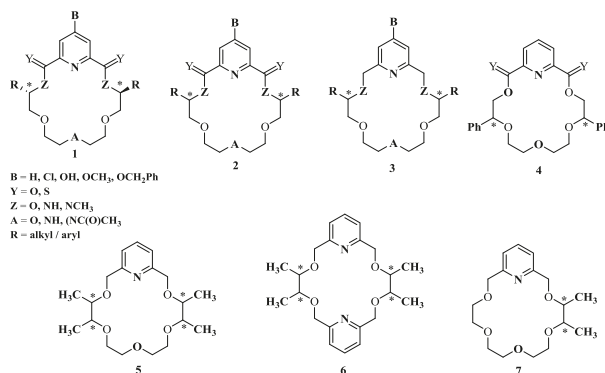


Figure 2. Chiral pyridine containing crown ether ligands.

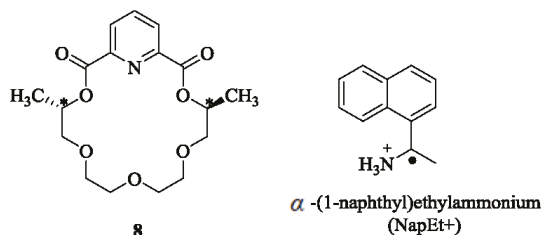
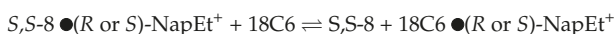


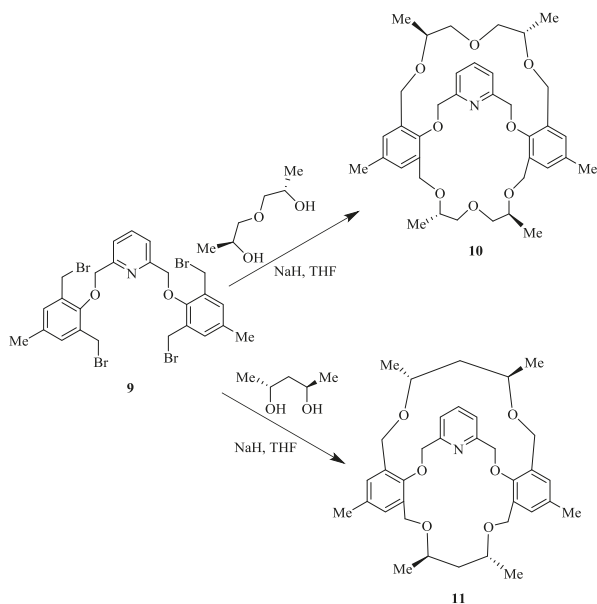
Figure 3. (*S,S*)-dimethyldiketopyridino-18-crown-6 (*S,S*-8) and α -(1-naphthyl)ethylammonium (NapEt⁺).



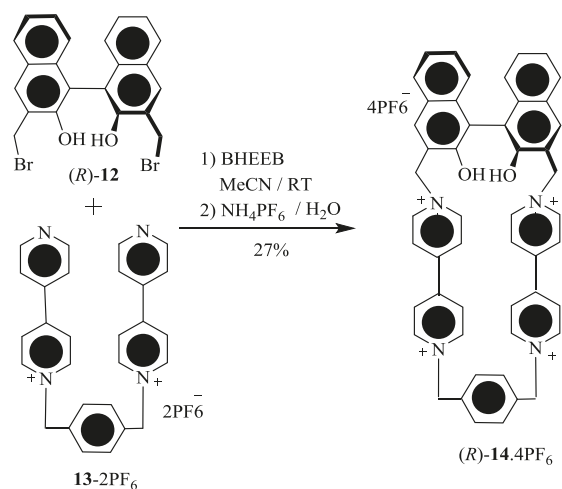
In their continuing efforts, same group then synthesized two chiral macrobicyclic cleft compounds containing a pyridine ring [62] as it possesses a three-dimensional cavity which might be useful for the recognition process. Treatment of pyridine-bridged tetrabromide **9** with the respective chiral glycols, chiral methyl-substituted diethylene glycol, (1*S*,5*S*)-3-oxapentane-1,5-diol or the (2*R*,4*R*)-pentanediol furnished the chiral tetramethyl-substituted macrobicyclic **10** and macrocycle **11**, respectively (Scheme 1). ¹H NMR spectroscopy has been used to determine the chiral recognition behavior of the synthesized compounds **10** and **11**. Indeed, (*S,S,S,S*)-**10**, as a chiral host demonstrated a high degree of the enantiomeric discrimination for (*S*)-enantiomers of α -(1-naphthyl)-ethylammonium perchlorate (NapEt) and phenyl ethyl ammonium perchlorate (PhEt) over their (*R*)-forms. However, a reverse sequence of the recognition was observed for the (*S,S*)-**8** host wherein it recognizes the corresponding (*R*) forms of NapEt and PhEt over their (*S*) forms. This high recognition ability of cleft compound was observed owing to its increased molecular rigidity after introduction of a second macro ring on the monocyclic pyridine-crown ligand. The chiral discrimination behavior was studied using binary solvent system, lower enantiomeric recognition was observed for MeOH/CHCl₃ in comparison with Ethanol:Dichloroethane (2:8) which revealed the effect of solvent.

Stoddart et al. [63] have developed new axially-chiral tetracationic cyclophanes, (*R*)-**14**.4PF₆ and (*R,R*)-**16**.4PF₆ (Scheme 2). Tetracationic cyclophane, (*R*)-**14**.4PF₆ was obtained by the reaction of (*R*)-**12** and **13**.2PF₆ and similarly D₂ symmetric tetracationic cyclophane, (*R,R*)-**16**.4PF₆ was synthesized using the treatment of (*R*)-**12** and (*R*)-**15**.2PF₆. These tetracationic cyclophane receptors were found to be effective for the chiral recognition in the case of several chiral amino acids, such as L- and

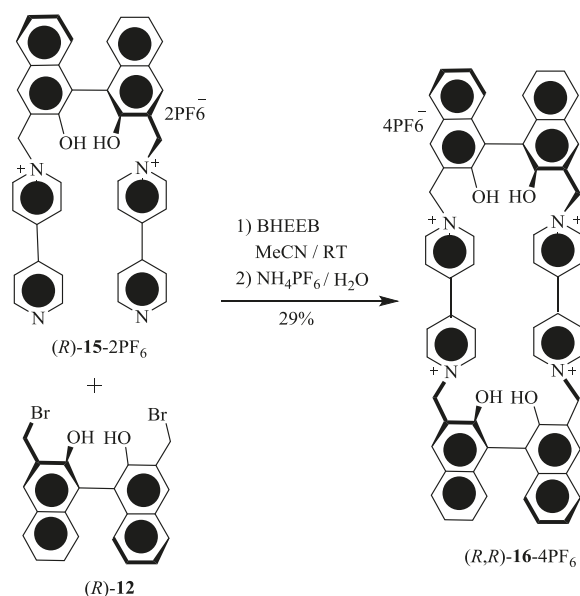
D-enantiomers of phenylalanine (Phe), tyrosine (Tyr), and tryptophan (Trp) as free forms, or methyl esters, or *N*-acetyls in H₂O and organic solvents, as determined by using UV-Vis titration. The binding constant and free energies of 1:1 host-guest complexation are provided in Table 1. As one can see, the enantioselective recognition ability decreases from *N*-acetyl-Trp to *N*-acetyl-Tyr (Table 1, entries 7 and 8) and further to less π -electron-rich *N*-acetyl-Phe (Table 1, entries 9 and 10). These results revealed a greater extent of the secondary stereoelectronic interactions between the functional groups of π -electron rich guest and bulky optically-active binaphthol spacer(s) of cyclophane(s), which can be attributed to the π -electron rich nature of guest (primary mode of binding).



Scheme 1. Synthesis of macrobicyclic cleft compounds 10 and 11.



Scheme 2. Cont.



Scheme 2. Synthesis of axially-chiral tetracationic cyclophanes (R)-14.4PF₆ and (R,R)-16.4PF₆.

Table 1. Binding constants (K_a) and free energies of complexation ($-\Delta G_0$) for the 1:1 complexes between cyclophanes (R)-14.X (X = PF₆ or Cl) and (R,R)-16.4 PF₆ and π -electron-rich amino acids ^a.

| Entry | Substrate | Solvent | K_2 (M ⁻¹) | | K_a (L)/ K_a (D) | | $-\Delta G_0$ (kcal/mol) | | $\Delta\Delta G_0$ (kcal/mol) ^b | |
|-------|---------------|-------------------------------|--------------------------|-----------------|----------------------|----------|--------------------------|----------|--|----------|
| | | | (R)-14 | (R,R)-16 | (R)-14 | (R,R)-16 | (R)-14 | (R,R)-16 | (R)-14 | (R,R)-16 |
| 1 | L-Trp | H ₂ O ^c | 2470 | ND ^d | | | 4.63 | | | |
| 2 | D-Trp | H ₂ O ^c | 5860 | ND ^d | 0.42 | | 5.14 | | | -0.51 |
| 3 | L-Trp OMe.HCl | H ₂ O ^c | 753 | ND ^d | | | 3.92 | | | |
| 4 | D-Trp OMe.HCl | H ₂ O ^c | 803 | ND ^d | 0.94 | | 3.96 | | | -0.04 |
| 5 | N-Ac-L-Trp | A ^e | 20700 | 4280 | | | 5.89 | 4.95 | | |
| 6 | N-Ac-D-Trp | A ^e | 2670 | 1080 | 7.75 | 3.96 | 4.67 | 4.14 | 1.22 | 0.81 |
| 7 | N-Ac-L-Tyr | B ^e | 10060 | 2340 | | | 5.45 | | | |
| 8 | N-Ac-D-Tyr | B ^e | 2125 | 1047 | 4.73 | 2.23 | 4.53 | 4.12 | 0.92 | 0.48 |
| 9 | N-Ac-L-Phe | A ^e | 1220 | 219 | | | 4.21 | 3.19 | | |
| 10 | N-Ac-D-Phe | A ^e | 2260 | 157 | 0.54 | 1.60 | 4.57 | 2.91 | -0.36 | 0.28 |

^a All binding constants were determined by UV/vis titration at 25 °C. ^b $\Delta\Delta G_0 = \Delta G_0$ (L) - ΔG_0 (D). ^c In H₂O as solvent.

^d Not determined. ^e Solvent mixture A: MeCN 90% DMF 10%; solvent mixture B: MeCN 90% DMSO 10%.

Hollosi et al. [64] have established the applicability of CD spectroscopy as an effective tool for the enantioselective discrimination of aryl alkyl ammonium salts **19–21** by pyridine-18-crown-6 type ligands, **17** and **18** (Figure 4). Furthermore, the stoichiometry and relative stability of host-guest complexes have been determined. Intriguingly, the study revealed that the heterochiral complexation of (R,R)-**17** with (S)-aralkyl ammonium salts **19** and **20** or (S,S)-**18** with (R)-salts **19** and **20** exhibited additional spectral effects in the spectral region ¹L_b and ¹L_a in the form of high amplitude of CD than homochiral complexation.

Mallouk et al. [65] have synthesized the (S)-valine-leucine-alanine cyclophane, **26** (Scheme 3). The bipyridine fragment, **23** of **26** was prepared by the reaction of 4, 4'-bipyridine with 4-(chloromethyl)benzoic acid followed by the treatment with 4-(bromomethyl)benzylamine hydrobromide. The standard solid phase synthesis was employed to produce the N-*t*-BOC-protected tripeptide unit, **24**. Finally, the bipyridine and N-*t*-BOC-protected tripeptide units **24** were coupled to obtain the required (S)-valine-leucine-alanine cyclophane, **26**. ¹H NMR titration for the complexation of chiral cyclophane host **26** in an aqueous media with diverse pharmaceutically interesting chiral

and racemic π -donor guest molecules, such as Non-steroidal Anti-inflammatory Drugs (NSAIDs), β -blockers, amino acids, and amino acid derivatives were performed confirming weak binding abilities in the range of 1–39 M⁻¹ (Table 2). Out of the studied guest molecules, racemic nandanol and DOPA exhibited the substantial binding with **26**. Interestingly, the (*R*)/(*S*) enantioselectivity ratio of 13 \pm 5 was found for dihydroxyphenylalanine (DOPA), indicating a strong π -electron donor cationic guest. Two-dimensional NOESY ¹H NMR spectra revealed the corresponding multiple intermolecular NOE's signals for (*R*)-DOPA and the host, **26** in the host-guest complex. This result unambiguously confirmed a strong and enantioselective binding of (*R*)-DOPA inside the cavity of **26**, while no measurable interaction was detected for (*S*)-DOPA under the same conditions.

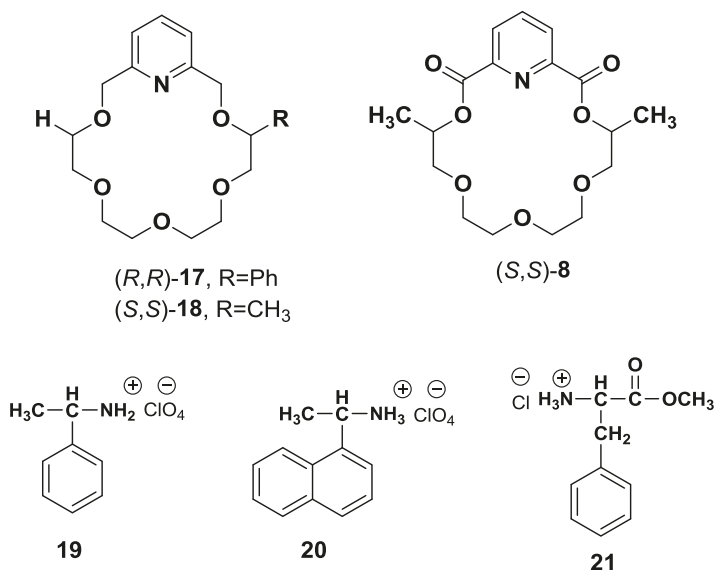


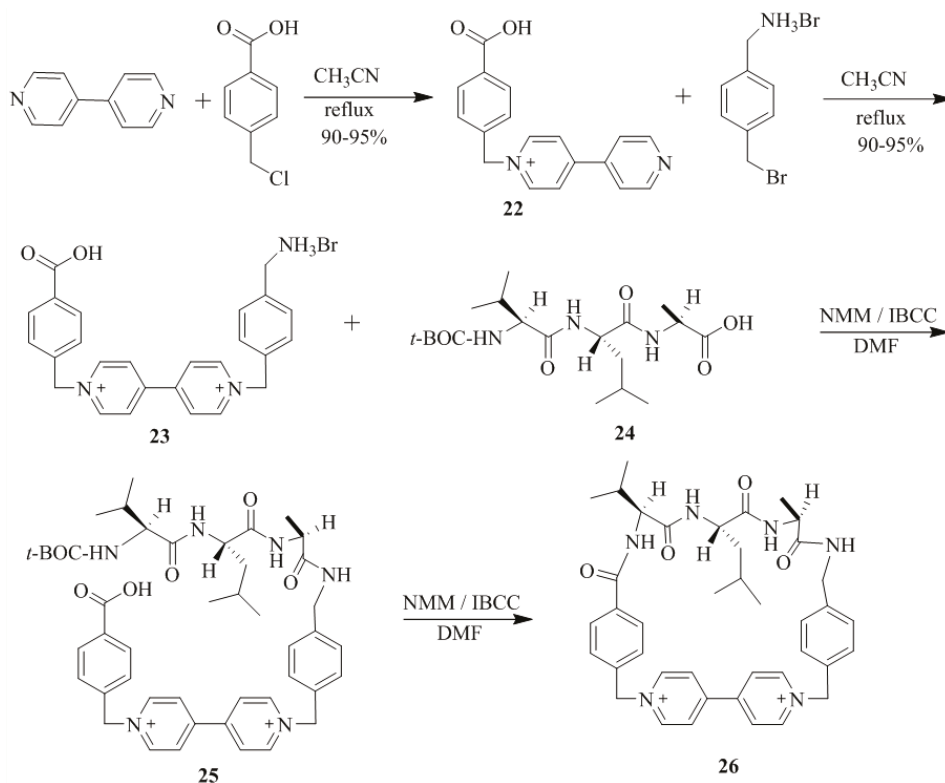
Figure 4. Pyridine-18-crown-6 (**17**, **18**) type ligands host for enantioselective recognition of aryl alkyl ammonium salts **19–21**.

Hua et al. [30] reported the synthesis of five pyridine-based macrocyclic receptors, **29a–e** (Schemes 4 and 5) by simple acylation of the chiral diamine dihydrobromide intermediates, **28a–c** with 2,6-pyridinedicarbonyl dichloride in a highly diluted solution. However, the acylation of chiral diamine dihydrobromides, **28a–b** with 2,6-pyridinedicarbonyl dichloride simultaneously afforded the [1 + 1] cyclization products, **29a–b** and [2 + 2] cyclization products **29c–d**. More importantly, under similar reaction condition, the acylation reaction of **28c** and 2,6-pyridinedicarbonyl dichloride, afforded the only [1 + 1] product **29e**, while the [2 + 2] product was not formed. The enantioselective interaction of synthesized chiral macrocyclic receptors, **29a–e** with D- and L-amino acid methyl ester hydrochlorides was evaluated by using fluorescence spectroscopy and the difference of fluorescence intensity confirmed significant chiral molecular recognition (Table 3).

As seen in Table 3, macrocycles, **29c,e** exhibit the better enantiomeric recognition for D- and L-Ala methyl ester hydrochlorides as compared to other chiral macrocycles, **29a,b,d**. Chiral macrocycles, **29a,c,e** all show excellent chiral discrimination for Phe methyl ester hydrochloride, whereas **29b,d** do not. In the case of D- and L-His methyl ester dihydrochloride, only **29b** displayed recognition.

Suh et al. [53] synthesized new pyridine-based chiral crown ether, **34** (Scheme 6) as follows. Diol, **30** obtained from the known five step methodology, was coupled with diiodide, **37** prepared from chelidamic acid (**35**) to furnish **32**. The reduction of cyano group of **32**, followed by the treatment

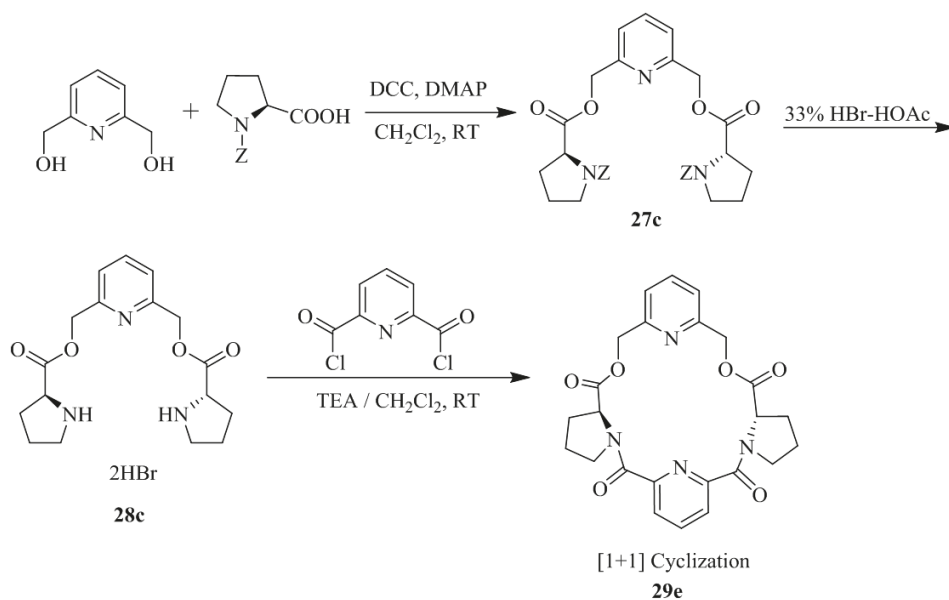
with ethyl isocyanate provided the required chiral host, **34**. The authors also synthesized chiral bis-pyridino-18-crown-6, **31** with the diphenyl substituent by similar methodology in order to compare it with the chiral host, **34**. These hosts exhibited chiral molecular recognition for the enantiomers of methyl ester hydrochlorides of Leu, Gly(Ph), and Phe, which was determined by enantiomer labeled (EL) guest method using fast atom bombardment mass spectrometry (FAB-MS). For host, **34** the IRIS values obtained are in the range of 1.12 to 1.44 indicating that the (*R*)-enantiomer of amino acids showed binding preference over the (*S*)-enantiomer. However, for the host, **31** the IRIS values for chiral recognition were found to be lower than for the chiral host, **34**.



Scheme 3. Synthetic of (*S*)-valine-leucine-alanine cyclophane, **26**.

Table 2. Results of NMR titrations using the dibromide salt of **26**. Association constants (K_a) represent the average of two or more proton chemical shifts.

| Guest | K_a (M^{-1}) | Solvent System | Structure |
|--|-------------------------|----------------------------|-----------|
| (<i>R</i>)-DOPA (<i>S</i>)-DOPA | 39 ± 6 3 ± 1 | $17D_2O:1acetone-d_6:1DCI$ | |
| (<i>R</i>)-Tryptophan (<i>S</i>)-Tryptophan | 5 ± 1 6 ± 1 | $17D_2O:1acetone-d_6:1DCI$ | |



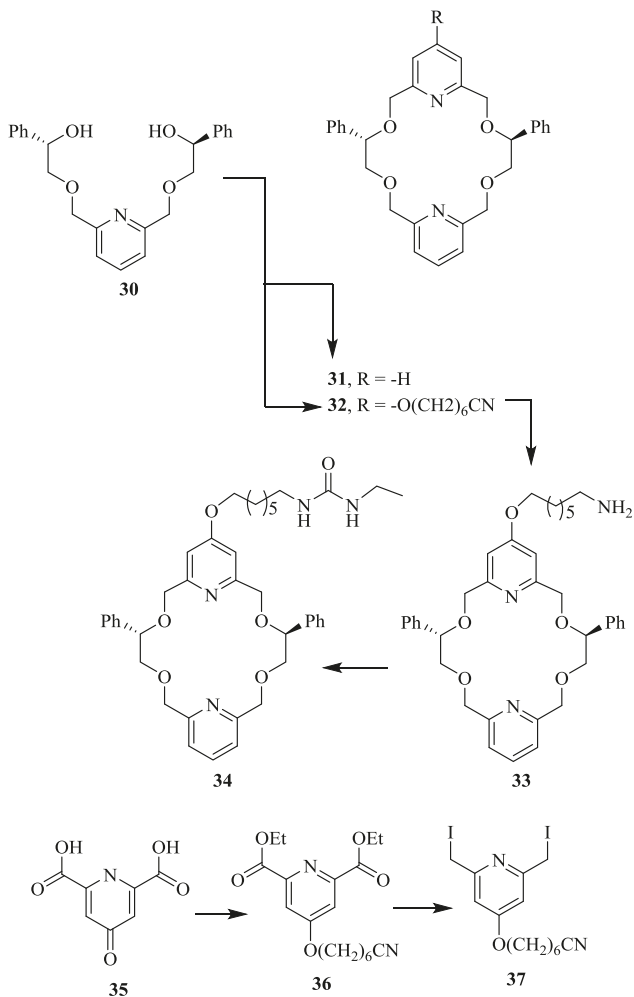
Scheme 5. Preparation of Chiral Macrocycle 29e.

Table 3. Chiral recognition data determined by fluorescence spectra for the interactions of pyridine-containing chiral ligands with enantiomers of amino acid methyl ester hydrochlorides.

| Ligand | Amino Acid Methyl Ester Hydrochlorides, Cation | λ_{\max} (nm) | $\Delta\lambda$ (nm) | I/I_0 (Rel. Intensity) |
|--------|--|-----------------------|----------------------|--------------------------|
| 29a | D-Ala | 350 | 8 | 0.68 |
| | L-Ala | 342 | | |
| | D-Phe | 350 | 50 | 0.84 |
| | L-Phe | 400 | | |
| | D-His | 350 | 0 | 0.67 |
| | L-His | 350 | | |
| 29b | D-Ala | 392 | 12 | 1.08 |
| | L-Ala | 362 | | |
| | D-Phe | 374 | 10 | 1.32 |
| | L-Phe | 360 | | |
| | D-His | 350 | 38 | 0.91 |
| | L-His | 362 | | |
| 29c | D-Ala | 348 | 52 | 0.37 |
| | L-Ala | 400 | | |
| | D-Phe | 348 | 48 | 0.69 |
| | L-Phe | 352 | | |
| | D-His | 400 | 1 | 0.72 |
| | L-His | 352 | | |
| 29d | D-Ala | 392 | 12 | 1.19 |
| | L-Ala | 354 | | |
| | D-Phe | 366 | 14 | 1.01 |
| | L-Phe | 380 | | |
| | D-His | 366 | 16 | 1.19 |
| | L-His | 350 | | |
| | | 364 | | 0.82 |

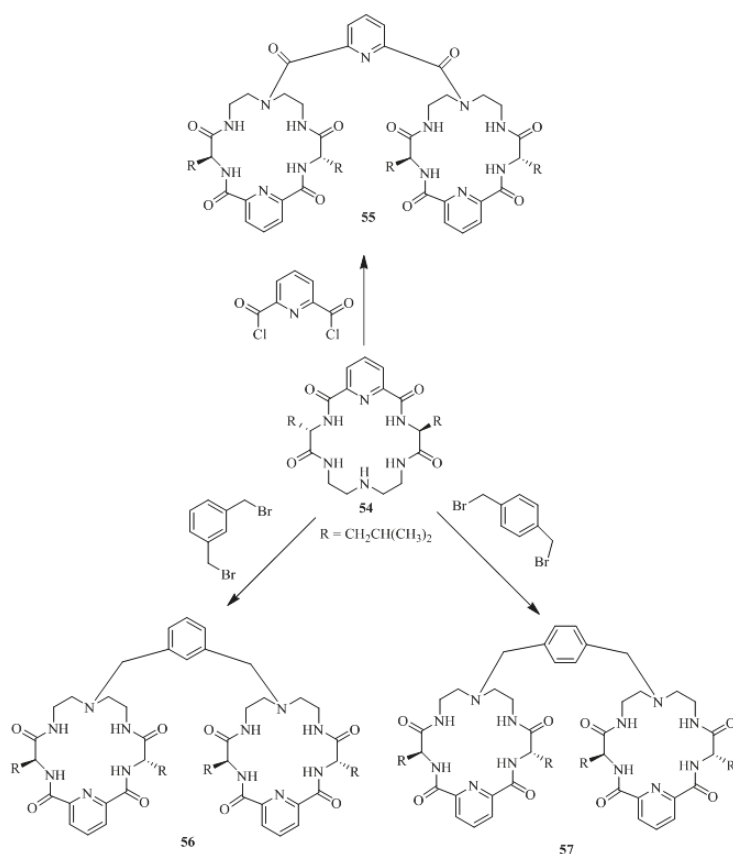
Table 3. Cont.

| Ligand | Amino Acid Methyl Ester Hydrochlorides, Cation | λ_{\max} (nm) | $\Delta\lambda$ (nm) | I/I_0 (Rel. Intensity) |
|--------|--|-----------------------|----------------------|--------------------------|
| 29e | D-Ala | 350 | 50 | 0.78 |
| | L-Ala | 400 | | |
| | D-Phe | 350 | 50 | 0.84 |
| | L-Phe | 400 | | |
| | D-His | 348 | 8 | 1.05 |
| | L-His | 340 | | |



Scheme 6. Synthesis of chiral macrocycles, 31 and 34.

The same group [23] has prepared C_2 -symmetric chiral bis-pyridino-18-crown-6, (*R,R,R,R*)-42 and 43 (Scheme 7) with tetraethyl tetracarboxylate and tetramethyl tetracarboxamide groups as chiral barriers in 2008. The synthesis was carried out by a simple alkylation of diethyl-*L*-tartarate (38) or *N,N,N',N'*-tetramethyl tartaramide (38) with 2,6-bis(iodomethyl)pyridine (40).



Scheme 8. Synthesis of bis-macrocyclic oxo-polyamine type molecular tweezers (55–57).

Table 5. Binding constants (K_a), the Gibbs free energy changes ($-\Delta G_0$), enantioselectivities K_L/K_D and $\Delta\Delta G_0$ calculated from $-\Delta G_0$ for the complexation of L/D-amino acid esters with the chiral receptors 54–57 in CHCl_3 at 25 °C ^a.

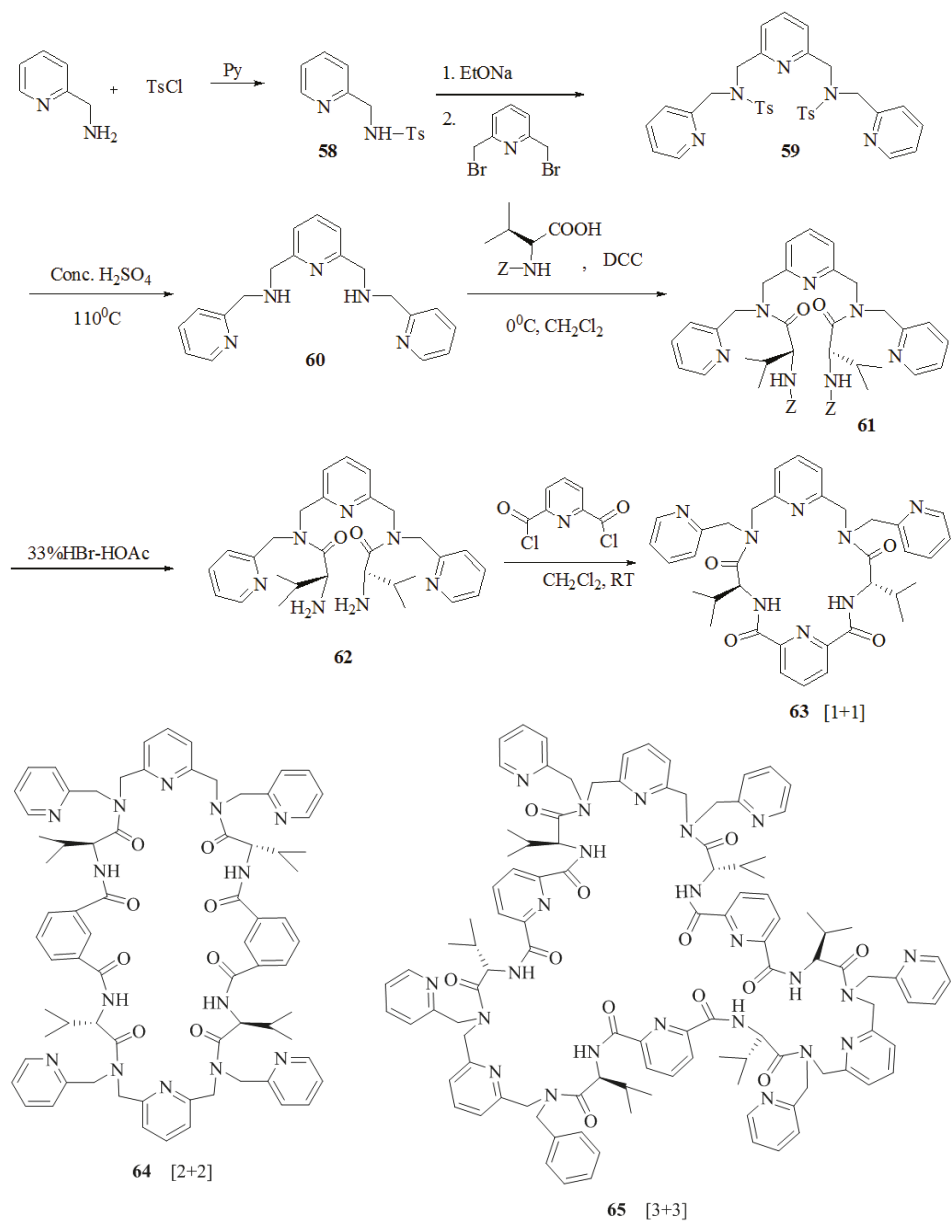
| Entry | Host | Guest ^b | K_a ($\text{dm}^3 \text{mol}^{-1}$) | K_L/K_D | $-\Delta G_0$ (kJ mol^{-1}) | $\Delta\Delta G_0$ (kJ mol^{-1}) ^c |
|-------|------|--------------------|---|-----------|--|--|
| 1 | 54 | L-Phe-OMe | 46.3 | 0.75 | 9.50 | 0.73 |
| 2 | 54 | D-Phe-OMe | 62.0 | | 10.23 | |
| 3 | 54 | L-Trp-OMe | 58.0 | 0.67 | 10.06 | 0.98 |
| 4 | 54 | D-Trp-OMe | 86.1 | | 11.04 | |
| 5 | 55 | L-Ala-OMe | 74.1 | 1.21 | 10.67 | −0.48 |
| 6 | 55 | D-Ala-OMe | 61.2 | | 10.19 | |
| 7 | 55 | L-Leu-OMe | 68.0 | 2.70 | 10.45 | −2.46 |
| 8 | 55 | D-Leu-OMe | 25.2 | | 7.99 | |
| 9 | 55 | L-Phe-OMe | 213 | 3.92 | 13.28 | −3.38 |
| 10 | 55 | D-Phe-OMe | 54.4 | | 9.90 | |
| 11 | 55 | L-Trp-OMe | 1280 | 7.90 | 17.72 | −5.12 |
| 12 | 55 | D-Trp-OMe | 162 | | 12.60 | |
| 13 | 56 | L-Leu-OMe | 59.9 | 2.0 | 10.14 | −1.71 |
| 14 | 56 | D-Leu-OMe | 30.0 | | 8.43 | |
| 15 | 57 | L-Leu-OMe | 36.8 | 1.33 | 8.93 | −0.72 |
| 16 | 57 | D-Leu-OMe | 27.7 | | 8.23 | |

^a The concentration of the receptors: $2.0 \times 10^{-4} \text{ mol dm}^{-3}$. ^b Ala-OMe: alanine methyl ester; Leu-OMe: leucine methyl ester; Phe-OMe: phenylalanine methyl ester; Trp-OMe: tryptophane methyl ester. ^c $\Delta\Delta G_0 = \Delta G_0 - \Delta G_0$.

Hua et al. [67] prepared seven C_2 -symmetrical pyridyl unit containing macrocycles. The tosylamine, **58** was reacted with 2,6-bis(bromomethyl)pyridine to afford compound, **59**. Further detosylation gave 2,6-bis(*N*-picolyaminomethyl)-pyridine, **60** followed by condensation with *Z*-protected Val to furnish **61**, while subsequent deprotection yielded **62**. Finally, all three chiral macrocycles, **63**, **64** and **65** were synthesized by acylation of the chiral diamine dihydrobromide intermediate, **62** with 2,6-pyridinedicarbonyl dichloride at high dilution (Scheme 9). These macrocycles, **63**, **64** and **65** were obtained by the [1 + 1], [2 + 2] and [3 + 3] cyclization in 15.6%, 5.1% and 3.7% yields, respectively. By following a similar methodology, the macrocycles, **66**, **67**, **68** and **69** (Figure 6) were synthesized from the respective acids. Macrocycle, **63** was investigated for the chiral molecular recognition of amino acid derivatives by using several spectroscopic techniques such as IR, FAB-MS, fluorescence and UV-vis. Macrocycle **63** showed significant enantiomeric discrimination by IR spectroscopy, wherein the IR frequency shift values of *D*-amino acid methyl esterhydrochlorides were greater than that of *L*-isomers. Furthermore, the FAB-MS data showed host-guest 1 + 1 molecular ion peaks for macrocycles **63** and **69** with benzene ring containing amino acid methyl ester hydrochlorides owing to π - π interactions with pyridine ring of the macrocycles showed excellent enantioselective binding. The fluorescence data demonstrated that the when macrocycles **63** and **66** mixed with guest amino acids, Ala-OMe and Ph-OMe, the fluorescence intensity increases. However, in the case of macrocycles **67** and **69** fluorescence intensity decreases probably because nitrogen in the pyridine ring as a binding site interacts with proton by static force.

Sakai et al. [68] designed and synthesized a series of the pyridine incorporated chiral bifunctional macrocyclic hosts, **70–74** (Figure 7) using two 2,6-diacylaminopyridine as binding units, chiral BINOL to provide an anisotropic ring-current effect, and amides giving rise to a V-shaped arrangement in **70–72**, while a parallel alignment in **73**. Out of the five chiral receptors, **70** was evaluated for the chiral discrimination ability using ^1H or ^{19}F NMR and was found to be an excellent versatile chiral solvating agent for a wide range of the chiral compounds (Figure 8) having the following functionalities: carboxylic acid, oxazolidinone, lactone, alcohol, sulfoxide, sulfoximine, isocyanate, or epoxide. In particular, **70**, having the NO_2 group, influenced the binding capacity as well as the degree of enantioselectivity and further host exhibited special characteristic features such as versatility, signal sharpness, high splitting ability, high sensitivity, wide detection window, and easy synthetic accessibility.

Wilhelm et al. [69] synthesized a series of the (–)-nicotine-based chiral ionic liquid as follows. (Schemes 10–12). (–)-Nicotine, **75** was treated with one equivalent of methyl iodide to furnish **79**, (Scheme 10) subsequently the anion metathesis was carried out and iodide was replaced by PF_6^- , BF_4^- , and NTf_2^- , respectively to obtain the chiral ionic liquids (Scheme 11). In order to produce the desired salt, **78**, **75** was reacted with ethyl bromide, however, the product, **83a** was isolated instead of **78**. As **83b** was not suitable, a different anion was then converted to *N*-ethyl nicotinium bromide **83a**, which upon the anion metathesis resulted in the chiral ionic liquids, **83b–d** (Scheme 12). The newly developed enantiopure ionic liquids were evaluated as chiral solvating agents using ^{19}F NMR spectroscopy. In the case of **79b** the best result was observed with Mosher's acid in the ^{19}F NMR and with mandelic acid in the ^1H NMR (Table 6, entry 3).



Scheme 9. Preparation of macrocycles 63–65.

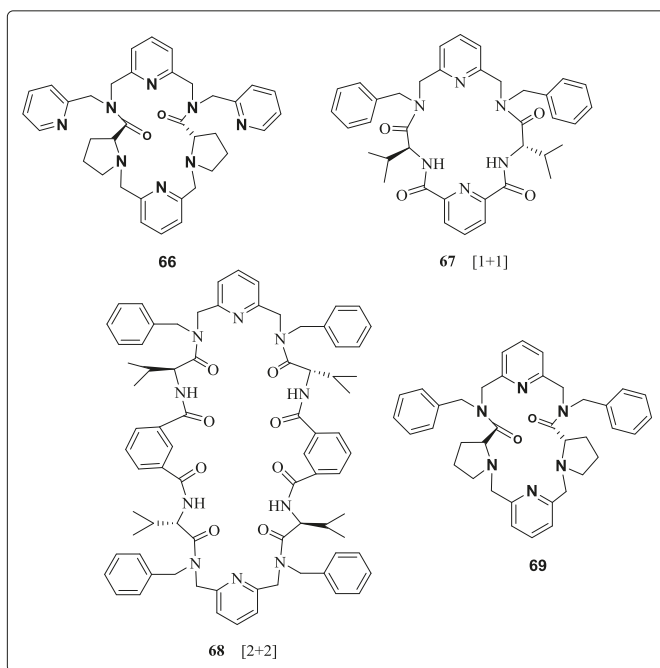


Figure 6. Macrocycle 66–69.

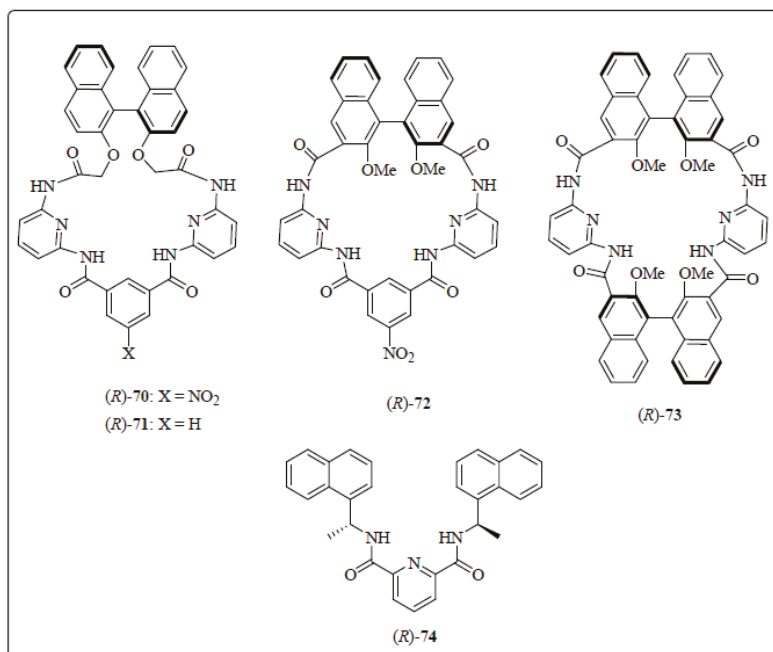


Figure 7. Chiral solvating agents, 70–74.

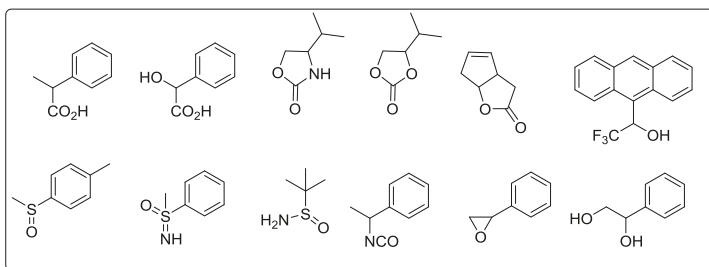
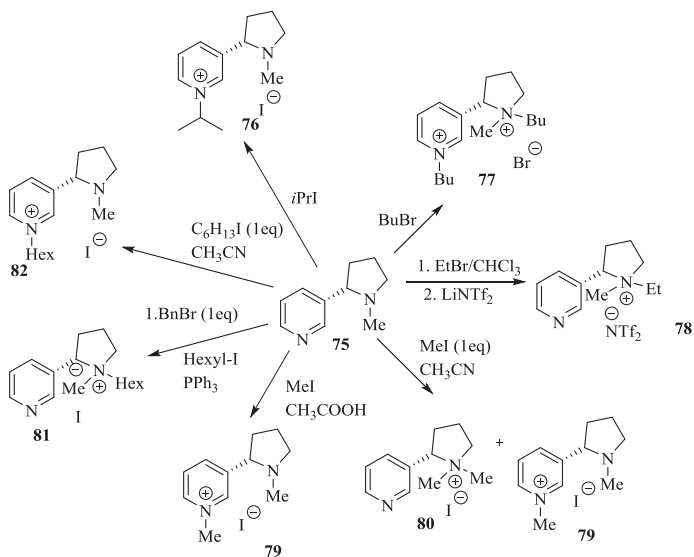
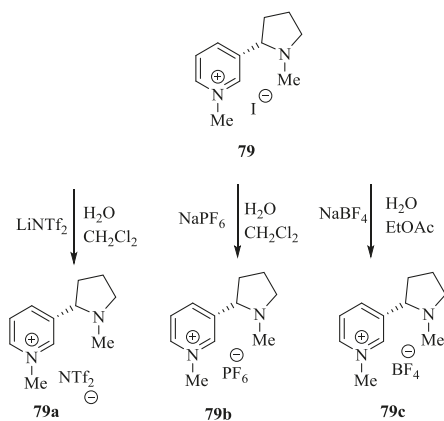


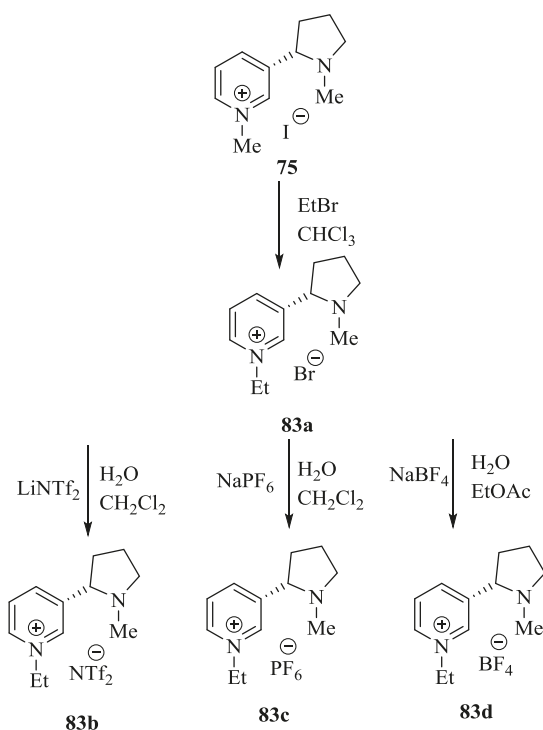
Figure 8. Chiral guests used for chiral recognition by (R)-70.



Scheme 10. Synthesis of Ionic liquid 76–82.



Scheme 11. Synthesis of Ionic liquid 79a–c.

Scheme 12. Synthesis of Ionic liquid **83b–d**.

Zhang et al. [70] developed a chiral shift reagent, macrocyclic compound, **85** (Scheme 13) by the simple alkylation of C_2 -symmetric aminonaphthol, **84** with pyridyl chloride in a high yield. Enantiomeric acids gave large nonequivalent chemical shifts (upto 0.80 ppm) in the presence of **85** in ^1H NMR (500 MHz) spectra. The quantitative analysis of mandelic acid with a different enantiomeric purity showed that the host, **85** is an excellent chemical shift reagent for chiral carboxylic acids. Indeed, **85** exhibited an excellent ability to discriminate (Table 7) the enantiomers of a broad variety of carboxylic acids (Figure 9) by ^1H NMR spectroscopy.

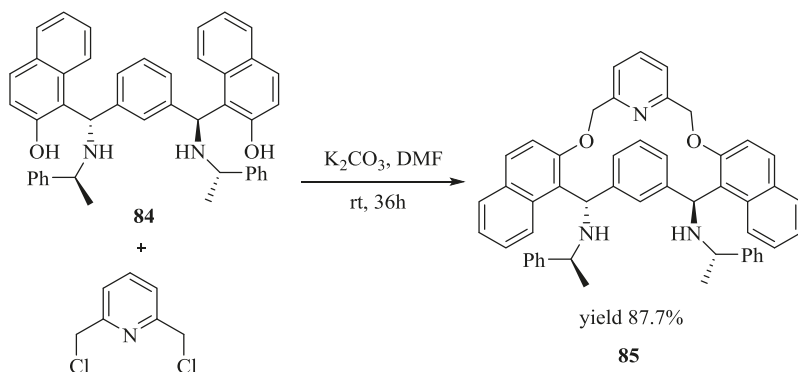
Scheme 13. Synthesis of **85**.

Table 6. ¹⁹F NMR chemical shifts (δ) of Mosher's acid or mandelic acid in ppm and resolution of Δδ values in Hz (282 MHz ¹⁹F NMR), (500 MHz ¹H NMR).

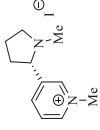
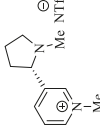
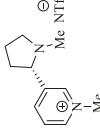
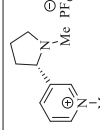
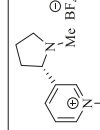
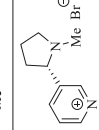
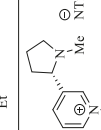
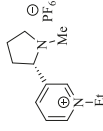
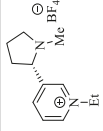
| Entry | Salts | CDCl ₃ | | | CD ₃ OD | | | | | |
|-------|---|---------------------------------|-----|--------------------------------|---------------------------------|------|--------------------------------|-----|-------------|-----|
| | | ¹⁹ F δ Mosher's Acid | Δ δ | ¹ H δ Mosher's Acid | ¹⁹ F δ Mandelic Acid | Δ δ | ¹ H δ Mosher's Acid | Δ δ | | |
| 1 |  | -71.0 | - | 3.56q | 5.25 | - | -73.17 | - | 3.57q | - |
| 2 |  | -70.61/-70.63 | 5.9 | 3.51/3.50 | 4.99/5.01 | 5.7 | - | - | - | - |
| 3 |  | -70.86/-70.89 | 9.0 | 3.44/3.40 | 4.96/4.98 | 10.0 | -71.26/-71.29 | 9.1 | 3.55q/3.56q | 4.0 |
| 4 |  | -71.09 | 0 | 3.54/3.53 | 5.19 | 0 | -71.11/-71.13 | 6.6 | 3.56q/3.57q | 5.0 |
| 5 |  | -70.90/-70.92 | 7.2 | 3.49/3.47 | 4.95/4.96 | 5.4 | -71.20 | 0 | 3.56q | 0 |
| 6 |  | -71.02/-71.04 | 5.0 | 3.47/3.46 | 5.01/5.03 | 6.8 | -71.18 | 0 | 3.57q | 0 |
| 7 |  | -69.90/-70.57 | 7.5 | 3.45/3.42 | 5.20 | 0 | -71.64/-71.65 | 4.3 | 3.55q/3.56q | 2.0 |

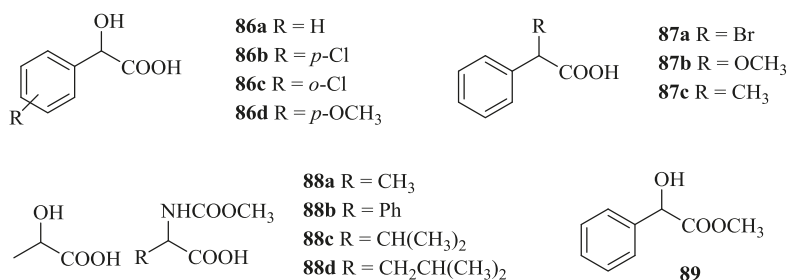
Table 6. *Cont.*

| Entry | Salts | CDCl ₃ | | | CD ₃ OD | | |
|-------|---|-----------------------------------|-----------------------------------|-----------------------------------|-----------------------------------|----------------------------------|----------------------------------|
| | | ¹⁹ Fδ Mosher's Acid Δδ | ¹ H δ Mosher's Acid Δδ | ¹ H δ Mandelic Acid Δδ | ¹⁹ Fδ Mosher's Acid Δδ | ¹ Hδ Mosher's Acid Δδ | ¹ Hδ Mosher's Acid Δδ |
| 8 |  | -70.67 / -70.68 | 3.54 / 3.53 | 4.99 / 5.00 | -70.85 / -70.88 | 8.1 | 3.58q / 3.57q |
| 9 |  | -71.10 | 3.50 / 3.48 | 5.24 / 5.26 | -71.69 / -71.70 | 5.5 | 3.57q / 3.56q |

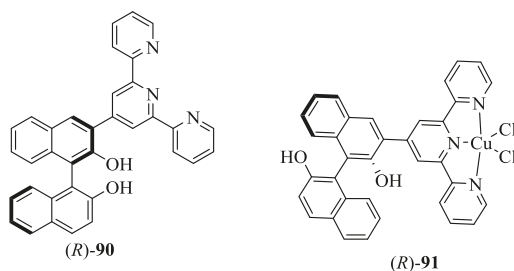
0.5 equiv. of Mosher's acid and mandelic acid with different salts in CDCl₃ and Mosher's acid with different salts in deuterated methanol.

Table 7. Measurements of ^1H Chemical Shift Inequivalencies $\Delta\Delta\delta$ of **86a** and **88b** in the presence of **85** by ^1H NMR Spectroscopy (500 MHz) in different solvents at 25 °C.

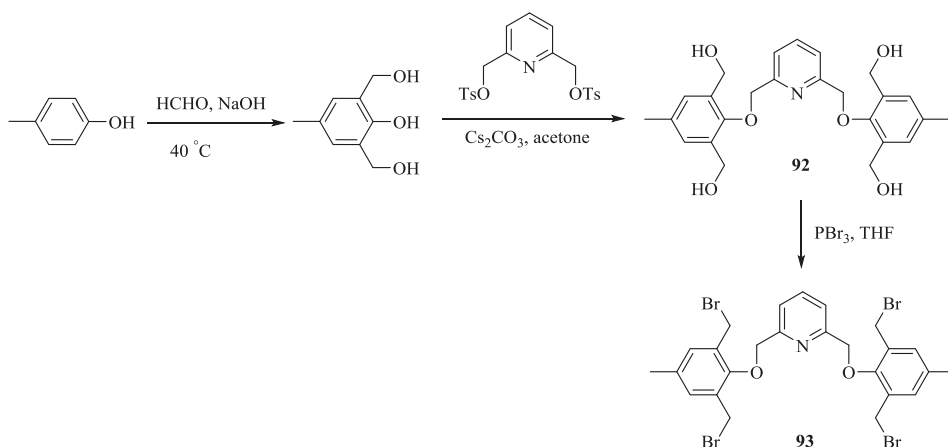
| Entry | Solvent | $\Delta\Delta\delta$ (ppm) | |
|-------|--|----------------------------|------|
| | | 4 | 13 |
| 1 | CDCl_3 | 0.62 | 0.39 |
| 2 | $\text{CDCl}_3/\text{C}_6\text{D}_6$ (10%) | 0.62 | 0.39 |
| 3 | $\text{CDCl}_3/\text{Acetone-}d_6$ (10%) | 0.53 | 0.27 |
| 4 | $\text{CDCl}_3/\text{CD}_3\text{OD}$ (10%) | 0.43 | 0.21 |
| 5 | $\text{CDCl}_3/\text{DMSO-}d_6$ (10%) | 0.13 | 0.04 |

**Figure 9.** Structures of the guests studied.

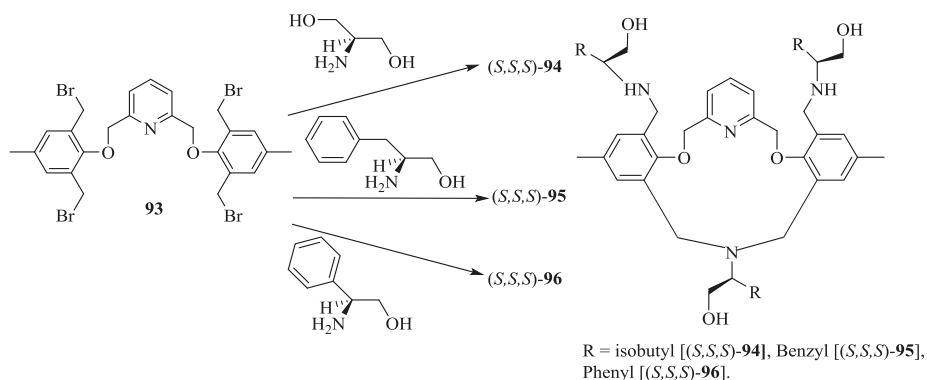
Pu et al. [71] reported the first example of enantioselective gel collapsing as a new means of the visual chiral sensing (Figure 10). The BINOL-terpyridine-Cu(II) complex, (*R*)-**91** was obtained as a green solid by reaction between the terpyridine conjugate, (*R*)-**90** and $\text{CuCl}_2 \cdot 2\text{H}_2\text{O}$. The enantioselective sensing of gel, (*R*)-**91** was studied upon interaction with chiral amino alcohols. It was observed that (*R*)-**91** in chloroform when mixed with (*R*)-phenylglycinol remained stable, whereas when mixed with (*S*)-phenylglycinol collapsed. This confirmed the enantioselective nature of gel towards chiral amino alcohols. This result was compared to the fluorescence response of (*R*)-**91** towards (*R*)- and (*S*)-phenylglycinol in solution. Intriguingly, enhancement in the fluorescence intensity was observed when (*R*)-**91** was treated with an excess of (*S*)-phenylglycinol. In contrast, weaker fluorescence was observed in the case of (*R*)-phenylglycinol. This difference is due to displacement of the Cu(II) ion in (*R*)-**91** by the chiral amino alcohol, which is enantioselective. Indeed, the reaction of (*R*)-**91** with (*S*)-phenylglycinol is more favorable than that with (*R*)-phenylglycinol. Moreover, other chiral amino alcohols including prolinol, valinol, phenylalaninol, leucinol, and 1-amino-2-propanol also exhibited significant fluorescent enhancement in the presence of (*R*)-**91**.

**Figure 10.** First example of enantioselective gel, **91** and its precursor, **90**.

Togrul et al. [27] synthesized a series of pyridine-macrocycles bearing amino alcohol subunits. A tetra-bromide building block, **93** was prepared for the macrocycle synthesis (Scheme 14) starting from 4-methylphenol, which was converted to 2,5-dihydroxymethyl-4-methylphenol followed by the reaction with pyridine ditosylate to give **92** and final bromination using PBr_3 . The chiral macrocycles, (*S,S,S*)-**94**, (*S,S,S*)-**95** and (*S,S,S*)-**96** (Scheme 15) were obtained by the treatment of **93** with respective amino alcohols and their enantiomeric recognition properties towards alkyl ammonium salts were investigated by UV-vis spectroscopy (Figure 11). The association constants are summarized in Table 8, demonstrated that the complex host bearing phenyl, (*S,S,S*)-**94** and isobutyl, (*S,S,S*)-**94** are more stable with an (*S*)-configuration of the enantiomer of guests of both **98** and **97**; over the (*R*)-configuration because the phenyl and cyclohexyl groups in the (*S*)-enantiomers are placed opposite to the isobutyl and phenyl side chains in the cavity of the host, whereas in opposite enantiomers, these groups are located in the same face, causing unfavorable steric interactions.



Scheme 14. Synthesis of compound, **93**.



Scheme 15. Synthesis of compound, **94**.

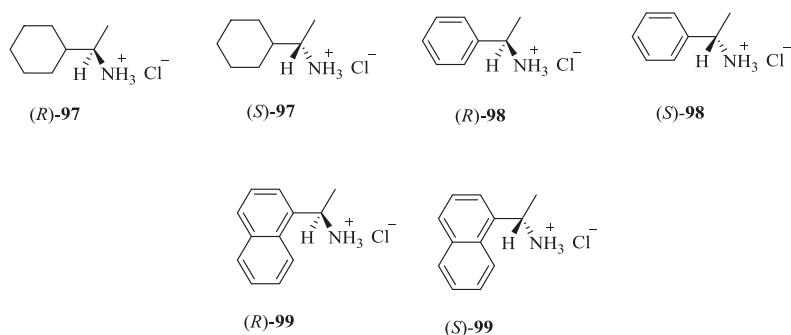
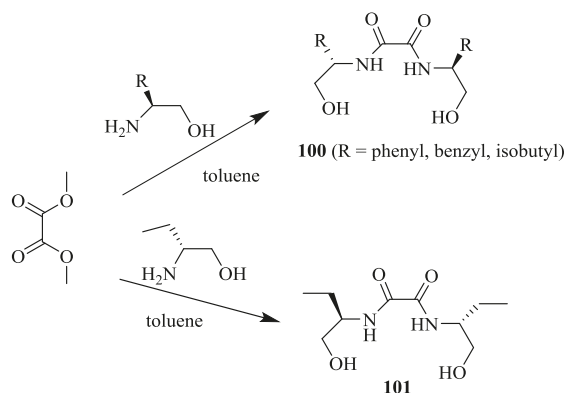


Figure 11. Ammonium hydrochloride salts used as guests.

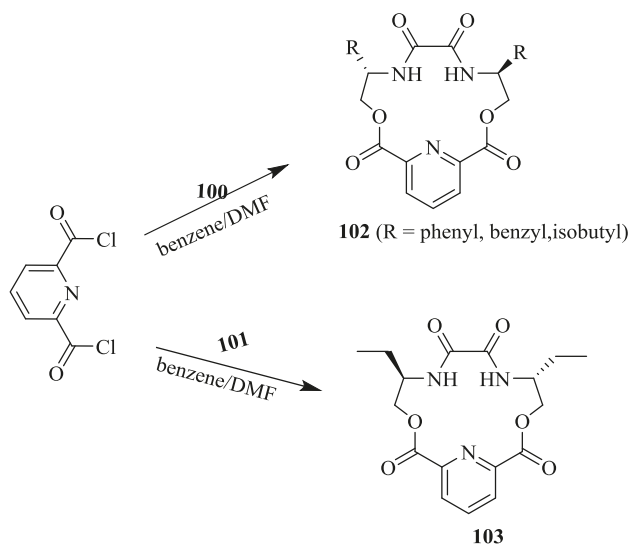
Table 8. Binding constant (K_a), the Gibbs free energy changes ($-\Delta G_0$), enantioselectivities K_S/K_R or $\Delta\Delta G_0$ for including the *R/S* guest with the chiral host macrocycles in CHCl_3 at 25 °C.

| Host | Guest | K_a (M^{-1}) | K_S/K_R | $-\Delta G_0$ (kJ mol^{-1}) | $\Delta\Delta G_0$ (kJ mol^{-1}) |
|--------------------|----------------|-------------------------------|-----------|--|---|
| <i>(S,S,S)</i> -94 | <i>(R)</i> -98 | $(2.0 \pm 0.23) \times 10^4$ | 2.0 | 24.62 | 1.63 |
| | <i>(S)</i> -98 | $(4.0 \pm 0.34) \times 10^4$ | | 26.25 | |
| | <i>(R)</i> -97 | $(1.0 \pm 0.42) \times 10^4$ | 5.0 | 22.82 | 3.99 |
| | <i>(S)</i> -97 | $(5.0 \pm 0.36) \times 10^4$ | | 26.81 | |
| <i>(S,S,S)</i> -95 | <i>(R)</i> -98 | $(2.0 \pm 0.31) \times 10^5$ | 0.9 | 30.24 | -0.26 |
| | <i>(S)</i> -98 | $(1.8 \pm 0.38) \times 10^5$ | | 29.98 | |
| | <i>(R)</i> -97 | $(1.67 \pm 0.19) \times 10^4$ | 2.4 | 24.09 | 2.16 |
| | <i>(S)</i> -97 | $(4.0 \pm 0.43) \times 10^4$ | | 26.25 | |
| <i>(S,S,S)</i> -96 | <i>(R)</i> -98 | $(1.5 \pm 0.26) \times 10^4$ | 2.1 | 23.82 | 1.80 |
| | <i>(S)</i> -98 | $(3.1 \pm 0.18) \times 10^4$ | | 25.62 | |
| | <i>(R)</i> -97 | $(1.0 \pm 0.34) \times 10^4$ | 5.0 | 22.82 | 3.99 |
| | <i>(S)</i> -97 | $(5.0 \pm 0.46) \times 10^4$ | | 26.81 | |

The same group [72] has developed a series of the C_2 -symmetric, pyridine and diamide–diester groups containing lactone type macrocycles (**102**, **103**) with different side arms by reacting chiral bis(aminoalcohol)oxalamides with acyl pyridine (Schemes 16 and 17).



Scheme 16. Synthesis of bis(aminoalcohol)oxalamides.



Scheme 17. Synthesis of pyridine-15-crown-5 type macrocycles.

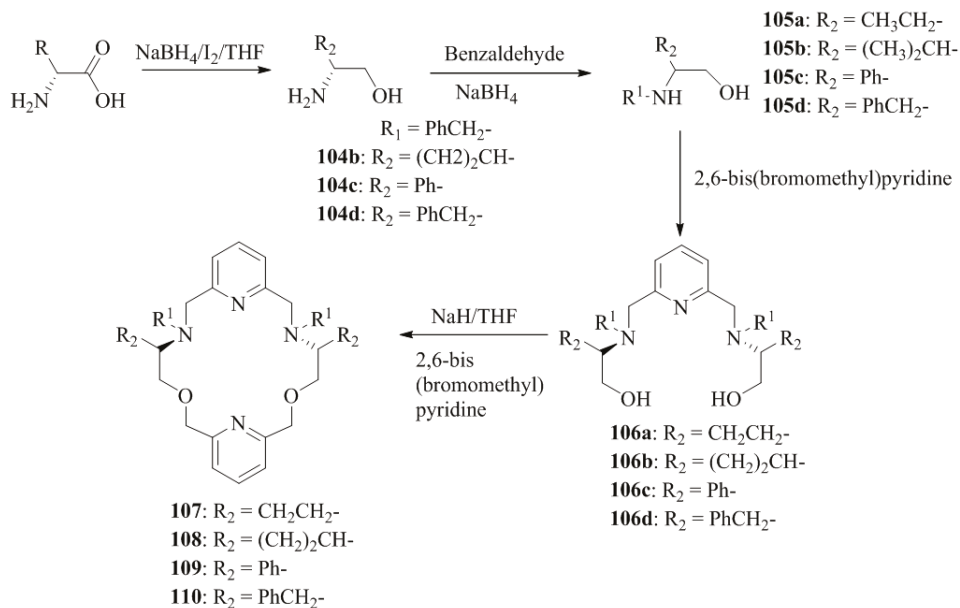
The standard ^1H NMR titration experiments were carried out in order to investigate the chiral discrimination ability and complex stability of **102** and **103** with enantiomeric perchlorate salts **98** and **99**. The detailed results are summarized in Table 9. The host **102** formed stable complexes with (*S*)-enantiomers of **98** and **99** whereas host **103** formed the stables complexes with (*R*)-enantiomers of guest as host **103** contains the inverted stereogenic center compare to host **102**. Interestingly, replacing the phenyl group with benzyl ring in the host **102b**, reversed discrimination observed and formed the more stable complexes with (*R*)-enantiomers of **98** and **99**.

Table 9. Binding constant (K_a), the Gibbs free energy changes (ΔG_0), enantioselectivities K_R/K_S or $\Delta\Delta G_0$ for including the *R/S* guest with the chiral host macrocycles in DMSO- d_6 at 25 °C.

| Entry | Host | Guest ^a | K_a (M^{-1}) ^b | K_a^S/K_a^R ^c | $-\Delta G_0$ (kJ mol^{-1}) ^d | $\Delta\Delta G_0$ (kJ mol^{-1}) ^e | ED ^f |
|-------|-----------------------------|-------------------------|--|----------------------------|---|--|-----------------|
| 1 | (<i>S,S</i>)- 102a | (<i>R</i>)- 98 | 33.6 ± 0.3 | 3.86 | 8.71 | 3.34 | 59(<i>S</i>) |
| 2 | (<i>S,S</i>)- 102a | (<i>S</i>)- 98 | 129.6 ± 0.5 | | 12.05 | | |
| 3 | (<i>S,S</i>)- 102a | (<i>R</i>)- 99 | 327.1 ± 0.2 | 31.0 | 14.35 | 8.50 | 94(<i>S</i>) |
| 4 | (<i>S,S</i>)- 102a | (<i>S</i>)- 99 | $10,138 \pm 71$ | | 22.85 | | |
| 5 | (<i>S,S</i>)- 102b | (<i>R</i>)- 98 | 1852 ± 17 | 1.44 | 18.64 | 0.91 | 18(<i>S</i>) |
| 6 | (<i>S,S</i>)- 102b | (<i>S</i>)- 98 | 2668 ± 10 | | 19.55 | | |
| 7 | (<i>S,S</i>)- 102b | (<i>R</i>)- 99 | 721.4 ± 3.1 | 0.36 | 16.31 | -2.51 | 47(<i>R</i>) |
| 8 | (<i>S,S</i>)- 102b | (<i>S</i>)- 99 | 262.6 ± 2.6 | | 13.80 | | |
| 9 | (<i>S,S</i>)- 102c | (<i>R</i>)- 98 | 2559 ± 7 | 1.05 | 19.44 | 0.20 | 2(<i>S</i>) |
| 10 | (<i>S,S</i>)- 102c | (<i>S</i>)- 98 | 2681 ± 5 | | 19.56 | | |
| 11 | (<i>S,S</i>)- 102c | (<i>R</i>)- 99 | 1126 ± 4 | 1.34 | 17.41 | 0.73 | 30(<i>S</i>) |
| 12 | (<i>S,S</i>)- 102c | (<i>S</i>)- 99 | 1511 ± 4 | | 18.14 | | |
| 13 | (<i>R,R</i>)- 103 | (<i>R</i>)- 98 | 5412 ± 17 | | 21.30 | | |
| 14 | (<i>R,R</i>)- 103 | (<i>S</i>)- 98 | nd ^g | | nd ^g | | |
| 15 | (<i>R,R</i>)- 103 | (<i>R</i>)- 99 | 4719 ± 9 | 0.60 | 20.96 | -1.27 | 25(<i>R</i>) |
| 16 | (<i>R,R</i>)- 103 | (<i>S</i>)- 99 | 2833 ± 7 | | 19.69 | | |

^a **98**: α -phenylethylammonium perchlorate salts; **99**: α -(1-naphthyl)ethylammonium perchlorate salts. ^b The binding constants between the hosts and the guests observed by ^1H NMR titration. ^c The ratios of binding constants for each enantiomer. ^d The binding free energy change for the complexes, calculated by $\Delta G_0 = -RT \ln K_a$. ^e $\Delta\Delta G_0 = -(\Delta G_{0(R)} - \Delta G_{0(S)})$. ^f Enantiomeric discrimination factor. ^g Not determined.

Yilmaz Turgut et al. [73] synthesized four C_2 -symmetric chiral pyridine containing 18-crown-6 macrocycles, each containing pairs of the following substituents: ethyl (107), isopropyl (108), phenyl (109), and benzyl (110). The synthetic strategy adopted was as follows: firstly, as a chiral source, D-Val, D-Pgly and D-Phe were reduced to the corresponding amino alcohols, D-valinol, 104b, D-Phenyl glycinol 104c and D-phenylalaninol, 104d. The compound, 104a and the reduced products, 104b–d were reacted with benzaldehyde to give imines, which subsequently were converted to the corresponding N-benzyl derivatives, 105a, 105b, and 105c (Scheme 18) followed by the treatment with 2,6-bis(bromomethyl) pyridine to afford 106a–d. The pyridine containing C_2 -symmetric 106a–d having ethyl-, isopropyl-, phenyl-, and benzyl-moieties in their side arms were cyclized in a 1:1 ratio with 2,6-bis(bromomethyl)pyridine to the desired chiral macrocycles, 107, 108, 109 and 110 possessing the dipyridine units (Scheme 18). The chiral recognition of macrocycles towards the D-, L-amino acid methyl ester derivatives was determined by the ^1H NMR titration method (Table 10). The compounds, 107 and 108 with the ethyl and isopropyl substituents at the stereogenic center, respectively, demonstrated the highest enantioselectivity and stable complexes, whereas the compounds, 109 and 110 with the corresponding phenyl and benzyl substituents possess a low-to-medium level of these properties. This inefficiency is a result of the fact that the phenyl and benzyl moieties prevent the guest cations from approaching the host.



Scheme 18. Synthesis of chiral amino alcohols and chiral macrocycles.

Kumares Ghosh et al. [74] prepared a series of pyridinium-based chiral compounds, 112–114, 119 and 122. The synthesis proceeds (Schemes 19 and 20) with the reaction of Boc-protected L-amino acids like Val (111a), Ala (111b) and Pgly (111c) and 3-aminopyridine to furnish the coupled products, 112a–c, respectively. Further removal of the Boc-groups in 112a–c yielded the corresponding amines, 113a–c, which upon reaction with 1-naphthyl isocyanate afforded the respective urea derivatives, 114a–c. The compounds, 114a–c reacted with the corresponding chloroamides, 119a–c to produce the chloride salts. Further, the anion exchange reactions with NH_4PF_6 yielded the desired compounds, 115, 116 and 117. On the other hand, reaction of 114a with benzyl bromide followed by the Br^- exchange with PF_6^- gave 118.

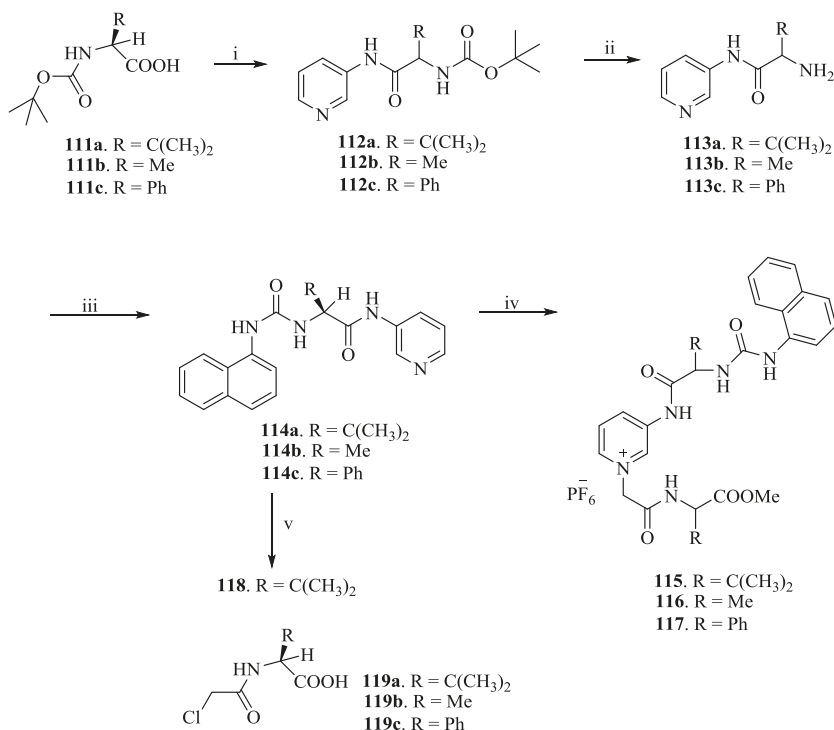
Table 10. Association constant (K_a), the Gibbs free energy changes ($-\Delta G_0$), enantioselectivities K_D/K_L for the complexation of D-/L-guest with the **107**, **108**, **109**, and **110** in $CDCl_3$ with 0.25% CD_3OD .

| Entry | Host | Guests | K_{ass} (M^{-1}) | K_D/K_L | $-\Delta G_0$ ($kJ\ mol^{-1}$) ^a | $-\Delta\Delta G_0$ ($kJ\ mol^{-1}$) ^b |
|-------|------------|--------------|------------------------|------------------------------|---|---|
| 1 | 107 | D-PheOMe.HCl | 1785 | 2.04 | 18.3 | 1.80 |
| 2 | 107 | L-PheOMe.HCl | 875 | | 16.5 | |
| 3 | 107 | D-ValOMe.HCl | 2325 | 2.63 | 18.9 | 2.30 |
| 4 | 107 | L-ValOMe.HCl | 885 | | 16.6 | |
| 5 | 108 | D-PheOMe.HCl | 2580 | 1.22 | 1.2 | 0.5 |
| 6 | 108 | L-PheOMe.HCl | 2105 | | 18.7 | |
| 7 | 108 | D-ValOMe.HCl | 13,590 | 5.08 | 23.3 | 4.00 |
| 8 | 108 | L-ValOMe.HCl | 2675 | | 19.3 | |
| 9 | 109 | D-PheOMe.HCl | 395 | 0.77 ($K_L/K_D = 1.29$) | 14.6 | 0.60 |
| 10 | 109 | L-PheOMe.HCl | 510 | | 15.2 | |
| 11 | 109 | D-ValOMe.HCl | 32 | 0.33 ($K_L/K_D = 3.00$) | 8.5 | 2.80 |
| 12 | 109 | L-ValOMe.HCl | 96 | | 11.3 | |
| 13 | 110 | D-PheOMe.HCl | 1190 | 1.21 | 17.3 | 0.50 |
| 14 | 110 | L-PheOMe.HCl | 983 | | 16.8 | |
| 15 | 110 | D-ValOMe.HCl | 660 | 0.72 ($K_L/K_D = 1.38$) | 15.8 | 0.8 |
| 16 | 110 | L-ValOMe.HCl | 914 | | 16.6 | |

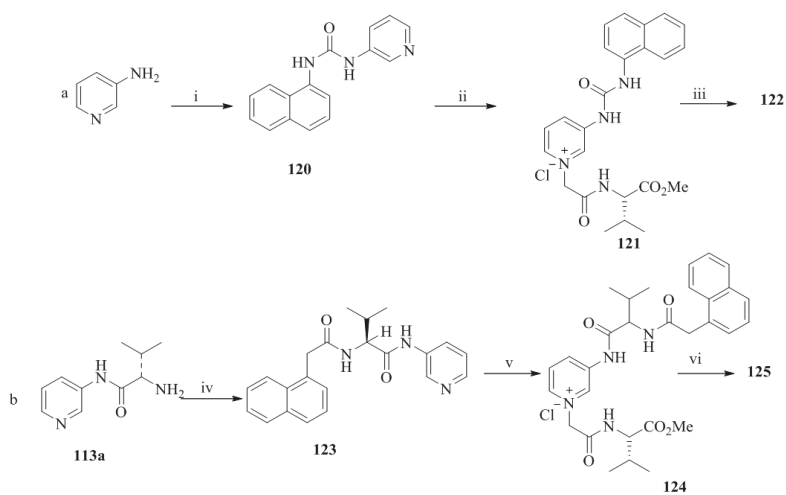
The treatment of 3-aminopyridine with 1-naphthylamine and phosgene afforded the urea, **120**, (Scheme 20) followed by the reaction with the chloroamide, **119a**, to give the chloride salt, **121**. Then the chloride exchange of **121** by using NH_4PF_6 gave the desired compound, **122**. Next, the amine, **113a** was coupled with 1-naphthylacetyl chloride to obtain the amide derivative, **123**, which, subsequently reacted with **119a** to yield the chloride salt, **124** followed by the ion exchange with NH_4PF_6 to furnish the desired compound, **122**. Among the synthesized compounds, **115–117**, **122**, and **125**, the structures, **115** and **125** have been established as effective fluorescent chiral receptors for the selective enantioselective recognition of D-lactate over L-lactate.

Bedekar et al. [75] synthesized two diastereomers of the optically active N, O-containing macrocycles, **129** and **130**. First, the ring opening reaction of cyclohexene oxide, **126** with (S)-2-phenylethyl amine afforded two diastereomers of aminocyclohexanol, **127a,b**, (Scheme 21) which after separation and subsequent condensation with m-xylene dibromide furnished the respective diols, **128a,b** (Scheme 22). The final transesterification with dimethyl 2, 6-pyridinedicarboxylate afforded the desired eighteen membered macrocycles, (S,S,S)-**129** and (R,R,S)-**130**. Using ^{31}P NMR as a detection tool, the macrocycles (S,S,S)-**129** and (R,R,S)-**130** were tested for the chiral discrimination of chiral BINOL-based phosphoric acid derivatives by measuring the corresponding chemical shifts (Table 11). The macrocycle, (R,R,S)-**130** showed better discrimination, while (S,S,S)-**129** was found to be ineffective. Further, the discrimination of chiral phosphoric acid **131a** was corroborated by fluorescence, where the quenching was observed with the interaction of chiral host molecules **129** and **130**. The fluorescence quenching efficiency, ratio of $K^{R-131a}_{sv} / K^{S-131a}_{sv}$ was observed to be 1.05 and 1.40 respectively for **129** and **130**.

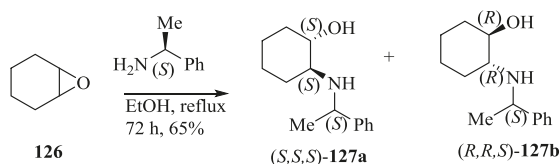
Interestingly, for the same set of macrocyclic chiral solvating agents (CSAs) **129** and **130**, interaction with the second group of analytes, such as α -substituted phosphonic acids (**132** to **136**) gave a reverse trend (Table 12). The authors proposed that these analytes being smaller in size were better accommodated in the partially closed cavity of macrocycle (S,S,S)-**129**. The formation of H-bond between the phosphonic acid analyte and H-bond acceptor sites of macrocyclic CSA is apparently favored by the partially closed cavity of (S,S,S)-**129**.



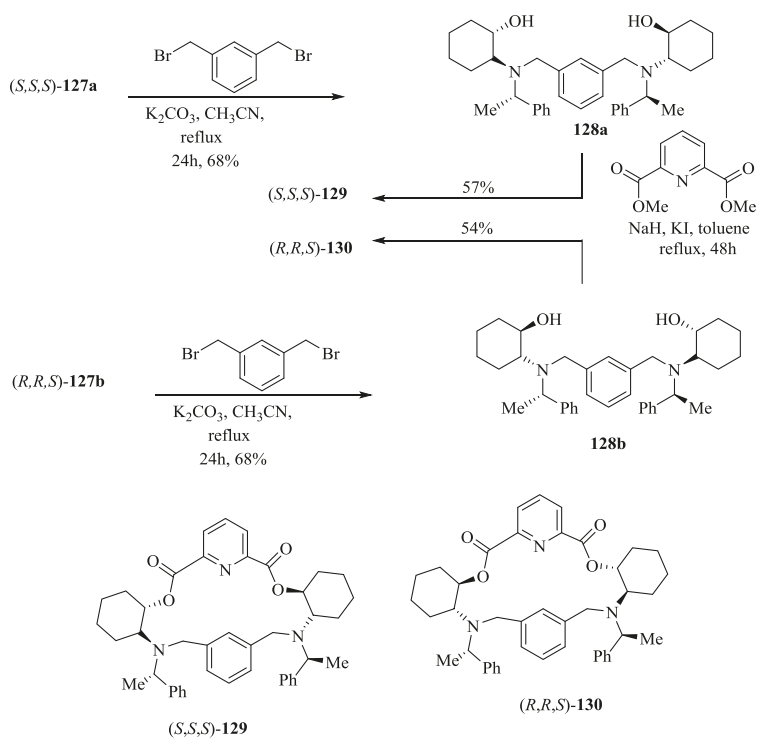
Scheme 19. (i) 3-Aminopyridine, DCC, CH₂Cl₂, 20 h; (ii) TFA, CH₂Cl₂, 3 h; (iii) 1-naphthylamine, triphosgene, Et₃N, CH₂Cl₂, 16 h; (iv) (a) **119a–c**, CH₃CN, reflux, 4 days; (b) NH₄PF₆, CH₃OH–H₂O; (v) (a) benzyl bromide, CH₃CN, reflux, 18 h; (b) NH₄PF₆, CH₃OH–H₂O.



Scheme 20. (a) (i) 1-Naphthylamine, triphosgene, Et₃N, CH₂Cl₂, 18 h; (ii) **119a**, CH₃CN, reflux, 4 days; (iii) NH₄PF₆, CH₃OH–H₂O; (iv) (b) (iv) 1-naphthylacetyl chloride, CH₂Cl₂, Et₃N, 12 h; (v) **119a** CH₃CN, reflux, 3 days; (vi) NH₄PF₆, CH₃OH–H₂O.



Scheme 21. Preparation of amino alcohols from cyclohexeneoxide.

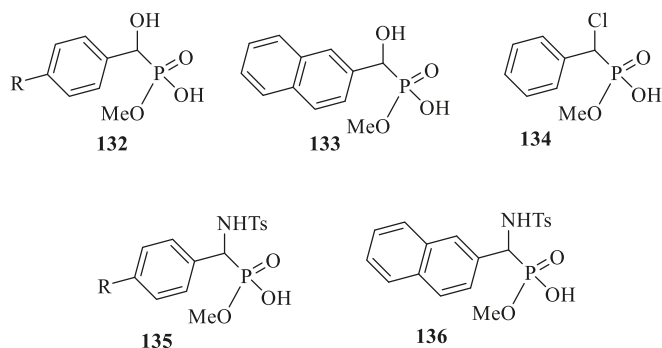


Scheme 22. Synthesis of macrocycles, 129 and 130.

Table 11. Discrimination of binaphthyl phosphoric acids 131^a.

| | | | | $\Delta\Delta\delta$ | (ppm) |
|-----|-----------|-----------------|----------------|----------------------|----------------------|
| No. | Comp. No. | R ₁ | R ₂ | (<i>S,S,S</i>)-129 | (<i>R,R,S</i>)-130 |
| 1 | 131a | H | H | 0.03 | 0.74 |
| 2 | 131b | H | Ome | _b | 0.68 |
| 3 | 131c | H | i-Pr | _b | 0.76 |
| 4 | 131d | NO ₂ | H | _b | 0.81 |
| 5 | 131e | Br | H | _b | 0.40 |

^a In CDCl₃ (20 mM), 162 MHz (³¹P NMR), ratio of 5:1 (2:1). _b Not resolved.

Table 12. Discrimination of monomethyl esters of substituted phosphoric acids **132** to **136**^a.

| No. | Comp. No. | R | (<i>S,S,S</i>)-129 | (<i>R,R,S</i>)-130 |
|-----|-----------|-----------------|----------------------|----------------------|
| 1 | 132a | H | 0.17 | 0.04 |
| 2 | 132b | Me | 0.19 | _b |
| 3 | 133c | Cl | 0.16 | _b |
| 4 | 133 | - | 0.17 | _b |
| 5 | 134 | - | _b | _b |
| 6 | 135a | H | 0.40 | _b |
| 7 | 135b | Me | 0.42 | _b |
| 8 | 135c | Cl | 0.45 | 0.10 |
| 9 | 135d | OMe | 0.43 | _b |
| 10 | 135e | NO ₂ | 0.40 | 0.12 |
| 11 | 136 | - | 0.37 | _b |

^a In CD₃OD (5%), in CDCl₃ (20 mM), 162 MHz (³¹P NMR), ratio of A to 10:4 (2:1). _b Not resolved.

5.2. Oxygen Containing Six Member Heterocycle

Oxygen containing six member heterocycles is another class of motif found as structural core in several natural and synthetic compounds. Oxygen atom in the heterocyclic ring has two unshared pairs of electrons and hence can effectively participate in many types of the non-bonded interactions mentioned above. Six-membered carbohydrate unit has been very widely used in commercially popular chiral chromatographic columns. It is also a harder Lewis base than nitrogen and consequently different types of ligands can be probed with these heterocycle containing receptors. The particularly chromene heterocycle is a well-known significant core unit in the molecular recognition [32]. Chromenone core has exclusively placed oxygen atoms in 1,4-arrangement in conjugation with a double bond which facilitates brisk electron movement upon change in the electronic environment and hence quick detection under spectroscopic techniques, while studying host-guest interactions (Chart 2). Hence chromenone becomes a molecule of choice for receptor construction. The general design of chromenone based hosts discussed here, contain one or more chromenone motifs present in the receptor backbone, of molecular cleft or macrocycles.

Moran et al. [33] for the first time synthesized the chromenone and Spiro-bifluorene containing chiral macrocyclic receptor, **141** by reaction of the bis-aminomethylspirobifluorene unit **137** with nitrochromenone 2-carboxylic acid chloride, subsequent reduction of the nitro groups, treatment with phosgene, and slow hydrolysis of the intermediate isocyanates (Scheme 23). Significant chiral recognition of hydroxycarboxylates such as lactic or mandelic acids has been achieved with the macrocyclic receptor, **141** by using ¹H NMR. Thus, the receptors **141** showed a good association of the carboxylate group owing to four efficient hydrogen bonds for the syn- and anti-lone pairs of oxo-anion. The resolution of racemic receptor, **141** was achieved on a TLC plate by taking the advantage of its complexing properties with (*R*)-mandelic acid tetramethylammonium salt.

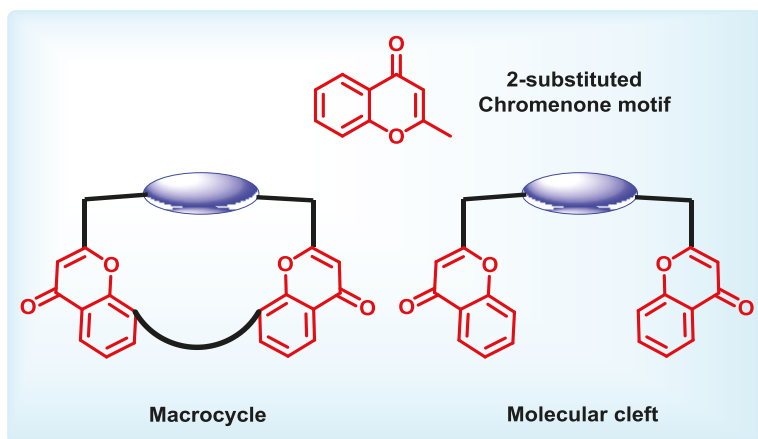
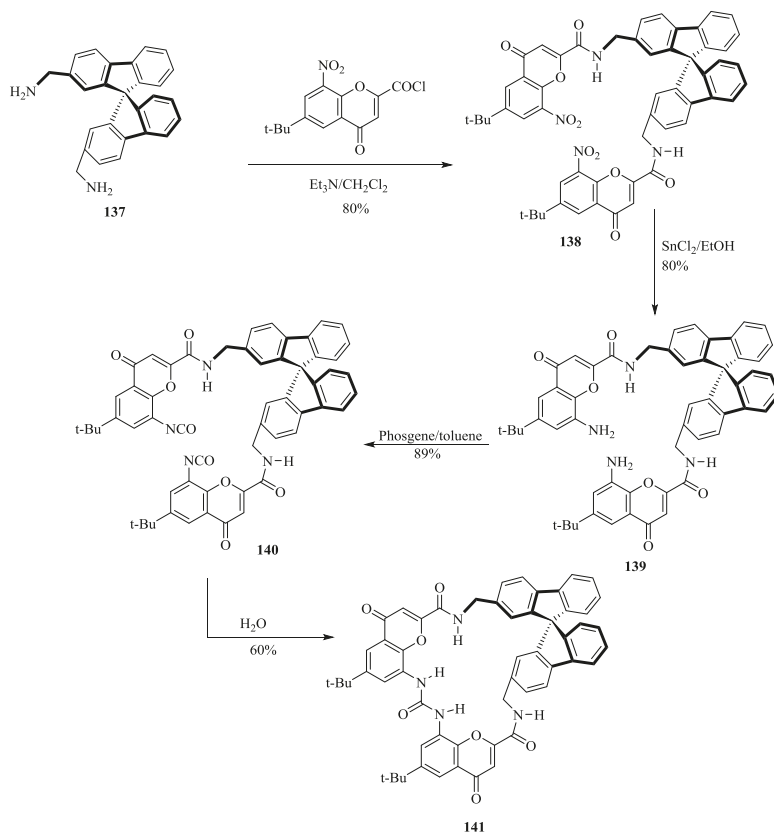


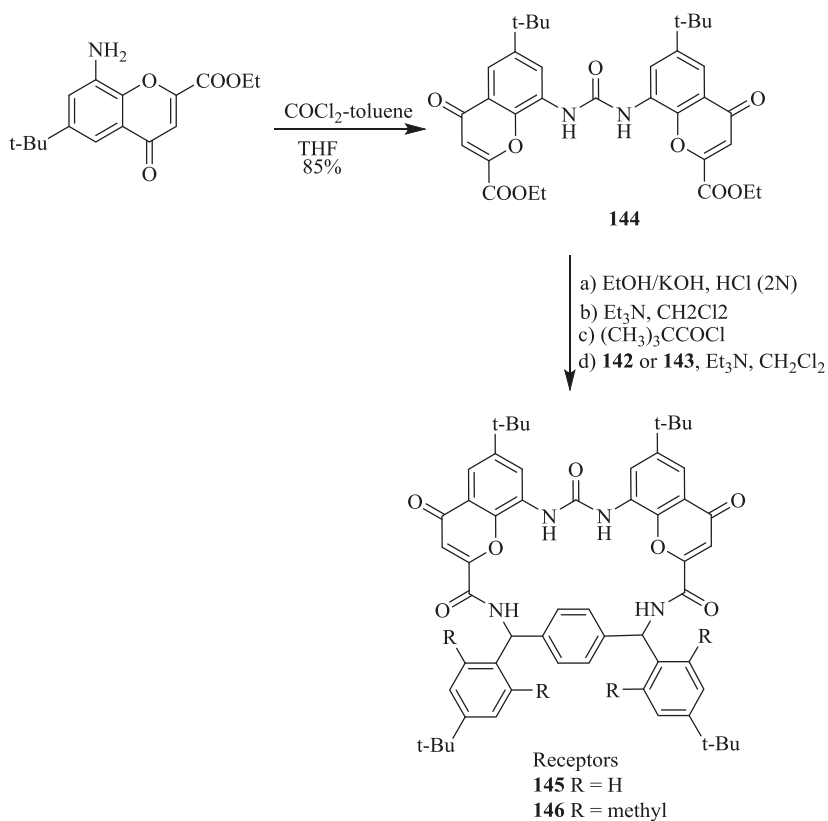
Chart 2. General design of chromenone containing hosts.



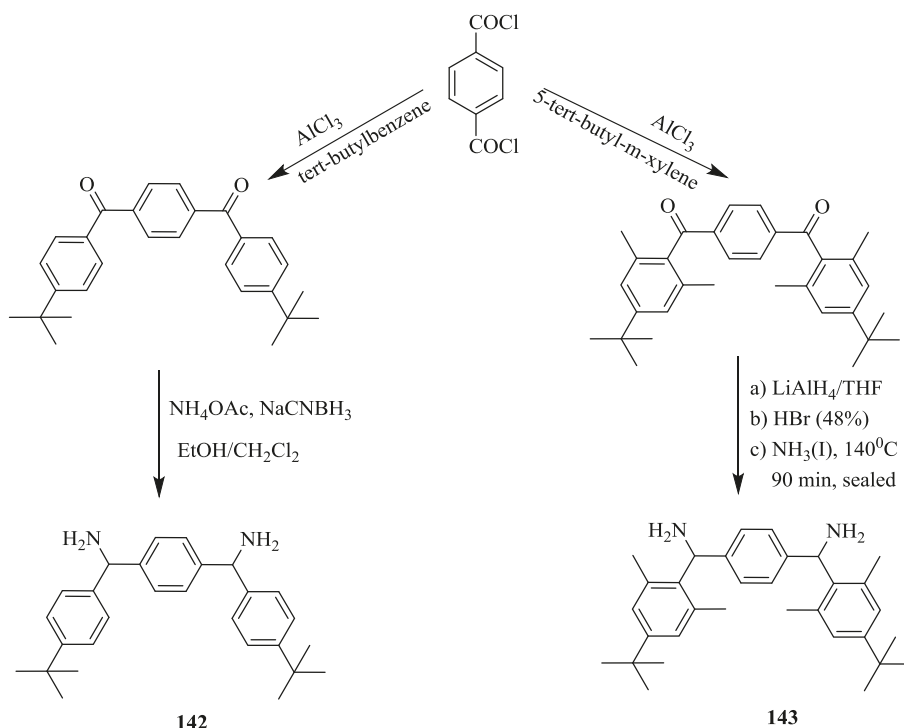
Scheme 23. Preparation of Receptor 141.

With the excellent recognition ability of bischromenylurea skeleton-based receptor **141** for chiral acids, this strategy was further extended [76]. Hence, bischromenylurea and α, α' -(*o,o'*-dialkyl)diphenyl-*p*-xylylenediamine spacer-based receptors (**145**, **146**) (Scheme 24) were prepared by a simple synthetic approach involving the hydrolysis of ethoxy carbonyl amino chromenone, **144** to give a dicarboxylic acid, which was subsequently coupled with the diamine, **142** or **143** (Scheme 25).

The chiral recognition behavior of racemic receptors, **145** and **146** has been tested with the enantiomers of naproxen by using ^1H NMR. However, only a slight chiral discrimination (ratio 1.2:1) was observed for the receptor **145** and (*S*)-naproxen. Intriguingly, high enantioselectivity of 7.2:1 was obtained for the racemic receptor, **146** and (*S*)-naproxen. Apparently this is because **146** possesses a rigid and hindered cavity, where the host-guest binding takes place without disturbing the required complementary geometry.



Scheme 24. Synthesis of receptors, **145** and **146**.



Scheme 25. Synthesis of diamines, 142 and 143.

6. Five Member Heterocycles Containing Receptors

Five member heterocycles such as imidazole, thiophene, furan, oxazole and oxazoline-based chiral compounds have attracted a widespread interest in the asymmetric synthesis and molecular recognition of metal ion, anion and chiral guests, owing to their striking structural features discussed in the Section 4. In the contemporary days several chiral receptors with five membered heterocycles have been developed and explored for the selective detection of chiral acids, chiral alcohols, chiral diamines and chiral amines. However, further chiral recognition using such receptors is used for the determination of concentration and enantiomeric excess of chiral analytes by high throughput methods. In this section, the recent developments in the receptor with five member heterocycles for chiral discrimination processes are presented.

6.1. Imidazole Ring Containing Receptors

Imidazole core has profound existence in nature, undoubtedly the synthetic community is inspired to construct receptors containing imidazole motifs. Imidazole moiety is bestowed with unique properties like basicity, nucleophilicity, and coordination ability. Acidity of the NH proton present in the imidazole ring can be tuned by changing the electronic properties of the imidazole substituents which is useful in anion binding. On the other hand, the presence of a donor pyridine-like nitrogen atom within the ring enables the imidazole ring towards selectivity in binding cationic species, thus making imidazole derivatives excellent metal ion sensors. The general receptor design of imidazole containing receptors discussed here, contain one or more imidazole motifs either separated by a chiral spacer to form a molecular cleft or 2,2'-linked bisimidazole motif as spacer itself with suitably placed terminal chiral arms (Chart 3).

Xie et al. [34] synthesized the chiral imidazole containing cyclophanes, **149–152** by highly selective *N*-alkylation of the imidazolyl 1*N*-position of **148** with the corresponding dibromides (Scheme 26).

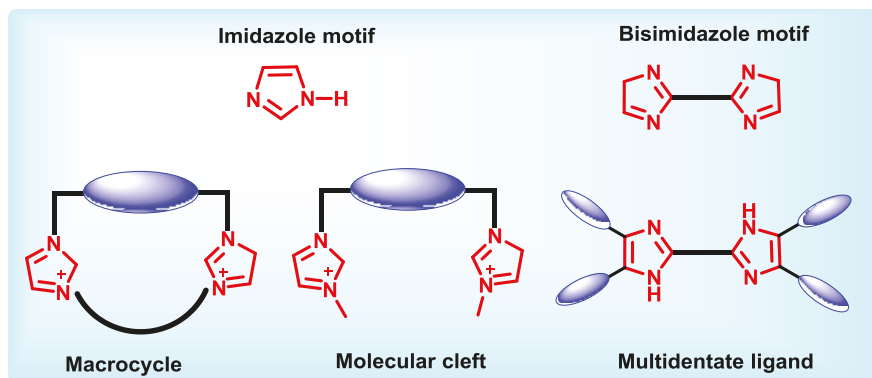
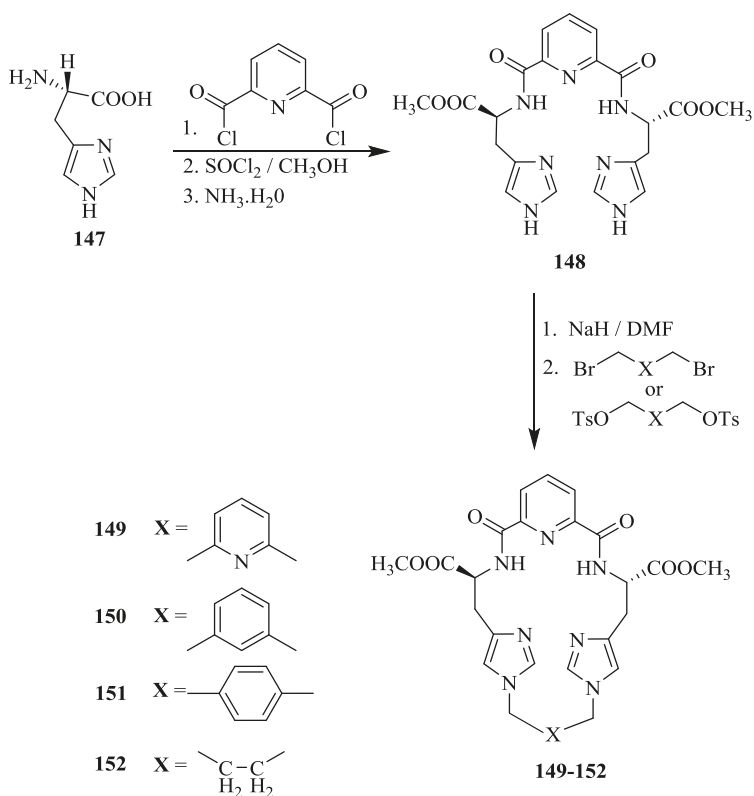


Chart 3. General design of imidazole containing hosts.



Scheme 26. Synthesis of chiral imidazole cyclophanes, **149–152**.

On the basis of differential UV spectroscopic studies, the association constants (K_a) of inclusion complexes of the chiral imidazole cyclophane receptors with amino acid esters along with the free

energy change (G_0) were determined (Table 13). The K_D values of **149** and **152** for D-Phe-OMe with the $-(\text{CH}_2)_4-$ moiety were found to be 1063 and 208 $\text{dm}^3 \text{mol}^{-1}$, respectively, which corresponds to the D/L-selectivity (K_D/K_L) of 3.33 and 1.40. The enantioselective recognition ability of **149** with α -amino acid esters and their hydrochlorides gave K_D/K_L in the range of 1.45–3.52 and G_0 from 20.93 to 23.11 kJ mol^{-1} . However, **149** gave fairly poor recognition ability for amino acid esters with the aliphatic side chain (Table 13, entries 3–8) due to absence of π - π stacking interactions with receptor.

Table 13. Association constants (K_a), the Gibbs free energy changes ($-\Delta G_0$), enantioselectivities K_D/K_L or $\Delta\Delta G_0$ calculated from $-\Delta G_0$ for the including complexation of L/D-amino acid esters with **148–152** in CHCl_3 at 25 °C ^a.

| Entry | Host | Guests | K_a (M^{-1}) | K_D/K_L | $-\Delta G_0$ (kJ mol^{-1}) ^a | $-\Delta\Delta G_0$ (kJ mol^{-1}) ^b |
|-------|------------|---------------|---------------------------|-----------|---|---|
| 1 | 148 | L-Phe-OMe | 89.4 | 1.12 | 11.13 | −0.27 |
| 2 | 148 | D-Phe-OMe | 99.8 | | 11.40 | |
| 3 | 149 | L-Ala-OMe | 437 | 1.45 | 15.06 | −0.93 |
| 4 | 149 | D-Ala-OMe | 634 | | 15.99 | |
| 5 | 149 | L-Val-OMe | 299 | 2.05 | 14.12 | −1.78 |
| 6 | 149 | D-Val-OMe | 613 | | 15.90 | |
| 7 | 149 | L-Leu-OMe | 260 | 2.24 | 13.78 | −2.00 |
| 8 | 149 | D-Leu-OMe | 583 | | 15.78 | |
| 9 | 149 | L-Phe-OMe | 319 | 3.33 | 14.28 | −2.99 |
| 10 | 149 | D-Phe-OMe | 1063 | | 17.27 | |
| 11 | 149 | L-Trp-OMe | 1238 | 2.68 | 17.64 | −2.44 |
| 12 | 149 | D-Trp-OMe | 3314 | | 20.08 | |
| 13 | 149 | L-Ala-OMe.HCl | 471 | 2.80 | 15.25 | −2.55 |
| 14 | 149 | D-Ala-OMe.HCl | 1319 | | 17.80 | |
| 15 | 149 | L-Leu-OMe.HCl | 327 | 3.52 | 14.35 | −3.11 |
| 16 | 149 | D-Leu-OMe.HCl | 1150 | | 17.46 | |
| 17 | 150 | L-Phe-OMe | 224 | 2.33 | 13.41 | −2.10 |
| 18 | 150 | D-Phe-OMe | 523 | | 15.51 | |
| 19 | 151 | L-Phe-OMe | 217 | 2.00 | 13.33 | −1.71 |
| 20 | 151 | D-Phe-OMe | 433 | | 15.40 | |
| 21 | 152 | L-Phe-OMe | 149 | 1.40 | 12.40 | −0.82 |
| 22 | 152 | D-Phe-OMe | 208 | | 13.22 | |

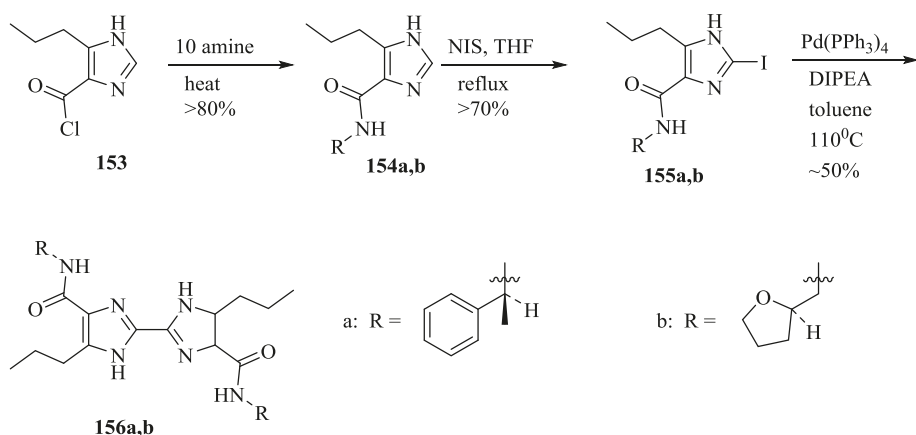
^a The concentration of the receptors: $2.0 \times 10^{-4} \text{ mol dm}^{-3}$. ^b Ala-OMe: alanine methyl ester; Val-OMe: valine methyl ester; Leu-OMe: leucine methyl ester; Phe-OMe: phenylalanine methyl ester; Trp-OMe: tryptophan methyl ester; Ala-OMe. HCl: alanine methyl ester hydrochloride; Leu-OMe.HCl: leucine methyl ester hydrochloride.

Allen et al. [77] prepared chiral 4,4'-diamido-2,2'-biimidazoles, **156a,b** (Scheme 27) by the treatment of acid chloride, **153** with (*S*)- α -methylbenzylamine and (*R*)-tetrahydrofurfurylamine to afford **154a,b**, followed by the corresponding iodination and coupling. The macromolecules, **156a,b** were found to be beneficial for the chiral recognition of *N*-protected amino acids as revealed by the NMR titration methods. In particular, **156a** discriminates the enantiomers of *N*-Boc-Phe, while **156b** discriminates the enantiomers of *N*-Boc-Ser (Table 14).

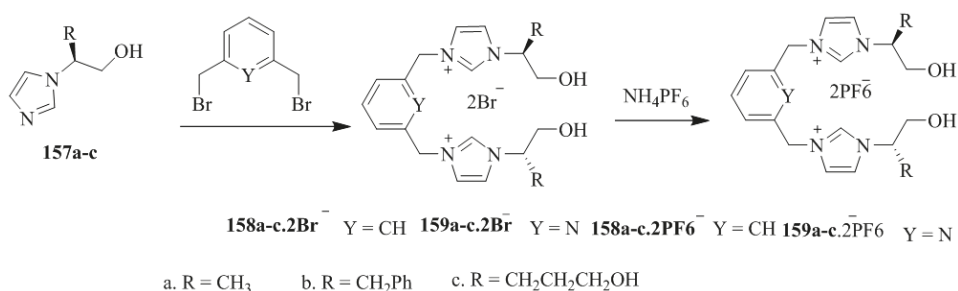
Table 14. Binding constants K_a (M^{-1}) ^a for chiral biimidazoles with amino acid derivatives in CDCl_3 at 23 °C.

| Complex | K_a |
|--|---------|
| 156a. <i>N</i> -Boc-L-Phe, -D-Phe | 100,65 |
| 156b. <i>N</i> -Boc-L-Ser, -D-Ser | <6065 |
| 156a. <i>N</i> -Boc-L-Phe, -D-Phe | 6565 |
| 156b. <i>N</i> -Boc-L-Ser, -D-Ser | 120,270 |

^a Values represent averages of at least two replicate titrations, rounded to the nearest $\pm 5 \text{ M}^{-1}$. Errors in individual fits were $\leq 15\%$.

Scheme 27. Synthesis of chiral 4,4'-diamido-2,2'-biimidazoles, **156a,b**.

Later Xie and coworkers [78,79] synthesized the imidazole-based chiral molecular tweezers (Scheme 28) spaced by 2,6-di(bromomethyl)-4-chlorophenol, 1,3-phenylenebis(methylene) and 2,6-pyridylenebis(methylene). The dibromide salts, **158a-c.2Br⁻** and **159a-c.2Br⁻** were obtained by the direct quaternization of **157a-c** with 2,6-di(bromomethyl)-4-chlorophenol or 1,3-bis(bromomethyl)benzene or 2,6-bis(bromomethyl)pyridine while the hexafluorophosphate salts **158a-c.2PF₆⁻** and **159a-c.2PF₆⁻** were prepared by the treatment with a saturated aqueous solution of NH_4PF_6 . The chiral discrimination of chiral molecular tweezers for amino acids or their derivatives (Tables 15 and 16) were evaluated by the UV-vis titration method.



Scheme 28. Synthesis of chiral molecular tweezers.

Table 15. Binding constants (K_a), Gibbs free energy changes ($-\Delta G_0$), enantioselectivities K_L/K_D or $\Delta\Delta G$ calculated from $-\Delta G$ for the including complexation of L/D-amino acids or their derivatives with hosts at 27 °C in water or acetonitrile.

| Entry | Host ^{a,b} | Guest | K/dm ³ mol | K_L/K_D | $-\Delta G_0/\text{KJ mol}^{-1}$ | $-\Delta\Delta G_0/\text{KJ mol}^{-1}$ |
|-------|----------------------------|-------|-----------------------|-----------|----------------------------------|--|
| 1 | 158a2Br⁻ | L-Phe | 10,328 | 1.29 | 23.05 | 0.63 |
| 2 | 158a2Br⁻ | D-Phe | 8012 | | 22.42 | |
| 3 | 158a2Br⁻ | L-Thr | 766 | 1.82 | 16.56 | 1.49 |
| 4 | 158a2Br⁻ | D-Thr | 421 | | 15.07 | |
| 5 | 158b2Br⁻ | L-Phe | 19,518 | 1.89 | 24.64 | 1.59 |
| 6 | 158b2Br⁻ | D-Phe | 10,324 | | 23.05 | |

Table 15. Cont.

| Entry | Host ^{a,b} | Guest | K/dm ³ mol | K _L /K _D | −ΔG ₀ /KJ mol ^{−1} | −ΔΔG ₀ /KJ mol ^{−1} |
|-------|-----------------------------------|---------------|-----------------------|--------------------------------|--|---|
| 7 | 158b2Br [−] | L-His | 7627 | 2.03 | 22.30 | 1.77 |
| 8 | 158b2Br [−] | D-His | 3761 | | 20.53 | |
| 9 | 158c2Br [−] | L-Phe | 14,026 | 1.71 | 23.82 | 1.34 |
| 10 | 158b2Br [−] | D-Phe | 8222 | | 22.48 | |
| 11 | 159a2Br [−] | L-Ala | 820 | 1.61 | 16.73 | 1.19 |
| 12 | 159a2Br [−] | D-Ala | 509 | | 15.54 | |
| 13 | 159a2Br [−] | L-Thr | 1901 | 2.10 | 18.83 | 1.85 |
| 14 | 159a2Br [−] | D-Thr | 904 | | 16.98 | |
| 15 | 159a2Br [−] | L-Phe | 13,053 | 2.51 | 23.64 | 2.75 |
| 16 | 159a2Br [−] | D-Phe | 5196 | | 20.89 | |
| 17 | 159a2Br [−] | L-His | 11,639 | 3.03 | 23.35 | 2.76 |
| 18 | 159a2Br [−] | D-His | 3841 | | 20.59 | |
| 19 | 159a2Br [−] | L-Phe | 28,321 | 3.35 | 25.57 | 3.02 |
| 20 | 159a2Br [−] | D-Phe | 8458 | | 22.55 | |
| 21 | 159a2Br [−] | L-His | 12,031 | 3.20 | 23.43 | 2.91 |
| 22 | 159a2Br [−] | D-His | 3741 | | 20.52 | |
| 23 | 159c2Br [−] | L-Phe | 14,733 | 2.14 | 23.94 | 1.90 |
| 24 | 159c2Br [−] | D-Phe | 6899 | | 22.04 | |
| 25 | 158a2PF ₆ [−] | BOC-L-His-Ome | 870 | 3.50 | 16.88 | 3.13 |
| 26 | 158a2PF ₆ [−] | BOC-D-His-Ome | 248 | | 13.75 | |
| 27 | 158b2PF ₆ [−] | BOC-L-His-Ome | 1001 | 4.07 | 17.23 | 3.50 |
| 28 | 158b2PF ₆ [−] | BOC-D-His-Ome | 246 | | 13.73 | |
| 29 | 159a2PF ₆ [−] | L-Ala-Ome | 610 | 1.72 | 16.00 | 1.50 |
| 30 | 159a2PF ₆ [−] | D-Ala-Ome | 355 | | 14.50 | |
| 31 | 159a2PF ₆ [−] | L-Phe-Ome | 9294 | 2.72 | 22.79 | 2.49 |
| 32 | 159a2PF ₆ [−] | L-Phe-Ome | 3421 | | 20.30 | |
| 33 | 159a2PF ₆ [−] | BOC-L-Phe-Ome | 9166 | 3.34 | 22.76 | 3.01 |
| 34 | 159a2PF ₆ [−] | BOC-D-Phe-Ome | 2741 | | 19.74 | |
| 35 | 159b2PF ₆ [−] | L-Phe-Ome | 10,720 | 3.14 | 23.15 | 2.86 |
| 36 | 159b2PF ₆ [−] | D-Phe-Ome | 3412 | | 20.29 | |
| 37 | 159b2PF ₆ [−] | BOC-L-Phe-Ome | 13,903 | 4.03 | 23.79 | 3.47 |
| 38 | 159b2PF ₆ [−] | BOC-L-Phe-Ome | 3446 | | 20.32 | |
| 39 | 159b2PF ₆ [−] | BOC-L-His-Ome | 1284 | 5.10 | 17.48 | 3.69 |
| 40 | 159b2PF ₆ [−] | BOC-D-His-Ome | 252 | | 13.79 | |

^a 158a-c2Br[−] and 159a-c2Br[−] in water, 158a-c2PF₆[−] and 159a2PF₆[−] in acetonitrile. ^b the concentration of hosts 5.0 × 10^{−5} mol dm^{−3}.

Table 16. Binding constants (K_a), Gibbs free energy changes ($-\Delta G_0$), enantioselectivities K_L/K_D or $\Delta\Delta G$ calculated from $-\Delta G$ for the complexation of L/D-amino acids or their methyl esters with 158a–159b at 27 ± 0.1 °C in water or acetonitrile.

| Entry | Host ^{a,b} | Guest ^c | K/dm ³ mol | K _L /K _D | −ΔG ₀ /Kj mol ^{−1} | −ΔΔG ₀ /Kj mol ^{−1} ^d |
|-------|---------------------|------------------------|-----------------------|--------------------------------|--|--|
| 1 | 158a | L-Ala D-Ala | 1623 897 | 1.81 | 18.44 16.95 | 1.49 |
| 2 | 158a | L-Phe D-Phe | 33,748 19,241 | 1.75 | 26.01 24.60 | 1.41 |
| 3 | 158a | L-His D-His | 7458 3876 | 1.92 | 22.24 20.61 | 1.63 |
| 4 | 159a | L-Phe-OMe D-Phe-OMe | 4099 2515 | 1.59 | 20.99 19.83 | 1.16 |

Table 16. Cont.

| Entry | Host ^{a,b} | Guest ^c | K/dm ³ mol | K _L /K _D | −ΔG ₀ /Kj mol ^{−1} | −ΔΔG ₀ /Kj mol ^{−1} ^d |
|-------|---------------------|--------------------|-----------------------|--------------------------------|--|--|
| 5 | 158b | L-Ala | 1682 | 1.82 | 18.53 | 1.51 |
| | | D-Ala | 921 | | 17.02 | |
| 6 | 158b | L-Phe | 68,274 | 3.36 | 27.76 | 3.02 |
| | | D-Phe | 20,310 | | 24.74 | |
| 7 | 158b | L-His | 9510 | 3.04 | 22.85 | 2.78 |
| | | D-His | 3129 | | 20.07 | |
| 8 | 159b | L-Ala-OMe | 1704 | 1.95 | 18.55 | 1.86 |
| | | D-Ala-OMe | 874 | | 16.69 | |
| 9 | 159b | BOC-L-Ala-OMe | 1453 | 2.10 | 18.16 | 1.86 |
| | | BOC-D-Ala-OMe | 690 | | 16.30 | |
| 10 | 159b | L-Phe-OMe | 6882 | 2.22 | 22.04 | 1.98 |
| | | D-Phe-OMe | 3105 | | 20.06 | |
| 11 | 159b | BOC-L-Phe-OMe | 6736 | 2.68 | 21.99 | 2.47 |
| | | BOC-D-Phe-OMe | 2510 | | 19.52 | |
| 12 | 159b | BOC-L-His-OMe | 2941 | 4.10 | 19.92 | 3.52 |
| | | BOC-D-His-OMe | 717 | | 16.40 | |

^a 158a,b in water; 159a,b in acetonitrile. ^b the concentration of hosts 5.0×10^{-5} mol dm^{−3}; ^c Phe-OMe: phenylalanine methyl ester; BOC-Phe-OMe: BOC-phenylalanine methyl ester; BOC-Ala-OMe: BOC-alanine methyl ester; BOC-His-OMe: BOC-Histidine methyl ester. ^d $\Delta\Delta G_0 = -(\Delta G_{0(L)} - \Delta G_{0(D)})$.

Yu et al. [29] designed and synthesized the imidazolium-functionalized BINOLs, (*R*)-160, (*S*)-161 and (*S*)-162 (Figure 12). These hosts were evaluated for chiral recognition with various amino acid derivatives, tetrabutylammonium salts of *t*-Boc-amino acids, such as Ala, Ser, Leu, and Phe. However, *R*-160 exhibited a noteworthy binding ability only for *t*-BOC alanine anion with the high enantioselectivity (K_D/K_L) of 4.5, while (*S*)-161, bearing imidazolium rings attached to a flexible methylene linker, showed the higher association constant but furnished moderate enantioselectivity, K_L/K_D value of 2.9 for the same chiral guest. This is a result of the reduction of the steric factor between the BINOL unit and imidazolium due to the flexible methylene linker.

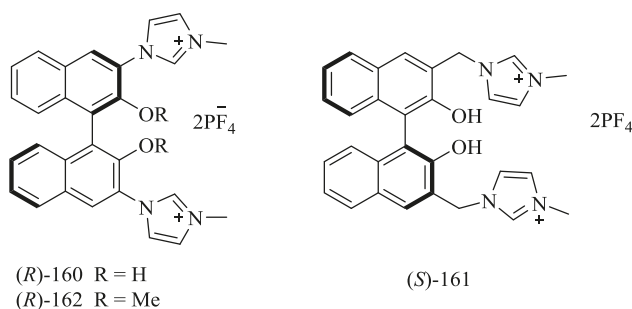
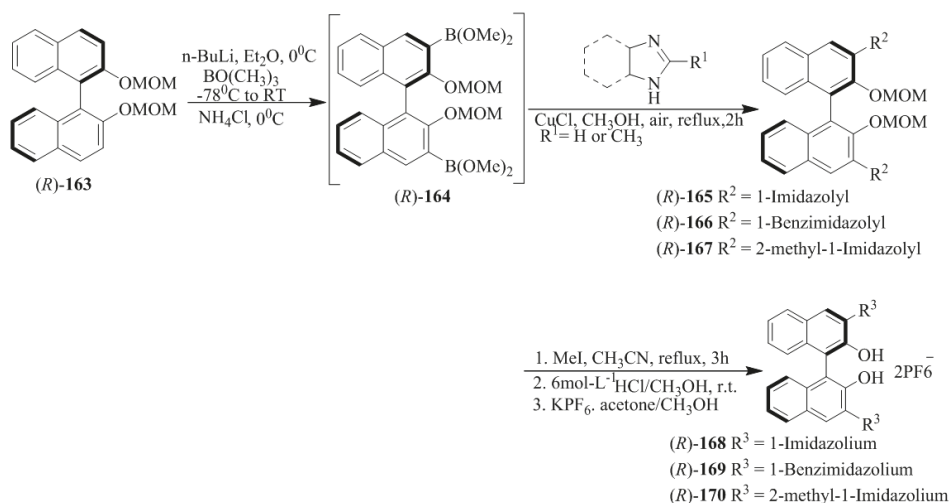


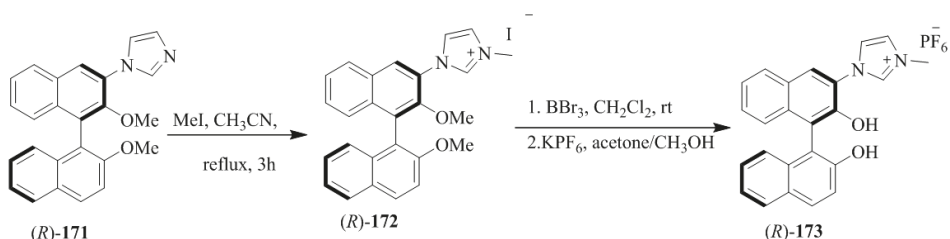
Figure 12. Imidazolium-functionalized anion-binding receptors.

Yu et al. [24] developed the imidazolium/benzimidazolium-containing receptors, (*R*)-168, (*R*)-169, (*R*)-170, (*R*)-173, and (*R*)-176. At first, MOM-protected boronic acid ester, (*R*)-164 upon the *N*-arylation with imidazole derivative or benzimidazole yielded the respective coupled products (165–167) followed by methylation to give the desired hosts, 168–170 (Scheme 29). Further, (*R*)-171 and (*R*)-174 (Schemes 30 and 31) were converted to (*R*)-173 and (*R*)-176, respectively. The synthesized compounds were then evaluated for the chiral discrimination of amino acid derivatives, such as Ala, Ser, Leu, and Phe, and tetrabutylammonium salts of *t*-Boc-amino acids studied by using fluorescence spectroscopy. The association constants of (*R*)-178 with L- and D-Boc alanine were found to be 4.55×10^5 and

$1.02 \times 10^5 \text{ L mol}^{-1}$, respectively, with the K_L/K_D value of 4.5. While (*R*)-**176** displayed larger association constants with both L- and D- *t*-Boc alanines, the enantioselectivity was very similar ($K_L/K_D = 4.1$). However, when (*R*)-**173** containing only one 3-imidazolium substituent was tested with two enantiomers of *t*-Boc-alanine, the enantioselectivity was as low as 1.1. Thus, the C_2 symmetric sensors, (*R*)-**168** and (*R*)-**176** were more efficient than the C_1 symmetric (*R*)-**173** in the chiral recognition.

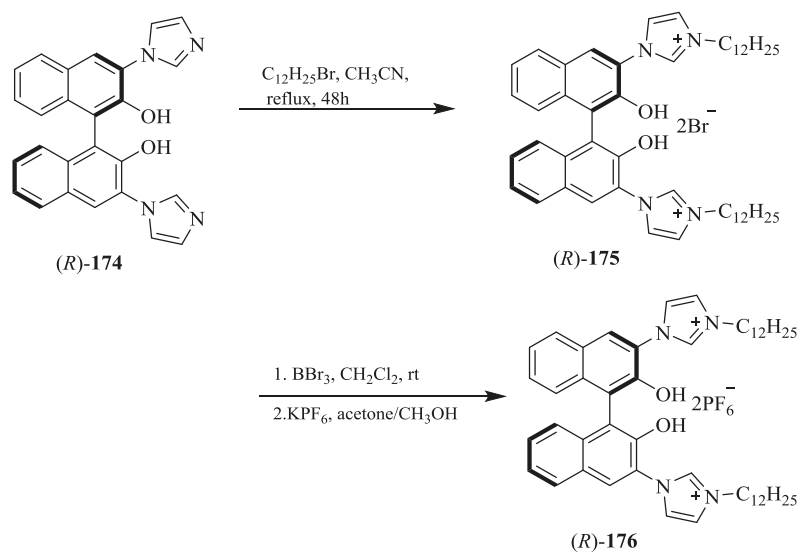


Scheme 29. Synthesis of receptors, (*R*)-**168**, (*R*)-**169** and (*R*)-**170**.

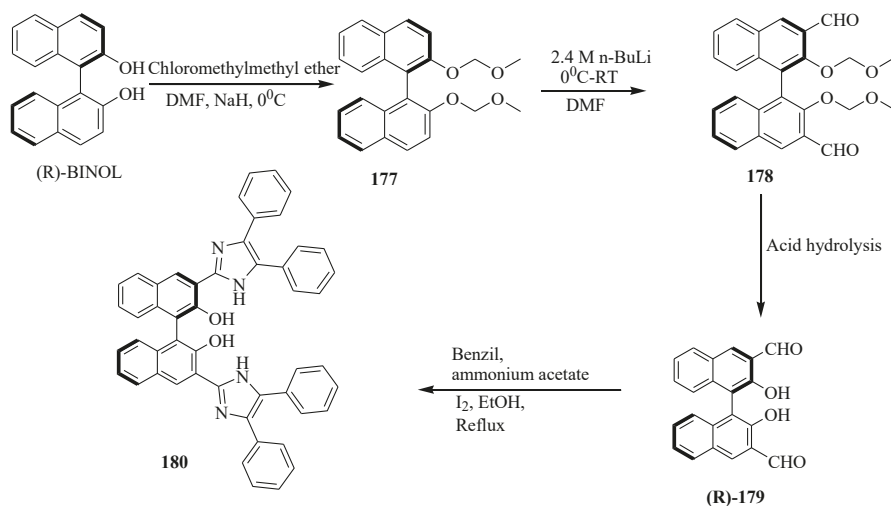


Scheme 30. Synthesis of the mono-imidazolium substituted receptor, (*R*)-**173**.

Iyer et al. [80] developed the BINOL-imidazole-based fluorescent sensor, **180** (Scheme 32). It was synthesized by the first formylation of MOM-protected BINOL, **177** followed by the deprotection of MOM and treatment with benzil in the presence of iodine to afford the desire product. This compound was found to be useful as a fluorescent sensor for Cu(II). Furthermore, the in situ generated complex, Cu(II)-**180** was studied for the fluorescent enantioselective recognition of unmodified amino acids (Table 17). L-ala displayed a large enhancement in the fluorescence intensity; whereas D-enantiomer has a small influence under the similar experimental conditions with an enantiomeric fluorescence difference ratio [$ef = I_L - I_D / I_D - I_0$] of 1.52 at the 1:50 molar ratio.



Scheme 31. Synthesis of (R)-176.



Scheme 32. Synthesis procedure of the sensor, 180.

6.2. Benzimidazole Ring Containing Receptors

Benzimidazole is a member of benzo-fused heterocycles. It has received more attention compared to the other members of the same class is possibly because generation of chiral benzimidazoles by easy synthetic protocol. A chiral center can be easily incorporated in the heterocycle and this has led to use of these molecules as a chiral organo-catalyst or as a metal atom containing catalysts [9]. Several such reports have appeared periodically. The use of this molecule in chiral molecular recognition has not received the attention it deserved. Endowed with aromatic electron cloud and almost rigid conformation for the small sized macrocycles can be good structural features for use of chiral benzimidazoles in chiral molecular recognition. Due to the synthetic ease and freedom in

structural tuning that benzimidazole core offers, it is a popular structural motif to be included in chiral ligand design. Our group has been exploring the benzimidazole core in an effective manner for over two decades and very recently we were successful in using it as a chiral host for enantiomeric guests. The Chart 4 ahead, depicts the various manners in which 2-substituted chiral benzimidazole cores can be included in ligand design. Several open chained molecular clefts with benzimidazole motif as end groups can be created using the general receptor design. Using the benzimidazole core, we have successfully synthesized few unsymmetrical macrocycles. Symmetrical macrocycles can also be prepared using various spacer (Chart 4).

Table 17. Amino acids employed in enantioselective sensing studies and their respective enantiomeric fluorescent difference ratio.

| Amino Acid ^a | ($\Delta I/I_0$)max | Ef |
|-------------------------|-----------------------|------|
| Ala | 1.50 | 1.52 |
| Phe | 1.58 | 1.68 |
| Pro | 1.44 | 1.61 |
| Ser | 2.60 | 4.04 |
| Met | 1.44 | 1.33 |

^a Methionine (Met), Proline (Pro).

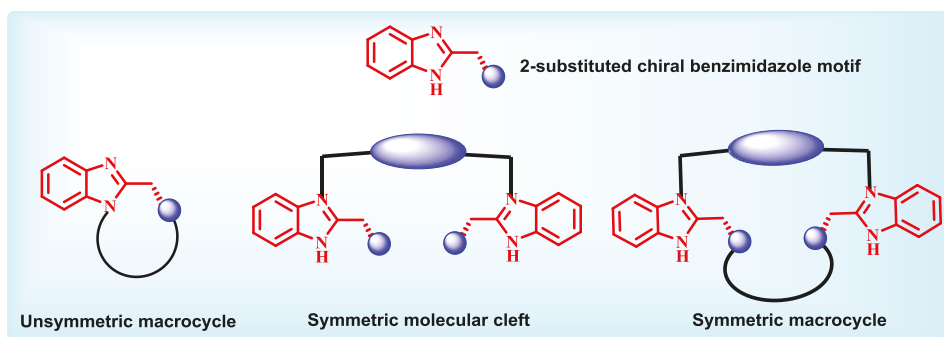


Chart 4. General design of benzimidazole containing hosts.

Recently, our group [36] has synthesized the chiral benzimidazole-based receptors (Figure 13), mono aza-15-crown-5 **181**, monoaza-[18]crown-6 (*S,R*)-**182**, (*S,S*)-**183**, and [18]crown-6-sized aza-crown **184**.

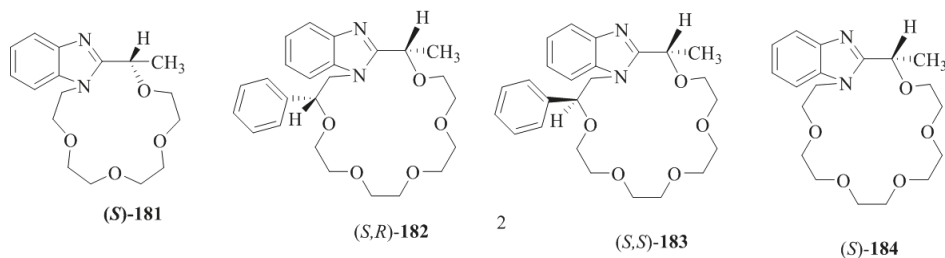


Figure 13. Chiral benzimidazole-based receptors **181**–**184**.

Supramolecular interactions between the aza-crown host, **181** and enantiomerically pure amine guests in the ionic and neutral forms displayed the enantio-discrimination ability for phenylethyl

amine and naphthylethyl amine. However, the reversed enantioselective binding was observed for [18]crown-6, aza-crowns (*S,R*)-**182**, (*S,S*)-**183** and (*S*)-**184**.

This was the first report which revealed the opposite steric preferences in chiral supramolecular systems. The experimental study was supported by single-crystal XRD data (Figures 14 and 15) and DFT studies. Size-dependent pre-organization effects leading to the corresponding molecular models was invoked to explain the origins of size-dependent enantioselective binding in aza-crowns (*S,R*)-**182**, (*S,S*)-**183** and (*S*)-**184** and (*S*)-**181**. It was established that these effects influence the preferences for guests with the opposite absolute configuration. Numerous known components, in particular nonbonding interactions responsible for the effective enantioselective binding are known, such as ligating size, hydrogen bonding, dipole-dipole interaction, pi-stacking etc. With these findings, an additional component of size-dependent pre-organization effects for the effective binding of enantiomeric guests was introduced.

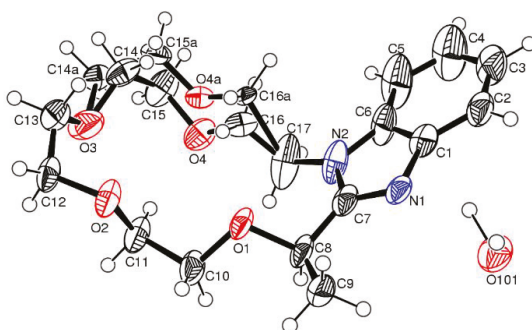


Figure 14. ORTEP representation of the X-ray crystal structure of **181**.

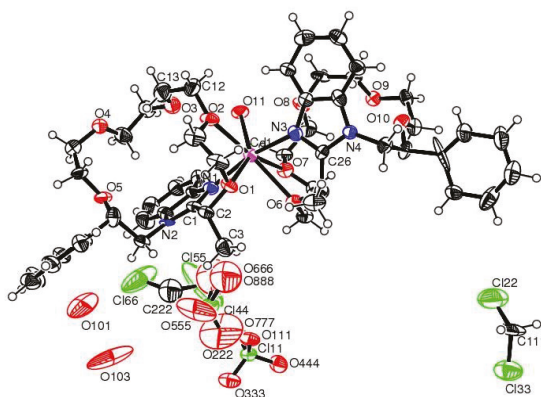
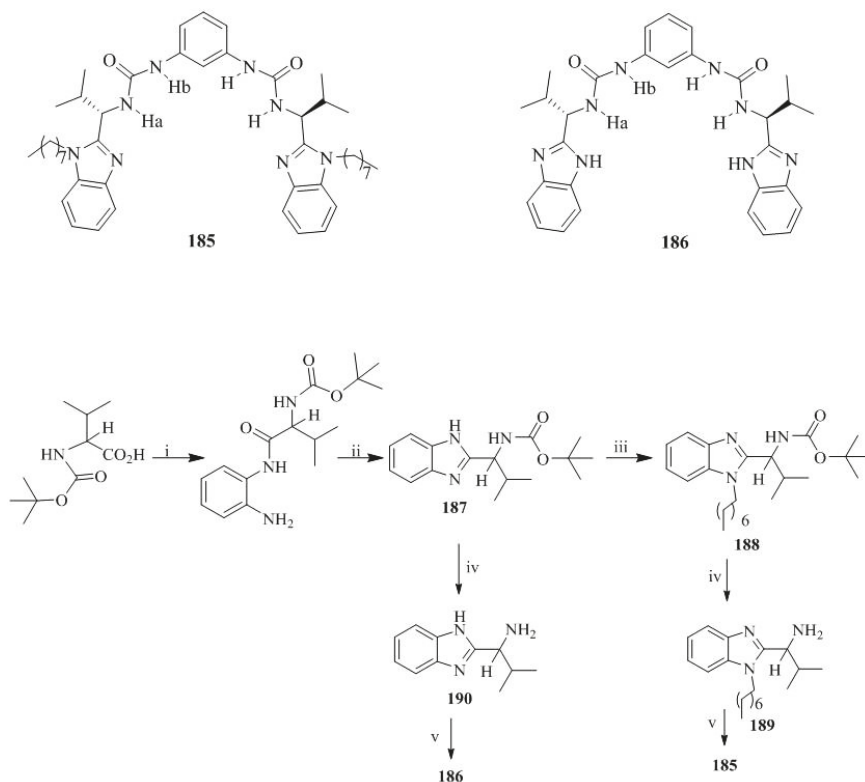


Figure 15. ORTEP diagram of the Cd^{2+} complex of (*S,R*)-**182**. Ellipsoids are given at the 50% probability level.

Ghosh et al. [81] prepared the L-Valine derived benzimidazole-based bis-ureas, **185** and **186**, according to the procedure illustrated in Scheme 33. Alkylation of the ring nitrogen of chiral benzimidazole, **187** yielded **188** and subsequent deprotection afforded the **189**. Coupling of **189** with 1,3-diisocyanatobenzene furnished the desired compound, **185**, whereas deprotection of **187** gave **190** followed by the treatment with 1,3-diisocyanatobenzene to obtain compound **186**.



Scheme 33. Reagents and conditions (i) *o*-phenylenediamine, DCC, DMAP, stirred in CH_2Cl_2 for 19 h; (ii) AcOH, heat, 2 h; (iii) NaH, THF, *n*-octyl bromide, heat 4 h; (iv) 50% TFA in CH_2Cl_2 , stirred for 3 h; (v) 1,3-dicyanobenzene, *N,N*-diisopropyl ethylamine stirred in CH_2Cl_2 for 9 h.

The fluorescence titration of **185** was performed with the tetrabutylammonium salts of tartaric and mandelic acids. The receptor, **185** exhibited clear fluorometric discrimination for D and L tartarates, while a low level of discrimination was found for mandelates. Interestingly, the compound, **186** exhibited a small preference for D-tartrate with the enantiomeric fluorescence difference ratio (*ef*) of 1.44, which signifies the steric crowding around the binding zone in **185** as the key feature for its enantioselective sensing of tartrate.

Katagiri et al. [82] reported a new achiral host on the basis of Cu(II) complex of pyridine-benzimidazole, **192**, $[\text{Cu}(\text{bmb-bpy})(\text{H}_2\text{O})(\text{OTf})_2]$ where (bmb-bpy = 6,6'-bis([(1-methylbenzimidazol-2-yl)thio)methyl]-2,2'-bipyridine) (Figure 16) for the enantioselective and chemoselective recognition of chiral carboxylic acids. Hence, the binding of chiral carboxylic acids, 2-phenylbutyric acid (PBA), 2-phenylpropionic acid (PPA), 2-bromopropionic acid (BPA) and *N*-*boc*-2-piperidinecarboxylic acid (PCA) to $[\text{Cu}(\text{bmb-bpy})(\text{H}_2\text{O})(\text{OTf})_2]$ produced an exciton-coupled circular dichroism signal. The (*R*)-PBA, (*R*)-PPA, (*R*)-PCA gave the positive first Cotton effect and negative second Cotton effect, while (*R*)-showed the negative first Cotton effect and positive second Cotton effect. Further, the opposite (*S*) enantiomers exhibited the mirror image relationship. The linear discriminant analysis (LDA) allowed the assignment of the absolute configuration, the five replicates for the each enantiomers of each carboxylic acids were analyzed at four different wavelength (333, 313, 295, and 285 nm). The LDA plot of chiral carboxylic acids with a positive first Cotton effect appear at a negative position on F1-axis, whereas the plots of the negative first Cotton effect appear at a positive

position. A stronger CD intensity shows a larger absolute value of F1, whereas a weaker CD intensity shows a smaller absolute value. F2-axis shows a small difference in the CD profile for each sample. Furthermore, enantiomeric excess of chiral carboxylic acids, have established using the eight unknown samples in the range of -100% (S) to $+100\%$ (R) plotted on the calibration line with linear regression.

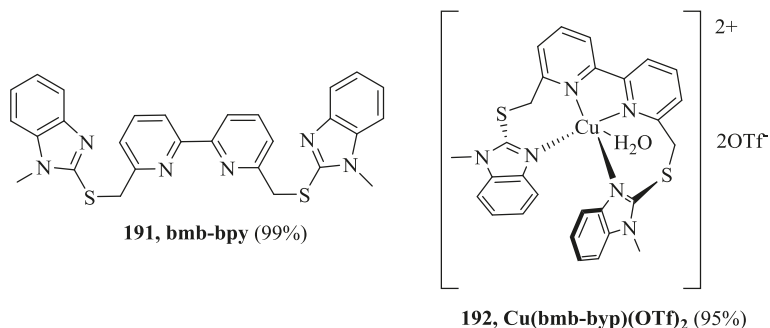


Figure 16. Pyridine-benzimidazole-based host **191**, **192**.

6.3. Triazole Ring Containing Receptors

Triazole has both pyridine and pyrrole type of nitrogens and satisfactory basic character. The chiral center can be easily attached by N-alkylation or N-acylation reactions. Presence of multiple ligating centers and aromatic nature were good enough reasons to attract attention of chiral chemists. Triazole linked hosts are considered to be better chelators for chiral guests for its electron rich nature due to the presence of three nitrogen atoms adjacent to each other. As per reports, the orientation of nitrogen atom at the third position is important for chiral discrimination of amino acids [69]. The general structural design existing in the triazole based receptors discussed in this report, incorporates one or more triazole motifs at terminal ends separated by a chiral spacer to form a molecular cleft. Triazoles could be further attached to chiral arms which function as chiral discriminators. Few macrocyclic receptors are also prepared in which triazoles are placed in macrocyclic cavity, with nitrogen atoms facing inwards to enable participation during recognition events. (Chart 5).

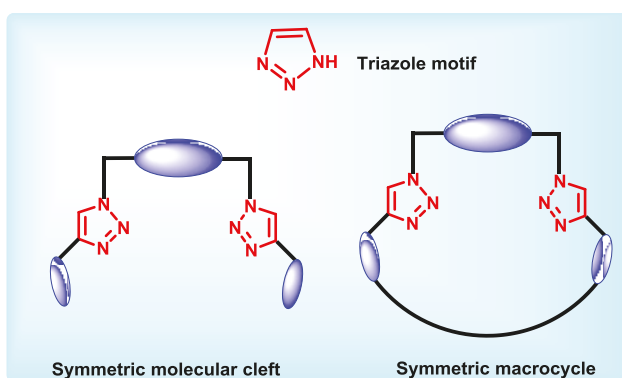


Chart 5. General design of triazole containing hosts.

Sato et al. [83] synthesized the new triazole linked hosts, (**193**, **194**) (Figure 17) by versatile, rapid and high yield copper catalyzed Huisgen-1,3-dipolar cycloaddition (Click Chemistry) of linker azide with saccharide alkyne. These two compounds, **193**, **194** then were investigated for the chiral

recognition ability. It was established that the orientation of nitrogen atoms at the 3-position of triazole rings was the most important factor for the enantiodiscrimination of amino acid esters. Thus, UV titrations revealed the triazole linked host **193** exhibited the chiral recognition preference for (*R*)-alanine isopropyl ester with $K_R/K_S = 2.13$ and for host **194** the strong complexes were formed with both the enantiomers of alanine isopropyl ester but no enantioselectivity observed. Further, the similar recognition ability of alanine isopropyl ester by the host **193** and **194** corroborated by the Fast Atom Bombardment Mass spectroscopy method.

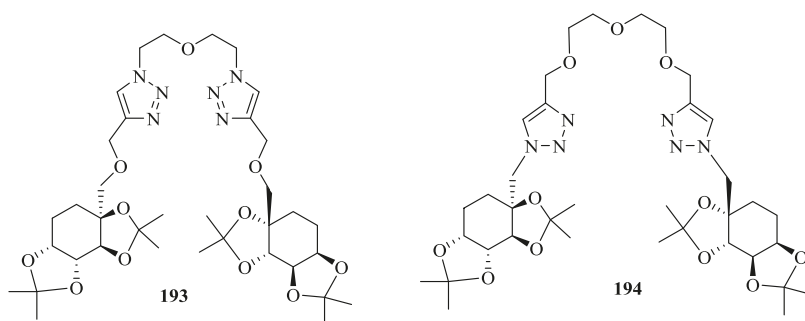
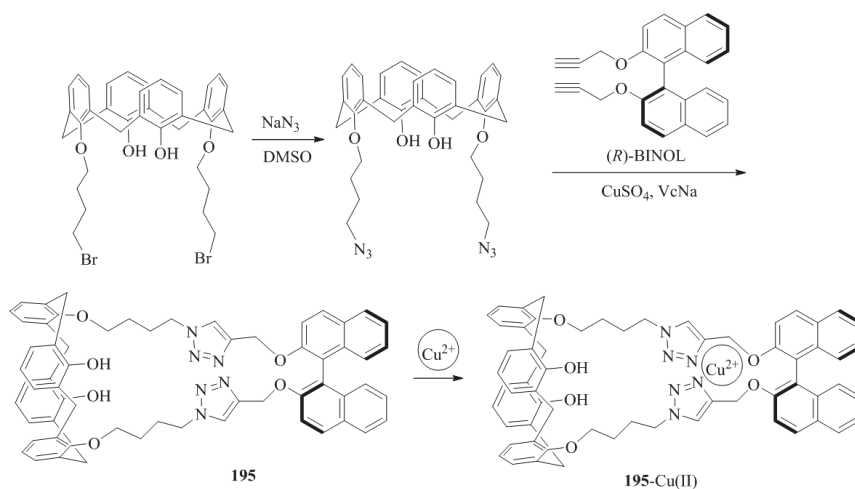


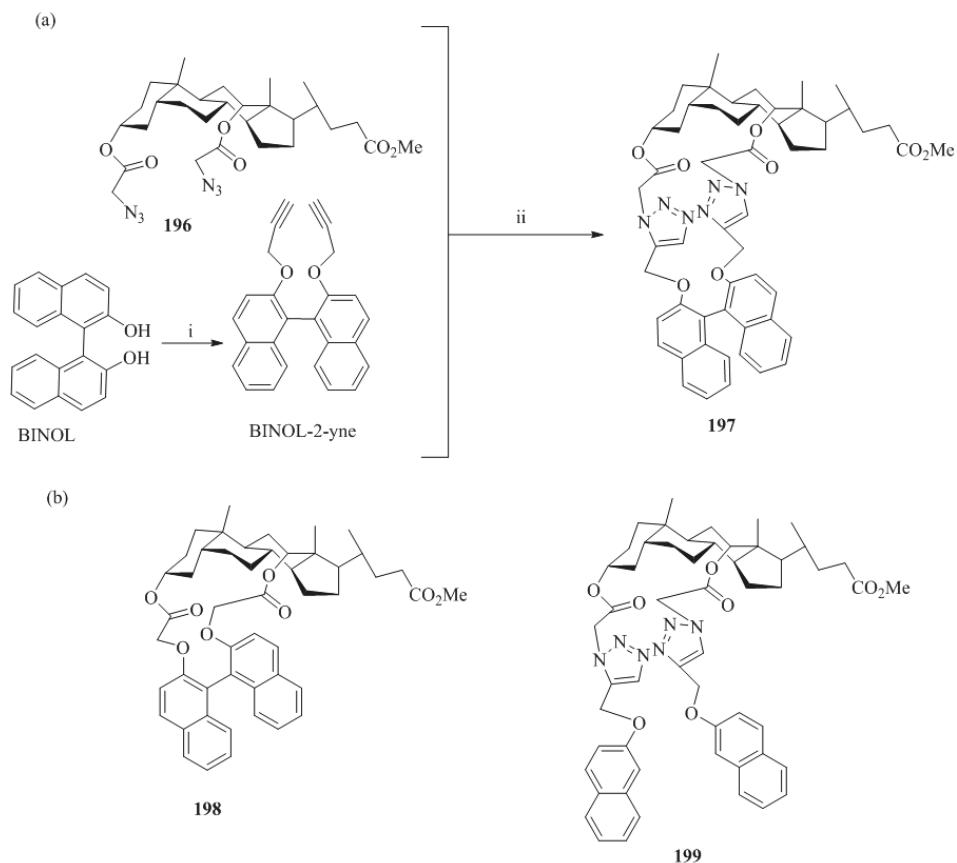
Figure 17. Triazole linked host compounds, **193** and **194**.

Li et al. [84] synthesized the fluorescent calix-[4]arene bearing a chiral 1,1'-bi-2-naphthol unit-based receptor, **195** (Scheme 34). The in situ generated complex Cu(II)-**195** were evaluated for the chiral discrimination of performance of the, (*R*)- and (*S*)-Mandelic acid using fluorimeter. The fluorescent intensity of Cu(II)-**195** complex upon addition of (*R*)-Mandelic acid increased 6.35 fold and with (*S*)-Mandelic acid increased up to 4.87 fold. Thus, the enantiomeric fluorescence difference was found to be 1.69. The tartaric acid and malic acid were also investigated and showed the increased in the fluorescence intensity for *R* enantiomers over the *S* enantiomers. Further, by using the dynamic light scattering, for mandelic acid a remarkable 100-fold detection sensitivity was increased with the detection limit of 2.0×10^{-7} M as compared to fluorescent method.



Scheme 34. Synthesis of calix-[4]arene, **195** bearing a chiral 1,1'-bi-2-naphthol and its Cu complex.

Ju et al. [85] synthesized **197** (Cyclic Deoxycholate-Triazole-BINOL conjugate) (Scheme 35) from azido-deoxycholic acid ester **196** and BINOL-2-yne via the “CuAAC” click reaction. This macrocycle is able to serve as a fluorescent turn-off sensor for Hg^{2+} ion due to the 1,2,3-triazole motif, which has an outstanding binding ability to transition metal ions. Furthermore, the corresponding $[\mathbf{197}\cdot\text{Hg}^{2+}]$ complex exhibited recognition ability for amino acids with certain enantioselectivity (Table 18). Hence, L-amino acids showed larger K_a as compared to D-amino acids. The stronger interaction of $[\mathbf{197}\cdot\text{Hg}^{2+}]$ complex with L-amino acids than with D-amino acids is a result of the chiral spatial structure provided by the deoxycholic acid scaffold.



Scheme 35. (a) Synthesis of **197**; (b) Structure of control molecules **198** and **199**.

Table 18. Association constants between $[\mathbf{197}\cdot\text{Hg}^{2+}]$ or $[\mathbf{199}\cdot\text{Hg}^{2+}]$ complex and amino acids.

| Amino Acids | $[\mathbf{197}\cdot\text{Hg}^{2+}]$ | | | $[\mathbf{199}\cdot\text{Hg}^{2+}]$ | | |
|-------------|-------------------------------------|---------------------------------|-----------|-------------------------------------|---------------------------------|-----------|
| | K_L (10^5 M^{-1}) | K_D (10^5 M^{-1}) | K_L/K_D | K_L (10^5 M^{-1}) | K_D (10^5 M^{-1}) | K_L/K_D |
| Ala | 1.284 | 1.252 | 1.026 | 0.4664 | 0.4646 | 1.004 |
| Val | 1.226 | 1.199 | 1.023 | 0.4358 | 0.4352 | 1.001 |
| His | 2.201 | 2.002 | 1.100 | 0.8610 | 0.8455 | 1.018 |
| Cys | 2.510 | 2.121 | 1.183 | 1.630 | 1.616 | 1.008 |
| Met | 2.032 | 1.841 | 1.104 | 0.7667 | 0.7764 | 0.9875 |

6.4. Benzo-Fused Furan Heterocycles Containing Receptors

Benzo-fused furans are electron rich units and hence are expected to exhibit anisotropic effects due to the presence of ring current. There are innumerable heterocycles containing benzo-fused furans. The use of this heterocyclic unit in stereo-discrimination reactions are very few. One solution to this situation was to incorporate this unit in receptors with different elements of chirality, such as the presence of chiral axis.

The benzofuran containing hosts are bestowed with excellent fluorescence properties and hence are ideal substrates for development of fluorescent sensor. Our group has designed and synthesized several interesting receptors with benzofuran motifs. The receptors discussed here originate from synthetically simple benzofuran motif which are axially linked or helically linked benzofuran rings (Chart 6). Benzofuran units can be used as a synthon to prepare crowded binols and the free hydroxyl groups of the furo fused binols can be exploited to synthesize macrocycles.

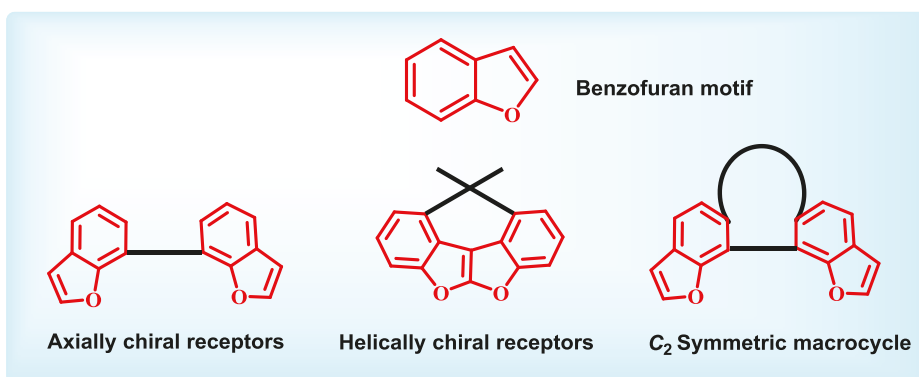
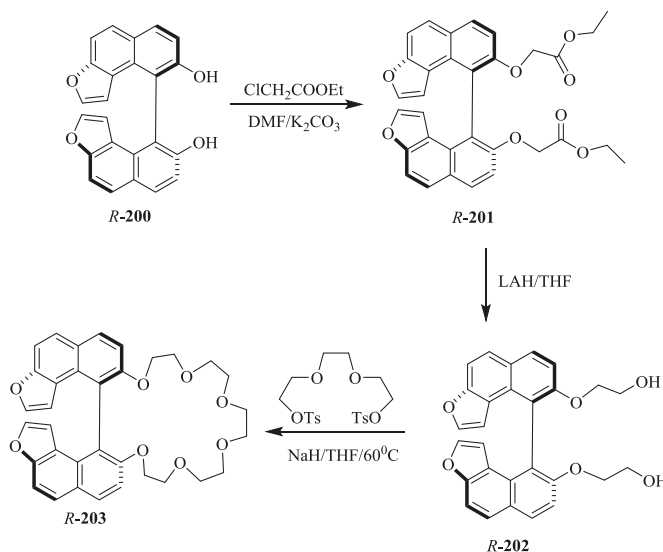


Chart 6. General design of benzofuran containing hosts.

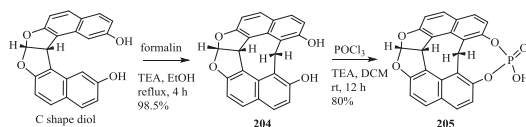
Our group [86–89] synthesized several furan ring incorporated chiral receptors. In 2007 [37] the synthesis of chiral furo fused BINOL-based crown ether, (*R*)-**203** has been reported (Scheme 36). Parent furo fused BINOL, **200** was alkylated with ethyl chloroacetate followed by the corresponding reduction and treatment with triethylene glycol tosylate to yield (*R*)-**203**.

The furo-fused BINOL derivative (*R*)-**203** has the following special features: C_2 symmetry, a sufficiently enlarged dihedral angle for better stereo-discrimination and modified electronic properties as compared to BINOL. This macrocycle (*R*)-**203** was useful as an enantioselective chiral sensor for phenylethylamine and ethyl ester of valine. Fusion of furan to BINOL resulted in a highly stereodiscriminating backbone for the chiral crown moiety. This receptor, (*R*)-**203** exhibited fluorescence enhancement differences of 2.97 and 2.55 times between two enantiomers of phenylethylamine and ethyl ester of valine, correspondingly. The ratio of association constants for two diastereomeric complexes on the basis of two enantiomers of these guests was found to be 11.30 and 7.02, respectively.

Further in 2016 [25] the C_s -symmetric rigid organophosphoric acid host, **205** (Scheme 37) was developed by the treatment of helicene diol [72], **204** with phosphoryl chloride and explored for the supramolecular induced circular dichroism sensing of chiral amino alcohol. The study revealed that the rigidity of tautomers, **205A** (Figure 18) or **205B** (Figure 19) and bulkiness of chiral amino alcohols were responsible for the resultant ICD signals (Table 19).



Scheme 36. Synthesis of furo fused BINOL-based crown ether.



Scheme 37. Synthesis of 205.

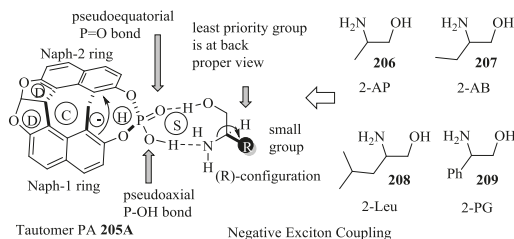


Figure 18. Proposed exciton coupling model for amino alcohols, 206–209 having small R group, binding with tautomer, 205A.

In the case of amino alcohols, 206–209 (Figure 18) with small substituents such as $-\text{CH}_3$, $-\text{C}_2\text{H}_5$, or $-\text{CH}_2\text{CH}(\text{CH}_3)_2$ present at the stereogenic center, the tautomer 205A of achiral phosphoric acid 205 is preferred. This could be possible due to cooperative hydrogen bonding, amino group of guest accepts the acidic hydrogen P–O–H of 205A, occupying a pseudoaxial position, whereas the alcohol part of the chiral guest acts as a hydrogen bond donor to P=O of the PA group, with a pseudoequatorial position on the H ring. The resultant nine membered spirocyclic hydrogen-bonded S ring is able to transfer the information on the R/S configuration at the stereogenic center of guest to host via H ring, directly attached to the chromophores, exhibited the corresponding ICD signal (negative exciton coupling). The R-enantiomers of chiral amino alcohol gave the negative sign in the ICD spectrum while S-enantiomer exhibited the mirror image.

Intriguingly, the chiral amino alcohols, **210–213** (Figure 19) with bulky substituent at the stereogenic center on interaction with the achiral phosphoric acid preferred the 189B tautomer to result into reversed induced CD pattern to the amino alcohols with small substituent at stereogenic center. This is attributed owing to the amino group of guest hydrogen bonded with an acidic P–O–H group, occupies a pseudoequatorial position. Simultaneously, the –OH group acts as hydrogen bond donor to the P=O group of **205B** and occupies a pseudoaxial position to the rigid, conformationally locked H ring, the newly formed. Resulted complex of host and guest able to transfer the chiral information of guest by the S-ring to H ring and to the chromophore of the host to induced the signals in the CD. Thus, this mechanistic demonstration exemplified the binding mode of the host dependent on the bulk of the substituent present at stereogenic center of guest chiral amino alcohols.

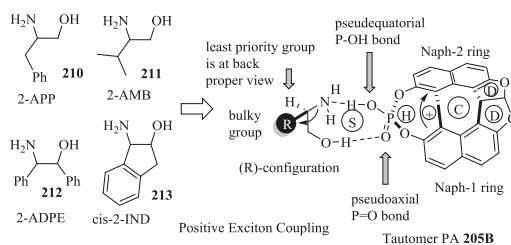


Figure 19. Proposed exciton coupling model for amino alcohols, **210–213** having bulky R group, binding with tautomer, **205B**.

Complexation of host phosphoric acid, **205A** mode, with guest, **206** (2-AP) gave the highest $\Delta \epsilon$ value at $498.65 \text{ cm}^{-1} \text{ M}^{-1}$. Similarly, the **205B** mode resulted in highest $\Delta \epsilon$ value of $641.13 \text{ cm}^{-1} \text{ M}^{-1}$ for **211** (2-AMB) (Table 19).

Table 19. ICD Results for Amino Alcohols, **206–213** with **205**.

| Guests | First CE | Second CE | $\Delta \epsilon (\text{cm}^{-1} \text{ M}^{-1})$ | $g = \Delta \epsilon / \epsilon \times 10^{-3}$ (at First CE) | Binding Mode |
|---------------------|----------|-----------|---|--|--------------|
| (R)- 206 | – | + | 498.65 | 35.9 | A |
| (R)- 207 | – | + | 121.10 | 15.16 | A |
| (R)- 208 | – | + | 85.48 | 10.8 | A |
| (R)- 209 | – | + | 7.12 | 10.0 | A |
| (R)- 210 | + | – | 124.66 | 10.5 | B |
| (R)- 211 | + | – | 641.13 | 9.3 | B |
| (1R,2S)- 212 | + | – | 4.63 | 0.1 | B |
| (1R,2S)- 213 | + | – | 3.21 | 0.4 | B |

Subsequently in 2017, [48] Hasan et al. developed the dioxa[6]helicenes-based supramolecular chirogenic system (**214**) for chiral recognition of enantiopure *trans*-1,2-cyclohexanediamine (Figure 20). The host, **214** was obtained using the reaction of dioxa[6]helicenes and (1S)-camphanic chloride and the enantioselective fluorescence study revealed that **214** serves as a turn-on fluorescent sensor for *trans*-cyclohexyl diamine with the excellent enantioselective factor, $\alpha = K_{SS}/K_{RR} = 6.3$ in benzene as a solvent.

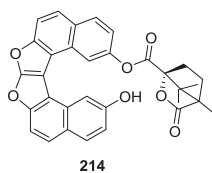


Figure 20. Helicene camphanate.

6.5. Receptors with Nitrogen and Oxygen Containing Five Membered Heterocycles

Chiral Oxazolines and oxazolidinones have played one of the most noticeable roles [90,91] in chiral processes, by providing Evans' chiral auxiliaries, chiral organo-catalysts and chiral metal-based catalysts. The use of these molecules in the chiral receptors has received some attention. Oxazoline coordinates to a wide range of transition metals. Stereochemical outcome of the metal catalyzed reaction is strongly governed by the favorable placement of stereogenic centre, the chelating nitrogen atom of oxazoline ligand and the metal ion.

The oxazoline based C_3 -symmetric receptors discussed in this report have tripod like structures with terminal oxazolines or in another case, the free arms of the tripod linked to benzene motif, forming a molecular cage (Chart 7). The types of interactions which are observed in such hosts are π - π interactions due to aromatic oxazoline rings and tripod hydrogen bonding interactions due to the flexible arms containing oxazolines.

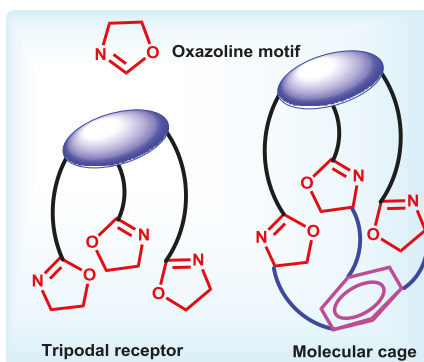


Chart 7. General design of oxazoline containing receptors.

In 2003, Ahn et al. [22] developed the benzene-based tripodal C_3 -symmetric oxazoline receptors, **215a–c** (Figure 21) for the chiral molecular recognition of α -chiral primary ammonium ions (Table 20). Surprisingly, a good level of the enantioselectivity was observed by one of the receptors **215a**, as it provides the C_3 symmetric chiral environment on guest binding. The general results of chiral discrimination for α -substituted guests revealed that the π - π interaction is an important factor. Binding studies using NMR and isothermal titration calorimetry confirmed the host guest complexes formation influenced by the enthalpy changes and minor negative contribution of entropy changes.

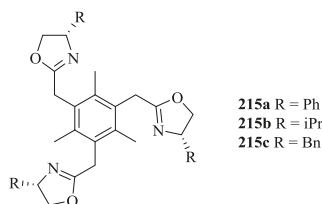


Figure 21. C_3 -symmetric oxazoline receptors, **215a–c**.

The same group [92] later established the use of C_3 symmetric receptor, **215a** for the enantioselectivity of β -chiral primary ammonium ions by utilizing a bifurcated H-bonding. Further, the extraction experiments confirmed that this interaction plays a crucial role in the chiral discrimination between the host and guest. The X-ray data proved the existence of such H-bonding.

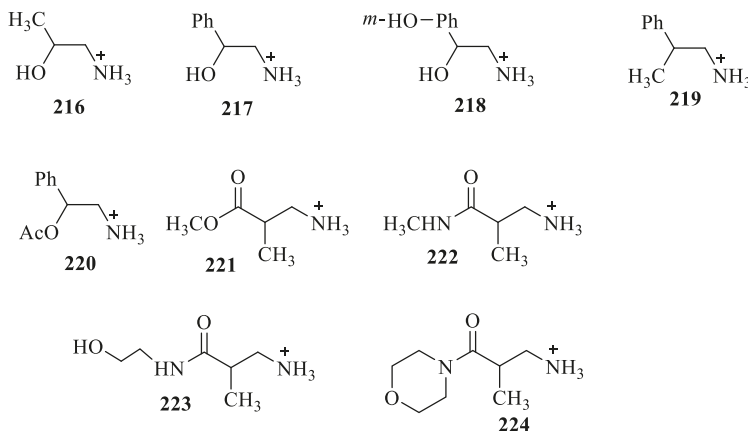
Hence, this article demonstrated that this type of binding is suitable for the chiral molecular recognition with C_3 -symmetric tripodal oxazoline receptors and further extended toward ammonium ions of α -, β -, and α , β -chiral primary amines Tables 21 and 22.

Table 20. Enantioselective binding of Tris(oxazoline), **215a** toward Racemic Ammonium Salts.

| Racemic Ammonium Guest | Enantioselectivity ^a | Extraction (%) ^b |
|----------------------------------|---------------------------------|-----------------------------|
| α -phenylethylamine | 71(<i>R</i>):29(<i>S</i>) | 82 |
| α -(1-naphthyl)ethylamine | 70:30 | 99 |
| Phenylglycine methyl ester | 78(<i>S</i>):22(<i>R</i>) | 60 |
| Tryptophan methyl ester | 67(<i>S</i>):33(<i>R</i>) | 57 ^c |
| Alanine methyl ester | 53(<i>S</i>):47(<i>R</i>) | 41 |
| Phenylalanine methyl ester | 55(<i>S</i>):45(<i>R</i>) | 36 |

^a Enantioselectivity of the ammonium ion extracted from excess racemic salts ($\text{RNH}_3^+\text{Cl}^-$, 10 M equivalent, 0.5 M in D_2O ; 0.6 M NaPF_6) by tris(oxazoline) **215a** (0.05 M in CDCl_3) at 25 °C. ^b Percentage of the ammonium salts extracted into CDCl_3 with respect to tris(oxazoline) **1a**. ^c Extraction at 45 °C.

Table 21. Selective binding of **215a** toward racemic ammonium salts of β -chiral amines, **216–224**.



| Entry | Racemic Guest | Enantioselectivity ^a | Extraction (%) ^b |
|-------|---------------|---------------------------------|-----------------------------|
| 1 | 216 | 63:37 ^c | 50 |
| 2 | 217 | 75:25 | 60 |
| 3 | 218 | 72:28 | 40 |
| 4 | 219 | 50:50 | 97 |
| 5 | 220 | 58:42 | 72 |
| 6 | 221 | 58:42 | 71 |
| 7 | 222 | 71:29 | <5 |
| 8 | 223 | 61:39 | 10 |
| 9 | 224 | 83:17 | <5 |

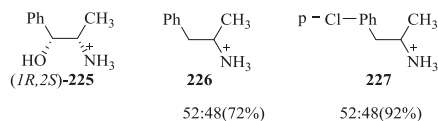
^a Enantiomeric ratio of the extracted guest from excess racemic salts (10 M equiv., 0.5 M in D_2O) by PhBTO **215a** (0.05 M in CDCl_3) at 25 °C. ^b Percentage of the ammonium salt extracted into CDCl_3 with respect to PhBTO **215a**. ^c Major: (*R*)- isomer.

Removing the β -OH group from **225**, as in **226** or **227**, (Figure 22) results in low enantioselectivities, hence indicating that the secondary H-bond interaction is critical to secure the necessary environment for chiral discrimination as confirmed by the crystallographic structure of the corresponding **215–225** complex.

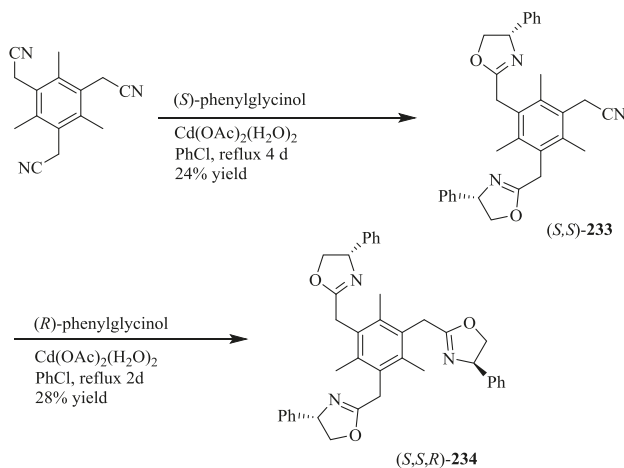
Table 22. Selective Binding of **215** toward Racemic Ammonium Salts of α -alkyl-substituted Chiral Amine.

| Entry | Racemic Guest | Enantioselectivity | Extraction (%) |
|-------|---------------|--------------------|----------------|
| 1 | 228 | 66:34 ^c | 74 |
| 2 | 229 | 61:39 | 20 |
| 3 | 230 | 56:44 | 26 |
| 4 | 231 | 53:37 ^c | 41 |
| 5 | 232 | 55:45 ^c | 36 |

^a Enantiomeric ratio of the extracted guest from excess racemic salts (10 M equiv., 0.5 M in D₂O) by **215** (0.05 M in CDCl₃) at 25 °C. ^b Percentage of the ammonium salt extracted into CDCl₃ with respect to **215**. ^c Major: (*S*)-isomer.

**Figure 22.** Chiral ammonium analytes, **225–227**.

In the next article [93] the development of a benzene-based tripodal oxazoline receptor with C₁-symmetry, **234** upon changing the symmetry of chiral environment from C₃ to C₁ was reported (Scheme 38). The synthetic strategy was based on the coupling of tris-(cyanomethyl)mesitylene with (*S*)-phenylglycinol in the presence of 5 mol % Cd(OAc)₂ to furnish (*S,S*)-bis(oxazoline), **233** and subsequent treatment with (*R*)-phenylglycinol under the similar reaction conditions afforded (*S,S,R*)-**234** in 28% isolated yield.

**Scheme 38.** Synthesis of (*S,S,R*)-**234**.

Subsequently, **234–237** were explored for the chiral discrimination by using extraction experiment. The tripodal receptors with two phenylglycinol-derived oxazolines displayed significant enantioselectivity for racemic α -chiral ammonium ions (Table 23, entries 1–8). It was revealed that the changing receptor's symmetry, from C_3 to C_1 , causes intense improvement in the binding mode and chiral recognition. Table 24 shows that **234** was more enantioselective than other hosts, but less selective than **235**. However, **234** gave significantly lower values of the % extraction than other receptors. Furthermore, the receptor **236** and **237** (Figure 23) extracted (*S*)- α -phenylethylammonium ion preferentially over the (*R*)-guest demonstrated the reverse sense of the chiral discrimination in comparison with that of **234**.

Table 23. Enantioselective Extraction Experiments Using **234–237** towards α -Chiral Organoammonium Guests.

| Entry | Receptor | Ammonium Guest | Enantioselectivity | Extraction (%) |
|-------|-------------|--|-------------------------------|----------------|
| 1 | 235 | PhCH(NH ₃ ⁺) CH ₃ | 71(<i>R</i>):29(<i>S</i>) | 82 |
| 2 | 235 | PhCH(NH ₃ ⁺) CO ₂ Me | 78(<i>S</i>):22(<i>R</i>) | 60 |
| 3 | 234 | PhCH(NH ₃ ⁺) CH ₃ | 64(<i>R</i>):36(<i>S</i>) | 51 |
| 4 | 234 | PhCH(NH ₃ ⁺) CO ₂ Me | 70(<i>S</i>):30(<i>R</i>) | 22 |
| 5 | 236a | PhCH(NH ₃ ⁺) CH ₃ | 59(<i>S</i>):41(<i>R</i>) | 100 |
| 6 | 236a | PhCH(NH ₃ ⁺) CO ₂ Me | 62(<i>S</i>):38(<i>R</i>) | 91 |
| 7 | 236b | PhCH(NH ₃ ⁺) CH ₃ | 58(<i>S</i>):42(<i>R</i>) | 80 |
| 8 | 236b | PhCH(NH ₃ ⁺) CO ₂ Me | 69(<i>S</i>):31(<i>R</i>) | 69 |
| 9 | 236c | PhCH(NH ₃ ⁺) CH ₃ | 50(<i>S</i>):50(<i>R</i>) | - |
| 10 | 237 | PhCH(NH ₃ ⁺) CH ₃ | 50(<i>S</i>):50(<i>R</i>) | 70 |

Table 24. Enantioselective Binding of Receptors, **235**, **240a**, and **240b** toward Organoammonium Ions **98** and Ala Methyl Ester.

| Receptor-Guest | Temp (°C) | Enantioselectivity | Binding (%) ^a |
|------------------------------------|-----------|--|--------------------------|
| 235-(R,S)-98 | 25 | 71(<i>R</i>):29(<i>S</i>) ^c | 82 |
| 240a-(R,S)-98 | −30 | 57(<i>R</i>):43(<i>S</i>) | ~100 |
| | −50 | 60(<i>R</i>):40(<i>S</i>) | ~100 |
| 240b-(R,S)-98 | −30 | | |
| | −50 | 61(<i>R</i>):39(<i>S</i>) | 73 |
| 235-(R,S)-Ala Methyl ester | 25 | 47(<i>R</i>):53(<i>S</i>) ^c | 41 |
| 240a-(R,S)-Ala Methyl ester | 10 | 61(<i>R</i>):39(<i>S</i>) | 62 |
| | −10 | 60(<i>R</i>):40(<i>S</i>) | 65 |
| | −30 | 61(<i>R</i>):39(<i>S</i>) | 67 |
| | −50 | 64(<i>R</i>):36(<i>S</i>) | 68 |
| 240b-(R,S)-Ala Methyl ester | −10 | 64(<i>R</i>):36(<i>S</i>) | 79 |
| | −30 | 66(<i>R</i>):34(<i>S</i>) | 83 |
| | −50 | 72(<i>R</i>):28(<i>S</i>) | 76 |

^a Percentage of receptor-guest adduct with respect to unbound guest, calculated for 1 equiv. of receptor.

Further this group [94] reported the preparation of chiral cage-like receptors, **240a** and **240b** (Scheme 39) via the reaction of corresponding 3-hydroxyphenyl-substituted tripodal oxazolines, **238** with capping molecules, **239**. The chiral recognition behavior of **240a** and **240** was studied for two typical chiral guests; α -phenylethylammonium **98** and alanine methyl ester as α -aryl- and α -alkyl substituted amines by using ¹H NMR (Table 24). However, **240** preferentially binds to (*R*)-**98** with a lower enantioselectivity as compared to **202**. Furthermore, **240** is able to recognize alanine methyl ester with excellent enantioselectivity (7:3), but chiral discrimination is not effective in the case of **235**. The degree of chiral discrimination with the cage-like receptors is distinctive from the open sensors, attributed to narrowed space offered for the guest.

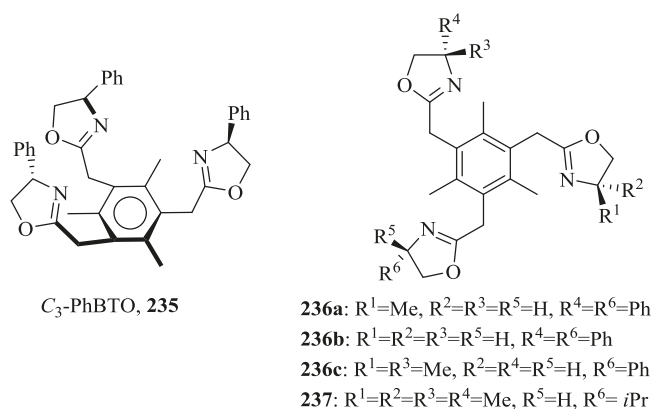
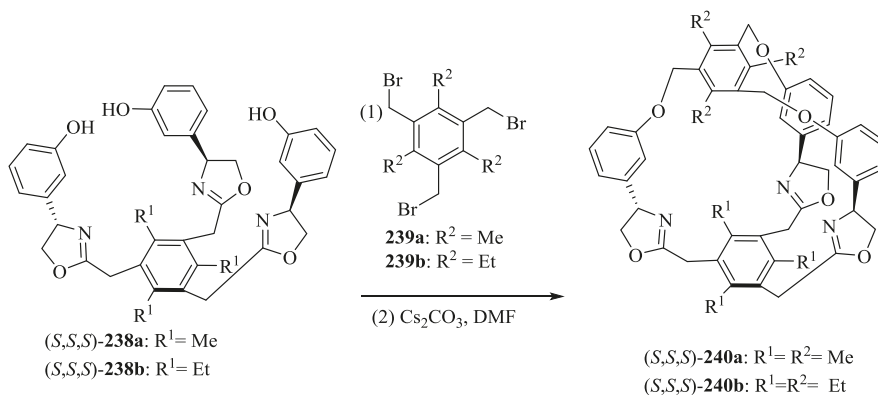


Figure 23. Receptor 235, 236, and 237.

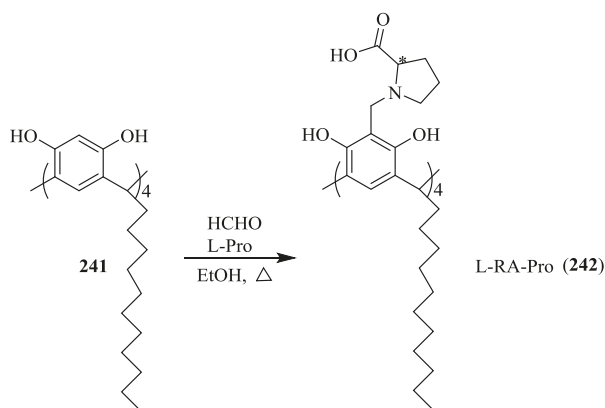
Scheme 39. Synthesis of cage-like receptors, (S,S,S) -**240a** and (S,S,S) -**240b**.

7. Miscellaneous Heterocyclic Receptors

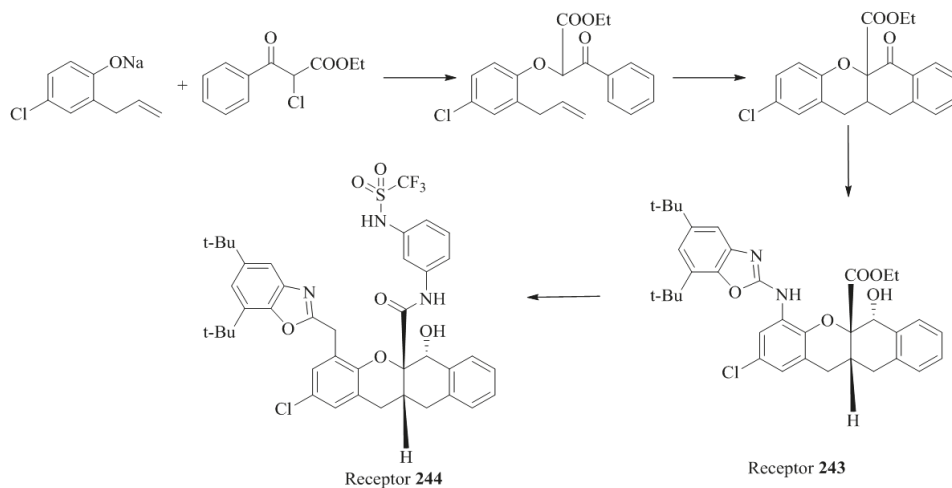
Apart from the heterocycles mentioned above, there exists a group of heterocyclic receptors which have a few but significant experimental findings. Given below is the group of such group used in chiral recognition receptors. Hegner et al. [28] described the synthesis of chiral amphiphilic calix[4]resorcinarene, tetrakis(*N*-methylprolyl)tetraundecylcalix-[4]resorcinarene, **242** (Scheme 40), bearing four *L*-prolyl moieties at the macrocyclic upper rim and four undecyl chains at the lower rim. The methodology consists of the Mannich-type reaction of tetraundecylcalix[4]resorcinarene, **241**, *L*-proline, and formaldehyde to yield the desired product. The supramolecular complex of calixresorcinarene and Cu(II) displayed the enantioselective recognition properties for phenylalanine with the stronger binding for *D*-phenylalanine.

Moran et al. [95] synthesized the *cis*-tetrahydrobenzoxanthene receptors, **243**, **244** by following the synthetic route given in Scheme 41. The binding properties of **243** have been evaluated by 1H NMR titration with decanoic acid and Cbz-glycine (Cbz = benzyloxycarbonyl) to give $K_a = 1.2 \times 10^4 M^{-1}$ and $1.5 \times 10^4 M^{-1}$, respectively. However, the titration of a racemic mixture of **243** with the amino acid derivatives, such as Cbz-phenylglycine, exhibited the association ($K_a = 2.3 \times 10^4 M^{-1}$) but neither splitting of the 1H NMR signals of host nor chiral discrimination were observed. Further, the receptor, **243** was converted to **244** by treatment with the lithium salt of *m*-phenylenediamine, followed by the

reaction with trifluoromethanesulfonic anhydride. The titrations of racemic host carried out with enantiomeric pure guests (amino acid derivatives, Table 25), resulted in splitting of the $^1\text{H-NMR}$ signals of **244**, owing to the chiral discrimination, and confirming significant enantioselectivity for **244**. The racemic receptor, **244** then was treated with ethoxycarbonyl-L-leucine and two corresponding enantiomers of the host have been separated on preparative TLC.



Scheme 40. Synthetic route to L-RA-Pro, **242**.

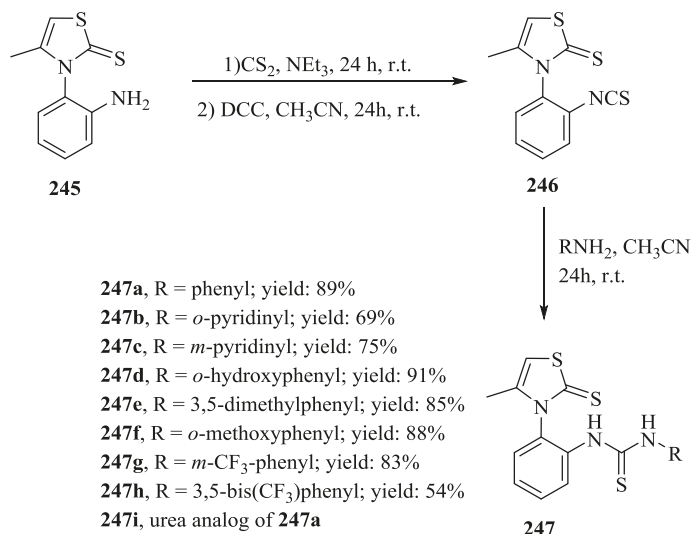


Scheme 41. *cis*-tetrahydrobenzoxanthene receptors **243**, **244**.

Table 25. Enantioselective discrimination for receptor, **244** with different guests in CDCl_3 at 20°C .

| Guest | K_a |
|--------------------------|-------|
| Ethoxycarbonyl-L-proline | 57.0 |
| Cbz-L-phenylglycine | 16.0 |
| Cbz-L-phenylalanine | 15.0 |
| Ethoxycarbonyl-L-alanine | 8.4 |
| Ethoxycarbonyl-L-leucine | 7.6 |
| BOC-L-leucine | 4.0 |

Roussel et al. [96] reported the non-racemic atropisomeric 1-(2-(4-methyl-2-thioxothiazol-3(2*H*)-yl)phenyl)-3-(hetero)aryl(thio)ureas, **247a–h** (Scheme 42). The synthesis was carried out on the basis of parent enantiopure amino-thiazoline-2-thione, **245**, which was converted into the corresponding isothiocyanate, **246** followed by the reaction with the desired aniline derivatives. These thioureas were investigated as neutral anion receptors for the chiral recognition of some amino-acids derivatives using NMR showing moderate binding affinities and discrimination (Table 26). It was exemplified that the intramolecular H-bonding apparently play a noticeable role in the fine tuning of binding and lead to the activation or deactivation depending upon the interaction site.



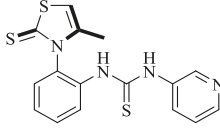
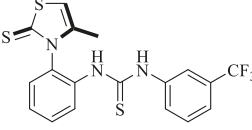
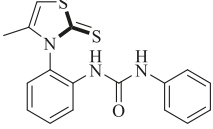
Scheme 42. Synthesis of thiourea, **247a–h** from amino-2-thiazoline, **245**.

Periasamy et al. [97] synthesized the Troger's base, **248** (Scheme 43) by reported synthetic methodology via the reaction of *p*-anisidine with paraformaldehyde in the presence of AlCl₃ and followed by the enantioseparation with *O,O'*-dibenzoyl-L-tartaric acid as a resolving agent. Further, the amino alcohol, **249** was prepared from the chiral methoxy Troger's base, **248** by using a standard procedure for the α -alkylation of tertiary amines. These chiral compounds, **248** and **249** demonstrated a good chiral recognition behavior for several carboxylic acids as determined by NMR (Table 27).

Table 26. Binding constant (K_a) for the 1:1 complexes formed between thioureas, **247a,c,g** and urea **247i** and tetrabutylammonium salts of some *N*-Acetyl amino-acid or naproxen in CD₃CN at 20 °C (¹H NMR titration).

| Chiral Selectors | <i>N</i> -Ac-amino acid Tetrabutyl Ammonium Salt | Association Constants (M ⁻¹) | Discrimination |
|-------------------------|---|---|-----------------------------------|
| <p>247a (aR)</p> | (L)- <i>N</i> -Ac-Phe-COO ⁻ | 540 | L/D 1.60 D/L 1.15 ^a |
| | (D)- <i>N</i> -Ac-Phe-COO ⁻ | 330 | |
| | (L)- <i>N</i> -Ac-Val-COO ⁻ | 600 | |
| | (D)- <i>N</i> -Ac-Val-COO ⁻ | 700 | |

Table 26. Cont.

| Chiral Selectors | N-Ac-amino acid Tetrabutyl Ammonium Salt | Association Constants (M ⁻¹) | Discrimination |
|---|--|---|--|
|  247c (aS) | (L)-N-Ac-Phe-COO ⁻ (D)-N-Ac-Phe-COO ⁻ | 1150 2300 | D/L 2.00 |
|  247g (aS) | (L)-N-Ac-Phe-COO ⁻ (D)-N-Ac-Phe-COO ⁻ | 800 960 | D/L 1.20 ^a |
|  247i (aR) | (L)-N-Ac-Phe-COO ⁻ (D)-N-Ac-Phe-COO ⁻ (L)-N-Ac-Val-COO ⁻ (D)-N-Ac-Val-COO ⁻ | 1250 1550 2150 2350 | L/D 1.25 ^a D/L 1.10 ^a |
| (aR) 247i (aS) 247i | (L)-N-Ac-Leu-COO ⁻ | 2750 3900 | 1.42 |
| (aR) 247i (aS) 247i | (S)-Naproxenate | 1330 1900 | 1.43 |
| (aR) 247i (aS) 247i | (L)-N-Ac-Trp-COO ⁻ | 825 1150 | 1.47 |

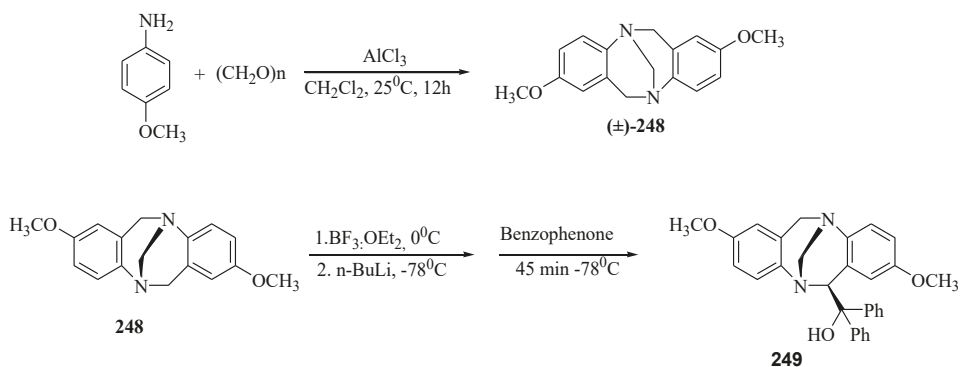
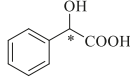
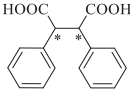
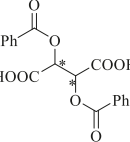
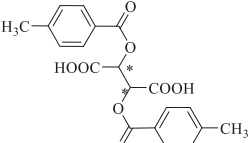
^a Ratio less than 1.3 are under the limit of confidence.Scheme 43. Synthetic methodology for Troger's base, **248** and its amino alcohol derivative, **249**.

Table 27. Chemical Shift changes ($\Delta\delta$) and chemical shift non-equivalence ($\Delta\Delta\delta$) observed in ^1H NMR spectra of guest acids in the presence of hosts, **248** and **249**.

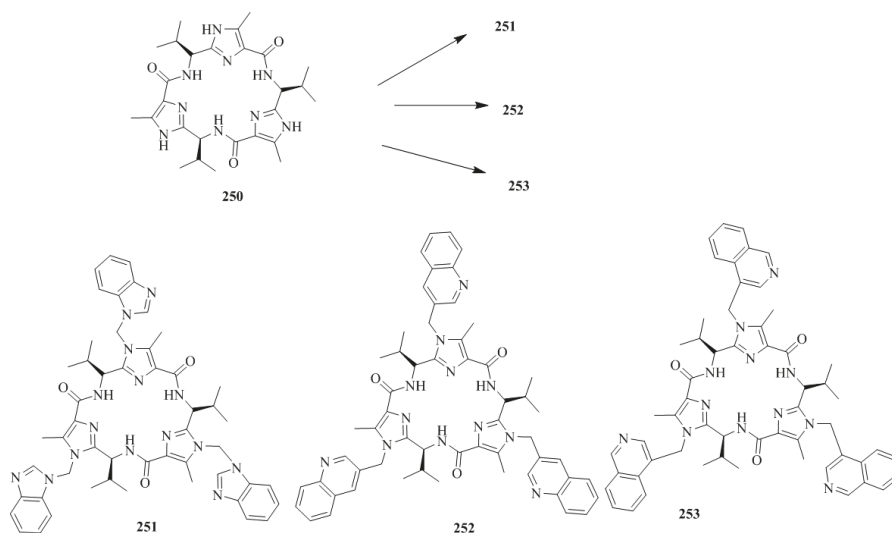
| Guests | Observed Signals | $\Delta\delta(\text{ppm})$ | | $\Delta\Delta\delta$ (Hz) | |
|---|--------------------------|------------------------------------|----------------------|---------------------------|-------------------|
| | | 248 | 249 | 248 | 249 |
|  Mandelic acid | -CH | -0.13 -0.12 -0.205 -0.217 | -0.122 -0.14 - | 4 4.8 ^b | 7.2 - |
|  2,3-diphenylsuccinic acid | -CH | -0.08 -0.11 | - | 12 | 0 |
|  O,O'-dibenzoyl tartaric acid | Ortho CH of phenyl ring | -0.060 -0.008 | -0.101 -0.137 | 21.2 | 14.4 ^c |
|  O,O'-ditoluoyl tartaric acid | Ortho CH of toluoyl ring | -0.001 -0.050 | -0.05 0.102 | 20.8 | 20.4 ^c |

The chiral recognition study (Table 27) established that the chiral methoxy Troger's base **248** exhibited better enantiodiscrimination towards the C_2 -symmetric acids such as 2,3-diphenylsuccinic acid, *o,o'*-dibenzoyl tartaric acid, and *o,o'*-ditoluoyl tartaric acid. Whereas, the C_1 -symmetric **249** was showed better discrimination towards unsymmetrical acids mandelic acid and 1,1'-binaphthyl-2,2'-diylphosphoric acid.

Haberhauer et al. [98] synthesized the C_3 -symmetric imidazole-containing macrocyclic peptide receptors, (**251**–**253**) (Scheme 44) with different binding arms. The simple using *N*-alkylation of known scaffold, **250** with the corresponding halogenomethyl compounds afforded the desired receptors.

These hosts were employed as chiral scaffolds for the enantioselective recognition of chiral primary organoammonium ions by using the ^1H NMR titration techniques. The arms of receptors, nitrogen-containing aromatic heterocycles were selected as simple units due to their rigidity, bulkiness, and ability to transfer the chiral information of the scaffold to the active binding site, thereby making the enantioselective discrimination possible. The results obtained for the chiral discrimination with several guests are summarized in Tables 28 and 29. The binding constant of receptors **251**–**253** with perchlorate salts of (*R*)-PEA and (*S*)-PEA were determined Table 28. The benzimidazole receptor, **251** on interaction with the (*R*)-PEA and (*S*)-PEA influenced the protons towards upfield around 0.10 ppm. The titration curve obtained demonstrated the pseudo linear progression, and found smaller binding constants less than 1 M^{-1} owing to receptor, **251** could not orient basic nitrogens of benzimidazole in such a way to form the stable complex. For the quinoline receptor **252**, obtained the quite low value of binding constant as 200 M^{-1} for (*R*)-PEA and 480 M^{-1} for (*S*)-PEA respectively for both enantiomers with maximum 0.03 ppm and 0.06 ppm chemical shift. In the case of isoquinoline receptor, **253** large

chemical shift around 0.3 ppm observed with binding constants, 4500 M⁻¹ for (S)-PEA and 30,000 M⁻¹ for (R)-PEA.



Scheme 44. Synthesis of C₃-symmetric imidazole-containing macrocyclic peptides receptor (251–253).

Table 28. Binding constants K_a (M⁻¹) for the formation of 1:1 complexes of 218–220 with the perchlorates of (R)- and (S)- α -phenylethylamine in CDCl₃ at 298 K^a.

| Entry | Guest | 218 | 219 | 220 |
|-------|---------|-----|-----------|-----------------------------|
| 1 | (R)-PEA | <1 | 200(± 30) | 30000(± 11000) ^b |
| 2 | (S)-PEA | <1 | 480(± 60) | 4500(± 590) |

^a The association constants K_a (M⁻¹) for the formation of 1:1 complexes were measured using ¹H NMR spectroscopic titrations. ^b A host concentration of 2.5×10^{-4} M was used for titration studies, because of the high binding constant.

For the titration of quinoline receptor 252 with other guests (Table 29) revealed the maximum chemical shift observed in the range of 0.01 ppm and 0.05 ppm and binding constants for the complexes were more similar for (R)-PEA and (S)-PEA. Further, quite small binding constant were obtained for 251*(R)-AH and 251*(S)-AH with the respective values of 360 M⁻¹ and 100 M⁻¹. More interestingly, high enantioselectivities were furnished for the complexes of 252 with (R)-BA vs. (S)-BA and for the complexes of 252 with (R)-PAM vs. (S)-PAM. Intriguingly, the binding constant values of isoquinoline receptor 253 with the both the enantiomers of guests were found to be ten times larger than that of quinolone receptor 252. In general comparison of receptors 252 and 253 exemplified the high sensitivity to small change in the guest molecules.

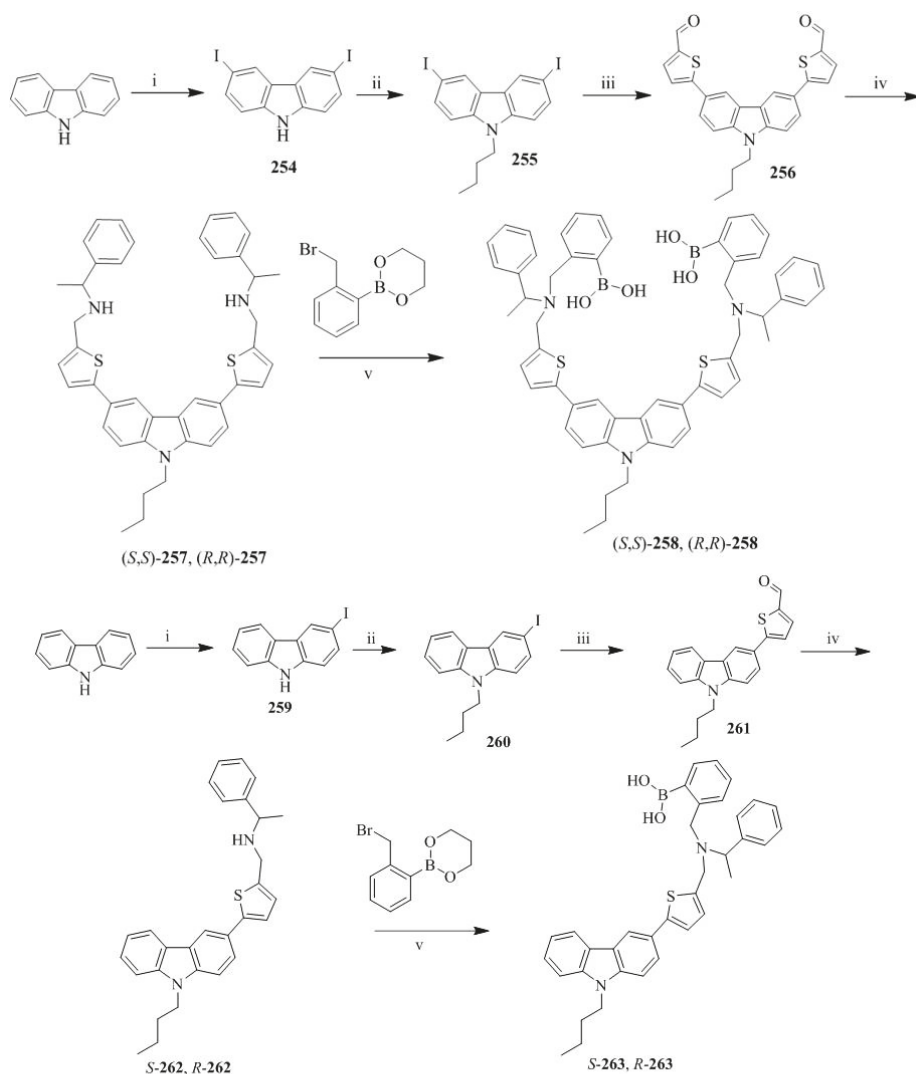
Zhao et al. [38] prepared the chiral fluorescent bisboronic acid sensors, 258, 263 with 3,6-dithiophen-2-yl-9H-carbazole as a fluorophore (Scheme 45). The thiophene units were used to extend the π -conjugation of carbazole and to enhance the electron-donating ability of fluorophore. The synthetic strategy was based on the first iodination of carbazole core and subsequent attachment of 2-formyl-5-thiopheneboronic acid to the carbazole moiety by Pd(0)-catalyzed Suzuki cross-coupling. The chirogenic center was introduced by reductive amination with α benzylamine. Finally, the boronic acid units were attached by a simple N-alkylation with 2-(2-bromomethylphenyl)-1,3,2-dioxaborinane. The monoboronic acid sensor, 230 was also prepared from mono iodinate carbazole in the similar manner and used for comparison in the binding studies.

Table 29. Binding constants K_a (M^{-1}), maximum observed chemical shifts ($\Delta \delta_{\max}$), Gibbs free energy changes ($-\Delta G_0$), selectivity coefficients, and differences of the Gibbs free energy changes ($\Delta \Delta G_0$ above) for the formation of 1:1 complexes of **219** and **220** with different salts of α -chiral primary organoammonium ions in $CDCl_3$ at 298 K.

| Guest | K_s | $\Delta \delta_{\max}$ | Selectivity Coefficients | $-\Delta G_0$ kJ mol $^{-1}$ | $\Delta \Delta G_0$ kJ mol $^{-1}$ |
|-------------|-----------------------|------------------------|--------------------------|------------------------------|------------------------------------|
| 252*(R)-PEA | 200(\pm 40) | 0.03 | | 13.1 | |
| 252*(S)-PEA | 480(\pm 70) | 0.06 | 2.4 | 15.3 | -2.2 |
| 252*(R)-PAM | 16,000(\pm 4900) | 0.01 | | 24 | |
| 252*(S)-PAM | 1900(\pm 500) | 0.02 | 8.4 | 18.7 | 5.3 |
| 252*(R)-BA | 130(\pm 40) | 0.01 | | 12.1 | |
| 252*(S)-BA | 940(\pm 240) | 0.01 | 7.2 | 17 | -4.9 |
| 252*(R)-NEA | - | -d | | - | |
| 252*(S)-NEA | d | -d | - | - | - |
| 252*(R)-BEA | 560(\pm 210) | 0.01 | | 15.7 | |
| 252*(S)-BEA | 540(\pm 50) | 0.05 | 1.0 | 15.6 | 0.1 |
| 252*(R)-AH | 360(\pm 70) | 0.01 | | 14.6 | |
| 252*(S)-AH | 100(\pm 20) | 0.02 | 3.6 | 11.4 | 3.2 |
| 253*(R)-PEA | 30,000(\pm 11,000) | 0.25 | | 25.5 | |
| 253*(S)-PEA | 4500(\pm 590) | 0.30 | 6.7 | 20.8 | 4.7 |
| 253*(R)-PAM | 2000(\pm 240) | 0.22 | | 18.8 | |
| 253*(S)-PAM | 1100(\pm 270) | 0.22 | 1.8 | 17.4 | 1.5 |
| 253*(R)-BA | 1600(\pm 260) | 0.17 | | 18.3 | |
| 253*(S)-BA | 2400(\pm 930) | 0.20 | 1.5 | 19.3 | -1.0 |
| 253*(R)-NEA | 1000(\pm 180) | 0.06 | | 17.1 | |
| 253*(S)-NEA | 610(\pm 110) | 0.06 | 1.6 | 15.9 | 1.2 |
| 253*(R)-BEA | 6600(\pm 1600) | 0.30 | | 21.8 | |
| 253*(S)-BEA | 3200(\pm 450) | 0.28 | 2.1 | 20 | 1.8 |
| 253*(R)-AH | 9700(\pm 3100) | 0.13 | | 22.7 | |
| 253*(S)-AH | 2400(\pm 710) | 0.16 | 4.0 | 19.3 | 3.5 |

The host containing diboronic acid, **258** exhibited the enantioselective recognition of tartaric acid at acidic pH, and the enantioselectivity was found to be 3.3. The L-tartaric acid showed 5 fold enhancements in the fluorescence while for D-tartaric acid exhibited 3 fold enhancement in the fluorescence. Thus, fluorescence enhancement factor ($I_F^{\text{Sample}}/I_F^{\text{Blank}}$) for **258** upon interaction with tartaric acid was 3.5-fold at pH 3.0. Further, **258** was useful for the enantioselective recognition of D- and L-mandelic acid, whereas **263** containing monoboronic acid failed to display the corresponding chiral recognition of these guests.

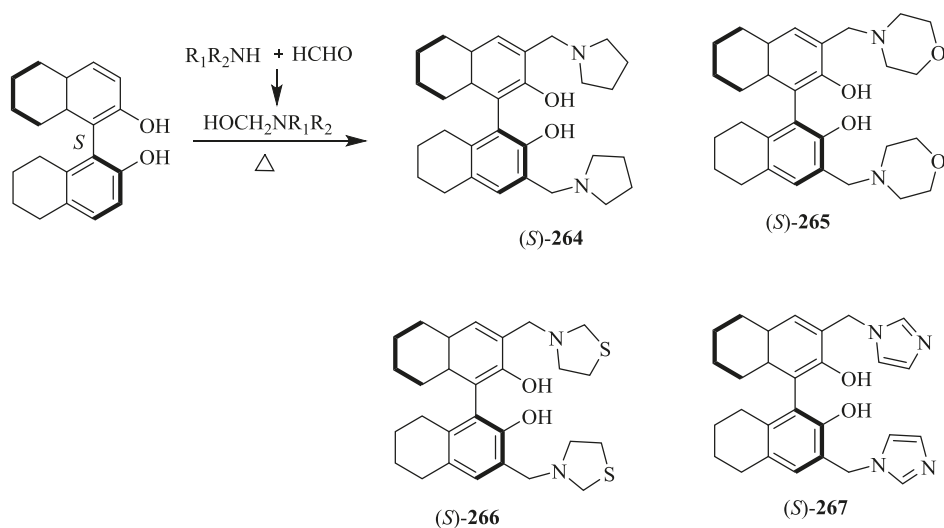
Pu and coworkers [99] developed the H_8 -BINOL-aminomolecules, (S)-**264**-(S)-**267** as a promising new class of the enantioselective fluorescent sensors by using their recently developed one-step reaction of H_8 -BINOL with in situ generated aminomethanol (Scheme 46). The NMR studies revealed that the difference between the fluorescence spectra of (S)-**264**-(S)-**267** apparently arises from the different capability of their nitrogen atoms to form intramolecular hydrogen bonds. When (S)-**267** was treated with enantiomer (R)-MA result into the substantial fluorescent enhancement with $I_R/I_0 = 3.2$. This was anticipated that the involvement of nitrogen of (S)-**267** in the complexation with (R)-MA to form a structurally more rigid fluorophore. However, for (S)-MA, the fluorescence enhancement was smaller with $I_R/I_0 = 2.1$. This indicates that (S)-**267** is a promising candidate for the enantioselective fluorescent recognition of MA in the shorter emission wavelength. Greater fluorescence enhancement at the short wavelength ($\lambda_{em} = 330$ nm) was observed upon the interaction of (S)-**268** (Figure 24) with (R)-MA, whereas (S)-MA gave smaller enhancement at the same wavelength. Thus, a good enantioselective fluorescent response was observed in this case with $ef = 3.5$. This study demonstrated that the H_8 -BINOL-based molecules are promising as a new class of the enantioselective fluorescent sensors.



Reagents and conditions: (i) KI, KIO₃, CH₃COOH, reflux, 10 min, 42.1%; (ii) NaH, DMF, n-C₄H₉Br, rt 1 h, 85.0%; (iii) THF, K₂CO₃, Pd(PPh₃)₄, 5-formylthiophene-2-boronic acid, N₂ atmosphere, reflux, 10 h, 62.4%; (iv) R- and S-1-phenylethylamine, DCM, ethanol, reflux, 8 h, then NaBH₄, rt 1 h, 79.4% (S,S-12), 64.6% (R,R-12); (v) acetonitrile, DCM, K₂CO₃, 2-(2-bromomethylphenyl)-1,3,2-dioxaborinane, reflux, 10 h, 27.5% (S,S-1), 31.2% (R,R-1); (vi) KI, KIO₃, CH₃COOH, reflux, 10 min, 40.0%; (vii) NaH, DMF, n-C₄H₉Br, rt 1 h, 90.2%; (viii) THF, K₂CO₃, Pd(PPh₃)₄, 5-formylthiophene-2-boronic acid, N₂ atmosphere, reflux, 10 h, 52.0%; (ix) R- and S-1-phenylethylamine, DCM, ethanol, reflux, 8 h, then NaBH₄, rt 1 h, 71.2% (S-16), 78.4% (R-16); (x) acetonitrile, DCM, K₂CO₃, 2-(2-bromomethylphenyl)-1,3,2-dioxaborinane, reflux, 10 h, 42.0% (S-2), 44.5% (R-2).

Scheme 45. Synthesis of bisboronic acid sensors, **258**, **263** bearing 3,6-dithiophen-2-yl-9H-carbazole as a fluorophore.

Jurczak et al. [31] prepared the tweezer-type compound, **271** by functionalization of 7,7'-diamino 2,2'-diindolylmethane, **269** with peracetylated D-glucuronic acid (**270**) (Figure 25), as a source of chirality, to form the corresponding amide linkage. Similarly, the reference receptor, **272** was synthesized from 7-aminoindole.



Scheme 46. Synthesis of the H₈BINOL-amine compounds, (S)-264–(S)-267.

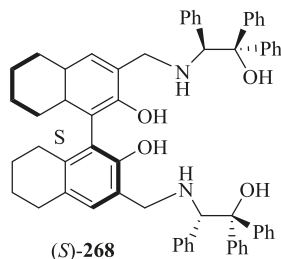


Figure 24. H₈BINOL-amino alcohol, (S)-268.

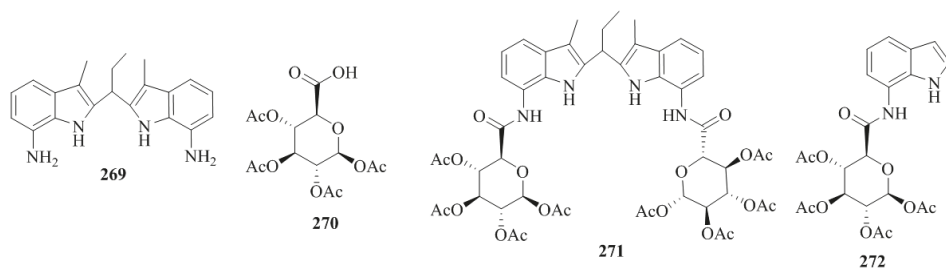
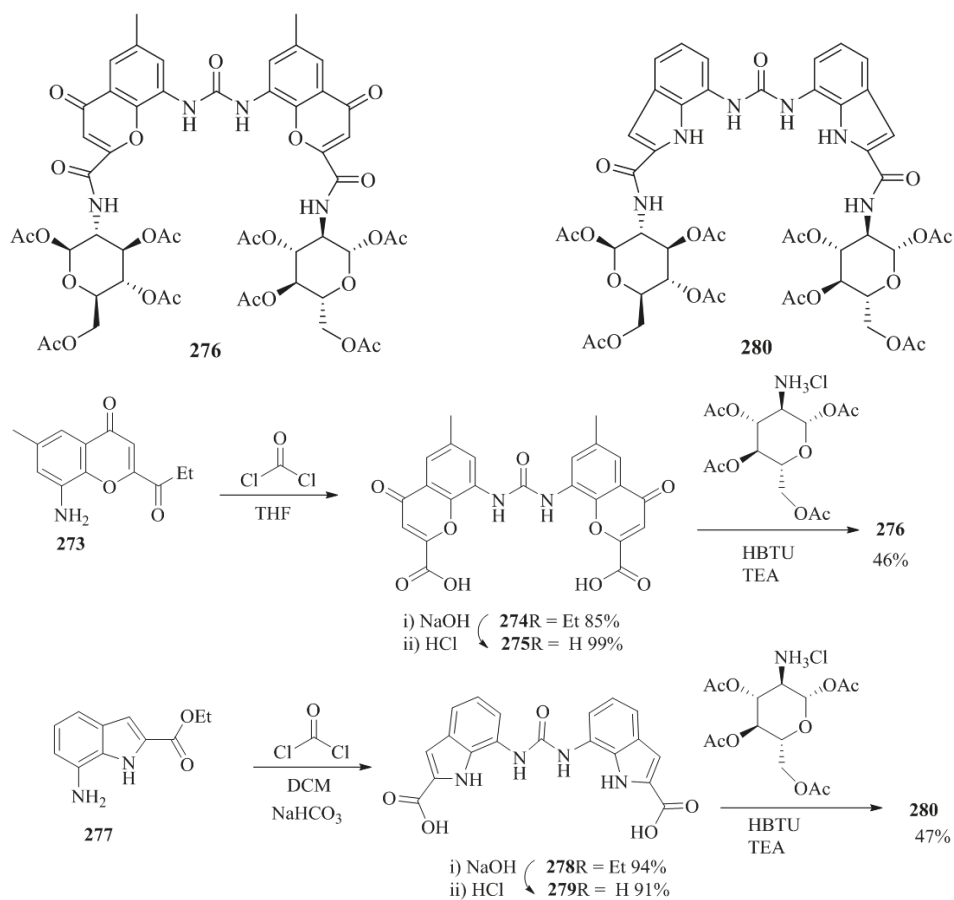


Figure 25. Structures of 7,7'-diamino-2,2'-dindolylmethane (**269**), peracetylated D-glucuronic acid, **270**, and chiral anion receptors **271** and **272**.

The enantioselective recognition of **271** and **272** were studied by ¹H NMR titrations for model chiral anionic guests; *S*-(+)-mandelate or *R*-(−)-mandelate. It was found that the association constant of (*R*)-MA is larger than that of (*S*)-MA. ROESY spectrum of the host-guest system between **271** and (*R*)-MA shows the corresponding correlations between the aromatic protons of guest and sugar protons (H3 and H5) of host. For weaker bounded (*S*)-MA, additional cross peaks were also found indicating a

deeper penetration of the anion into the receptor cavity. This was also confirmed by different ROESY signals arising from the (*R*)-mandelate protons and sugar moiety protons of host.

The same group [100] developed the chromenone- and indole-urea-based C_2 -symmetrical receptors, **276** and **280** functionalized with easily accessible 1,3,4,6-tetra-*O*-acetyl-D-glucosamine, starting from amines **273** and **277** (Scheme 47). Subsequently, the condensation with phosgene resulted in **274** and **278** followed by the hydrolysis of ester groups to yield **275** and **279**. These acid compounds were then coupled with the D-glucosamine derivative to furnish the desired products, **276** and **280**.

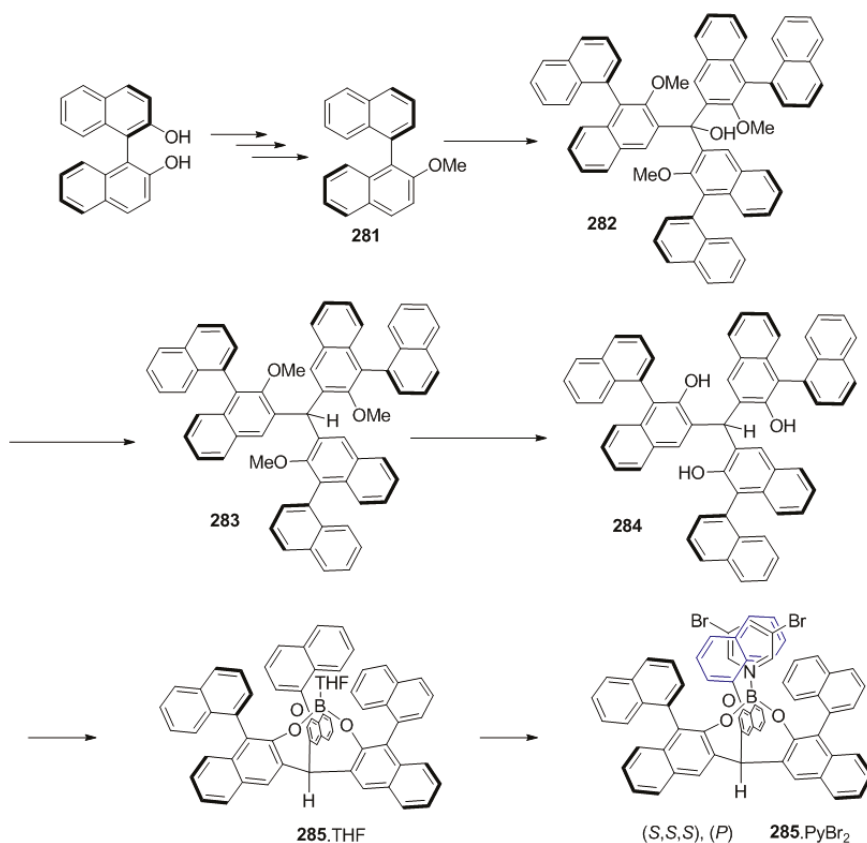


Scheme 47. Synthesis of receptors **276** and **280**.

The receptors, **276** and **280** were evaluated for their binding properties with various anions derived from chiral acids and having a stereogenic center in the α position. It was observed that **276** binds the *S* enantiomers of anions more strongly than the *R* enantiomers in all cases, with the enantioselectivities in the range of 1.2–2.0. A similar trend but with weaker preference for binding the *S* enantiomers was observed for **280** in the most cases. Also, **276** recognizes the chiral guests by steric interaction with the sugar moieties. This hypothesis was further supported by the relative stability constants (K_S/K_R) in the mandelate anion series. Hence, reducing the steric hindrance on the α carbon in the anion by substituting Ph with PhCH₂ results in increasing the overall stability constants and decreasing the K_S/K_R value, whereas enhancing this steric hindrance by replacing the hydrogen atom

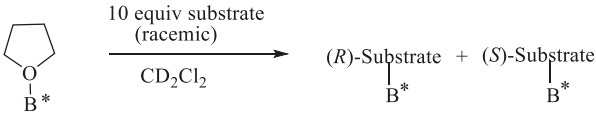
with the CF_3 group significantly decreases both the stability constants and the K_S/K_R value. In the case of **280** the sugar parts do not interact with the side chain of anions during the complexation, which was explained by the weak enantiodiscrimination.

Yasuda et al. [101] prepared the cage-shaped borate, **285** starting from readily available (*R*)-BINOL, which was converted to methoxybinaphthyl, **281** followed by lithiation at the ortho-position and subsequent condensation with ethyl chloroformate to yield tris(2-methoxybinaphthyl)methanol, **282** (Scheme 48). Further reduction of **282** with a $\text{Me}_2\text{SiHCl}/\text{InCl}_3$ system and deprotection of the methoxy groups afforded tris(2-hydroxybinaphthyl) methane, **284** with the axial chirality at all three binaphthyl moieties. Finally, mixing **284** with $\text{BH}_3 \cdot \text{THF}$ generated the cage shaped borate, **285**, which was subsequently converted to **285**· PyBr_2 .

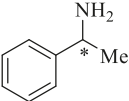
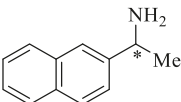
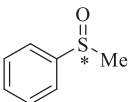


Scheme 48. Synthesis of homochiral cage-shaped borate, **285** with C_3 -symmetry.

The chiral recognition of a mixture of the excess amount of racemic phenyl ethyl amine **98** with **285**·THF in CD_2Cl_2 have been studied by ^1H NMR measurement. The ratio between the *R* and *S* enantiomers of phenyl ethyl amine, 1-(2-naphthyl)ethylamine and adducts with **285** found to be 18:1, 23:1 respectively (entry 1, 2 in Table 30), showing the highly enantioselectivity. Further, the *R* and *S* enantiomers ratio for the racemic methyl phenyl sulfoxide with host **285**, was observed to be 7:1 owing to low Lewis basicity of the sulfoxide as compared to amines.

Table 30. Recognition of chiral substrates by complexation with **285**.THF.


C1CCOC1 $\xrightarrow[\text{CD}_2\text{Cl}_2]{10 \text{ equiv substrate (racemic)}}$ $(R)\text{-Substrate}_{\text{B}^*} + (S)\text{-Substrate}_{\text{B}^*}$

| Entry | Substrate | R/S ^a |
|-------|---|-------------------|
| 1 |  98 | 18:1 ^b |
| 2 |  99 | 23:1 ^c |
| 3 |  286 | 7:1 ^d |

^a The ratios and absolute configurations except entry 3 were determined by ¹H NMR measurement; ^b heating for 43 h at 80 °C; ^c heating for 216 h at 80 °C; ^d the absolute configuration was not determined.

8. Summary

Chiral molecular recognition is a crucial branch of modern chemistry facilitating the qualitative and quantitative analysis of chiral molecules. It is also a basis of the industrially relevant chromatographic technique for bulk separation of racemates. There exists a huge global market for chiral separation technology for qualitative and quantitative estimations of chiral analytes. This review focuses on chiral supramolecular systems with the presence of heterocyclic ring(s) in the host structures. The hosts with the pyridine ring(s) form the major group in both the macrocyclic structures and the open chain tweezers. So far, different spectral and analytical techniques to detect and to estimate the binding between the host and the guest with a noticeable difference in the association constants of two enantiomeric guests have been employed. The fluorescence and NMR spectroscopic methods have been more commonly used for the chiral recognition purpose. Different types of intermolecular interactions between the corresponding hosts and guests involved in each supramolecular system have been proposed and discussed. An additional method on the basis of induced chirality detected by CD has been included in the review, though strictly speaking it is amplification of chirality of the guests based on supramolecular interactions between achiral host and chiral guests. Hosts with presence of different chiral elements have been employed. So far the incorporation of heterocyclic units in chiral hosts seems to be driven by ease of access, presence of aromatic ring and presence of multiple ligating centers. Though crowns and macrocycles of different sizes have been employed for chiral recognition studies, size-dependent enantio-discrimination factor has been noticed only in the last few years. Given the importance of chiral analysis, this branch is poised to achieve momentum in the coming decade.

Acknowledgments: Authors thank Mohammed Hasan and Sushil Khot for critical reading and suggestions. Vaibhav N. Khose thanks UGC-NET for the JRF and SRF awards. Victor Borovkov acknowledges funding from the European Union's Seventh Framework Programme for Research, Technological Development, and Demonstration under Grant Agreement no. 621364 (TUTIC-Green).

Conflicts of Interest: The authors declare no conflict of interest.

References

- Zupancic, V.; Kikelj, D. Chiral drugs in pharmaceutical industry-development and applications. *Farm. Vestnik* **2001**, *52*, 259–272.
- Gao, Y.; Boschetti, E.; Guerrier, L. Synthesis and separation of optically active compounds. Part I. *Ann. Pharm. Fr.* **1994**, *52*, 184–203. [[PubMed](#)]
- Hembury, G.A.; Borovkov, V.V.; Inoue, Y. Chirality sensing supramolecular systems. *Chem. Rev.* **2008**, *108*, 1–73. [[CrossRef](#)] [[PubMed](#)]
- Ball, P. Giving life a hand. *Chem. World* **2007**, *4*, 30–31.
- Talele, T.T. Natural-products-inspired use of the gem-dimethyl group in medicinal chemistry. *J. Med. Chem.* **2017**. [[CrossRef](#)] [[PubMed](#)]
- Blaskovich, M.A.T. Unusual amino acids in medicinal chemistry. *J. Med. Chem.* **2016**, *59*, 10807–10836. [[CrossRef](#)] [[PubMed](#)]
- Karnik, A.V.; Patil, S.T.; Patnekar, S.S.; Semwal, A. A convenient route to optically active γ -substituted γ -lactones. *New J. Chem.* **2004**, *28*, 1420–1422. [[CrossRef](#)]
- Karnik, A.V.; Kamath, S.S. Cascade enantioselective synthesis of γ -aryl- γ -butyrolactones with a delayed stereoselective step. *Tetrahedron* **2008**, *64*, 2992–2996. [[CrossRef](#)]
- Tawde, T.S.; Wagh, S.J.; Sapre, J.V.; Khose, V.N.; Badani, P.M.; Karnik, A.V. Reversal of enantioselectivity induced by the achiral part of an organocatalyst in a Diels-Alder reaction. *Tetrahedron Asymmetry* **2016**, *27*, 130–135. [[CrossRef](#)]
- Buchbauer, G.; Shafii-Tabatabai, A. Enones of (+)- and (–)-3-pinanone: Influence of chirality on flavour. *Flavour Fragr. J.* **2003**, *18*, 441–445. [[CrossRef](#)]
- Leffingwell, J.C.; Leffingwell, D. Chiral chemistry in flavours & fragrances. *Spec. Chem. Mag.* **2011**, *31*, 30–33.
- Pietro Paolo, A. *Ideas in Chemistry and Molecular Sciences: Where Chemistry Meets Life*; Pignataro, B., Ed.; Wiley: Hoboken, NJ, USA, 2010; pp. 293–312.
- Venkatakrishnarao, D.; Sahoo, C.; Mamonov, E.A.; Novikov, V.B.; Mitetelo, N.V.; Naraharisetty, S.G.; Murzina, T.V.; Chandrasekar, R. Chiral organic photonics: Self-assembled micro-resonators for an enhanced circular dichroism effect in the non-linear optical signal. *J. Mater. Chem. C* **2017**, *5*, 12349–12353. [[CrossRef](#)]
- Cram, D.J. The design of molecular hosts, guests, and their complexes. *Science* **1988**, *240*, 760–767. [[CrossRef](#)] [[PubMed](#)]
- Bao, W.; Wang, Z.; Li, Y. Synthesis of chiral ionic liquids from natural amino acids. *J. Org. Chem.* **2003**, *68*, 591–593. [[CrossRef](#)] [[PubMed](#)]
- Bako, P.; Fenichel, L.; Toke, L. A Novel diaza-crown ether and cryptands from glucopyranose and their complex-forming properties. *Eur. J. Org. Chem.* **1990**, *1990*, 1161–1164. [[CrossRef](#)]
- Bako, P.; Vizvardi, K.; Toppet, S.; Eycken, E.; Hoornaert, G.; Fenichel, L.; Toke, L. Synthesis, extraction ability and application in asymmetric synthesis of aza crown ethers derived from D-glucose. *Tetrahedron* **1998**, *54*, 14975–14988. [[CrossRef](#)]
- Bradshaw, J.S.; Huszthy, P.; McDaniel, C.W.; Oue, M.; Zhu, C.Y.; Izatt, R.M.; Lifson, S. Enantiomeric recognition of organic ammonium salts by chiral pyridino-18-crown-6 ligands: A short review. *J. Coord. Chem.* **1992**, *27*, 105–114. [[CrossRef](#)]
- Fernandez-Gonzalez, A.; Guardia, L.; Badía-Laiño, R.; Díaz-García, M. Mimicking molecular receptors for antibiotics—analytical implications. *Trends Anal. Chem.* **2006**, *25*, 949–957. [[CrossRef](#)]
- Kaushansky, K. Small molecule mimics of hematopoietic growth factors: Improving on Mother Nature? *Leukemia* **2001**, *15*, 673–674. [[CrossRef](#)] [[PubMed](#)]
- Dickert, F.L. Biomimetic receptors and sensors. *Sensors* **2014**, *14*, 22525–22531. [[CrossRef](#)] [[PubMed](#)]
- Kim, S.; Kim, K.; Jung, J.; Shin, S.; Ahn, K. Unprecedented Chiral Molecular Recognition in a C₃-Symmetric Environment. *J. Am. Chem. Soc.* **2002**, *124*, 591–596. [[CrossRef](#)] [[PubMed](#)]

23. Kim, J.; Seo, J.; Yim, E.; Jin, Y.; Song, S.; Suh, H. Enantiomeric recognition in host-guest complexation using chiral bis-pyridino-18-crown-6 ethers, by electrospray ionization mass spectrometry (ESI-MS) enantiomer-labelled (EL) guest method. *Bull. Korean Chem. Soc.* **2008**, *9*, 1069–1072.
24. Lu, Q.; Hou, J.; Wang, J.; Xu, B.; Zhang, J.; Yu, X. Multichannel Chromogenic and Chiral Anions Recognition by Imidazolium Functionalized BINOL Derivatives. *Chin. J. Chem.* **2013**, *31*, 641–650. [[CrossRef](#)]
25. Hasan, M.; Khose, V.N.; Pandey, A.D.; Borovkov, V.; Karnik, A.V. Tailor-Made Supramolecular Chirogenic System Based on Cs-Symmetric Rigid Organophosphoric Acid Host and Amino Alcohols: Mechanistic Studies, Bulkiness Effect, and Chirality Sensing. *Org. Lett.* **2016**, *18*, 440–443. [[CrossRef](#)] [[PubMed](#)]
26. Artz, S.P.; de Grandpre, M.P.; Cram, D.J. Host-guest complexation. Search for new chiral hosts. *J. Org. Chem.* **1985**, *50*, 1486–1496. [[CrossRef](#)]
27. Ozer, H.; Kocakaya, S.O.; Akgun, A.; Hosgoren, H.; Togrul, M. The enantiomeric recognition of chiral organic ammonium salts by chiral pyridino-macrocycles bearing aminoalcohol subunits. *Tetrahedron Asymmetry* **2009**, *20*, 1541–1546. [[CrossRef](#)]
28. Shahgaldian, P.; Pielek, U.; Hegner, M. Enantioselective recognition of phenylalanine by a chiral amphiphilic macrocycle at the air-water interface: A copper-mediated mechanism. *Langmuir* **2005**, *21*, 6503–6507. [[CrossRef](#)] [[PubMed](#)]
29. Lu, Q.; Dong, L.; Zhang, J.; Li, J.; Jiang, L.; Huang, Y.; Qin, S.; Hu, C.; Yu, X. Imidazolium-functionalized binol as a multifunctional receptor for chromogenic and chiral anion recognition. *Org. Lett.* **2009**, *11*, 669–672. [[CrossRef](#)] [[PubMed](#)]
30. Zhao, H.; Hua, W. Synthesis and characterization of pyridine-based polyamido-polyester optically active macrocycles and enantiomeric recognition for D- and L-amino acid methyl ester hydrochloride. *J. Org. Chem.* **2000**, *65*, 2933–2938. [[CrossRef](#)] [[PubMed](#)]
31. Granda, J.M.; Jurczak, J. Sweet anion receptors: Recognition of chiral carboxylate anions by D-glucuronic-acid-decorated diindolylmethane. *Org. Lett.* **2013**, *15*, 4730–4733. [[CrossRef](#)] [[PubMed](#)]
32. De la Torre, M.F.; Campos, E.G.; Gonzalez, S.; Moran, J.R.; Caballero, M.C. Binding properties of an abiotic receptor for complexing carboxylates of α -heterocyclic and α -keto acids. *Tetrahedron* **2001**, *57*, 3945–3950. [[CrossRef](#)]
33. Tejada, A.; Oliva, A.I.; Simon, L.; Grande, M.; Caballero, M.; Moran, J.R. A macrocyclic receptor for the chiral recognition of hydroxycarboxylates. *Tetrahedron Lett.* **2000**, *41*, 4563–4566. [[CrossRef](#)]
34. You, J.; Yu, X.; Zhang, G.; Xiang, Q.; Lan, J.; Xie, R. Novel chiral imidazole cyclophane receptors: Synthesis and enantioselective recognition for amino acid derivatives. *Chem. Commun.* **2001**, *0*, 1816–1817. [[CrossRef](#)]
35. Pandey, A.; Mohammed, H.; Karnik, A. Chiral benzimidazole-derived mono azacrowns: Synthesis and enantiomer recognition studies with chiral amines and their ammonium salts. *Tetrahedron Asymmetry* **2013**, *24*, 706–712. [[CrossRef](#)]
36. Pandey, A.D.; Mohammed, H.; Pissurlenkar, R.S.; Karnik, A.V. Size-induced chiral discrimination switching by (S)-(–)-2-(α -hydroxyethyl)-benzimidazole-derived azacrowns. *ChemPlusChem* **2015**, *80*, 475–479. [[CrossRef](#)]
37. Upadhyay, S.P.; Pissurlenkar, R.S.; Coutinho, E.C.; Karnik, A.V. Furo-fused BINOL based crown as a fluorescent chiral sensor for enantioselective recognition of phenylethylamine and ethyl ester of Valine. *J. Org. Chem.* **2007**, *72*, 5709–5714. [[CrossRef](#)] [[PubMed](#)]
38. Wu, Y.; Guo, H.; James, T.D.; Zhao, J. Enantioselective recognition of mandelic acid by a 3,6-dithiophen-2-yl-9H-carbazole-based chiral fluorescent bisboronic acid sensor. *J. Org. Chem.* **2011**, *76*, 5685–5695. [[CrossRef](#)] [[PubMed](#)]
39. Shcherbakova, E.G.; Brega, V.; Minami, T.; Sheykhi, S.; James, T.D.; Anzenbacher, P. Toward fluorescence-based high-throughput screening for enantiomeric excess in amines and amino acid derivatives. *Chem. Eur. J.* **2016**, *22*, 10074–10080. [[CrossRef](#)] [[PubMed](#)]
40. Jo, H.H.; Lin, C.Y.; Anslyn, E.V. Rapid optical methods for enantiomeric excess analysis: From enantioselective indicator displacement assays to exciton-coupled circular dichroism. *Acc. Chem. Res.* **2014**, *47*, 2212–2221. [[CrossRef](#)] [[PubMed](#)]
41. Velazquez, H.A.; Hamelberg, D. Electrochemical detection. In *Chemosensors: Principles, Strategies, and Applications*, 1st ed.; Wang, B., Anslyn, E.V., Eds.; John Wiley & Sons, Inc.: Hoboken, NJ, USA, 2011.
42. Lynnf, B.C.; Tsesarskaja, M.; Schall, O.F.; Hernandez, J.C.; Watanabe, S.; Takahashit, T.; Kaifer, A.; Gokel, G.W. Hydrogen bonding in macrocyclic receptor systems. *Supramol. Chem.* **1993**, *1*, 253–260. [[CrossRef](#)]

43. Muehldorf, A.V.; Engen, D.V.; Warner, J.C.; Hamilton, A.D. Aromatic-aromatic interactions in molecular recognition: A family of artificial receptors for thymine that shows both face-to-face and edge-to-face orientations. *J. Am. Chem. Soc.* **1988**, *110*, 6561–6562. [[CrossRef](#)]
44. Mecozzi, S.; West, A.P.; Dougherty, D.A. Cation- π interactions in aromatics of biological and medicinal interest: Electrostatic potential surfaces as a useful qualitative guide. *Proc. Natl. Acad. Sci. USA* **1996**, *93*, 10566–10571. [[CrossRef](#)] [[PubMed](#)]
45. Price, S.L.; Stone, A.J. The electrostatic interactions in van der Waals complexes involving aromatic molecules. *J. Chem. Phys.* **1987**, *86*, 2859–2868. [[CrossRef](#)]
46. Gibb, B.C. Van der waals interactions and the hydrophobic effect. In *Chemosensors: Principles, Strategies, and Applications*, 1st ed.; Wang, B., Anslyn, E.V., Eds.; John Wiley & Sons, Inc.: Hoboken, NJ, USA, 2011.
47. Mei, X.; Wolf, C. Enantioselective sensing of chiral carboxylic acids. *J. Am. Chem. Soc.* **2004**, *126*, 14736–14737. [[CrossRef](#)] [[PubMed](#)]
48. Hasan, M.; Khose, V.N.; Mori, T.; Borovkov, V.; Karnik, A.V. Sui Generis Helicene-Based Supramolecular Chirogenic System: Enantioselective Sensing, Solvent Control, and Application in Chiral Group Transfer Reaction. *ACS Omega* **2017**, *2*, 592–598. [[CrossRef](#)]
49. Li, G.; Cao, J.; Zong, W.; Lei, X.; Tan, R. Enantiodiscrimination of carboxylic acids using the diphenylprolinol NMR chiral solvating agents. *Org. Chem. Front.* **2016**, *3*, 96–102. [[CrossRef](#)]
50. Fukui, F.; Fukushi, Y. NMR Determinations of the Absolute Configuration of α -Chiral Primary Amines. *Org. Lett.* **2010**, *12*, 2856–2859. [[CrossRef](#)] [[PubMed](#)]
51. Parker, D. NMR determination of enantiomeric purity. *Chem. Rev.* **1991**, *91*, 1441–1457. [[CrossRef](#)]
52. Davankov, V.A. Separation of enantiomeric compounds using chiral HPLC systems. A brief review of general principles, advances, and development trends. *Chromatographia* **1989**, *27*, 475–482. [[CrossRef](#)]
53. Kim, J.; Lee, J.; Lee, S.; Seo, J.; Hong, J.; Suh, H. Chiral molecular recognition in fast atom bombardment mass spectrometry (FAB-MS) enantiomerlabeled (EL) guest method using new chiral bis-pyridino-18-crown-6. *Bull. Korean Chem. Soc.* **2002**, *23*, 543–544.
54. Bayly, S.R.; Chen, G.Z.; Beer, P.D. Electrochemical Detection. In *Chemosensors: Principles, Strategies, and Applications*, 1st ed.; Wang, B., Anslyn, E.V., Eds.; John Wiley & Sons, Inc.: Hoboken, NJ, USA, 2011.
55. Shaw, S.A.; Aleman, P.; Vedejs, E. Development of chiral nucleophilic pyridine catalysts: Applications in asymmetric quaternary carbonsynthesis. *J. Am. Chem. Soc.* **2003**, *125*, 13368–13369. [[CrossRef](#)] [[PubMed](#)]
56. Ishii, T.; Fujioka, S.; Sekiguchi, Y.; Kotsuki, H. A new class of chiral pyrrolidine-pyridine conjugate base catalysts for use in asymmetric Michael addition reactions. *J. Am. Chem. Soc.* **2004**, *126*, 9558–9559. [[CrossRef](#)] [[PubMed](#)]
57. Ager, D.J.; Prakash, I.; Schaad, D.R. 1,2-amino alcohols and their heterocyclic derivatives as chiral auxiliaries in asymmetric synthesis. *Chem. Rev.* **1996**, *96*, 835–876. [[CrossRef](#)] [[PubMed](#)]
58. Fu, G.C. Asymmetric Catalysis with “Planar-Chiral” Derivatives of 4-(Dimethylamino)pyridine. *Acc. Chem. Res.* **2004**, *37*, 542–547. [[CrossRef](#)] [[PubMed](#)]
59. Jolly, S.T.; Bradshaw, J.S.; Izatt, R.M. Synthetic chiral macrocyclic crown ligands: A short review. *J. Heterocycl. Chem.* **1982**, *19*, 3–18. [[CrossRef](#)]
60. Bradshaw, J.S.; Peter Huszthy, P.; Redd, J.T.; Zhang, X.X.; Wang, T.; Hathaway, J.K.; Young, J.; Izatt, R.M. Enantiomeric recognition of chiral ammonium salts by chiral pyridino- and pyrimidino-18-crown-6 ligands: Effect of structure and solvents. *Pure Appl. Chem.* **1995**, *67*, 691–695. [[CrossRef](#)]
61. Chu, I.; Dearden, D.V.; Bradshaw, J.S.; Huszthy, P.; Izatt, R.M. Chiral host-guest recognition in an ion-molecule reaction. *J. Am. Chem. Soc.* **1993**, *115*, 4318–4320. [[CrossRef](#)]
62. Hellier, P.C.; Bradshaw, J.S.; Young, J.J.; Zhang, X.X.; Izatt, R.M. Chiral pyridine-based macrobicyclic clefts: Synthesis and enantiomeric recognition of ammonium salts. *J. Org. Chem.* **1996**, *61*, 7270–7275. [[CrossRef](#)] [[PubMed](#)]
63. Asakawa, M.; Brown, C.L.; Pasini, D.; Stoddart, J.F.; Wyatt, P.G. Enantioselective recognition of amino acids by axially-chiral π -electron-deficient receptors. *J. Org. Chem.* **1996**, *61*, 7234–7235. [[CrossRef](#)] [[PubMed](#)]
64. Somogyi, L.; Huszthy, P.; Bradshaw, J.S.; Izatt, R.M.; Hollosi, M. Enantiomeric recognition of aralkyl ammonium salts by chiral pyridino-18-crown-6 ligands: Use of circular dichroism spectroscopy. *Chirality* **1997**, *9*, 545–549. [[CrossRef](#)]
65. Gavin, J.A.; Garcia, M.E.; Benesi, A.J.; Mallouk, T.E. Chiral molecular recognition in a tripeptide benzylviologen cyclophane host. *J. Org. Chem.* **1998**, *63*, 7663–7669. [[CrossRef](#)]

66. Du, C.; You, J.; Yu, X.; Liu, C.; Lan, J.; Xie, R. Homochiral molecular tweezers as hosts for the highly enantioselective recognition of amino acid derivatives. *Tetrahedron Asymmetry* **2003**, *14*, 3651–3656. [[CrossRef](#)]
67. Chen, X.; Du, D.; Hua, W. Synthesis of novel chiral polyamide macrocycles containing pyridyl side-arms and their molecular recognition properties. *Tetrahedron Asymmetry* **2003**, *14*, 999–1007. [[CrossRef](#)]
68. Ema, T.; Tanida, D.; Sakai, T. Versatile and practical macrocyclic reagent with multiple hydrogen-bonding sites for chiral discrimination in NMR. *J. Am. Chem. Soc.* **2007**, *129*, 10591–10596. [[CrossRef](#)] [[PubMed](#)]
69. Heckel, T.; Winkel, A.; Wilhelm, R. Chiral ionic liquids based on nicotine for the chiral recognition of carboxylic acids. *Tetrahedron Asymmetry* **2013**, *24*, 1127–1133. [[CrossRef](#)]
70. Ma, F.; Ai, L.; Shen, X.; Zhang, C. New macrocyclic compound as chiral shift reagent for carboxylic acids. *Org. Lett.* **2007**, *9*, 125–127. [[CrossRef](#)] [[PubMed](#)]
71. Chen, X.; Huang, Z.; Chen, S.; Li, K.; Yu, X.; Pu, L. Enantioselective gel collapsing: A new means of visual chiral sensing. *J. Am. Chem. Soc.* **2010**, *132*, 7297–7299. [[CrossRef](#)] [[PubMed](#)]
72. Seker, S.; Baris, D.; Arslan, N.; Turgut, Y.; Lu, N.P.; Togrul, M. Synthesis of rigid and C₂-symmetric pyridino-15-crown-5 type macrocycles bearing diamide-diester functions: Enantiomeric recognition for chiral primary organoammonium perchlorate salts. *Tetrahedron Asymmetry* **2014**, *25*, 411–417. [[CrossRef](#)]
73. Deniz, P.; Turgut, Y.; Togrul, M.; Hosgoren, H. Pyridine containing chiral macrocycles: Synthesis and their enantiomeric recognition for amino acid derivatives. *Tetrahedron* **2011**, *67*, 6227–6232. [[CrossRef](#)]
74. Ghosh, K.; Majumdar, A. L-Amino acid derived pyridinium-based chiral compounds and their efficacy in chiral recognition of lactate. *RSC Adv.* **2015**, *5*, 24499–24506. [[CrossRef](#)]
75. Khanvilkar, A.N.; Bedekar, A.V. Synthesis and characterization of chiral aza-macrocycles and study of their enantiomer recognition ability for organo-phosphoric acid and phosphonic acid derivatives by ³¹P NMR and fluorescence spectroscopy. *Org. Biomol. Chem.* **2016**, *14*, 2742–2748. [[CrossRef](#)] [[PubMed](#)]
76. Gonzalez, S.; Pelaez, R.; Sanz, F.; Jimenez, M.B.; Moran, J.R.; Caballero, M.C. Macrocyclic chiral receptors toward enantioselective recognition of naproxen. *Org. Lett.* **2006**, *8*, 4679–4682. [[CrossRef](#)] [[PubMed](#)]
77. Barnhill, D.K.; Sargent, A.L.; Allen, W.E. Participation of host spacer atoms in carboxylic acid binding: Implications for amino acid recognition. *Tetrahedron* **2005**, *61*, 8366–8371. [[CrossRef](#)]
78. Su, X.; Luo, K.; Xiang, Q.; Lan, J.; Xie, R. Enantioselective recognitions of chiral molecular tweezers containing imidazoliums for amino acids. *Chirality* **2009**, *21*, 539–546. [[CrossRef](#)] [[PubMed](#)]
79. Luo, K.; Jiang, H.; You, J.; Xiang, Q.; Guoa, S.; Lan, J.; Xie, R. Chiral di-imidazolium molecular tweezers: Synthesis and enantioselective recognition for amino acid derivatives. *Lett. Org. Chem.* **2006**, *3*, 363–367.
80. Munusamy, S.; Muralidharan, V.P.; Iyer, S.K. Enantioselective recognition of unmodified amino acids by ligand-displacement assays with in situ generated 1:1 Cu(II)-BINOL imidazole complex. *Sens. Actuators B Chem.* **2017**, *250*, 244–249. [[CrossRef](#)]
81. Ghosh, K.; Sarkar, T. L-Valine derived benzimidazole based bis-urea in enantioselective fluorescence sensing of L-tartrate. *Tetrahedron Lett.* **2013**, *54*, 4568–4573. [[CrossRef](#)]
82. Zhao, S.; Ito, S.; Ohba, Y.; Katagiri, H. Determination of the absolute configuration and identity of chiral carboxylic acids using a Cu(II) complex of pyridine-benzimidazole-based ligand. *Tetrahedron Lett.* **2014**, *55*, 2097–2100. [[CrossRef](#)]
83. Sato, H.; Shizuma, M. Triazole-linked host compounds for chiral-discrimination toward amino acid ester guests. *J. Oleo Sci.* **2008**, *57*, 503–511. [[CrossRef](#)] [[PubMed](#)]
84. Miao, F.; Zhou, J.; Tian, D.; Li, H. Enantioselective recognition of mandelic acid with (R)-1,1-bi-2-naphthol-linked calix[4]arene via fluorescence and dynamic light scattering. *Org. Lett.* **2012**, *14*, 3572–3575. [[CrossRef](#)] [[PubMed](#)]
85. Wu, J.; Lu, J.; Liu, J.; Zheng, C.; Gao, Y.; Hu, J.; Ju, Y. A deoxycholic acid-based macrocycle: Recognition of mercury ion and cascade enantioselective sensing toward amino acids. *Sens. Actuators B* **2017**, *241*, 931–937. [[CrossRef](#)]
86. Karnik, A.V.; Upadhyay, S.P.; Gangrade, M.G. [9,9′]Bi[naphtho(2,1-b)furanyl]-8,8′-diol, a furo-fused BINOL derivative: Synthesis, resolution and determination of absolute configuration. *Tetrahedron Asymmetry* **2006**, *17*, 1275–1280. [[CrossRef](#)]
87. Upadhyay, S.P.; Karnik, A.V. Enantioselective synthesis of (R) and (S)-[9,9′]bi[naphtho(2,1-b)furanyl]-8,8′-diol. A furo-fused BINOL derivative. *Tetrahedron Lett.* **2007**, *48*, 317–318. [[CrossRef](#)]
88. Kotwal, S.B.; Pandey, A.D.; Khose, V.N.; Karnik, A.V. A convenient route to enantiomerically enriched furo-fused BINOL derivative. *Indian J. Chem. B* **2015**, *54*, 940–943.

89. Hasan, M.; Pandey, A.D.; Khose, V.N.; Mirgane, N.A.; Karnik, A.V. Sterically congested chiral 7,8-dioxo[6]helicene and its dihydro analogues: Synthesis, regioselective functionalization, and unexpected domino prins reaction. *Eur. J. Org. Chem.* **2015**, *17*, 3702–3712. [CrossRef]
90. Ollevier, T. Iron bis(oxazoline) complexes in asymmetric catalysis. *Catal. Sci. Technol.* **2016**, *6*, 41–48. [CrossRef]
91. Wolf, C.; Xu, H. Asymmetric catalysis with chiral oxazolidine ligands. *Chem. Commun.* **2011**, *47*, 3339–3350. [CrossRef] [PubMed]
92. Kim, S.; Kim, K.; Kim, Y.K.; Shin, S.K.; Ahn, K.H. Crucial role of three-center hydrogen bonding in a challenging chiral molecular recognition. *J. Am. Chem. Soc.* **2003**, *125*, 13819–13824. [CrossRef] [PubMed]
93. Kim, J.; Kim, S.; Seong, H.R.; Ahn, K.H. Breaking the C_3 -symmetry of chiral tripodal oxazolines: Enantio-discrimination of chiral organoammonium ions. *J. Org. Chem.* **2005**, *70*, 7227–7231. [CrossRef] [PubMed]
94. Sambasivan, S.; Kim, S.; Choi, U.M.; Rhee, Y.M.; Ahn, K.H. C_3 -symmetric cage-like receptors: Chiral discrimination of *R*-chiral amines in a confined space. *Org. Lett.* **2010**, *12*, 4228–4231. [CrossRef] [PubMed]
95. Oliva, A.I.; Simon, L.; Hernandez, J.V.; Muniz, F.M.; Lithgow, A.; Jimenez, A.; Moran, J.R. Enantioselective recognition of α -amino acid derivatives with a *cis*-tetrahydrobenzoxanthene receptor. *J. Chem. Soc. Perkin Trans.* **2002**, *2*, 1050–1052. [CrossRef]
96. Roussel, C.; Roman, M.; Andreoli, F.; Del Rio, A.L.; Faure, R.; Vanthuyne, N. Non-racemic atropisomeric (thio)ureas as neutral enantioselective anion receptors for amino-acid derivatives: Origin of smaller K_{ass} with thiourea than urea derivatives. *Chirality* **2006**, *18*, 762–771. [CrossRef] [PubMed]
97. Satishkumar, S.; Periasamy, M. Chiral recognition of carboxylic acids by Troeger's base derivatives. *Tetrahedron Asymmetry* **2009**, *20*, 2257–2262. [CrossRef]
98. Schnopp, M.; Haberhauer, G. Highly selective recognition of α -chiral primary organoammonium ions by C_3 -symmetric peptide receptors. *Eur. J. Org. Chem.* **2009**, 4458–4467. [CrossRef]
99. Yu, S.; DeBerardinis, A.M.; Turlington, M.; Pu, L. Study of the Fluorescent Properties of partially hydrogenated 1,1'-Bi-2-naphthol-amine molecules and their use for enantioselective fluorescent recognition. *J. Org. Chem.* **2011**, *76*, 2814–2819. [CrossRef] [PubMed]
100. Lichosyt, D.; Wasilek, S.; Jurczak, J. Stereoselective chirality extension of *syn,anti*- and *syn,syn*-oxazine and stereochemical analysis of chiral 1,3-oxazines: Stereoselective total syntheses of (+)-1-deoxygalactonojirimycin and (–)-1-deoxygulonojirimycin. *J. Org. Chem.* **2016**, *81*, 7342–7348. [CrossRef] [PubMed]
101. Konishi, A.; Nakaoka, K.; Maruyama, H.; Nakajima, H.; Eguchi, T.; Baba, A.; Yasuda, M. C_3 -symmetric boron lewis acid with a cage-shape for chiral molecular recognition and asymmetric catalysis. *Chem. Eur. J.* **2017**, *23*, 1273–1277. [CrossRef] [PubMed]



© 2018 by the authors. Licensee MDPI, Basel, Switzerland. This article is an open access article distributed under the terms and conditions of the Creative Commons Attribution (CC BY) license (<http://creativecommons.org/licenses/by/4.0/>).

Review

Helicene-Based Chiral Auxiliaries and Chirogenesis

Mohammed Hasan and Victor Borovkov *

Department of Chemistry and Biotechnology, Tallinn University of Technology, Akadeemia tee 15, 12618 Tallinn, Estonia; mhasanfive@gmail.com

* Correspondence: victor.borovkov@ttu.ee; Tel.: +372-620-4382

Received: 7 December 2017; Accepted: 26 December 2017; Published: 29 December 2017

Abstract: Helicenes are unique helical chromophores possessing advanced and well-controlled spectral and chemical properties owing to their diverse functionalization and defined structures. Specific modification of these molecules by introducing aromatic rings of differing nature and different functional groups results in special chiroptical properties, making them effective chiral auxiliaries and supramolecular chirogenic hosts. This review aims to highlight these distinct structural features of helicenes; the different synthetic and supramolecular approaches responsible for their efficient chirality control; and their employment in the chirogenic systems, which are still not fully explored. It further covers the limitation, scope, and future prospects of helicene chromophores in chiral chemistry.

Keywords: helicene; chiral auxiliaries; supramolecular chirogenesis; chirality

1. Introduction

Aromatic characteristics in organic compounds are very interesting due to the resonance electronic features, stability, and inter- and intramolecular π - π interactions along with the specific geometric properties and reactivity, making it an important topic for researchers. Among the diverse aromatic compounds, there is a class of the molecules carrying *ortho*-annulated polyaromatic structures, classified as helicenes. In order to understand their unique structural features, helicenes should be compared with the conventional aromatic molecules (Figure 1).

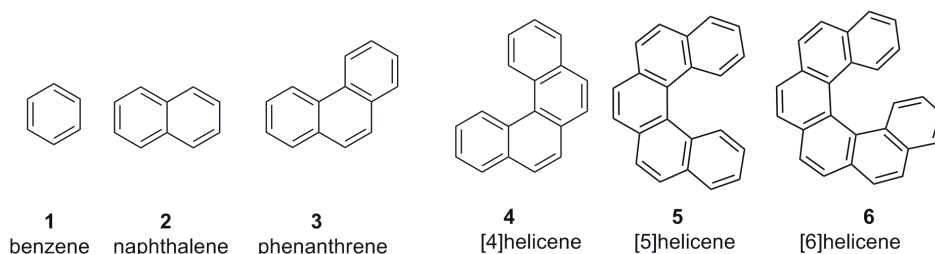


Figure 1. Conventional aromatic compounds, 1–3, and helicene compounds, 4–6 (numbers in bracket represent *ortho*-fused aromatic rings).

Benzene **1**, naphthalene **2**, and phenanthrene **3** are spatially flat aromatic structures (Figure 1); hence, they are not helicenes. As the number of *ortho*-fused aromatic rings is increased beyond three units, such as in **4–6** (Figure 1), the space constraint in the molecule is also enhanced, forcing it to adopt a nonplanar helical arrangement. These types of aromatic structures are called helicenes. As a consequence, the electron resonance ability is restricted throughout the molecule. Similar to

conventional aromatics, helicenes can be functionalized by various synthetic protocols to further enhance their spectral and chemical properties. However, the diversity of helical aromatic structures makes helicenes into unique and advanced chromophoric systems with tunable electronic and steric properties for corresponding applications in all types of stereochemical processes, including chiral auxiliaries and supramolecular chirogenesis. It is of note that, whilst there is a great variety of aromatic structures used in different chiral fields [1], helicenes still lag behind, despite their attractive properties discussed below.

2. Overview of Latest Reviews

Firstly, the existing reviews on helicenes from within the last five years should be briefly analyzed. Indeed, the chemistry of helicenes has existed for more than a century. However, this topic has been reviewed only recently to a rather limited extent [2–11]. Furthermore, these reviews mainly focused on the synthesis of helicenes and much less on their applications. One of the most comprehensive reviews was published in 2012 by Chen et al., describing helicene synthesis and applications [2]. In 2013, Gingras accumulated three sets of reviews targeting only carbohelicenes and covering the topics of its non-stereoselective [3] and stereoselective synthesis, chiral separation [4], and applications, along with the corresponding properties [5]. Yet, in 2014, three small review articles appeared on the topics of photochemical methods of helicene synthesis [6], helicene-based transition metal complexes [7], and helicene-like chiral auxiliaries [8]. Further, in 2015, Virieux [9] summarized the synthesis and application of helical phosphorus derivatives, where the helicene-based phosphorus ligands were also described. Thus, it is clear that—despite several consecutive reviews and monographs—this field is not fully covered, especially from the point of view of chiral applications. Further, the helicenes, being polyaromatic compounds, have been discussed in several chapters of a few books devoted to polyaromatic compounds and material chemistry [10]. Very recently, in 2017, a book on helicene chemistry [11] was published, covering most of the topic as it had appeared in previous reviews and presenting the progress up until the period of 2015.

Despite these recent efforts described above, a general tutorial and critical summary devoted to the design and tuning of helicene structures for suitable general and specific applications in the areas of chiral auxiliaries and chirogenesis is not yet available. Hence, the present review aims to fill in this gap, with a specific focus on the potential applicability and usefulness of helicene chemistry in these chirality fields—including the latest updates.

3. Classification and Nomenclature

3.1. Structural Diversity

In order to understand the structure and type of helicene molecules, a brief introduction into the classification and nomenclature should be made. As a part of classical organic chemistry, helicenes can be structurally divided into two major groups: carbohelicenes and heterohelicenes.

3.1.1. Carbohelicenes

Carbohelicenes are all benzenoid (aromatic) *ortho*-fused systems and named as [n]helicenes, where n represents the number of rings forming a helix in the *ortho*-fused fashion. Thus, the structures 4 [12], 5 [13,14], and 6 [15,16], are [4]helicene, [5]helicene, and [6]helicene, respectively (Figure 1). However, any fused ring which is not present in the *ortho*-fused manner is not included in the n counting. For example, structures 7 [17], 8 [18], and 9 [19] are all [5]helicenes, but not [6]helicenes, despite the presence of six aromatic rings in total (Figure 2). The functionalized helicenes such as 10 [20], 11 [21], and 12 [22] (Figure 2) which have a heteroatom as a substituent on the aromatic ring, as in the case of amino, hydroxyl (phenolic or alcoholic), thiol, or phosphorus-containing groups, are still carbohelicenes but not heterohelicenes. In order to specify the position of functional group(s), a numbering system is used, as shown in the structure 10. The numbering starts from the

innermost position at one end and goes to another end via the outer helical core in such a way that the functional group has the minimal number. Secondly, only unfused carbons (with hydrogen or other groups as substituents) are counted sequentially (shown in blue), whereas fused carbon atoms (of the helicene core) have the previous number with the corresponding a, b, c suffixes based on the sequence order of fused 1, 2, 3 atoms, and so on (shown in red). Thus, the structure **10** can be named as 2-acetoxy[5]helicene.

In the case of nonsymmetric heterohelicene, the numbering should be started from the peripheral ring which will give the least number to the heteroatomic ring core. In the case of more than one substituent, a general nomenclature rule of numbering should be applied. Yet, in both the cases mentioned, one should always follow the sequential numbering of the helicene core (starting from one innermost atom to another innermost atom of the two peripheral rings).

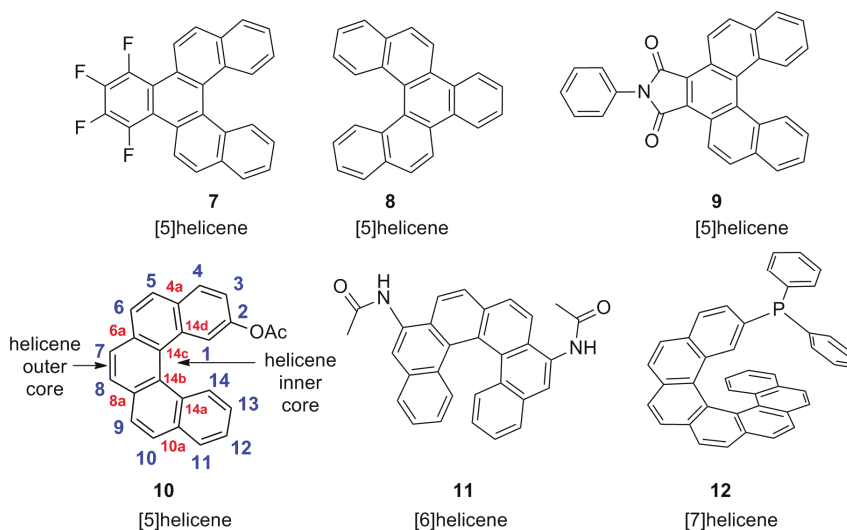


Figure 2. Examples of carbohelicenes: [5]carbohelicenes **7–9** with additional fused rings and functionalized [5]-**10**, [6]-**11**, and [7]-**12** carbohelicenes.

3.1.2. Heterohelicenes

Another class of helicenes is the heterohelicenes, in which one or more benzenoid ring is substituted with a heteroatomic ring (Figure 3). Heterohelicenes are generally based on five-membered rings such as thiophene, pyrrole, furan, etc., and six-membered rings mostly containing pyridine. Additionally, they can be fused and functionalized.

The corresponding heteroatom must be a part of the ring present in the fused *ortho* fashion but not as the substituent either in a functional group or in a heteroatomic ring. In the latter, whilst the overall molecule is heterocyclic, the helicene core is not. Further, depending on the heteroatom nature, the helicene structures are named aza[5]helicenes (**13** [23], **14** [24]), oxa[5]helicenes (**15** [25]), and thia[7]helicenes (**16** [26]). If there is more than one heteroaromatic ring or heteroatom, the helicene names are simplified as hetero[n]helicenes, [n]heterohelicenes, or simply [n]helicenes. For two or three similar heteroatomic rings, the prefixes “di”, “tri”, etc., are added with or without indicating the exact position. For example, the structure **17** [27] is called 7,8-dioxa[6]helicene or simply dioxa[6]helicene. Heterohelicenes containing phosphorus **18** [28], silicon **19** [29], and boron **20** [30] atoms are relatively rare and their chiral properties have not been well studied so far; therefore, they are excluded from this review.

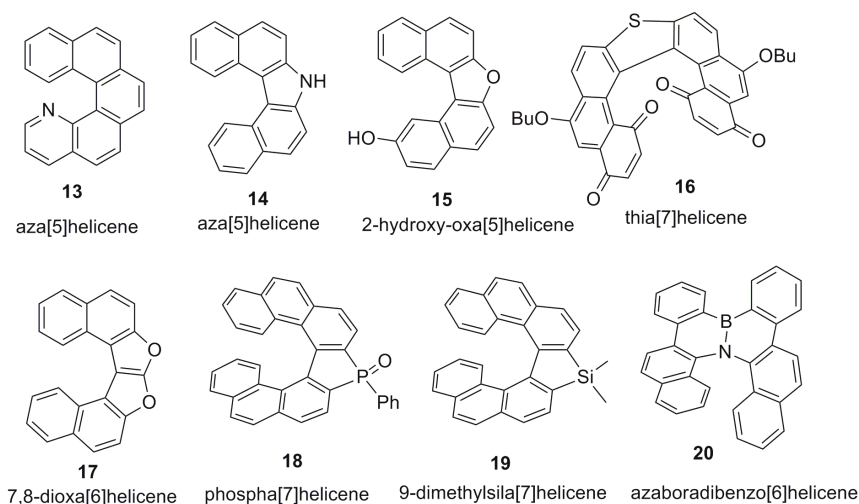


Figure 3. Examples of heterohelicenes, 13–20.

3.1.3. Charged Helicenes

Helicenes can also be categorized into neutral and charged helicene molecules. Most of the above examples are neutral helicene molecules, where the charge of the aromatic moiety is zero. However, if there is a charge on the helicene structure, a counter ion should be presented to balance the overall charge, hence resulting in different properties and applications. In such helicenes, exchanging the counter ion can easily enhance a number of the corresponding derivatives, controlling the solubility and pH effect. This counter ion exchange can sometimes offer a new approach towards optical resolution by changing an achiral counter ion to a chiral one in the case of thermodynamically stable structures. For example, quarternized azahelicene **21** [31] and cationic helicene **22** [32] stabilized by electron resonance/conjugation represent typical charged helicenes (Figure 4).

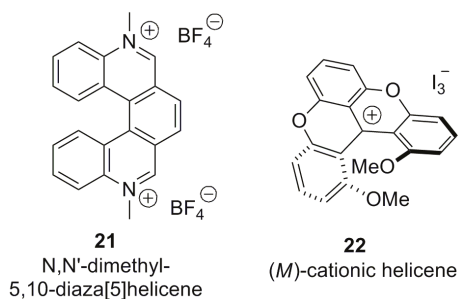


Figure 4. Charged helicenes, 21–22.

3.1.4. Special Structural Type of Helicene-Like Molecules

Besides the traditional definition of helicene molecules, there are several special cases which belong to this structural category but are not associated with the above-described major groups of carbo- and heterohelicenes; these are discussed below. Naphthalene **2** and phenanthrene **3** are the simplest *ortho*-fused flat molecules without any steric constraint and, hence, are not helicenes, whilst four fused aromatic rings induce a certain steric hindrance at the innermost peripheral hydrogen

atoms, setting up the first member of helicene family. Thus, in [n]helicenes, n should be >3 to be classified as a helicene molecule. However, there are some exceptions to this general rule. Interestingly, phenanthroline-*N,N*-dioxide **23** [33] (Figure 5) is also classified as a helicene in the literature, despite the fact that $n = 3$. This is due to the fact that the *N,N*-dioxide functionalities at the peri positions in the bay area of the phenanthroline are able to introduce the corresponding spatial constraint to force the molecule to adopt a configurationally stable helical conformation.

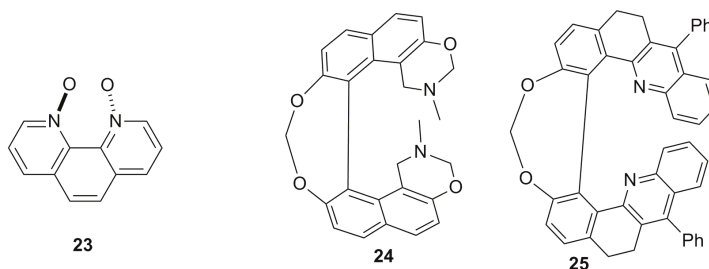


Figure 5. Special structural types of helicene **23** and helicene-like molecules **24–25**.

Besides the well-defined helicene molecules, there also exist helical structures, such as **24** [34] and **25** [35], called helicene-like molecules or helicenioids (Figure 5). Helicenioids usually contain at least one saturated atom as a part of the ring system in the helicene-type core system. Thus, the saturated ring is not able to adopt a flat structure, resulting in the enhancement of helicity. For example, a series of 1,1'-Bi-2-naphthol (BINOL)-based helical systems, sometimes referred to as oxahelicenioids, have been reported so far as configurationally stable structures [34,35]. Other types of saturated hydrocarbon-containing helicenioids, which are actually dihydrohelicenes, are also well documented in literature as precursors for helicene synthesis.

3.2. Spatial Diversity

Besides the structural diversity described above, helicenes can also be categorized, based on their stereochemistry, into four different categories: achiral (flat structures), stereodynamically labile (when *P* and *M* spatial conformations are in fast equilibrium; for the *P* and *M* definitions, see Section 3.2.1), chiral (enantiomerically stable structures), and *meso* helicenes (helical structure with some symmetry elements). This categorization is highly important for their applications in chiral auxiliaries and for chirogenic systems.

3.2.1. Chiral (Configurationally Stable) Helicenes

In order to understand the helicene spatial structures and this classification, the term “in-plane turn angle” needs to be introduced. Due to the *ortho* fusion mode, each aromatic ring contributes to the overall helicity of the molecule via an in-plane turn angle (Figure 6a). When the sum of the in-plane angles of the contributing rings becomes 360° or more, the helicene is forced to adopt a helically chiral structure caused by the corresponding steric clashes between the terminal/peripheral rings. Conventional six-membered (hexagon) aromatic rings such as benzene and pyridine have an in-plane turn angle of 60° [36]. However, in the case of five-membered heteroaromatic (pentagon) rings, the value is considerably smaller at 45° (thiophene), 35° (pyrrole), and 32° (furan) [36] due to the different geometric properties of aromatic rings as a result of the variable atomic sizes of heteroatoms and bond length of C–X bond ($X =$ heteroatom S, N, O in the five-member aromatic rings, correspondingly). Therefore, the helicenes with at least one five-membered heteroaromatic ring need $n > 6$ to become intrinsically chiral, whereas for the helicenes containing all six-membered carbo/hetero aromatic rings, $n = 6$ is sufficient to make them helically chiral.

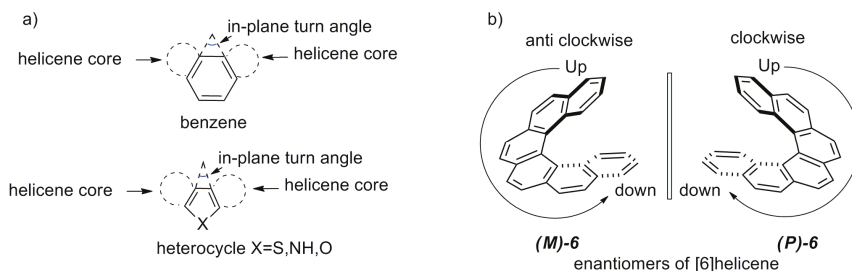


Figure 6. Schematic representation of (a) in-plane turn angle and (b) helicity and enantiomers of [6]helicene.

In general, a chiral helicene molecule exists in two enantiomeric forms. The right-handed helical structure (moving from up to down) is assigned the name (*P*)-enantiomer, whereas the left-handed helical structure (moving from up to down) is designated the (*M*)-enantiomer, according to the Cahn–Ingold–Prelog rule (Figure 6b). This type of helicene tends to give configurationally stable enantiomers as the racemization process is expected to go through the highly energetic, strained C_2 -symmetrical transition state [37]. Along with this thermodynamic stability of enantiomers, helicenes also exhibit notable enhanced (chir)optical properties, making them suitable candidates for chiral auxiliaries and other chirogenic processes. Interestingly, in general, (*P*)-carbohelicenes are observed as dextrorotatory, whereas (*M*)-enantiomers display a levorotatory nature [38].

3.2.2. Achiral Helicenes

Another type of helicene is the achiral flat molecules; for example, *ortho*-condensed polyaromatic molecules consisting of four rings with at least one ring being a five-membered (pentagon) heteroaromatic ring, as in [4]heterohelicenes. Whilst these structures are less interesting from the viewpoint of chirality, they possess enhanced conjugation, electron transfer, and emission properties, making them suitable candidates for various material chemistry applications.

3.2.3. Stereodynamic Helicenes

Holding an intermediate position between the chiral and achiral helicenes are the stereodynamic helicene structures. The geometry of these molecules is close to flat, whilst the van der Waals radii of the innermost hydrogens touch each other, making the structure stereodynamic and nonresolvable in solution, owing to the low (*P*)–(*M*) interconversion energy barrier. These include helicenes consisting of five benzenoid (hexagon) rings or [6]heterohelicenes with two five-membered (pentagon) heteroaromatic rings. However, in a solid state, these structures are able to adopt a chiral helical conformation. The dioxo[6]helicene **16** [27] is a typical example of such a system.

Stereodynamic helicenes are also highly fluorescent in nature due to the extended conjugation, whilst lacking any intrinsic chiroptical properties in solution. Yet, applying host–guest chemistry with suitable enantiopure guests, the corresponding chiroptical properties can be induced and controlled in this type of helicene. Additionally, the stereodynamic helicenes can be made helically chiral by introducing a bulky substitution at the innermost (C1) carbon atom. Computational analysis confirmed that attachment of just one methyl group at the innermost position results in the same steric strength as introduction of one additional *ortho*-fused benzene ring. Thus, [5]helicene with a methyl group at the innermost position has a structure more helical than that of [6]helicene, thus increasing the racemization barrier for the former [37].

3.2.4. Meso Helicenes

Meso helicenes are achiral, yet need to be classified separately. Two helicene fragments in one molecule, with the presence of a plane of symmetry, produce an achiral *meso* helicene.

Each equivalent helical part of this molecule possesses the opposite helical sense, whilst the whole molecule is symmetrical. Potentially, it can be suitably desymmetrized by a covalent bond or supramolecular interaction, making it chiroptically active and, hence, usable in various chirogenic processes. However, this area has not been well investigated yet, as selective modification of only one helicene moiety out of two is an arduous task; this is due to the fact that both the helicene parts are chemically equivalent. For example, carbocyclic helicene **26** [39] and heterocyclic helicene **27–28** [40] are *meso* double helicenes (Figure 7). It should be noted that the double helicenes have three stereoisomers, out of which two are optically active (*(P,P)* and *(M,M)*) and one is optically inactive (*(P,M)* or *(M,P)*), defined as a *meso* structure.

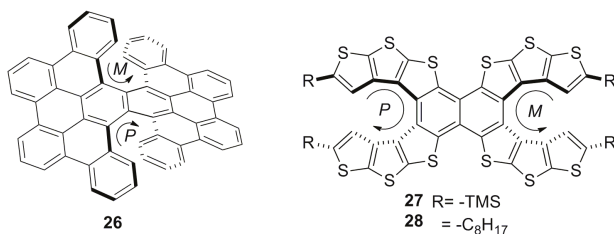


Figure 7. Examples of *meso* double helicenes **26–28**.

4. General Description and Main Synthetic Approaches toward Helicene-Based Chirogenic Systems

The early pioneering work on helicene synthesis, resolution, and chiroptical properties has been performed by Newman [15,16,41], Wynberg [36,38], Martin [42], and Katz [26]. In general, classical methods of helicene synthesis include the following approaches: oxidative photocyclization, Diels–Alder reactions, and various aromatic and metal-catalyzed coupling reactions [2–6,11]. The synthesis of helicenes is always a challenging task for organic chemistry due to the steric factors involved and difficulty in controlling the regioselectivity of reactions. The same factors are also responsible for the unique reactivity of the helicene skeleton.

The current advances in synthetic chemistry, resolution, and chiral separation are essentially helpful in designing and obtaining novel enantiopure helicene molecules in sufficient quantities to be used for various applications. As BINOL, (2,2'-bis(diphenylphosphino)-1,1'-binaphthyl) (BINAP), and related biaryl systems have been successfully applied as ligands, catalysts, and hosts in stereodiscriminating processes [43–45], it is theoretically possible to thoroughly design helicene-based helical systems possessing advantageous chiral properties. Progress in this area is highlighted below with several selected examples.

Let us look closely at a general structure of (*M*)-[6]helicene **6** (Figure 8a), where the benzene rings at the beginning and at the end of the helical arrangement are called the terminal or peripheral rings. It can be clearly seen that the helix experiences steric clashes towards the inner sides (interior), called the helicene's inner core. This structural organization results in a helical chiral cavity. The restricted space available between and around the two peripheral rings can be explored effectively for various chiral discriminating processes. In general, the introduction of suitable functional groups at the peripheral rings can act as a binding site to hold the reactant or guest molecules to facilitate the enantioselectivity, where the chiral cavity space of the helicene is able to influence the corresponding (diastereomeric) transition state and/or complexation mode. In contrast, the opposite outer skeleton of the helicene, termed as the helicene outer core (exterior), can be functionalized and used to covalently link these molecules on surfaces and for other applications.

The tailor-made design of helicenes for a suitable application can be of two types; first, where the functionalization at one peripheral ring is sufficient (monodentate), and second, where functionalization on both the terminal rings is required (bidentate) (Figure 8b). The bidentate helicenes can be C₂-symmetric (R = R') or nonsymmetric (R ≠ R') molecules. In accordance with the structural

features and substituent patterns of helicenes, their efficiency in chirogenic processes is observed, as demonstrated throughout this review.

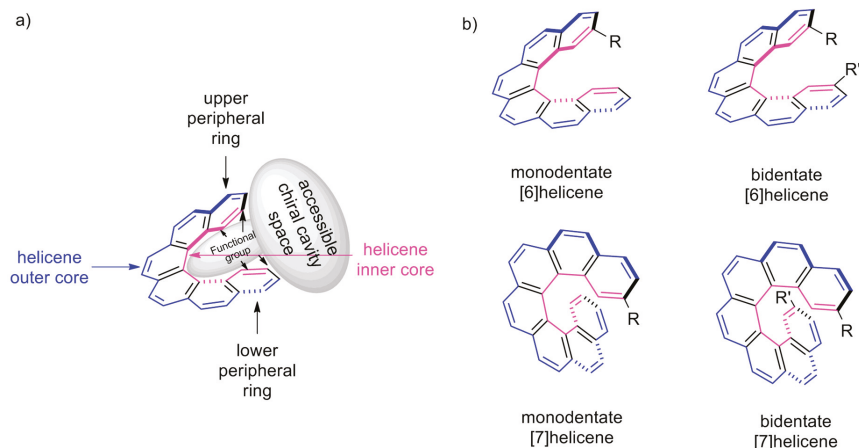
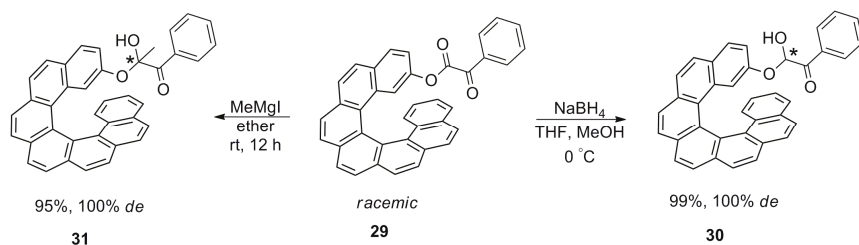


Figure 8. (a) General explanation of terms used for helicene structures and chiral cavity (shaded area); (b) representative [6]- and [7]helicenes ($R = R'$ or $R \neq R'$) with mono- or di-functionalized peripheral rings.

However, since the majority of recently published reviews [2–6] have focused on helicene synthetic chemistry, there is no need to describe this topic here in detail. Alternatively, this review addresses the structural design and stereochemical aspects of helicene chromophores suitable for various applications in chiral processes, whilst synthesis of these molecules will only be highlighted in brief upon necessity to emphasize their spatial and chiral properties.

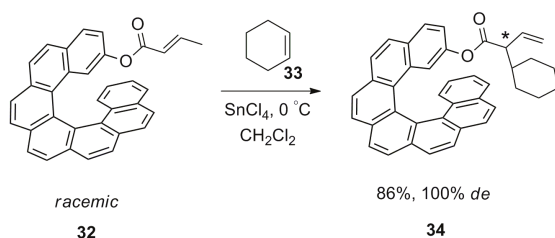
5. Helicenes as Chiral Auxiliary/Reagent or Additive

Due to the difficulties associated with the synthesis of helicenes and obtaining the corresponding enantiopure forms in sufficient amounts, their application as a chiral auxiliary in stoichiometric reactions is limited. However, one of the first results on the use of helicenes as chiral auxiliaries in few diastereoselective reactions was reported in 1985–1987 by Martin et al. with racemic 2-substituted-[7]helicene [46–50]. Hence, racemic **29** was employed as an inbuilt chiral auxiliary for the diastereoselective reaction of the carbonyl group of α -keto esters upon reduction with NaBH_4 , yielding **30** (99% yield; 100% *de*) [46], and on the nucleophilic addition of Grignard reagent to give **31** (95% yield; 100% *de*) [47] (Scheme 1).



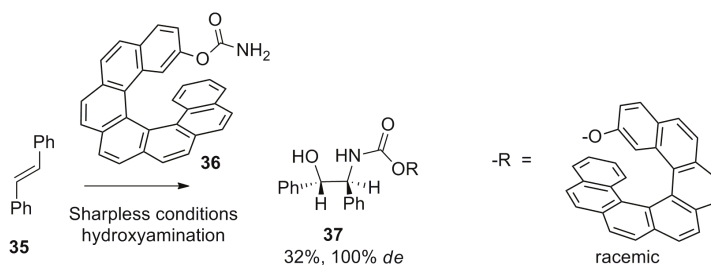
Scheme 1. Diastereoselective reaction using racemic [7]helicene **29** as a chiral auxiliary.

Although high diastereoselectivity (100%) was observed, the overall process requires attaching (protection) and detaching (deprotection) the helicene auxiliary, thereby making it difficult to scale up. Similarly, [7]helicene-attached unsaturated ester **32** was also utilized for the highly diastereoselective ene reaction with cyclohexene **33** in the presence of SnCl₄ to afford **34** with high yield (86%) and 100% *de* [48] (Scheme 2).



Scheme 2. Diastereoselective ene reaction using racemic [7]helicene **32** as a chiral auxiliary.

Further, hydroxyamination of *E*-stilbene **35** under the Sharpless condition by using helicene **36** as a chiral auxiliary resulted in **37** with 32% yield with 100% *de* [49] (Scheme 3).



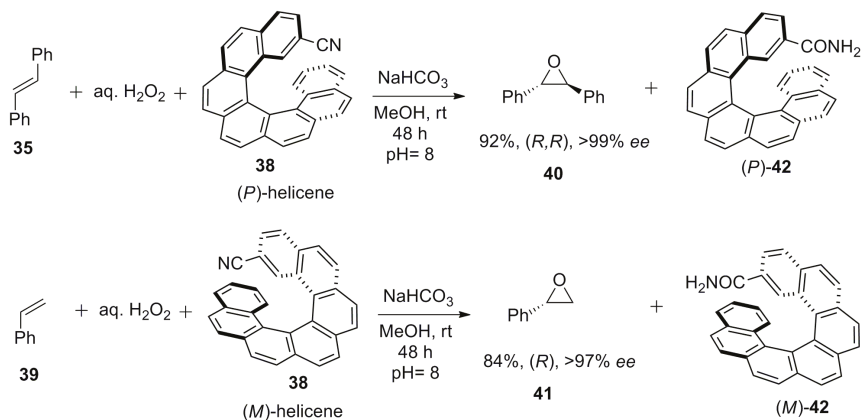
Scheme 3. Diastereoselective hydroxyamination of stilbene reaction using racemic [7]helicene **33** as a chiral auxiliary.

Another example is based on enantioenriched 2-cyano-[7]helicene **38** employed as a stoichiometric chiral additive (reagent) for the epoxidation of alkenes **35** and **39** using H₂O₂ as an oxidant to give enantiopure epoxides **40** (92%, 99% *ee*) and **41** (84%, 97% *ee*), respectively [50] (Scheme 4). The mechanism includes the initial reaction between enantiopure 2-cyano-[7]helicene **37** and H₂O₂ to generate in situ the corresponding chiral hydroperoxyimine, which serves as a chiral oxidizing reagent for the subsequent epoxidation of alkenes **35** and **39**, whilst itself converting finally to [7]helicene-2-carboxamide **42**.

These examples (Schemes 1–4) [46–50] are the first cases of helicenes being used as chiral auxiliaries resulting in a high asymmetric conversion (*de* or *ee*), yet noncatalytic in nature. These excellent results were due to the judicious selection of [7]helicene with corresponding functionalization at the 2-position (monodentate) (refer, Figure 8), which locates inside the helical chiral cavity with sufficient accessibility to the reactants. Besides this, a geometric feature of [7]helicenes is that the two peripheral rings are located one above another, hence inducing steric hindrance to one of the reacting prochiral faces and generating high selectivity via the stereospecific approach.

It is of note that most of the helicene-based catalytic research is focused on the use of [6]helicene and substituted [5]helicene-based systems. In cases where functionalization at both the rings is needed, substituted [5]helicenes and [6]helicenes are more suitable due to possibility of the geometrical accessibility of these groups (refer, Figure 8b). These groups are located on the same side; hence, they

are capable of coordinating or bonding together with the reactive partners. However, this situation is difficult to obtain in [7]helicenes, as seven benzenoid rings give the in-plane turn angle of 420° ($7 \times 60^\circ$), forcing the functional groups present on the terminal rings to exist in opposite directions, thus unable to work co-operatively (refer, Figure 8b). Yet, when only one of the peripheral rings is functionalized and acts as an active catalytic site, the [7]helicene-based systems have an additional advantage over substituted [5]- and [6]helicenes. This is owing to the same in-plane turn angle property allowing another peripheral ring to block one of the prochiral faces of the reactant. Nevertheless, surprisingly, asymmetric catalysis with [7]helicenes is not well explored in comparison with that with [5]- and [6]helicenes.



Scheme 4. Enantioselective epoxidation of alkenes **35** and **39** using entioenriched [7]helicene **38** as a chiral additive.

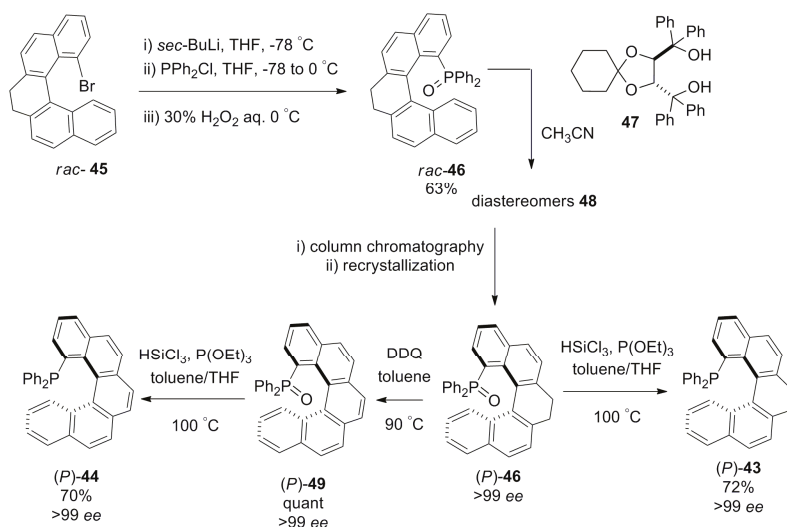
6. Helicenes as Chiral Catalysts

Since various helicene-based phosphine-related ligands have been reviewed [2,5,7–9], only recent selected examples capable of delivering exceptionally high *ee* values are summarized here.

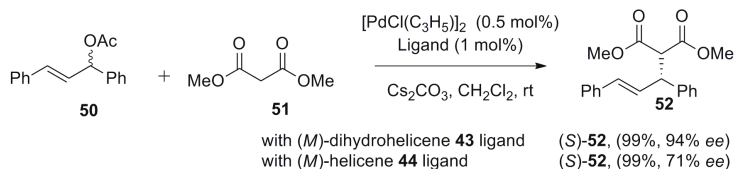
In 2016, the [5]carbohelicene-based phosphine ligands **43** and **44** were rationally designed for application in Pd-catalyzed asymmetric synthesis [51]. Both the systems were prepared from corresponding *rac*-bromo substituted **45** via lithiation and subsequent reaction with chlorodiphenylphosphine followed by oxidation with hydrogen peroxide to afford *rac*-phosphine oxide **46** with 63% yield. It was successfully resolved by using spiro-TADDOL ($\alpha,\alpha,\alpha,\alpha$ -tetraphenyl-1,3-dioxolane-4,5-dimethanol) **47** as a resolving agent to form the insoluble diastereomer **48** with (P) -**46**, which in turn gave pure (P) -**46** with greater than 99% *ee* on subsequent treatment. Then, (P) -**46** was aromatized to **49** quantitatively by using 2,3-dichloro-5,6-dicyano-1,4-benzoquinone. Both the phosphine oxides **48** and **49** were reduced to the corresponding phosphines, **43** and **44**, with trichlorosilane and $\text{P}(\text{OEt})_3$ with 70–72% yield and 99% *ee* (Scheme 5) [51].

In general, unsubstituted [5]helicenes are configurationally unstable and tend to racemize easily. However, introduction of the diphenylphosphine group at the 1-position results in the configurational stability of **43** and **44**. Of these two structures, the 7,8-dihydro-derivative **43** tends to be more helical due to the saturated ethane unit, which has greater conformational flexibility. From X-ray analysis, it was confirmed that the helical pitch diameter of dihydrohelicene **43** is 3.54–3.50 Å, which is larger than that of fully aromatic **44**, found to be 3.39–3.34 Å. This rationally changed spatial arrangement has a noticeable influence on its application as a ligand owing to the favorable geometry and distance, which was clearly demonstrated by the metal–ligand and arene interaction. Hence, the double bond (C8a–C14b) is coordinated with the palladium metal center of ligand **44** in a side-on (η^2) fashion,

which is not possible in the case of dihydrohelicene **43**. This difference in geometric features controls the outcome of Pd-catalyzed reactions. For example, the alkylation of *rac*-1,3-diphenylallyl acetate **50** with dimethyl malonate **51** by using (*M*)-dihydrohelicene **43** as a chiral ligand was highly efficient, resulting in the corresponding (*S*)-enantiomer **52** with 99% yield and 94% *ee* (Scheme 6) [51]. In contrast, the fully aromatic (*M*)-helicene **44**, whilst affording the same configuration of the product **52**, gave similar yield, but only 71% *ee* (Scheme 6). This clearly demonstrates that the ligands' geometry allowed them to opt for different transition states.



Scheme 5. Synthesis and resolution of enantiopure phosphine ligands **43** and **44**.



Scheme 6. Pd-catalyzed asymmetric alkylation of *rac*-1,3-diphenylallyl acetate **50** using helical phosphine ligands **43** and **44**.

Similar types of C1 position substituted phosphinite ligands, helicene **53** [52] and helicene **54** [52] (Figure 9), were also prepared and successfully explored for the Pd-catalyzed asymmetric allylic alkylation between **50** and **51** (see Scheme 5). In both cases, the high yields and *ee* of **52** were obtained as with **53** (96%, 90% *ee*) and with **54** (97%, 99% *ee*) [52]. It is of note that this kinetic resolution reaction using helicene ligand **55** [53] was firstly reported in 2000 with 100% conversion and 81% *ee* (Figure 9). Although the results from using **55** are comparatively worse in terms of *ee*, the reaction requires less catalyst loading and proceeds faster compared with other ligands. Interestingly, **55**, whilst being a bidentate ligand, still acts as a monophosphine (monodentate) ligand during the catalytic process owing to the large distance (6.481 Å) between the two phosphorus atoms; this was the subject of pioneering work by Reetz et al. [53]. Thus, one can see that all phosphine (**43**, **44**) and phosphinite (**53**, **54**) ligands prepared later, possess only a mono phosphorus atom and are suitable for application as monodentate ligands in this reaction.

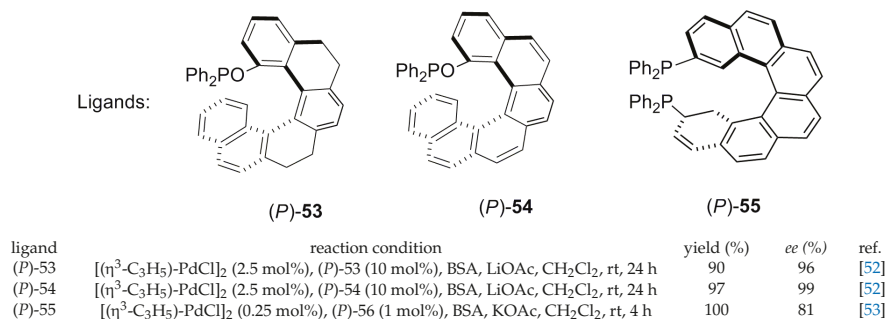
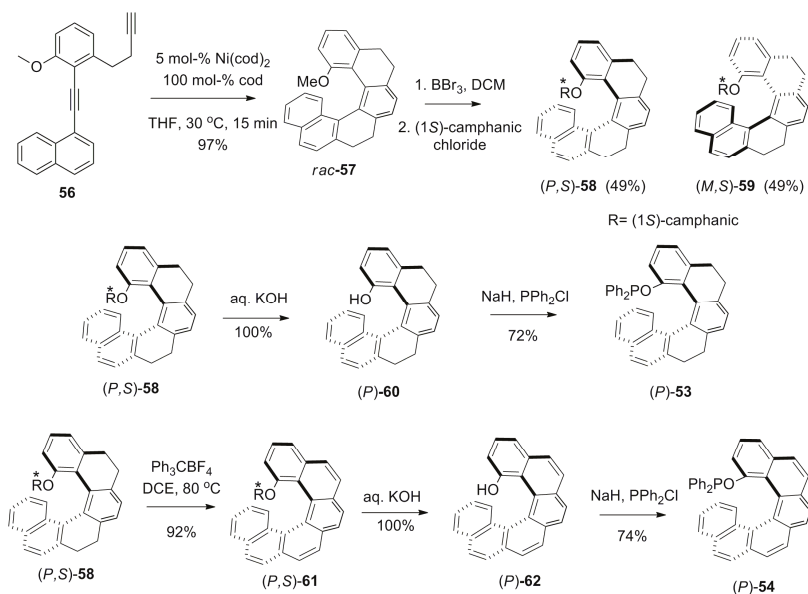


Figure 9. Other helicene-based phosphorus-containing ligands 53–55 used for Pd-catalyzed allylic substitution reaction of **50** and subsequent kinetic resolution.

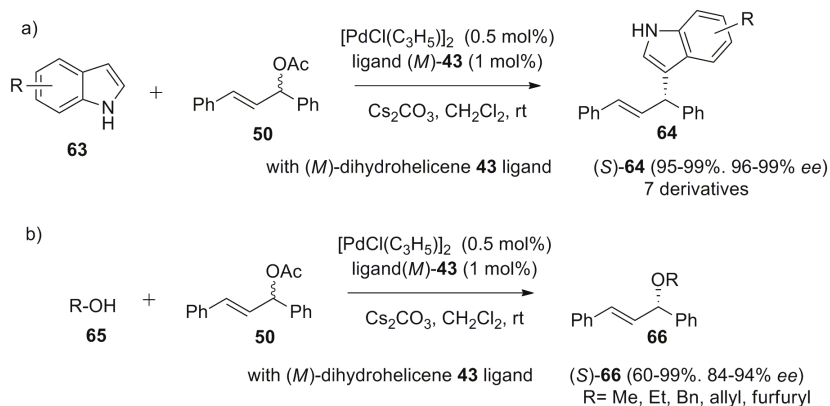
The corresponding enantiopure **53** and **54** were synthesized using the Ni-catalyzed [2 + 2 + 2] cycloaddition reaction of alkyne **56** to give **57** (97%), and the subsequent demethylation and esterification as (1*S*)-camphanate to yield the corresponding diastereomers, **58** and **59**. Further, the separated diastereomers were hydrolyzed with alkali to quantitatively produce the enantiomer **60**, which, on subsequent reaction with chlorodiphenylphosphine in the presence of sodium hydride, resulted in the tetrahydro phosphinite ligand, (P)-**53**. For **54**, an additional step of dehydrogenation using triphenylmethyl tetrafluoroborate (Ph_3CBF_4) was required to obtain the diastereomer **61** (92%), which upon hydrolysis gave [6]helicene-1-ol **62**, which was finally converted to phosphinite **54** with 74% yield (Scheme 7) [52].



Scheme 7. Synthesis and optical resolution of **53** and **54** by using the Ni-catalyzed [2 + 2 + 2] cycloaddition reaction as a key step.

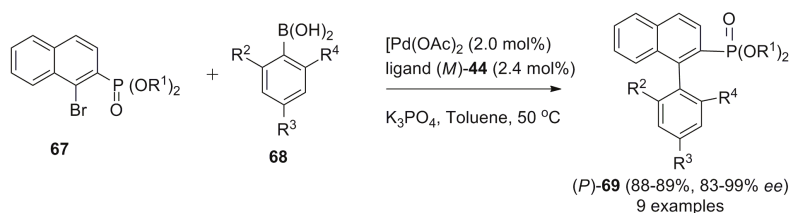
Inspired by the difference in the catalytic performance of **43** (94% *ee*) and **44** (71% *ee*) (Scheme 6) in Pd-catalyzed asymmetric allylic alkylation, the same group also applied these ligands in other

Pd-catalyzed reactions. Thus, in further investigation, the dihydrohelicene ligand **43** was found to be highly useful in the asymmetric allylation of indoles **63** with 1,3-diphenylallyl acetate **50** to give the 3-alkylated indole product **64** in up to 99% *ee*, and in the etherification with alcohols **65** to yield **66** in up to 94% *ee* (Scheme 8) [51].



Scheme 8. Pd-catalyzed asymmetric allylic substitution reactions of **50** by using (*M*)-helicenoid phosphine ligand **43** (a) with indole **63** and (b) with alcohols **65**.

In the case of fully aromatic helicene **44**, the ligand was highly effective in the stereocontrol of helical chirality in the Suzuki–Miyaura coupling reaction between bromide derivative **67** and boronic acid **68**, resulting in up to 99% *ee* for chiral biaryl products **69** of (*P*)-helicity (Scheme 9) [51].

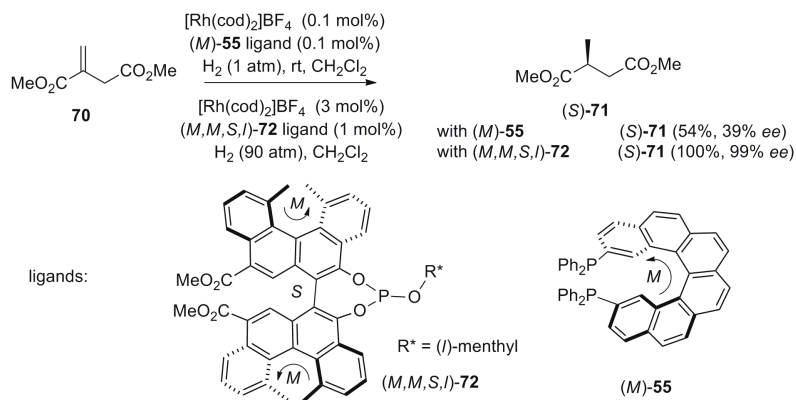


Scheme 9. Pd-catalyzed asymmetric Suzuki–Miyaura coupling between **67** and **68** using (*P*)-**44** as the helicene phosphine ligand.

These examples (**43** and **44**) clearly show that the helicity and space available in the helical groove suitable for a specific transition state play a vital role in the stereoselective control of the reaction pathway. The DFT-based calculation at the B3PW91/6-31G* level (LANL2DZ for the Pd atoms) revealed that the transition state with minimum steric repulsions between the helicene backbone and the reactant group is responsible for the (*S*)-configuration products (**52**, **64**, and **66**) and *P*-configuration product (**69**) obtained with high *ee* [51].

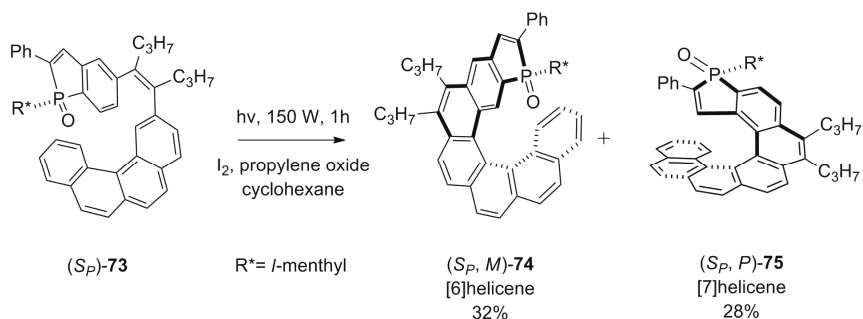
Helicene-based ligands have been also successfully investigated for the rhodium-catalyzed asymmetric hydrogenation of alkenes. In fact, the first enantioselective catalysis using helical diphosphane **55** was the asymmetric reduction of itaconate **70** as a model compound under mild conditions using in situ generated (*M*)-**55** and $[\text{Rh}(\text{cod})_2]^+\text{BF}_4^-$. This results in the corresponding diester (*S*)-**71** with 54% yield and 39% *ee* product, as reported by Reetz et al. [54] (Scheme 10). The synthesis of **55** is based on photochemical cyclization with subsequent conversion of the corresponding helicenedibromide derivative to phosphine **55**, followed by preparative chiral HPLC

separation of the enantiomers [54]. Yamaguchi et al. improved the yield (up to 100%) and enantioselectivity up to 96% *ee* for (*S*)-**71** using the (*M,M,S,I*)-configuration of the bis-helicenic phosphite ligand **72** [55] (Scheme 10). The excellent output in this reaction obtained with **72** was attributed to the matched (suitable) pair of asymmetries, i.e., two (*M*)-helical and one (*S*)-axial chirality. However, the central chirality derived from the *l*-menthyl part does not have much effect on the reaction *ee* outcome.

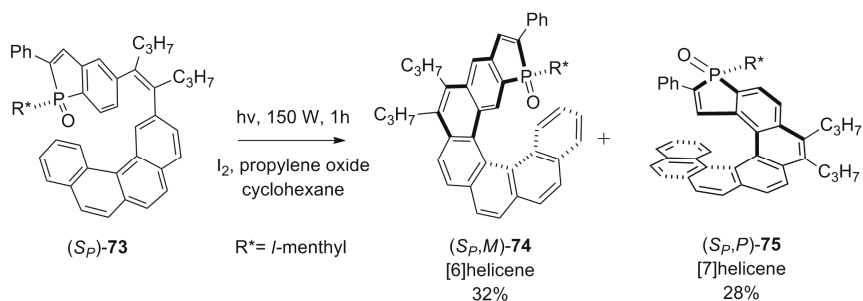


Scheme 10. Comparative Rh-catalyzed asymmetric hydrogenation of itaconate ester **70** using helicene-based ligands **55** and **72**.

Another approach adopted was to design a helicene with the fused phosphole heterocyclic unit at one of the terminal rings where the phosphorus atom has an additional point chirality, denoted as S_P or R_P . A key synthetic step includes the diastereoselective photochemical cyclization reaction of a suitable (S_P or R_P) enantiopure phosphole-bearing stilbene derivative **73**. The resulting regioisomeric [6]helicene phosphine oxide **74** and phospho[7]helicene **75** were chromatographically separated with 32% and 28% yield, respectively [56] (Scheme 11).

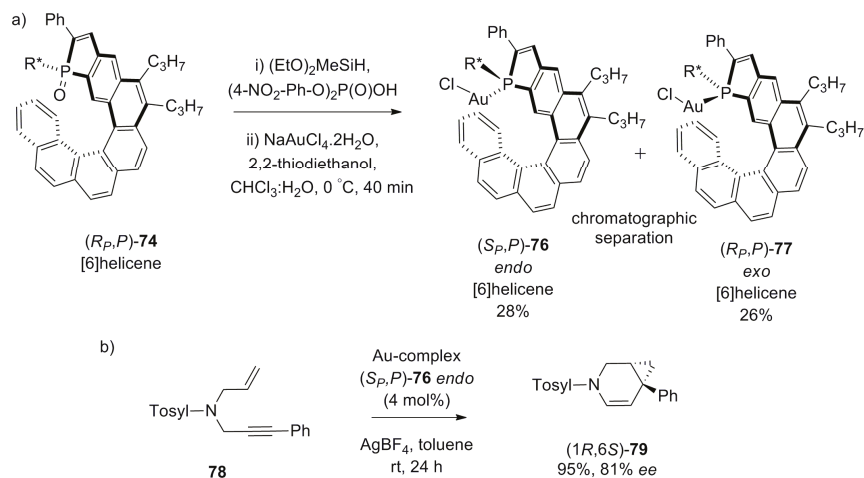


Scheme 11. Cont.



Scheme 11. Photochemical diastereoselective synthesis of [6]helicene phosphine oxide **74** and phospho[7]helicene **75**.

Subsequently, enantiopure **74** was reduced and in situ reacted with gold(I) salts to generate the phospho-substituted helicene–gold complexes, **76** (*endo*) and **77** (*exo*). In *endo*-**76**, the gold atom occupies the internal chiral cavity space, approaching towards the opposite terminal ring, whereas in *exo*-**77**, the gold atom is situated at the external face, being away from the helical moiety. Thus, chromatographically separated *endo*-**76** effectively catalyzes the enantioselective cycloisomerization of N-tethered 1,6-enyne **78** to give bicyclo[4.1.0]heptane **79** with 95% yield and 81% *ee*, whilst *exo*-**77** remained almost inactive [56] (Scheme 12). Meanwhile, various phosphole-containing ligands were also prepared and screened in similar reactions with success [8,9,57].



Scheme 12. (a) Synthesis of *endo* (S_P, P)-**76** and (b) its application as a catalyst for the enantioselective cycloisomerization of N-tethered enyne **78**.

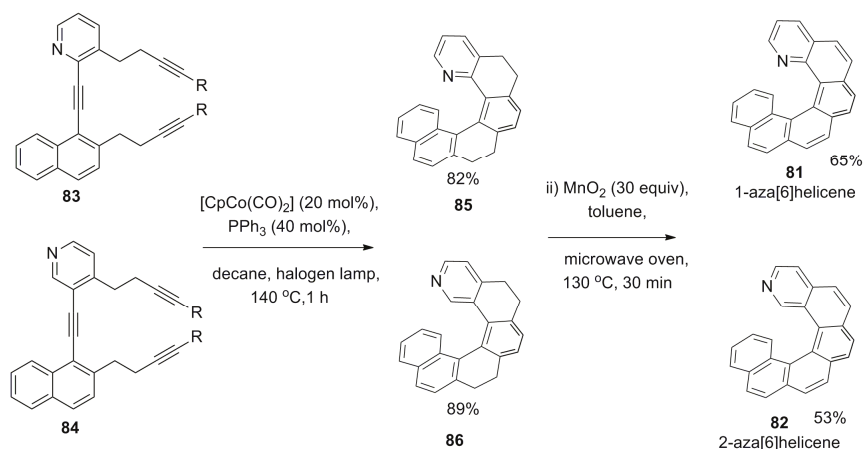
However, at present, the scope of the use of helicenes containing phosphorus functionality appears to be limited towards the metal-catalyzed reactions, as described above. A few other attempted asymmetric reactions such as ketimine reduction (22% *ee*), addition of thioester to benzaldehyde (22% *ee*), and reductive aldol reaction afforded quite low *ee* values, with tetrathia[6]helicene diphosphine oxides as a Lewis base catalyst [58].

Besides these phosphorus-containing helicenes, heterohelicenes with a nitrogen atom at the innermost 1- or 2-position are also able to provide a chiral cavity suitable for various asymmetric organocatalytic processes, where the nitrogen atom plays a crucial role as a Lewis base or hydrogen-bonding auxiliary.

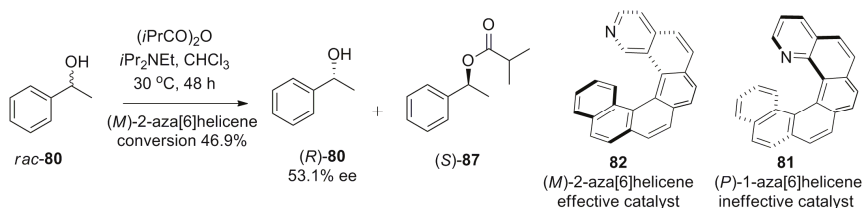
The classical synthetic approach for azahelicenes having a nitrogen atom at the peripheral ring as the pyridine subunit is based on the preparation of the corresponding stilbene derivative followed by the photocyclization reaction.

The first use of a pyridine-based helicene as a chiral organocatalyst for promoting the enantioselective acyl group transfer reaction and kinetic resolution of racemic phenylethanol **80** was reported by Stary et al. in 2009 [59]. The preparation of helicenes **81** and **82** [60] involves the [2 + 2 + 2] cyclotrimerization of regioisomeric aromatic triynes **83** and **84** using a Co(I)-catalyzed reaction as the major synthetic step to obtain tetrahydrohelicenes **85** (82%) and **86** (89%), respectively (Scheme 13). Finally, the MnO₂-based oxidation resulted in *rac* aza[6]helicene **81** (65%) and **82** (53%). The optical resolution of helicene **81** was carried out through the diastereomeric salt formation with optically pure (+)-*O,O'*-dibenzoyl-D-tartaric acid, whereas enantiopure **82** was obtained by separation of the corresponding racemic mixture with chiral HPLC (Scheme 13) [60].

It was found that (+)-(*P*)-1-aza[6]helicene **81** is an ineffective catalyst for this process with <5% yield, as the nitrogen atom at the most sterically congested position has very limited accessibility for the reactant. However, the isomeric (–)-(*M*)-2-aza[6]helicene **82**, due to the easily accessible nitrogen atom position, considerably improved the catalytic performance with 46.9% conversion to **87** and 53.1% *ee* for the unreacted starting alcohol **80** (*R*-configuration) with a selectivity factor of 7 for the corresponding (*S*)-enantiomer (Scheme 14) [59].



Scheme 13. Synthesis of azahelicenes **81** and **82** via Co⁺¹-catalyzed [2 + 2 + 2] cyclotrimerization reaction.



Scheme 14. Kinetic resolution of *rac*-phenylethanol **80** by (*M*)-**81** and (*M*)-**82**.

This example clearly demonstrates how the suitably tailor-made design of azahelicenes can provide a useful chiral pyridine-based nucleophilic organocatalyst comparable to other enantiopure amine-containing catalysts, whilst possessing different elements of asymmetry. In comparison to pyridine, dimethylaminopyridine (DMAP) and DMAP-containing compounds **88–90** [61–64] (Figure 10)

are better nucleophilic catalysts for acylation of alcohols due to the enhanced nucleophilicity provided by the electron donating nature of the dimethylamino group at the para position. Thus, (*P*)-helicenoids **88** containing a *p*-dialkyl amino substituent turned out to be a more effective enantiodifferentiating catalyst for the resolution of the (*S*)-enantiomer of racemic **80** with the selectivity factor of 17, in 5 h, as compared to 48 h with a selectivity factor of 7 using (*M*)-**82** as the catalyst.

The heliceneoidal DMAP **88** has a nitrogen atom at the 2-position and saturated N-alkyl group, whilst the helicene core ensures two additional advantages. Firstly, it enhances the nucleophilicity of the pyridine nitrogen at the 2-position by its electron donating ability (+I effect), and secondly, it increases the conformational flexibility to accommodate reactants inside the helical chiral cavity for efficient enantiodifferentiating processes. The attached ethyl substituents at the central ring of the helical outer core were responsible for increasing the lipophilic character and, thus, the solubility in organic solvents for better performance [61]. The heliceneoid DMAP **88** displayed a comparatively higher selectivity factor of 17–116, depending on the structure of the racemic aromatic ethanol. In comparison to **88**, the axially chiral DMAP catalyst **89** [62,63] showed selectivity factors of 12–52 (in ether) [62] and 32–95 (in *t*-amyl alcohol) [63] for enantioresolution of different racemic aromatic ethanols. However, the planar chiral DMAP catalyst **90** [64] displayed the smaller selectivity factor of 8.9–29. It is of note that, with planar chiral DMAP **89**, the acylating agent was acetic anhydride, whereas, in other cases, bulkier isobutyric anhydride was used. Thus, the helical DMAP **88** appears to be highly superior to **90** under similar experimental conditions.

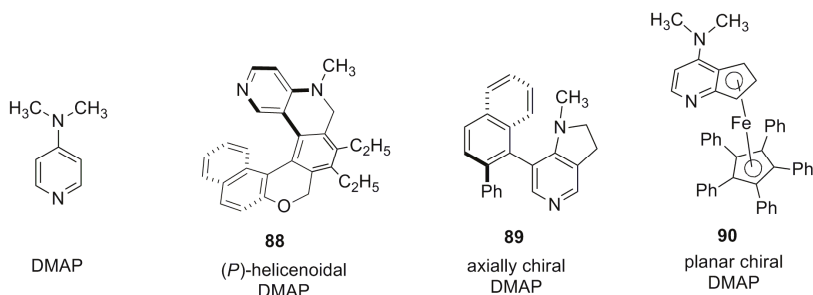
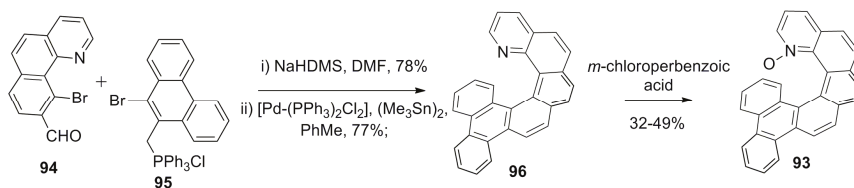


Figure 10. Structures of simple dimethylaminopyridine (DMAP) and helically, axially, and planar chiral DMAP catalysts **88–90**, respectively.

Indeed, the first use of unsubstituted aza[6]helicene **81** and **82** as an organocatalyst for the kinetic resolution of alcohols rationalized the corresponding steric constraint imposed at the 1-position for a bulky acyl moiety and its subsequent group transfer reaction to *rac*-alcohols. However, the additionally functionalized 1-aza[6]helicene was found to be an effective asymmetric catalyst for various reactions [65,66], probably due to the facile access to reactants in the chiral cavity in the transition state, as demonstrated in the following examples.

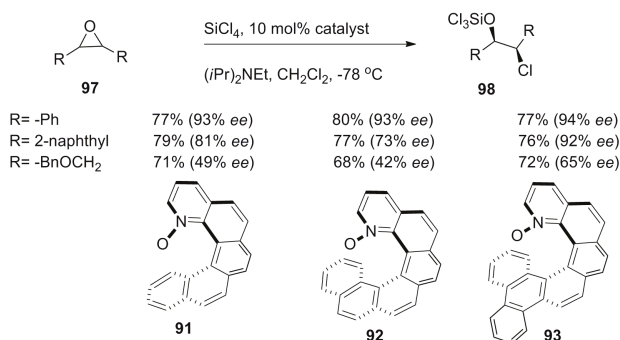
The azahelicene-based systems were converted to the corresponding *N*-oxides and investigated for the asymmetric ring opening of epoxides with chloride as a nucleophile. For example, 1-aza[6]helicene-*N*-oxide derivatives **91–93** (Schemes 15 and 16) [67] were prepared in the racemic form using a general three-step synthetic methodology, and their enantiomers were resolved over chiral HPLC [67]. The representative synthesis of **93** starts from the benzoquinoline aldehyde unit **94** and corresponding bromo-substituted phosphonium salt **95** in three steps, where the initial step involves the *Z*-selective Wittig condensation followed by the palladium-catalyzed Stille–Kelly coupling reaction to result in azahelicene **96**. Finally, oxidation with *meta*-chloroperbenzoic acid gave the desired helicene-*N*-oxide **93** with 32–49% yield (Scheme 15).



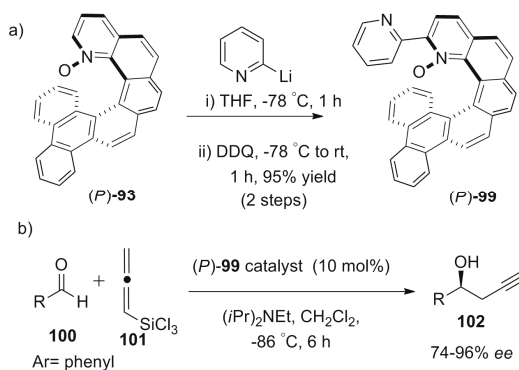
Scheme 15. Representative general synthetic scheme for 1-azahelicene-*N*-oxide **93** using Stille–Kelly coupling reaction.

Then, the enantiopure (*P*)-helical ligands **91–93** were screened for the desymmetrization of *meso* epoxide **97** with chloride as a nucleophile to obtain **98** with satisfactory yields and *ee* (Scheme 16) [67].

Similarly, enantiopure helical 2,2'-bipyridine-*N*-monoxide **99** was prepared in two steps from enantiopure **93** with 95% yield (Scheme 17a) and applied as a Lewis base type catalyst for the highly enantioselective reaction between aldehyde, **100**, and allenyltrichlorosilane **101** to obtain enantiomerically enriched homopropargylic alcohol **102** [68]. The reaction displayed high conversion (78–97%) and 74–96% *ee* for various *ortho*- and *para*-substituted aromatic aldehyde derivatives, with 18 examples in total (Scheme 17b). Further, the catalyst **99** can be recovered (~80%) without any loss of activity and selectivity after the reaction, making it highly attractive for industrial application.



Scheme 16. Desymmetrization of *meso* epoxide **97** using 1-azahelicene-*N*-oxide **91–93** as catalysts.



Scheme 17. (a) Two-step synthesis of helicene (*P*)-**99** from (*P*)-**93** and (b) asymmetric synthesis of (*S*)-propargylic alcohols **102** from aldehyde **100** and allenyltrichlorosilane **101** by using (*P*)-**99** as a catalyst.

The (*S*)-alcohol **102** was the major product with (*P*)-helicene **99** as a catalyst. It was also observed that *ortho*-substituted aldehydes **100** always provided higher *ee* than the corresponding *para*-substituted derivatives, regardless of the functional group attached. This key experimental observation indicated that, out of two possible transition states (Figure 11a,b), in one of them, the hydrogen or substituent at the *ortho* position of aldehyde **100** results in steric clash with catalyst **99**, which is responsible for the stereoselectivity. Thus, the suggested transition state model showed preference for the *Si*-face addition with π - π stacking between the bound aldehyde **100** and the bezofused helicene framework of **99** (Figure 11a), whereas the *Re*-face approach is disfavored due to the steric hindrance in the transition state (Figure 11b), where the reactants **100** and **101** and catalyst **99** are coordinated through the silicon atom. A separate DFT-based computational study also supported this mechanism [69].

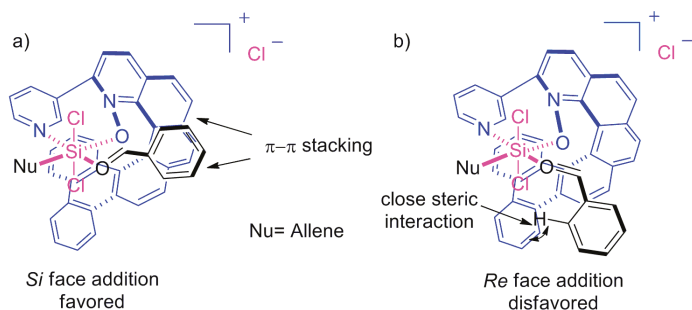


Figure 11. Proposed transition state models showing preference for (a) favorable *Si*-face attack and (b) unfavorable *Re*-face attack, with (*P*)-**99** catalyst. The bottom and top parts of the transition state models are marked in blue and black, respectively, whilst the coordinated SiCl_2 group with the corresponding bonds are marked in magenta.

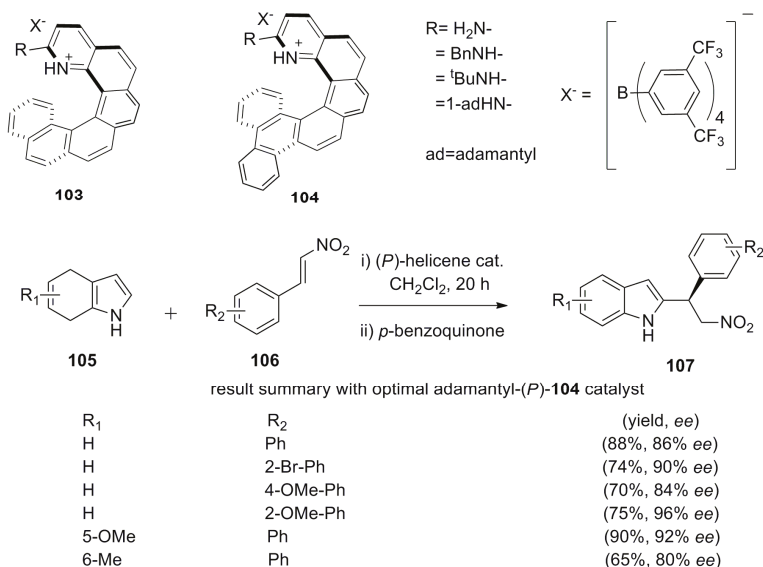
Azahelicenes have also been investigated as hydrogen bond donor chiral catalysts. The asymmetric addition of azole nucleophiles to nitroalkenes using various hydrogen bond catalysts is known. In this respect, aminopyridinium salts are also capable of activating nitroalkenes through the hydrogen bond donating ability to the nitro group. For this purpose, aza[6]helicene derivatives **103** and **104**, having a 2-aminopyridinium ring at the peripheral position, have been prepared [70]. Hence, the asymmetric addition of 4,7-dihydroindole **105** to nitrostyrene **106** using chiral (*P*)-helicenes **103** and **104** as catalysts, followed by oxidative aromatization, afforded exclusively β -nitro-indol-2-yl **107** with relatively high yield and *ee* (Scheme 18).

It was observed that the increased bulkiness of the amino group gives a higher *ee*. Thus, the results of (*P*)-**104** in terms of *ee* ratio were as follows for the corresponding R: H (69:31) = Bn (69:31) < *t*-Bu (92:8) = 1-adamantyl (92:8). Further, the yields were noticeably improved from 79% (for the *t*-Bu derivative) to 88% (for the adamantyl derivative) under similar conditions; hence, adamantyl-containing (*P*)-**104** is the optimal organocatalyst for this reaction (see the corresponding results summarized in Scheme 18). Further, the enhanced effectiveness of **104** in comparison with **103** indicates that the benzofused helicene framework affects the *ee* value by covering the space beneath the two hydrogen bonds [70], and is thus similar to the case shown in Figure 11.

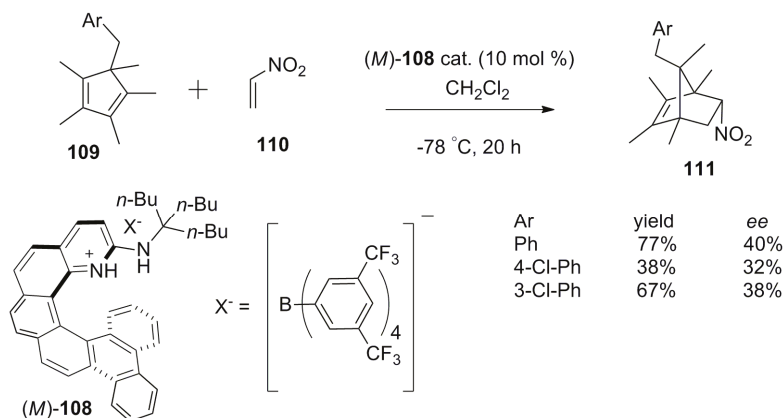
Another example of the activation of nitroalkenes via the hydrogen bonding donor characteristics was demonstrated by using aminopyridinium-based (*M*)-[6]helicene **108** in the asymmetric Diels–Alder reaction between cyclopentadienes **109** and nitroethylene **110** to give the cycloadduct product **111** in moderate 30–40% *ee* [71]. A traditional hydrogen bonded catalyst generally requires the complementary donor–acceptor units in both reactants to orient specifically for asymmetric induction in the addition reaction. However, here is a case where one counterpart is a nonfunctionalized cyclopentadiene **109**, unsuitable for hydrogen bonding. Therefore, the (*M*)-helicene catalyst **108** used has an aminopyridinium

peripheral ring which only binds to nitroethylene **110** (dienophile) through the corresponding hydrogen bonding. The stereospecificity of this reaction was achieved in the following manner: the helical backbone of (*M*)-**108** blocks one of the faces of **110**, leaving another face accessible to **109** (diene), hence making the whole reaction enantioselective in nature (Scheme 19).

Most of the successful examples of azahelicenes (**91–93**, **99**, **103**, **104**, **108**) as organocatalysts described here have a nitrogen atom at the 1-position of the innermost part of the helicene with additional substituents at the 1- or 2-position to modify the reactivity as well as the helicity (chiral cavity space), to facilitate accessibility of the reactant in a stereospecific manner, and to enhance asymmetric output.



Scheme 18. Asymmetric addition reaction between 4,7-dihydroindole **105** and nitrostyrene **106** using chiral (*P*)-helicenes **103** and **104** as hydrogen bond donor catalysts.



Scheme 19. (*M*)-helicene **108** as a hydrogen bond catalyst for asymmetric Diels–Alder reaction between cyclopentadiene **109** and nitroethylene **110**.

Carbohelicenes **5** and **6** and heterohelicene **112**, devoid of any functional group, are also able to act as chirality inducers in selected asymmetric reactions. Soai et al. have successfully used electron-rich nonfunctionalized carbohelicenes **5** and **6** [72] and heterohelicene **112** [73] for the nucleophilic addition of diisopropylzinc to electron-deficient pyrimidine-5-carbaldehyde **113**. In this case, the chirality induction was a result of two main reasons. Firstly, the formation of a charge transfer complex between helicenes **5**, **6**, and **112** and the carbonyl group of **113** results in the blocking of one reactive face while another face is left to react. Secondly, the final alcohol product **114** obtained can catalyze this reaction by itself, leading to overall chirality amplification to yield up to 95–99% *ee* (Scheme 20). In all these cases, the use of (*P*)-enantiomers of **5**, **6**, and **112** as catalysts resulted in the (*S*)-configuration of **114**, whereas the (*M*)-enantiomer produced the corresponding *R*-configuration. Further, even carbohelicenes **5** and **6** with a very low *ee* such as 0.13% and 0.54% were also able to act as chiral inducers, ensuring considerable stereospecificity and affording 56% and 60% *ee* of **114**, respectively, as a result of chirality amplification by asymmetric autocatalysis [72].

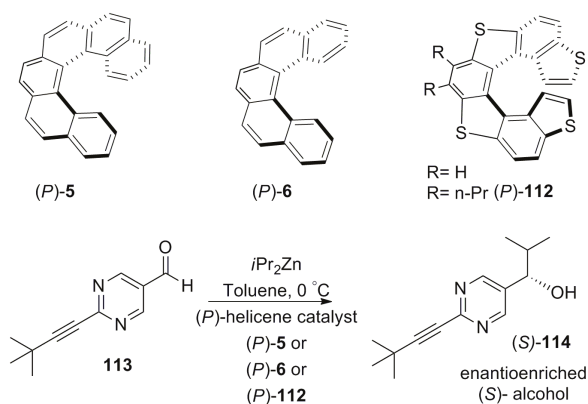
This is an interesting example where chiral inducers with a very low *ee* generate significantly enhanced *ee* of the product. This type of chiral amplification is a “soldiers-and-sergeant” principle and often observable in the field of supramolecular chirogenesis [1]. However, this scope appears to be limited in the case of asymmetric autocatalysis.

Indeed, the asymmetric nucleophilic addition of an organozinc compound to the carbonyl group has been mainly investigated with the use of biaryl-based systems such as BINOL and 2,2'-Diphenyl-(4-biphenanthrol)—axially chiral diol systems capable of coordinating to Lewis acids. Inspired by this, Katz et al. developed the bis[5]helicene-based diol system ([5]HELOL) **115**, which contains two identical units of (*P*)-[5]helicene-1-ol **116** connected by a single biaryl bond at the 2-position. Interestingly, the hydroxyl group is attached at the 1-position (the innermost position of [5]helicene), which makes **116** configurationally stable, and hence provides increased steric hindrance for racemization. The HELOL **115** was synthesized in a total of eight steps on the multigram scale with an overall 44% yield (Scheme 21a) [74]. The helicene backbone **117** was synthesized by Diels–Alder reaction between protected enol ether **118** and quinone **119**. The enantiopure (*P*)-[5]helicene-1-ol **116** was oxidatively coupled using Ag₂O, to selectively give (*P,P*)-[5]HELOL **115**, with only ~2% of the *meso* isomer. The energy barrier for the racemization of **115** ($\Delta H^\ddagger = 106 \pm 3 \text{ kJ mol}^{-1}$ and $\Delta S^\ddagger = -10.0 \pm 0.1 \text{ J mol}^{-1} \text{ K}^{-1}$) as determined by ¹H NMR was found to be even higher than that of (*P*)-[5]helicene **116** ($\Delta H^\ddagger = 95.8 \text{ kJ mol}^{-1}$ and $\Delta S^\ddagger = -17.2 \text{ J mol}^{-1} \text{ K}^{-1}$) [74] with the optical rotation value of +2580 in acetonitrile (*c* = 0.01 M). Further, the thermal racemization at 45 °C did not occur in 72 h as indicated by circular dichroism (CD) spectroscopy. Additionally, in degassed acetonitrile solution, it was configurationally stable for six days at room temperature as also analyzed by CD measurement. The enantiomeric stability toward conversion to the *meso* isomer and racemization made it a suitable candidate for screening in asymmetric catalysis.

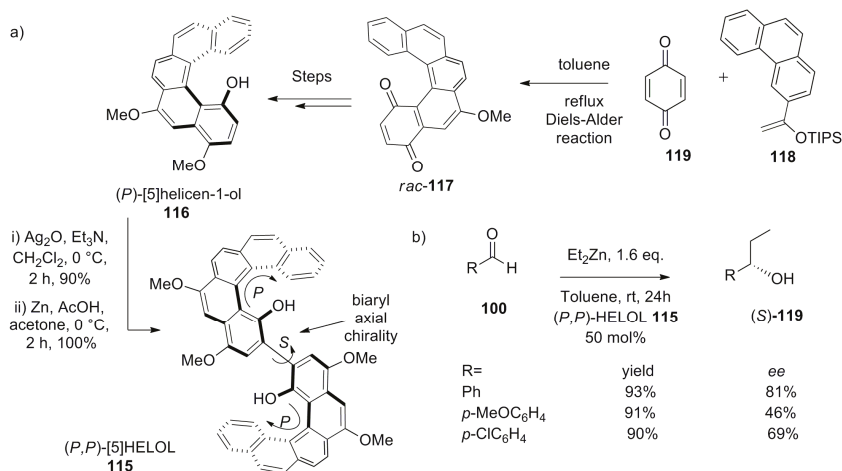
The catalyst **115** was screened for diethylzinc addition to a series of aromatic aldehydes **100**. However, for appreciable catalytic activity, catalyst loading as high as 50 mol% was needed to obtain moderate to good *ee* values of the alcohol products (*S*)-**119** (Scheme 21b). Under similar conditions, the (*R*)-(+)-BINOL gave lower yield (56%) and *ee* (34%) for (*R*)-**119** in comparison to (*P,P*)-(+)-HELOL **115** giving (*S*)-**119** (93% yield, 81% *ee*). This high and opposite stereospecificity is apparently due to a greater steric hindrance of HELOL **115** in comparison to BINOL upon chelation of the zinc atom of the reactant diethyl zinc. Additionally, this crowding in **115** is also able to prevent the phenomenon of zinc–oxygen coordination-based aggregation, responsible for catalyst deactivation, making **115** comparatively more reactive than BINOL [74]. Further, the opposite stereochemical outcome of alcohol products **119** obtained with (*P,P*)-(+)-[5]HELOL **115** as a catalyst and (*R*)-(+)-BINOL as catalyst is in accordance with the stereochemistry of the biaryl bond present in HELOL **115**, which appears to be of (*S*)-configuration (see structure **115** in Scheme 21a).

Whilst unsubstituted [4]helicene **4** is a planar and achiral structure, the introduction of two methyl groups on both the peripheral rings at the innermost positions gives rise to a helical structure

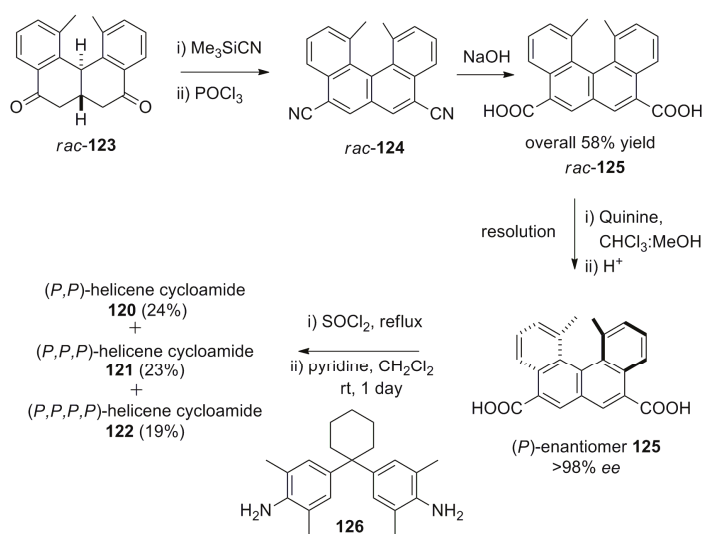
with configurational stability. In this respect, Yamaguchi et al. have extensively explored the synthetic chemistry and applications of functionalized dimethyl[4]helicene in different fields [75]. Thus, (*P,P*)-[4]helicene cycloamides **120–122** were prepared from well-known *rac*-diketone **123** via dicyanohelicene **124**, which was converted to helicene diacid **125** by alkaline hydrolysis. Then, helicene diacid **125** was resolved by using the chiral base quinine through diastereomeric salt formation. Finally, (*P*)-**125** was converted to acid chloride and then coupled with a suitable diamine linker **126** to obtain cycloamides dimer **120** (24%), trimer **121** (23%), and tetramer **122** (19%) (Scheme 22) [76].



Scheme 20. Asymmetric autocatalysis initiated by carbohelicenes (*P*)-5, (*P*)-6, and heterohelicene (*P*)-112.

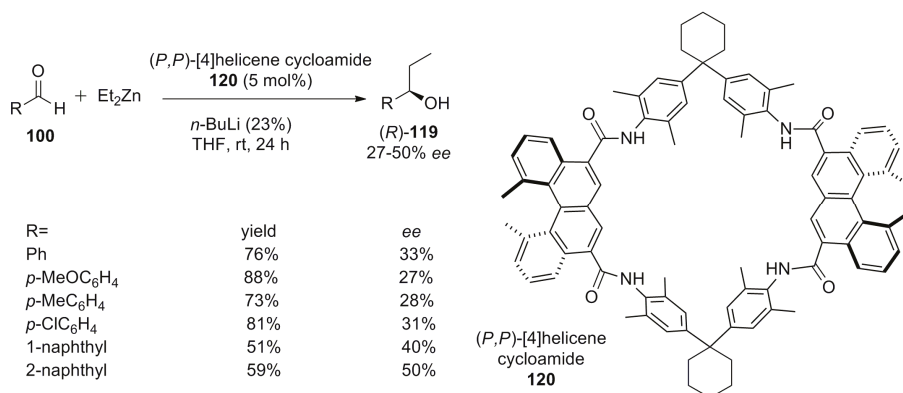


Scheme 21. (a) Synthesis of (*P,P*)-HELOL **115** and (b) its application in asymmetric diethyl zinc addition to benzaldehydes **100**.



Scheme 22. Synthesis of (*P,P*)-helicene cycloamides **120**–**122** from diketone **123**.

Interestingly, in this example, the functionalized amino groups are present at the outer core of the helicene but not at the helical chiral cavity as in previous examples; this makes it remarkably different. Yet, when it is dimerized with a suitable linker such as cycloamide **120**, the chirality of the helicene is transferred to a macrocycloamide, which essentially provides a chiral pocket for the asymmetric catalytic transformations. Macrocycloamides such as (*P,P*)-**120** have been applied for the asymmetric nucleophilic addition of diethyl zinc to aromatic aldehydes **100** with good yields (51–88%) and moderate enantioselectivities (27–50% *ee*) upon use of up to 5 mol % catalyst (Scheme 23) [76].



Scheme 23. (*P,P*)-helicene cycloamide dimer **120** catalyzed asymmetric diethyl zinc addition to aromatic aldehydes **100**.

It has been clearly demonstrated that helicene-based asymmetric organocatalysis is a highly promising and exciting field in terms of the enantioselectivity obtained with the lowest catalyst loading. Thus, this area of chemistry has exciting prospects to explore other well-known asymmetric reactions by using helicenes as organocatalysts, with foreseen advances in terms of the *ee* values in comparison

to conventional organocatalysts. For the most asymmetric organocatalysts, it is possible to design and develop helicene-based helical counterparts which are expected to give improved reactivity and stereoselectivity. However, the design of smart catalysts and their multigram synthesis in the enantiopure form still remain a major challenge to further investigations.

7. Helicene in Supramolecular Chirogenesis

Besides asymmetric catalysis, helicenes are efficiently used in a modern branch of chiral science called supramolecular chirogenesis, which covers all aspects of asymmetry induction, transfer, amplification, and modulation through noncovalent interactions. In numerous chromophoric systems [1] available to date, helicenes are also successfully employed. Indeed, helicenes have turned out to be one of the most attractive chromophores, which are suitable for several chirogenic applications including chiral recognition, sensors, and self-assembly, and are applicable to various areas ranging from classical solution chemistry, nanoparticles, and polymers, up to the sensing of biologically relevant molecules. Owing to their conjugated aromaticity, these chromophoric systems can be conveniently studied by diverse spectroscopic methods, such as UV, fluorescence, NMR, CD, etc., which are described below with selected examples.

7.1. Helicene-Based Chiral Recognition of Small Molecules

Since chirality is an essential part of life on Earth, its recognition and sensing play a vital role in such important fields of human activity as scientific research and modern technologies. Therefore, various methods of obtaining enantiopure molecules by optical resolution and by asymmetric synthesis are attractive areas of chemical research. Besides preparation, the analysis of all types of chiral molecules is also an equally important part of physical–organic chemistry. So far, existing analytical methods are based on the enantiodifferentiation procedure conventionally performed by using chiral HPLC, NMR, fluorescence, and CD techniques. In this respect, chiral helicenes are highly prospective host molecules to serve as specific chirality sensors.

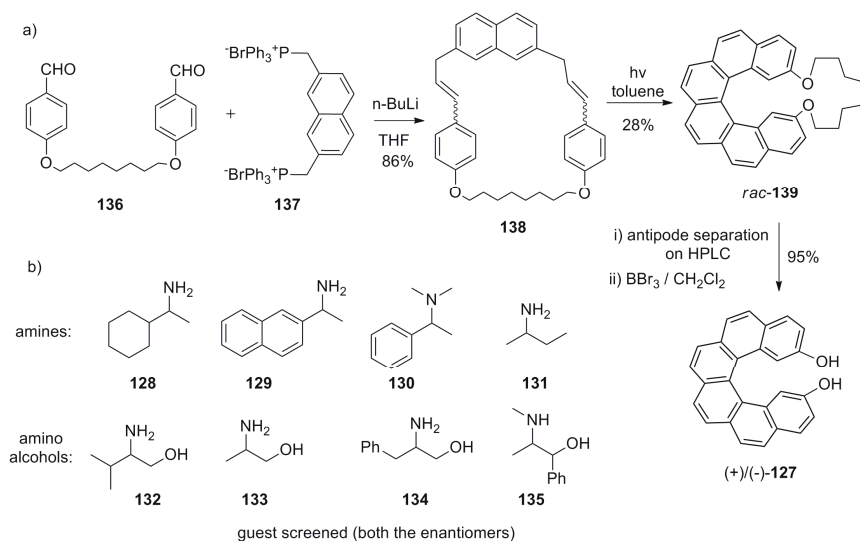
One of the first reports of such an application was published in 2001 by Reetz et al. [77]. To this end, 2,5-dihydroxy[6]helicene **127** (HELIXOL) was prepared for chiral recognition of amines **128–131** and amino alcohols **132–135** by using fluorescence as a detection tool (Scheme 24). The synthetic strategy includes classical Wittig olefination and photochemical cyclization steps. The condensation of **136** with **137** gives cyclic **138**, ether linkage of which ensures structural control during the double photocyclization reaction to obtain helicene cyclophane **139**. The chiral HPLC separation of racemic **139**, followed by the deprotection of the ether group using BBr_3 , affords enantiopure HELIXOL **127** (Scheme 24).

It was found that the host **127** served as an excellent fluorescent sensor, able to display enantioselective quenching by several amines and amino alcohols through the hydrogen bonding interactions. The best results were obtained for alaninol **133** with enantioselective factor $\alpha = K_R/K_S = 2.1$ upon using the levorotary (*M*)-**127**. Although the results obtained with **127** for chirality sensing are moderate, this work is a pioneering contribution for the use of helicenes for the purpose of chirality sensing. Further studies have demonstrated that this new, emerging area is challenging and highly prospective in chemical sciences.

Meanwhile, HELIXOL **127** is a bidentate compound with two hydrogen bonding units (phenolic groups) in the chiral space cavity, which can be used for stereodiscriminating recognition (Figure 8). Thus, it was assumed that amino alcohols may form the corresponding 1:1 host–guest complex, resulting in stronger fluorescence quenching than amines. Indeed, the best result among amines and amino alcohols was obtained for alaninol **133** due to the optimal steric matching in the chiral space available, while displaying the strongest fluorescence quenching output.

Another approach was demonstrated by the application of crown ether-based systems, which are known to bind various cations ranging from metal ions to organic ammonium ions. Hence, the helicene-based crown ethers **140** and **141** were firstly prepared in 1983 by using 1,14-dimethyl

pentahelicene and heptahelicene backbones [78,79]. The synthesis was performed by a classical strategy via Wittig condensation followed by photochemical cyclization. Finally, the construction of crown ethers and subsequent resolution of enantiomers using a chiral column packed with (+)-poly-(triphenylmethyl methacrylate) with methanol as an eluting solvent resulted in enantiomers of **140** and **141**. Then, enantiopure **140** and **141** were investigated towards application in the chiral discrimination of racemic amine salts **142–144** (Figure 12). This process was based on the selective differential transports of recognizable enantiomers from an aqueous solution to the corresponding organic solvent (CHCl_3) by a liquid–liquid extraction procedure. The ^1H NMR analysis of the extracted organic layer displayed two distinct $-\text{CO}_2\text{Me}$ signals of the representing diastereoisomeric complexes with the guest, **142**. Finally, the amount of transported guest was analyzed by a reverse extraction back to an aqueous acidic phase followed by the measurement of its UV absorption.



Scheme 24. (a) Synthesis and resolution of HELIXOL host, **127**; (b) Structures of chiral guest amines **128–131** and amino alcohols **132–135** used for enantioselective recognition studies.

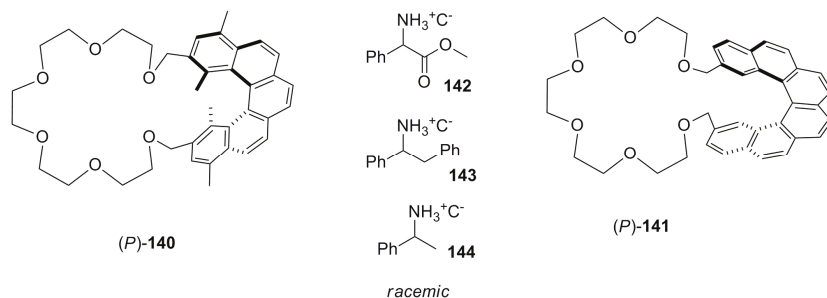
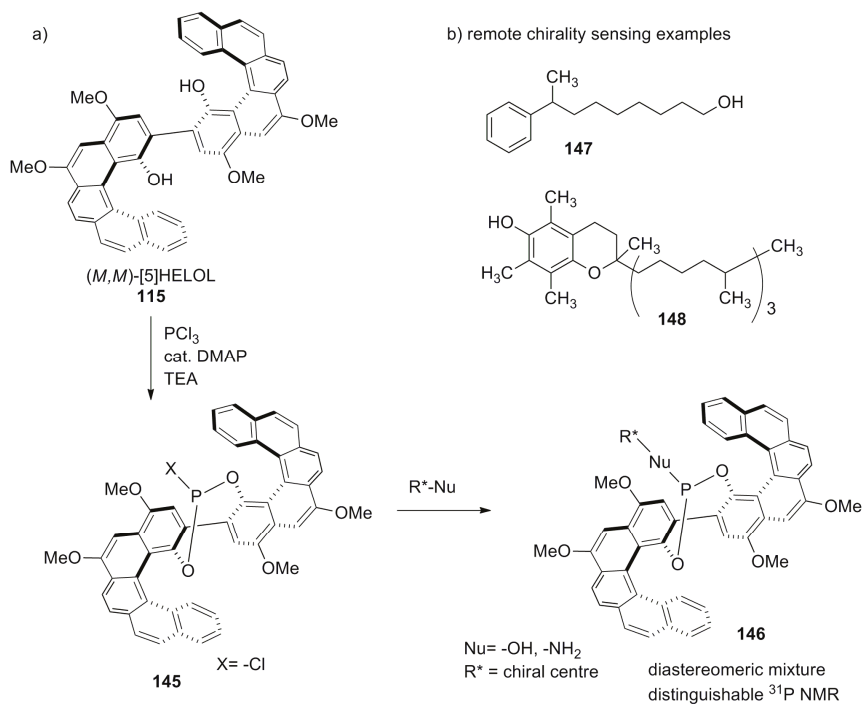


Figure 12. [5]helicene- and [6]helicene-bearing crown ethers **140** and **141** capable of enantioselective extraction of chiral amine salts **142–144** from aqueous to organic layer.

It was observed that the [5]helicene-based crown ether **140** showed higher enantioselective extracting ability than the [6]helicene-based crown ether **141**. For example, (*M*)-**140** was able to transport 6% of (*S*)-**142**, with optical purity of 75% in 6 h, comparatively better than (*M*)-**141** with

2% transport of 26% optical purity of opposite enantiomer (*R*)-**142** in the same time. The observed opposite enantioselectivity extraction using helicenes **140** and **141** with the same helical sense was rationalized by the phenomenon of changing the crown ether conformation [80]; this is evident in their CPK models. Additionally, the inner methyl groups also assist in the chiral recognition process, as suggested by the same models [78,79].

Another approach to chiral recognition was undertaken by Katz et al. via developing the helicene-based biaryl diol compound named (*M,M*)-[5]HELOL, **115** [81], which was based on enantiopure 1-hydroxy substituted [5]helicene (see **116** in Scheme 20). The in situ generated chloro phosphite derivative **145** was used as a chiral NMR derivatizing agent to discriminate alcohols or amines serving as nucleophilic guests. From the ^{31}P NMR analysis of diastereomeric mixture **146**, the enantiomeric excess of guests (alcohols or amines) was easily determined. An interesting feature of this sensor is its ability to sense a remote chirality, which locates far away from the phosphite group. This is related to the fact that the combined inner cavity formed by individual helicene units and the biaryl bond yields an extended chiral space in **115**. For example, this chiral space is able to recognize the asymmetric centers of 8-phenylnonanol **147** (as far as up to seven methylene units) and vitamin E **148** (Scheme 25). Additionally, the recognition ability of this sensor was related to 100% abundance of phosphorus as NMR active nuclei with high sensitivity and accuracy in measurement; thus, the enantiomeric excess of up to 3% can be easily analyzed [81]. The scope of this HELOL host and its structural analogue were further extended towards other nucleophiles such as alcohols, phenols, amines, and carboxylic acids, also containing a remote chirality, under similar methodology to the ^{31}P NMR-based enantiodiscrimination [82].

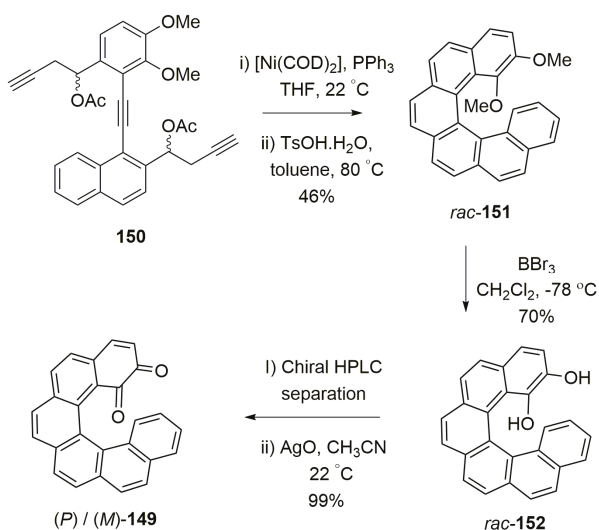


Scheme 25. (a) ^{31}P based diastereomeric NMR sensing of alcohols and amines using (*M,M*)-HELOL **115** and (b) examples of remote chirality sensing with molecules **147** and **148**.

A new chiral application as a chiroptical switch along with chiral recognition properties was demonstrated using enantiomerically pure [6]helicene *o*-quinone **149**. The synthesis was carried out by using the Nickel-catalyzed [2 + 2 + 2] cyclotrimerization reaction of triene **150**, followed by the deprotection of the methoxy group in **151** to result in helicene diol **152** in a racemic form. The enantiomers of **152** were separated on chiral HPLC, followed by the silver oxide-mediated oxidation, to give the quinone **149** in quantitative yield (Scheme 26) [83].

In general, quinones are electrochemically redox active molecules which undergo reduction as diol anions and re-oxidation back to quinone, with the corresponding measurable structural transformations in chromophoric absorption (Figure 13a). Therefore, the helicene-based quinone **149** was also tested for the same, with an additional possibility of chiroptical switching as observed by CD measurement. Both the enantiomers of **149** exhibited a one-electron reduction process to form the semiquinone radical anions, **149**^{•−}, as evident from cyclic voltammetry studies with $E_{1/2} = -1.00$ V (vs Fc⁺/0, $\Delta E_p = 0.07$ V) in acetonitrile, with a reversible electrochemical behavior. Since **149**^{•−} is a stable species, its UV and CD measurements were performed by using an optically transparent thin layer electrochemical cell. It was observed that the helicene quinone **149** is able to be reversibly reduced to the radical anion **149**^{•−} and re-oxidized over several cycles, and is an example of chiroptical switching to be conveniently monitored with CD spectroscopy at different wavelengths (Figure 13b) owing to the distinguishable spectral profiles of **149** and **149**^{•−}. However, as there is no change in the (*P*) or (*M*) helicity of the chromophore upon electrochemical transformations, the Cotton effect (CE) signs of **149** and **149**^{•−} remained the same.

Besides electrochemical switching, **149**^{•−} was tested for chiral recognition against 2,2'-bis(diphenylphosphanyl)-1,1'-binaphthylidioxide (BINAPO) using electron paramagnetic resonance and electron–nuclear double resonance (ENDOR) spectroscopy. The diastereomeric species formed by coordinated lithiated semiquinone radical anions [$\text{Li}+\{(\pm)\text{-149}^{\bullet-}\}$] and enantiomers of BINAPO generated noticeable changes of the lithium and proton hyperfine coupling measured by ENDOR spectroscopy. The diastereoisomeric complex **153** exhibits a hyperfine coupling constant (*A*) value for ⁷Li at -1.62 MHz, in comparison to -1.76 MHz for another diastereomeric complex **154**, indicating the appreciable difference between the diastereomers (Figure 14). It is of note that the racemic sample gives an average value of -1.69 MHz.



Scheme 26. Synthesis and resolution of helicene quinone **149** from triene **150** using the nickel-catalyzed [2 + 2 + 2] cyclotrimerization reaction as a key step.

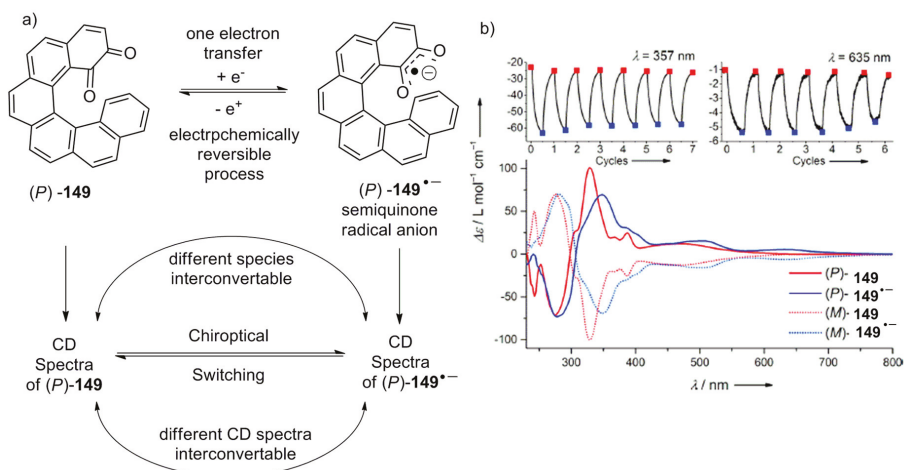


Figure 13. (a) Mechanism of reversible electrochemical switching of helicene quinone **149** to helicene semiquinone radical anions $149^{\bullet-}$; (b) observed reversible chiroptical switching between **149** and $149^{\bullet-}$; monitored by CD spectroscopy in acetonitrile. Reversible electrochemical switching for several cycles is shown for the (*M*)-(–) enantiomer at two different wavelengths (top right) along with the corresponding CD spectra. (Figure 13b) reprinted from [83]. © 2014, American Chemical Society.

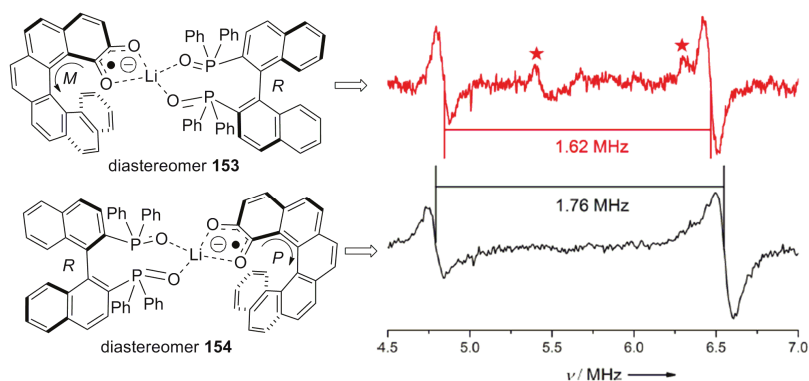
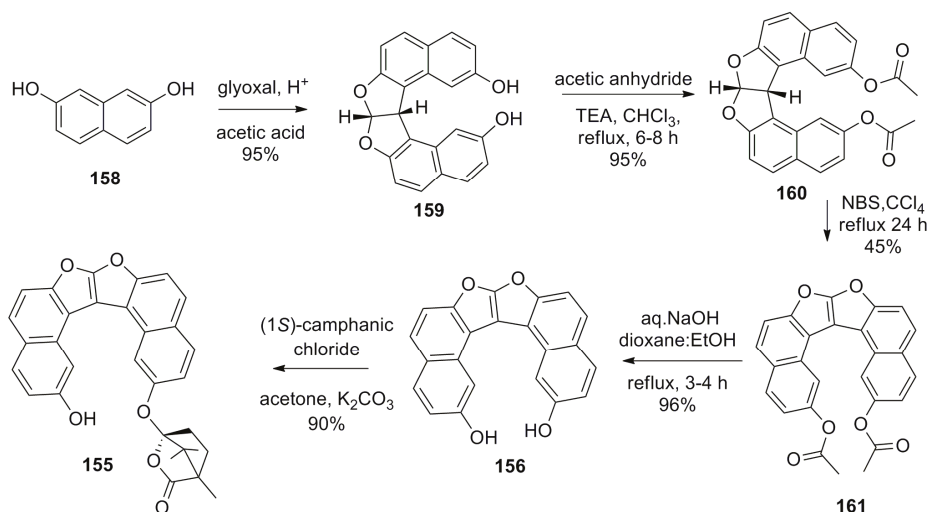


Figure 14. ENDOR spectra of diastereomeric species, **153** (black) and **154** (red) in THF at 210 K, only the low-frequency region is shown. Reprinted from [83]. © 2014, American Chemical Society.

The previously described examples, **127** [77] and **115** [81], represent the inbuilt chiral helicene chromophoric hosts for the chiral recognition of a general class of chiral molecules using some selected analytical techniques such as fluorescence and NMR spectroscopy. An essentially different approach has been recently developed by Karnik et al. on the basis of a new supramolecular chirogenic system, **155**, the key element of which was a stereodynamic dioxo[6]helicene diol **156** chromophore. This system was applied as a specific sensor, suitable for chirality sensing of *trans*-1,2-cyclohexanediamine **157** and monitored by various spectroscopic methods [84]. The helicene **156** was synthesized from 2,7-dihydroxynaphthalene **158** [85]. The first step involved acid-catalyzed condensation between two molecules of **158** and glyoxal to obtain dihydrofurofuran **159** (>95%), followed by the protection of phenolic groups to give acetate **160** (95%). Then, one-pot benzylic bromination and dehydrobromination (aromatization) of **160** using *N*-bromosuccinamide led to **161**

(45%), followed by basic hydrolysis resulting in dioxo[6]helicene diol **156** (96%). Finally, selective mono esterification with chiral (1*S*)-camphanic chloride in acetone afforded the desired host, **155**, with 90% yield (Scheme 27) [85].



Scheme 27. Multistep synthesis of helicene camphanate **155** from 2,7-dihydroxynaphthalene **158**.

Indeed, the parent dioxo[6]helicene diol **156** is almost a flat stereodynamic-type fluorescent compound, which was selectively modified with a chiral (1*S*)-camphanate group to give **155**, leaving one of the (phenolic) hydroxyl groups free. This inherently free phenolic group and (1*S*)-camphanate chiral handle on the opposite peripheral ring provided a suitable *sui generis* chiral space for guest **157**. In particular, this perfect stereospecific matching results in an effective turn-on fluorescent sensor for the (*S,S*)-enantiomer of **157** with a relatively high enantioselective factor, $\alpha = K_{SS}/K_{RR} = 6.3$ (in benzene). The favorable hydrogen-bonding interactions in nonpolar media (benzene and toluene) are responsible for the efficient chiral recognition observed by fluorescence spectroscopy (Figure 15a,b). In nonpolar media, the donor–acceptor type cooperative hydrogen bonding between host **155** and guest **157** (Figure 15c) resulted in a high turn-on enantioselective fluorescence response. The enantiodiscrimination behavior was found to be solvent-dependent as the polarity of solvent can influence the extent of hydrogen bonding between the host and guest. In turn, this induces a unidirectional switch in the helical conformation of the helicene chromophore, resulting in reverse selectivity for the (*R,R*)-enantiomer of **157** in acetonitrile, THF, and chloroform [84].

Further, the NMR studies performed in deuterated chloroform exhibited the chiral camphanate group transfer reaction (Scheme 28a) with the reaction rate of 5.83×10^{-6} and $5.97 \times 10^{-7} \text{ mol dm}^{-3} \text{ s}^{-1}$ for (*R,R*)-**157** and (*S,S*)-**157**, respectively, as monitored by ¹H NMR (Figure 15d). This tenfold increase of the reaction rate for the (*R,R*)-enantiomer allowed the host **155** to behave as a kinetic resolving agent for (*R,R*)-**157**, with up to 68% *de* at room temperature within 4 h (Figure 15d) [84].

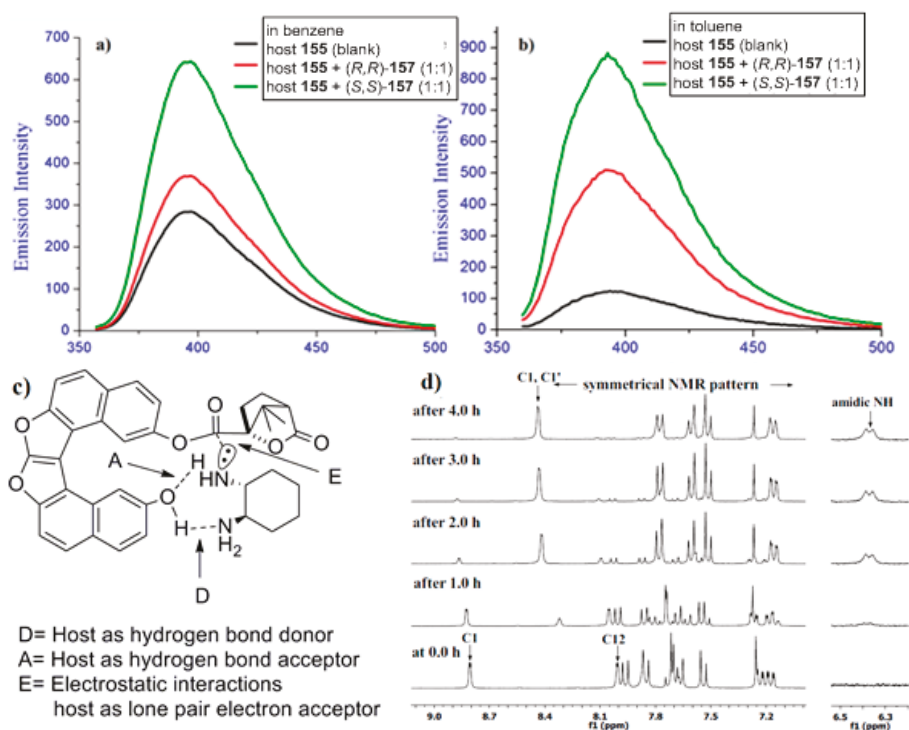
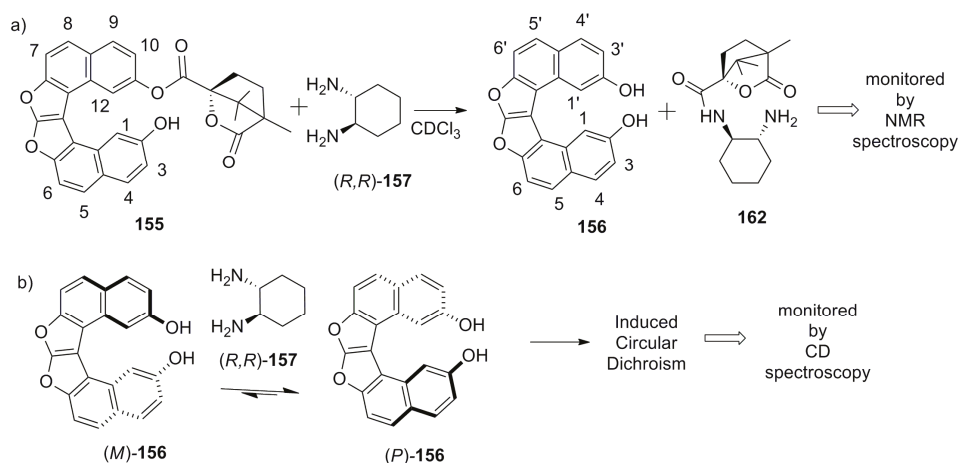


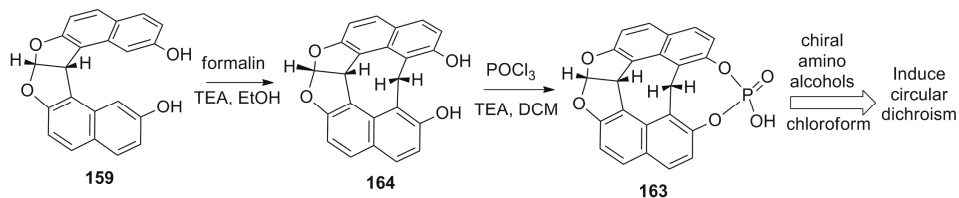
Figure 15. Fluorescence response of helicene camphanate **155** for *trans*-1,2-cyclohexanediamine **157** (a) in benzene and (b) in toluene solvent; (c) Schematic representation of the donor-acceptor hydrogen bonding between **155** and **157** in nonpolar solvent with turn-on fluorescence response; (d) Time-dependent changes observed in ¹H NMR spectra of host **155** with 1:1 (*R,R*)-**157** in CDCl₃. Reprinted from [84]. Source: <http://pubs.acs.org/doi/abs/10.1021/acsomega.6b00522>.

Indeed, this is a rare example of the *sui generis* host-guest pair as evident from the fact that diamine **157**, upon supramolecular interaction with the parent stereodynamic helicene diol **156** (Scheme 28b) is able to induce a specific helicity and shift the stereodynamic equilibrium of **156**, as monitored by CD spectroscopy in the region of helicene chromophore absorption.

Further, the same group also developed C_s-symmetric rigid achiral organophosphoric acid **163** in two steps, starting from dihydrofurofuran helicene **159** as a supramolecular chirogenic system for the absolute configuration determination of 1,2-amino alcohols by induced CD (ICD) studies [86]. The two-step synthesis includes the reaction of dihydrofurofuran helicene **159** with formaldehyde to form an additionally bridged diol, **164**, and subsequent reaction with POCl₃ to obtain the target, **163** (Scheme 29).



Scheme 28. (a) Chiral group transfer reaction between **155** and (R,R) -**157** in chloroform and (b) proposed shift in conformational dynamic equilibrium of **156** in the presence of (R,R) -**157** in chloroform.

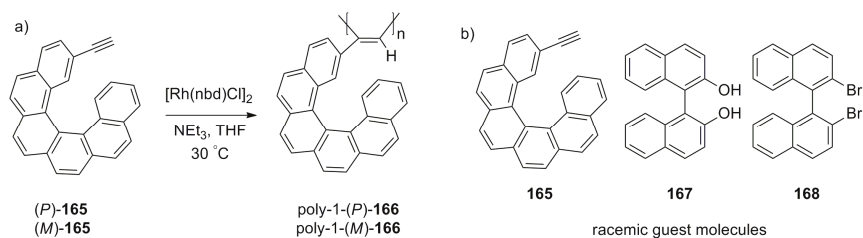


Scheme 29. Synthesis of **163** from dihydrofurofuran helicene **159**.

Interestingly, due to the C_s -symmetric nature of phosphoric acid, **163** has two tautomeric structures. This structural feature of **163**, in combination with the substituent bulkiness of the guest amino alcohols, together decide the preferred mode of two-point hydrogen bonding on equilibration, which gave a resultant ICD signal correlating with the absolute configuration of the guest [86].

7.2. Polymeric Helicene-Based Chiral Recognition

Polymer chains can also serve as suitable carriers for chiral helicenes, especially in the case of prospective applications. Thus, using 2-acetylene-[6]helicene **165**, Yashima et al. prepared a series of polymeric helicene pendants, poly-**166**, via the rhodium-catalyzed polymerization reaction (Scheme 30) [87]. This polymerization reaction gave stereoregular (*cis-transoidal*) polyacetylenes bearing the corresponding helicene pendants **166** with (P) - and (M) -polymeric chains with average molecular weight $M_n = 2.6 \times 10^3$. However, the formation of a precipitate during the reaction makes it difficult to reproduce. The careful analysis of the CD spectra of monomer **165** and polymers **166**, and their corresponding differential CD spectra, suggests that the helical polyacetylenes with the optically active pendant group exist as a single-handed structure, apparently due to the attractive intramolecular π - π interactions.



Scheme 30. (a) One step synthesis of polymeric helicene **166** and (b) its application against enantioselective adsorption of racemic guests **165**, **167**, and **168**.

The chiral recognition abilities of these polymers were studied in the context of the enantioselective adsorption of three racemic guests, namely, parent helicene **165**, BINOL **167**, and 2,2'-dibromo-binaphthalene **168**. The enantiomers were adsorbed by the polymer in methanol solution and desorbed in a mixture of methanol/THF [1:1, *v/v*] followed by chiral HPLC analysis. The poly-1-(*P*)-**166** preferentially adsorbed (*P*)-helicene **165** with 3.6% *ee*; both have similar configurations. As expected, in the case of **166** with opposite absolute configuration, the adsorption preference was observed for (*M*)-helicene **165** with a similar 3.7% *ee*. However, interesting results were obtained for binaphthyl derivatives **167** and **168**, where poly-1-(*P*)-**166** selectively adsorbed the opposite (*S*)-enantiomers with up to 36% *ee*, whilst poly-1-(*M*)-**166** showed similar selectivity towards the (*R*)-enantiomers of **167** and **168**. The calculated separation factor was sufficiently high (1.71–2.18), indicating that these polymers can be used as a stationary phase for the practical separation of racemic mixtures.

7.3. Helicene-Based Chiral Recognition via Nanoparticles

Another prospective approach for chiral recognition by helicene structures is based on nanomaterials. In this respect, individually racemic, (*P*)-, and (*M*)-helicene thiols **169** were grafted onto gold nanoparticles of 5–22 nm [88] in a mixture of ethanol/water (1:3, *v/v*) under sonication to form the corresponding Au-(*P/M*)-, (*P*)-, and (*M*)-**169**-nanoparticles (helicene-grafted nanoparticles) (Figure 16). These helicene-based nanoparticles show chirality-based inter(nano)molecular attractive interaction, resulting in the corresponding aggregation phenomenon followed by a time-dependent precipitation process, as analyzed by UV spectroscopy. All three types of nanoparticles dispersed in DMF gave a stable solution for a period of one week. The addition of the DMF solutions to an aromatic solvent such as benzonitrile resulted in different colors due to the surface plasmonic bands of the gold nanoparticles, as studied by UV–vis spectroscopy and a dynamic light scattering technique. Additionally, the time-dependent aggregates were of different sizes, based on the type of helicene nanoparticles present. The observed chiral recognition induced by the homo- (Au-(*P/M*)-**169** nanoparticle : Au-(*P/M*)-**169** nanoparticle, Au-(*P*)-**169** nanoparticle : Au-(*P*)-**169** nanoparticle, and Au-(*M*)-**169** nanoparticle : Au-(*M*)-**169** nanoparticle) and hetero self-aggregation (Au-(*M*)-**169** nanoparticle : Au-(*P*)-**169** nanoparticle) of the helicene nanoparticles was found to be enhanced according to the following sequence: Au-(*P/M*)-**169** nanoparticle : Au-(*P/M*)-**169** nanoparticle < Au-(*M*)-**169** nanoparticle : Au-(*M*)-**169** nanoparticle = Au-(*P*)-**169** nanoparticle : Au-(*P*)-**169** nanoparticle < Au-(*P*)-**169** nanoparticle : Au-(*M*)-**169** nanoparticle. This tendency relates to the interaction strength between the corresponding nanoparticles, which is controlled by stereochemical matching.

Another example of optically active nanoparticles **170** with 70 nm diameter size was obtained by grafting (*P*)-1,12-dimethyl-8-methoxycarbonylbenzo[*c*]phenanthrene-5-carboxamide on 3-aminopropylated silica (Figure 17) [89,90]. These nanoparticles were prepared by reacting 3-aminopropylated silica nanoparticles with the corresponding (*P*)-helicene carboxylic acid chloride by refluxing in isopropyl ether for 4 hours using ethyldiisopropylamine as a base.

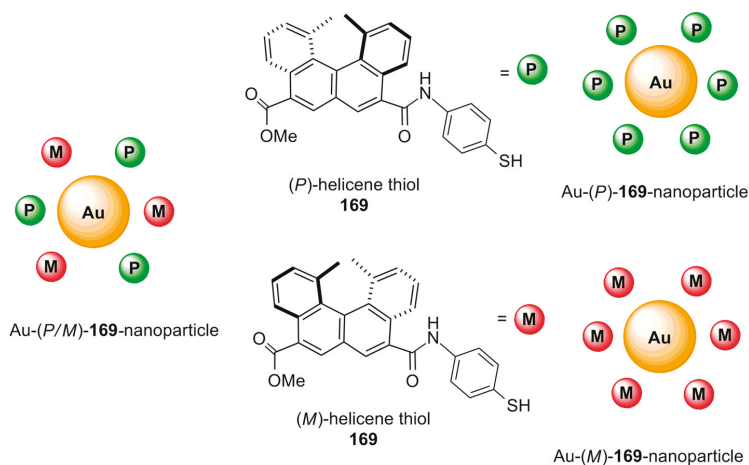


Figure 16. Enantiomeric structures of helicene thiol **169** and representations of the gold nanoparticles formed from **169**. Modified and reprinted, with permission from [88] © 2012, Royal Society of Chemistry.

It was found that these nanoparticles enantioselectively precipitated at a faster speed with (*S*)-configuration of aryl alcohols **80** (47% *ee*) and **171** (61% *ee*) [89] in *m*-bis(trifluoromethyl)benzene (Figure 17). To elucidate the corresponding *ee* values, the precipitate was centrifuged and separated, followed by mixing in 2-propanol. Then, the insoluble material (nanoparticles) was removed and the organic layer was concentrated and analyzed with chiral HPLC, indicating the optical resolution of up to 29–61% *ee* for various aromatic alcohols for the (*S*)-configuration [89]. The mechanism of this stereoselectivity was related to chiral recognition on the basis of the electrostatic aggregation phenomenon. This nanoparticle-based kinetic resolution requires a relatively smaller amount (10 mol %) of -nanoparticles **170** as the resolving agent compared with the requirement of conventional 0.5 equivalence, with providing additional possibility for resolving noncrystalline substances, making it an attractive and greener method of choice.

Further, the helicene-based nanoparticles **170** were able to recognize the shape of (*P*)-ethynylhelicene oligomers **172** in solution [90]. It preferentially forms the precipitate with a double helix of the oligomeric structure of **172** in comparison to its random coil structure in trifluoromethylbenzene (Figure 17). The analysis was carried out by CD spectroscopy, where the double helix oligomer shows a strong positive CE followed by a negative one, whilst in the case of the random coil oligomer, a weak CE of opposite sign was observed. This phenomenon was related to the chiral shape recognition on the surface of the nanoparticle by stereospecific absorption, resulting in the visualized selective aggregation-based precipitation, which is useful for the separation of the double helix structure of **172** from its random coil conformation [90]. These examples clearly show the potential of helicene-based chiral nanomaterials for applications in the resolution of chiral molecules ranging from a simple alcohol to complex polymeric structures.

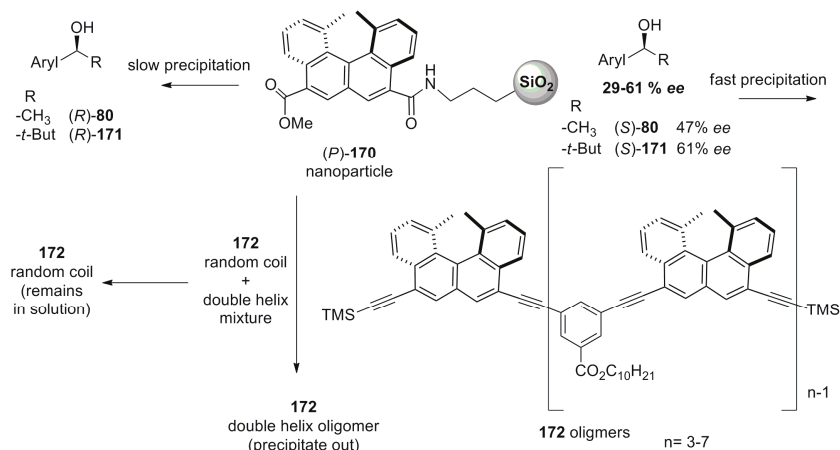


Figure 17. Helicene silica nanoparticle **170** and its ability towards chiral recognition and resolution of aromatic alcohol **80** and **171** and double helix oligomer **172**.

7.4. Helicene-Based Chiral Recognition Involving Biologically Relevant Molecules

The stereodynamic helicenes are also effectively employed for the induced CD-based sensing, where a chiral guest can induce a specific helicity via covalent or supramolecular interactions, thus generating the corresponding CD signals in the helicene absorption region. The guests range from simple organic molecules (Scheme 28b) to complicated biological molecules, as described here.

Thus, Yamada's group explored hydroxymethyl trithia[5]helicene **173** [91–96], which is a stereodynamic compound. Both the (*P*)- and (*M*)-enantiomeric structures are configurationally labile, nonresolvable, and exist in a fast equilibrium. However, due to the presence of an electron-rich aromatic chromophore and polar hydroxymethyl group capable of hydrogen bonding, suitable complexation of the chiral guest (such as biomolecules) [91,93–96] is able to shift the equilibria to one of unidirectional helicity, which, in turn, can be monitored by CD spectroscopy (Figure 18).

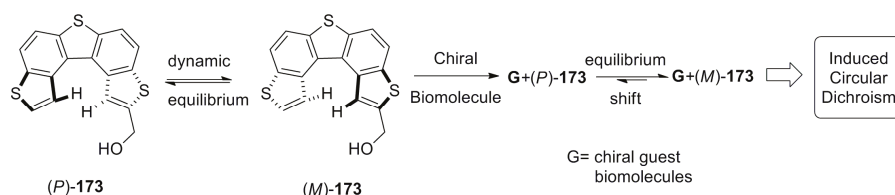
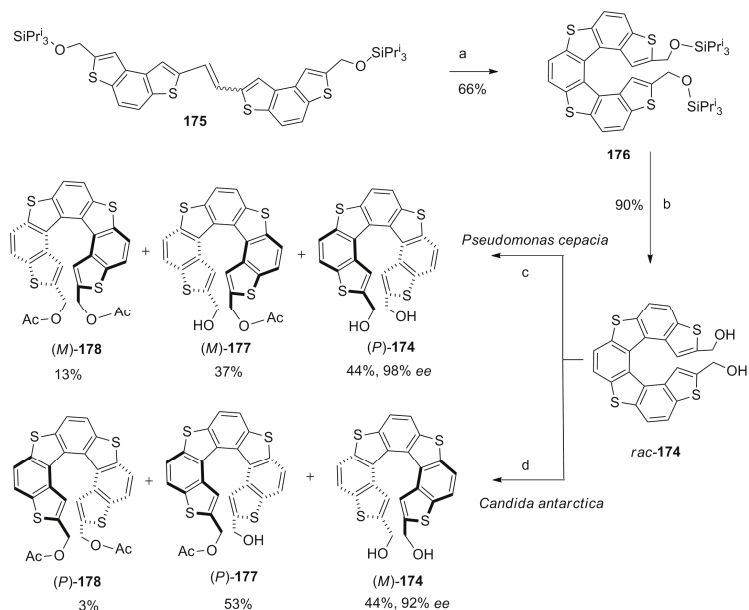


Figure 18. Stereodynamic hydroxymethyl trithia[5]helicene **173** and a principle of its use as an induced CD host.

The corresponding host–guest studies were successfully implemented with serum albumin [91], (*R*)-2-(2,4,5,7-tetranitrofluoren-9-ylideneaminoxy)propionic acid (TAPA) [92], alkyl b-D-pyranoside [93], and bilayered phosphatidylcholine vesicles [94–96] using CD spectroscopy as a major tool. As the extent of helicity induced in **173** by these guest molecules is small, the resultant CD signals are also small. Yet, as CD is a highly sensitive technique, even with a small signal, it can be applied for understanding molecular behavior and chirality in solution.

Tanaka et al. synthesized bis(hydroxymethyl)thia[7]helicene **174** to study its further synthetic chemistry and corresponding applications in the chirality recognition of biological molecules [97–100]. Hence, the helicene **174** was synthesized in a total of nine steps with an overall 33% yield, where the

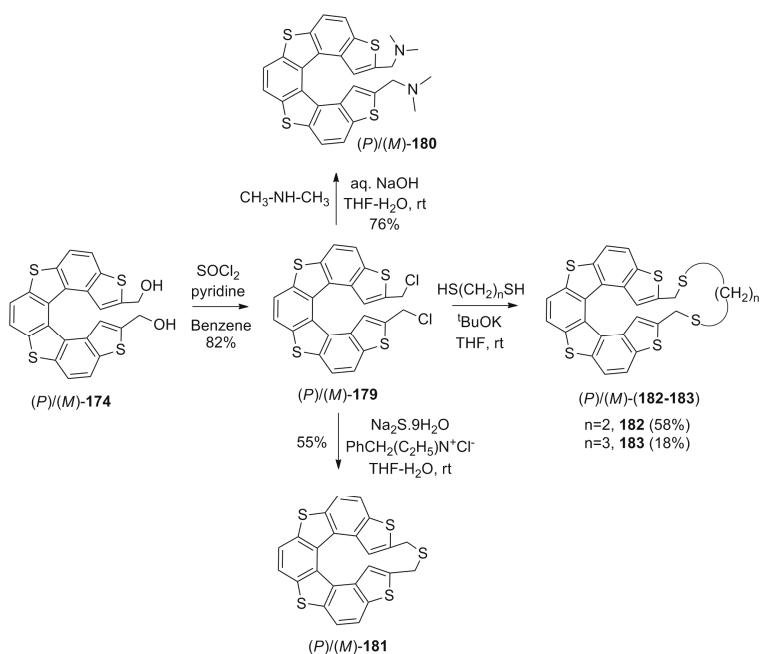
photochemical cyclization of alkene **175** was a key step to give silyl group protected *rac*-**176**. Further, deprotected racemic **174** was optically separated using the lipase-based enzymatic kinetic resolution method. For example, with the use of *Pseudomonas cepacia* enzyme, (*P*)-**174** (44%, 98% *ee*) was obtained as a slow reactive isomer with simultaneous formation of the corresponding mono- and diacetates, (*M*)-**177** and (*M*)-**178**. Similarly, the use of *Candida antarctica* enzyme resolved opposite (*M*)-**174** (44%, 92% *ee*) with the formation of mono- and diacetates, (*P*)-**177** and (*P*)-**178** (Scheme 31) [97].



Scheme 31. Photochemical synthesis and enzymatic resolution of helicene **174**; (a) *hν*, I₂, propylene oxide, benzene, room temperature; (b) tetra-*n*-butylammonium fluoride, THF, 0 °C; (c) *Pseudomonas cepacia*, CH₂Cl₂, vinyl acetate, room temperature, 25 h; (d) *Candida antarctica*, CH₂Cl₂, vinyl acetate, 28–29 °C, 9.5 h.

Further, enantiopure alcohol **174** was converted to its dichloride **179**, which was converted to **180** [98] and cyclic thia ethers **181–183** [99] using suitable synthetic procedures (Scheme 32). These helicene molecules were explored in terms of possible chiral recognition of biologically relevant molecules such as DNA [98,100].

It is well known that, under physiological conditions, a DNA duplex exists as a mixture of the right-handed B-DNA and left-handed Z-DNA forms. The supramolecular association of chiral C₂-symmetrical **180** with DNA revealed that the (*P*)-enantiomer of **180** displays chiral selection for binding Z-DNA over B-DNA [98]. The corresponding binding constants were found to be $(8.0 \pm 0.5) \times 10^4 \text{ M}^{-1}$ and $(1.4 \pm 0.3) \times 10^4 \text{ M}^{-1}$ for Z- and B-DNA, as measured by fluorescence titration. Besides, this interaction can be clearly monitored with CD spectroscopy, where, upon binding Z-DNA, there is a considerable decrease in the signal intensity of (*P*)-**180** of up to 70% at 330 nm at neutral pH. Under similar conditions, B-DNA failed to show any significant change in the CD spectra of (*P*)-**180**, indicating (*P*)-helicity-based recognition of Z-DNA. In contrast, although the (*M*)-**180** also showed a 20% reduction, it was observed upon binding both B- and Z-DNA, thus indicating the lack of its discrimination ability.



Scheme 32. Synthesis of functionalized helicene **180** and thiaethers **181–183** from [7]helicene **174**.

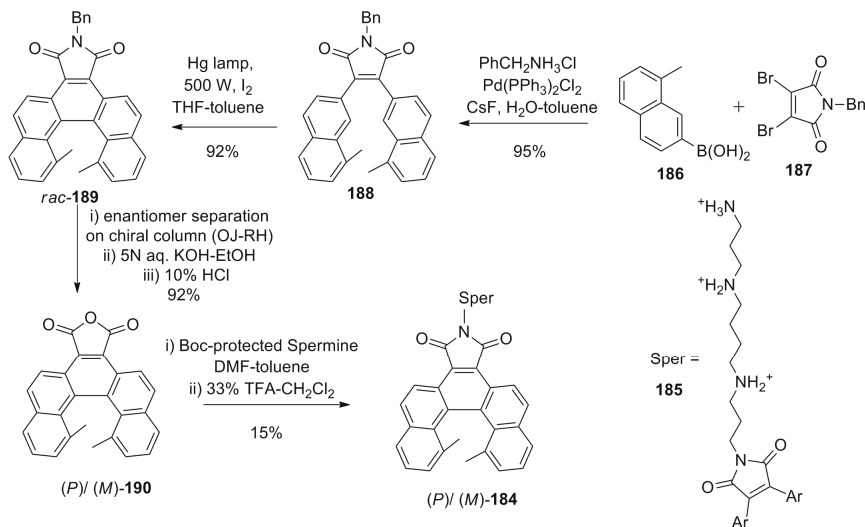
Additionally, it was observed that the (*P*)-**180** not only selectively binds Z-DNA but is also able to force B-DNA to adopt an opposite left-handed helical form, like Z-DNA. Apparently, the methylene-*N,N*-dimethylamine functionality in (*P*)-**180** plays a crucial role in this behavior, as the same helicene backbone but with hydroxy methyl substituents, as in the case of **174**, did not show any binding response towards B- and Z-DNA. It is likely that the protonated form of amino substituents in **180** becomes a crucial site for binding DNA, whilst the helicene chirality is an important factor in the enantioselective recognition of left-handed helical Z-DNA.

Further extending the chiral recognition research of biologically important molecules resulted in the development of cyclic helicenes with thiaether linkage, **181–183** (Scheme 32) [99,100]. The (*M*)-enantiomers of **181–183** turned out to be potential inhibitors against telomerase enzyme activity based on the chiral and steric matching, while binding to the G-quadruplex superhelical structure. The recognition phenomenon is based on the chiral space available at the cleft-pocket and the presence of Z-DNA assisting this helicene binding. Initially, **180** was studied and exhibited no chiral selectivity. This result led to the assumption that the dihedral angle in helicene chromophores plays a key role in the interaction efficiency. On this basis, three different cyclic helicene thiaethers, **181–183**, having different length of linkers, were designed to yield the dihedral angles of 22°, 53°, and 58°, respectively.

It was shown that the (*M*)-enantiomer of **181** with the smallest interplanar angle was able to inhibit the telomerase enzyme activity efficiently, presumably as a result of the chiral and steric matching. However, the exact binding mode of this helicene to the G-quadruplexes is not fully understood yet. Here, again, the binding studies relied on CD and fluorescence spectroscopy [100].

In 2013, chiral [5]helicene **184**, containing methyl groups at the innermost positions, was suitably connected with the spermine moiety **185** at the outer sphere of the helicene backbone to act as a host capable of recognizing the DNA conformation [101]. This host was synthesized by the Suzuki–Miyaura coupling of 8-methylnaphthalene-2-boronic acid **186** with dibromo-maleimide **187** to obtain **188**,

followed by photocyclization to result in racemic **189** with 92% yield. The enantiomers of **189** were separated on a chiral column followed by further transformation to **190** and, finally, to the target enantiopure **184** (Scheme 33) [101].



Scheme 33. Synthesis of helicene-spermine **184**.

The designing concept was such that the cationic spermine unit is able to provide the corresponding electrostatic interactions with the DNA's phosphate backbone of the minor groove, whereas the chiral helicene is expected to form end-stacking mode complexes, altogether resulting in a strong chiral recognition. Indeed, it was demonstrated that *(P)*-**184** binds preferentially to B-DNA over Z-DNA. The opposite trend was observed with *(M)*-**184**, which displayed strong binding for Z-DNA over B-DNA, as studied by performing CD, UV melting temperature, surface plasmon resonance measurements, and isothermal titration calorimetry. From the examples of **180** [98] and **184** [101], it appears that the cationic functional groups assist in binding with DNA through electrostatic interactions; along with this, the chiral helicity-based steric fit allows selectivity. The *(P)*-**180** prefers Z-DNA, whereas in the case of **184**, the *(M)*-enantiomer binds strongly to Z-DNA. As structures, tetrathia[7]helicene **180** having functional groups on the terminal rings (in chiral cavity space) and 1,14-dimethyl[5]helicene **184**, where spermine **185** is situated at the helicene outer core, are completely different in terms of the functional groups and their positions, therefore the exact mode of binding with DNA cannot be generalized and is still not completely understood.

Chiral cationic [4]helicenes **191** (Figure 19), having methoxy substituents at the innermost position, were also able to bind with DNA molecules, as evident from a noticeable change in absorption, fluorescence, and CD spectra obtained during the corresponding host-guest studies [102]. It was concluded that the molecular plane of the helicene dye lies essentially parallel to the DNA bases, implying intercalation mode rather than groove binding. Further, the chiral selectivity based on association constant evaluation indicates that the *(M)*-enantiomer of **191** interacts more strongly with DNA than the corresponding *(P)*-enantiomer of **191**.

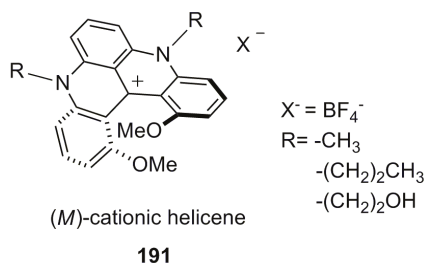
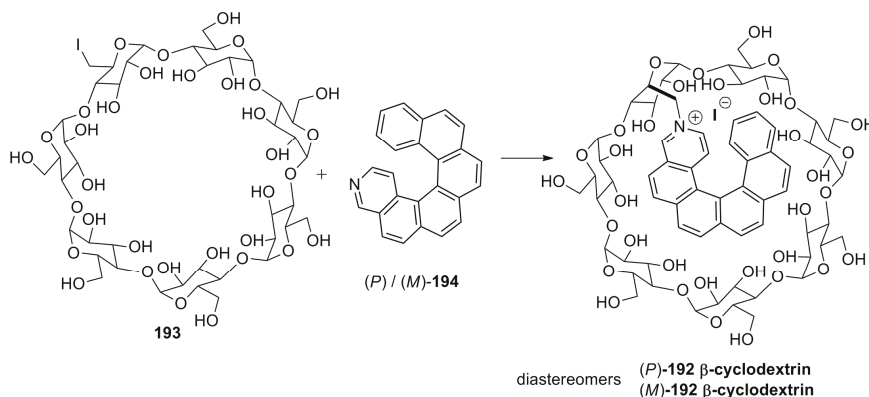


Figure 19. Structure of (*M*)-enantiomers of **191**.

Yang et al. developed chiral 3-aza[6]helicene-modified β -cyclodextrin **192** by reacting 6-iodo- β -cyclodextrin **193** with (*P*)/(*M*)-helicene **194**, resulting in two water soluble cationic charged diastereomeric species—(*P*)-**192**/ β -cyclodextrin, and (*M*)-**192**/ β -cyclodextrin (Scheme 34)—with different fluorescence behavior [103]. The concept was to use water-insoluble 3-aza[6]helicene **194** in aqueous media in combination with the β -cyclodextrin asymmetry for the chiral recognition of amino acids in water.



Scheme 34. Synthesis of 3-aza[6]helicene modified β -cyclodextrin **192** as a water-soluble amino acid sensor.

In polar solvents such as methanol, ethanol, and water, the helicene chromophore occupies the β -cyclodextrin cavity to a different extent in two diastereomers: (*P*)-**192**/ β -cyclodextrin and (*M*)-**192**/ β -cyclodextrin—favoring monomeric forms rather than self-aggregated species. Both the diastereomers were investigated for complexation towards proteinogenic amino acids by using the fluorescence technique in an aqueous buffer of pH 7.3. It turned out that hydrophobic interactions appeared to be a dominant binding mode with additional electrostatic forces between the cationic charge of helicene and carboxylate anion of corresponding amino acids; besides this, π - π interaction may also contribute in the case of aromatic guests. The chiral discrimination abilities were also found to be highly dependent on pH. A relatively high L/D selectivity of amino acids, up to 12.4, was observed as a consequence of the synergetic effects of the helicene auxiliary and β -cyclodextrin cavity [103].

7.5. Helicene-Based Chiral Recognition via Self-Assembly

A new approach for chiral recognition via self-assembly was applied by Yamaguchi et al. on the basis of functionalized chiral [4]carbohelicene. The overall studies demonstrated that the helicenes exhibit a noncovalent chiral recognition behavior via different functions, such as charge transfer

complexation, crystallization, homocoupling reaction, layer structure formation, self-aggregation, and even upon double helix formation [75]. Their observations indicated that the right-handed helix structure favors the same helicity of its counterpart, which is not generally observed in the case of point chirality (i.e., an *R*)- or (*S*)-host does not always prefer a guest of the same absolute configuration). Out of several examples, the following one is sufficient to understand this helicity matching phenomenon.

Tetranitro, dicyano-substituted [4]helicene **195**, being an electron-deficient system, strongly interacts with diamino-substituted [4]helicene **196** via a charge transfer complex [104], the formation of which was monitored by UV and NMR techniques. Particularly, in the UV spectrum, a charge transfer band was observed at 500–800 nm in THF. The association constant of the complex with the same configuration—(*M*)-**195** and (*M*)-**196**—was found to be 12.2 M^{-1} ; this was noticeably higher than the constant 10.2 M^{-1} observed for the opposite configuration—(*P*)-**195** and (*M*)-**196** (Figure 20). Further, the NMR-based NOE experiments revealed that the face-to-face *syn*-conformation of two 1,12-dimethyl groups was preferred over the *anti*-orientation in the corresponding charged transfer complexes [104].

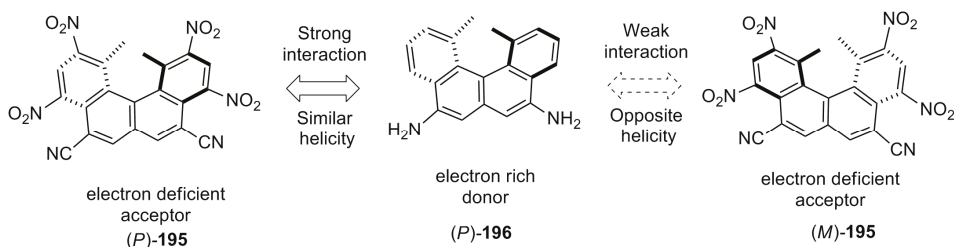


Figure 20. Helical discrimination upon supramolecular charge transfer complexation between electron-deficient helicene **195** and electron-rich helicene **196**.

In related studies, a series of racemic [7]helicene derivatives, **197–199**, containing pyridinone rings at both the terminals, were prepared using a classical methodology of Wittig olefination and photochemical cyclization, and were characterized both in solution and in solid state [105]. Despite a variety of self-assembly modes according to the stereochemical and topological relationships, these helicenes formed only enantiomerically pure dimers held together by two pairs of the cooperative hydrogen bonds. The self-assembly process was found to be enantiospecific in solution and diastereoselective in solid crystal (Figure 21).

The terminal pyridinone rings were capable of hydrogen bonding via the corresponding amidic N–H functionalities. The solution-phase NMR studies indicated that the helicenes exist as enantiomeric dimers. For example, the NH proton in 2-quinolinone **200** (10^{-4} – 10^{-2} M), as a reference, appeared at 12.9 ppm, whilst the position of this proton in **198** was downfield-shifted by 1 ppm in dilute solution ($>10^{-5} \text{ M}$), clearly indicating the cooperative hydrogen bonding and self-assembly phenomenon. In turn, the chemical shift was found to be concentration-independent in CDCl_3 and THF. In pyridine, as expected, it was concentration-dependent, as pyridine itself is able to compete for the hydrogen bonding. Additionally, the dimeric binding model was confirmed by dilution experiments with the association constant of 207 M^{-1} . The molecular modelling studies also indicated that each dimer is preferably constructed from a monomeric species of the same helicity.

The X-ray crystallographic structure of **199** showed only homochiral dimers; where the R-group (acetyl) is present in the *cis*-orientation to ensure the diastereoselective recognition process during crystallization. These enantiopure dimers are held together by four strong intermolecular hydrogen bonds between two terminal pyridinones.

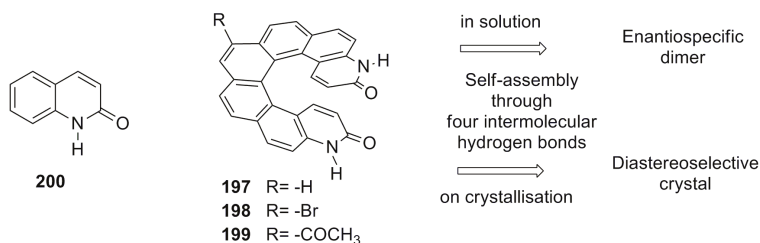


Figure 21. Hydrogen bonding-based self-assembly in pyridinone-containing helicenes **197–199** and 2-quinolinone **200**, as a NMR reference.

8. Enantiopure Helicenes: Enantioselective Synthesis, Chiral Separation, and Racemization

The chiroptical properties and applications discussed above prompted the development of efficient synthetic procedures to obtain enantiopure helicenes in sufficient quantities required for these investigations [2,4]. Although this topic is not directly related to the category of helicene applications, it is an important background for the whole helicene chemistry; hence, a brief description should be included as a special section. The major methods of obtaining enantiopure helicenes from a racemic mixture are based on optical resolution by chiral HPLC [60,77,78,83,101], diastereomeric salt formation [51,60,76] (for representative resolving agents, see Figure 22), chromatographic separation of diastereomers [52,56,74], and enzymatic-based approaches [97].

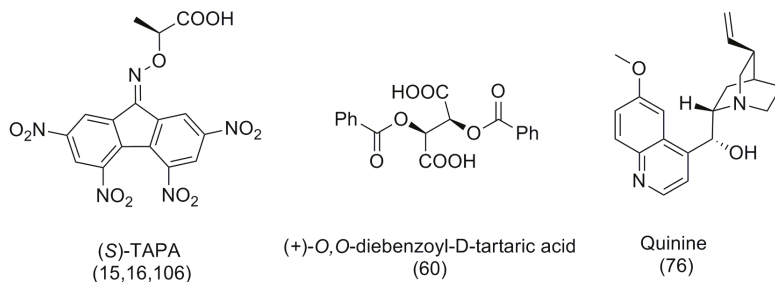
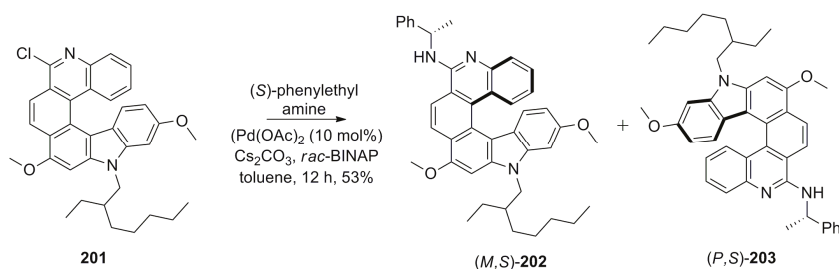


Figure 22. Selected examples of chiral reagents for helicene optical resolution.

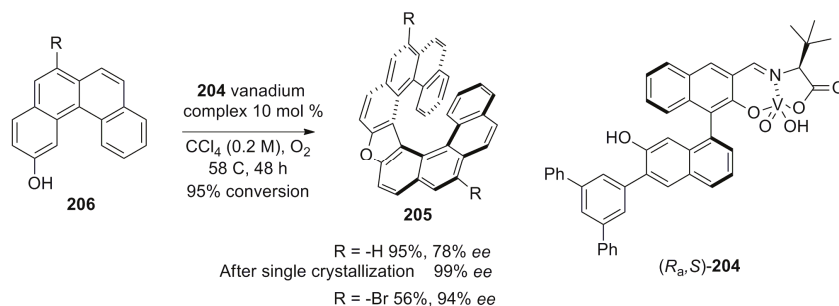
For example, racemic nonfunctionalized helicenes were successfully resolved through charge transfer complexation with electron-deficient molecules, such as TAPA [15,16] or HPLC-based separation with the use of silica coated with TAPA [106]. In the case of functionalized helicene-containing phenolic groups at the terminal ring, (1*S*)-camphanic chloride acts as the best resolving agent for chromatographically separable diastereomers obtained. Furthermore, their absolute configuration determination was carried out by the 2D ROESY NMR technique [52,74,107]. Particularly, it was observed that in 19 examples of helicenes studied, (*M,S*)-diastereomers were less polar, whilst (*P,S*)-diastereomers were more polar, hence eluting as the first and second fractions, correspondingly, upon the chromatographic separation on silica gel [107]. Another resolving agent, which is also frequently employed for optical resolution, is an *l*-menthyl derivative [4,56]. This approach has a distinct advantage of attaching and detaching a chiral auxiliary before and after the diastereomeric separation, making the whole procedure recyclable and highly efficient. Interestingly, in the case of azahelicene **201** containing the chloro group as a substituent on the outer peripheral pyridine ring, the use of Pd-catalyzed Buchwald–Hartwig coupling with (*S*)-phenylethyl amine gave chromatographically separable diastereomers **202** and **203** (Scheme 35) [108,109]. However, the absolute configuration of the 2-ethylhexyl alkyl chain was not discussed in the paper [108].



Scheme 35. Synthesis of chromatographically separable diastereomers **202** and **203** obtained by Pd-catalyzed reaction between *rac*-azahelicene **201** and (*S*)-phenylethylamine.

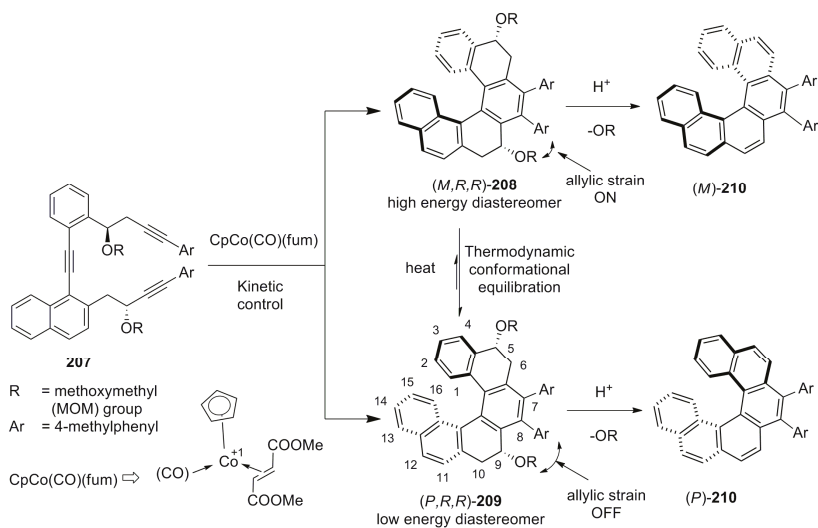
Besides the optical resolution of racemates, another approach to enantiopure helicenes is based on the stereospecific synthesis, where the originally chiral precursors or reagents are converted into the corresponding helicenes with unidirectional helicity [110]. In particular, the asymmetric synthesis of helicene can be performed by using various synthetic methods, such as photocyclization, Diels–Alder reaction, or metal-catalyzed annulation, in the presence of chiral auxiliaries attached to the reactant(s). These topics have been comprehensively covered in previous reviews [2,4]. Therefore, only a few of those recently published examples of asymmetric helicene synthesis are highlighted below.

In 2016, Sako et al. successfully used the modified BINOL-based vanadium(V) complex **204**, capable of functioning both as redox and Lewis acid catalysts, for the enantioselective synthesis of oxa[9]helicenes **205** starting from polycyclic phenols **206**. The reaction proceeds via oxidative coupling at first, followed by intramolecular cyclization. This results in the one-step enantioselective synthesis of oxa[9]helicenes in good yields with up to 94% *ee* [111] (Scheme 36).



Scheme 36. Modified BINOL-based vanadium complex **204**, catalyzed asymmetric synthesis of oxa[9]helicenes **205** from polycyclic phenols **206**.

In 2015, a new general asymmetric synthetic methodology was successfully developed for [5]-, [6]-, and [7]helicenes with ultimate enantioselectivity (*ee* >99) based on the controlled transfer of reactant point chirality to the product with unidirectional helicity [112]. At first, triyne **207**, having inbuilt point chirality, was converted into tetrahydrohelicene diastereomers **208** and **209**, being in the thermodynamic equilibrium, by cobalt-catalyzed tandem [2 + 2 + 2] cycloisomerization. The (*M*)-conformational helicity results in the 1,3-allylic strain, hence making **208** a highly energetic diastereomer in comparison to **209**, the (*P*)-conformational helicity of which gives relief from this strain, when the point chirality is of (*R*)-configuration at the 9-position. Subsequently, the favored diastereomer under acidic conditions yielded fully aromatic helicenes **210** with greater than 99% *ee* (Scheme 37). Thus, (*P*)- and (*M*)-helicenes can be readily prepared starting from the (*R*)- and (*S*)-absolute configurations at the 9-position of the precursor, correspondingly.



Scheme 37. Asymmetric synthesis of helicenes **210** based on the principle of point-to-helical chirality conversion.

One of the most important points of chiral helicenes is their configurational stability, which can be analyzed by using CD spectroscopy and chiral HPLC in combination with other techniques. Evidently, understanding the mechanism of racemization helps in designing more stable helicene structures. Recently, detailed theoretical racemization studies have been performed on $[n]$ helicenes where $n = 4$ – 24 [113]. Consequently, it was found that $n = 4$ – 7 involves the one-step concerted mechanism of racemization. The smallest member of the carbohelicene family, [4]helicene has a C_{2v} symmetric transition state (TS) with an energy barrier of $4.0 \text{ kcal mol}^{-1}$. However, the TS of $n = 5$ – 7 possesses a C_s -geometry with the energy barriers of 24.4 , 36.9 , and $42.0 \text{ kcal mol}^{-1}$, respectively. This is a result of the steric hindrance, which accounts for the high TS energies of racemization. For $n \geq 8$, besides the steric hindrance, an additional factor of the π - π interaction starts to contribute to the overall structural stability, making the racemization process a multistep process and thus further increasing the energy barrier. For example, when $n = 8, 9$, or 10 , helicenes displayed 2, 4, and 6 intermediates for the racemization process, respectively. Thus, in general, when $n = 8$ – 24 , helicenes involve $(2n-14)$ consecutive displacements, traversing intermediates in the molecule during the racemization process for corresponding carbohelicenes. These theoretical results should be taken into account to control the desired properties of helicene structures in future research.

9. Conclusions

Helicenes are versatile compounds existing in achiral, stereodynamic, meso, and chiral forms. Additionally, they could be neutral, charged, carbocyclic, heterocyclic, or polymeric in nature, with electron-rich or -deficient characteristics. These conjugated molecules exhibit unique physical properties such as fluorescence and strong chiroptical features, making them exclusively useful for the chirogenesis processes, including chiral recognition using both fluorescence and circular dichroism spectroscopies. Their polyaromatic helical structures are also suitable for providing shielding and deshielding effects, making them potentially applicable as chiral NMR sensors.

The high configurational stability and facile functionalization of the helicene structures open intriguing prospects in the fields of chiral catalysts and auxiliaries for various asymmetric reactions. In the last three decades, there has been much research effort focusing on newer, simpler, and

multigram synthetic procedures including different asymmetric methodologies for obtaining sufficient quantities of enantiopure helicenes for various practical applications, including chirogenesis. It has been established that modified helicene molecules with important properties can be developed by merging the helical structure with other (central, axial, and planar) chirality elements for specific applications. The helicity control may be conveniently achieved by means of the intramolecular cyclization of terminal rings, resulting in a decrease in the helicity. Alternatively, the introduction of functional groups on the terminal rings or presence of saturated bond(s) inside the molecule (helicenoid) increases the helicity. These modifications also govern the helicene chiral cavity space properties, and may thus be adopted for desired applications.

Besides chiral auxiliaries and chirogenesis, the helicene structures are good candidates for material chemistry and nanotechnology. We believe that there is still a large and diverse scope for helicene chemistry and application to be studied in the upcoming future, which will result in novel and interesting discoveries. We are yet to fully explore the real potential of helicene and related molecules.

Acknowledgments: M.H. and V.B. acknowledge funding from the European Union's Seventh Framework Programme for Research, Technological Development, and Demonstration under Grant Agreement No. 621364 (TUTIC-Green).

Conflicts of Interest: The authors declare no conflict of interest.

References

- Hembury, G.A.; Borovkov, V.V.; Inoue, Y. Chirality sensing supramolecular systems. *Chem. Rev.* **2008**, *108*, 1–73. [[CrossRef](#)] [[PubMed](#)]
- Shen, Y.; Chen, C.F. Helicenes: Synthesis and applications. *Chem. Rev.* **2012**, *112*, 1463–1535. [[CrossRef](#)] [[PubMed](#)]
- Gingras, M. One hundred years of helicene chemistry. Part 1: Non-stereoselective syntheses of carbohelicenes. *Chem. Soc. Rev.* **2013**, *42*, 968–1006. [[CrossRef](#)] [[PubMed](#)]
- Gingras, M.; Félix, G.; Peresuttiab, R. One hundred years of helicene chemistry. Part 2: Stereoselective syntheses and chiral separations of carbohelicenes. *Chem. Soc. Rev.* **2013**, *42*, 1007–1050. [[CrossRef](#)] [[PubMed](#)]
- Gingras, M. One hundred years of helicene chemistry. Part 3: Applications and properties of carbohelicenes. *Chem. Soc. Rev.* **2013**, *42*, 1051–1095. [[CrossRef](#)] [[PubMed](#)]
- Hoffmann, N. Photochemical reactions applied to the synthesis of helicenes and helicene-like compounds. *J. Photochem. Photobiol. C Photochem. Rev.* **2014**, *19*, 1–19. [[CrossRef](#)]
- Saleh, N.; Shena, C.; Crassous, J. Helicene-based transition metal complexes: Synthesis, properties and applications. *Chem. Sci.* **2014**, *5*, 3680–3694. [[CrossRef](#)]
- Aillard, P.; Voituriez, A.; Marinetti, A. Helicene-like chiral auxiliaries in asymmetric catalysis. *Dalton Trans.* **2014**, *43*, 15263–15278. [[CrossRef](#)] [[PubMed](#)]
- Virieux, D.; Sevrain, N.; Ayad, T.; Pirat, J.-L. Helical phosphorus derivatives. In *Advances in Heterocyclic Chemistry*; Eric, F.V.S., Christopher, A.R., Eds.; Academic Press: Cambridge, MA, USA, 2015; Volume 116, pp. 37–83.
- Rajca, A.; Miyasaka, M. *Functional Organic Materials*; Wiley-VCH Verlag GmbH & Co. KGaA: Weinheim, Germany, 2007; Chapter 15, pp. 547–558.
- Chen, C.-E.; Shen, Y. *Helicene Chemistry—From Synthesis to Applications*; Springer: Berlin/Heidelberg, Germany, 2017; ISBN 978-3-662-53168-6.
- Weitzenbock, R.; Lieb, H. New synthesis of chrysene. *Monatshefte Chem.* **1913**, *33*, 549–565. [[CrossRef](#)]
- Weitzenbock, R.; Klingler, A. Synthesis of the isomeric hydrocarbons 1,2,5,6-dibenzanthracene and 3,4,5,6-dibenzophenanthrene. *J. Chem. Soc.* **1918**, *114*, 494.
- Cook, J.W. Polycyclic aromatic hydrocarbons. Part XII. The orientation of derivatives of 1:2-benzanthracene, with notes on the preparation of some new homologues, and on the isolation of 3:4:5:6-dibenzphenanthrene. *J. Chem. Soc.* **1933**, *0*, 1592–1597. [[CrossRef](#)]
- Newman, M.S.; Lutz, W.B.; Lednicer, D. A new reagent for resolution by complex formation; the resolution of phenanthro-[3,4-c]phenanthrene. *J. Am. Chem. Soc.* **1955**, *77*, 3420–3421. [[CrossRef](#)]

16. Newman, M.S.; Lednicer, D. The synthesis and resolution of hexahelicene. *J. Am. Chem. Soc.* **1956**, *78*, 4765–4770. [[CrossRef](#)]
17. Morrison, D.J.; Trefz, T.K.; Piers, W.E.; McDonald, R.; Parvez, M. 7:8:9:10-Dibenzo-1,2,3,4-tetrafluoro-triphenylene: Synthesis, structure, and photophysical properties of a novel [5]helicene. *J. Org. Chem.* **2005**, *70*, 5309–5312. [[CrossRef](#)] [[PubMed](#)]
18. Xue, X.; Scott, L.T. Thermal cyclodehydrogenations to form 6-membered rings: Cyclizations of [5]helicenes. *Org. Lett.* **2007**, *9*, 3937–3940. [[CrossRef](#)] [[PubMed](#)]
19. Minuti, L.; Taticchi, A.; Marrocchi, A.; Gacs-Baitz, E. Diels-Alder reaction of 3,3',4,4'-tetrahydro-1,1'-binaphthalene. One-pot synthesis of a pentahelicenebenzoquinone. *Tetrahedron* **1997**, *53*, 6873–6878. [[CrossRef](#)]
20. Ogawa, Y.; Ueno, T.; Tarikomi, M.; Seki, K.; Haga, K.; Uyehara, T. Synthesis of 2-acetoxy[5]helicene by sequential double aromatic oxy-Cope rearrangement. *Tetrahedron Lett.* **2002**, *43*, 7827–7829. [[CrossRef](#)]
21. Pieters, G.; Gaucher, A.; Prim, D.; Marrot, J. First expeditious synthesis of 6,11-diamino-[6]carbohelicenes. *Chem. Commun.* **2009**, *32*, 4827–4828. [[CrossRef](#)] [[PubMed](#)]
22. El Abed, R.; Aloui, F.; Genet, J.-P.; Ben Hassine, B.; Marinetti, A. Synthesis and resolution of 2-(diphenylphosphino)heptahelicene. *J. Organomet. Chem.* **2007**, *692*, 1156–1160. [[CrossRef](#)]
23. Abbate, S.; Bazzini, C.; Caronna, T.; Fontana, F.; Gambarotti, C.; Gangemi, F.; Longhi, G.; Mele, A.; Sora, I.N.; Panzeri, W. Monoaza[5]helicenes. Part 2: Synthesis, characterisation and theoretical calculations. *Tetrahedron* **2006**, *62*, 139–148. [[CrossRef](#)]
24. Meisenheimer, J.; Witte, K. Reduction of 2-nitronaphthalene. *Chem. Ber.* **1903**, *36*, 4153–4164. [[CrossRef](#)]
25. Sundar, M.S.; Sahoo, S.; Bedekar, A.V. Synthesis and study of the structural properties of oxa[5]helicene derivatives. *Tetrahedron Asymmetry* **2016**, *27*, 777–781. [[CrossRef](#)]
26. Dreher, S.D.; Weix, D.J.; Katz, T.J. Easy synthesis of functionalized hetero[7]helicenes. *J. Org. Chem.* **1999**, *64*, 3671–3678. [[CrossRef](#)] [[PubMed](#)]
27. Eskildsen, J.; Krebs, F.C.; Faldt, A.; Sommer-Larsen, P.; Bechgaard, K. Preparation and structural properties of 7,8-dioxa[6]helicenes and 7a,14c-dihydro-7,8-dioxa[6]helicenes. *J. Org. Chem.* **2001**, *66*, 200–205. [[CrossRef](#)] [[PubMed](#)]
28. Nakano, K.; Oyama, H.; Nishimura, Y.; Nakasako, S.; Nozaki, K. k5-Phospha[7]helicenes: Synthesis, properties, and columnar aggregation with one-way chirality. *Angew. Chem. Int. Ed.* **2012**, *51*, 695–699. [[CrossRef](#)] [[PubMed](#)]
29. Oyama, H.; Nakano, K.; Harada, T.; Kuroda, R.; Naito, M.; Nobusawa, K.; Nozaki, K. Facile synthetic route to highly luminescent sila[7]helicene. *Org. Lett.* **2013**, *15*, 2104–2107. [[CrossRef](#)] [[PubMed](#)]
30. Hatakeyama, T.; Hashimoto, S.; Oba, T.; Nakamura, M. Azaboradibenzo[6]helicene: Carrier inversion induced by helical homochirality. *J. Am. Chem. Soc.* **2012**, *134*, 19600–19603. [[CrossRef](#)] [[PubMed](#)]
31. Zhang, X.; Edward, L.; Clennan, E.L.; Arulsamy, N. Photophysical and electrochemical characterization of a helical Viologen, N,N'-dimethyl-5,10-diaza[5]helicene. *Org. Lett.* **2014**, *16*, 4610–4613. [[CrossRef](#)] [[PubMed](#)]
32. Guin, J.; Besnard, C.; Lacour, J. Synthesis, resolution, and stabilities of a cationic chromenoxanthene [4]helicene. *Org. Lett.* **2010**, *12*, 1748–1751.
33. Rozen, S.; Dayan, S. At Last, 1,10-Phenanthroline-N,N'-dioxide, A new type of helicene, has been synthesized using HOF small middle dotCH(3)CN. *Angew. Chem. Int. Ed.* **1999**, *38*, 3471–3473. [[CrossRef](#)]
34. Talele, H.R.; Sahoo, S.; Bedekar, A.V. Synthesis of chiral helical 1,3-oxazines. *Org. Lett.* **2012**, *14*, 3166–3169. [[CrossRef](#)] [[PubMed](#)]
35. Jierry, L.; Harthong, S.; Aronica, C.; Mulatier, J.-C.; Guy, L.; Guy, S. Efficient dibenzo[c]acridine helicene-like synthesis and resolution: Scaleup, structural control, and high chiroptical properties. *Org. Lett.* **2012**, *14*, 288–291. [[CrossRef](#)] [[PubMed](#)]
36. Wynberg, H. Some observations on the chemical, photochemical, and spectral properties of thiophenes. *Acc. Chem. Res.* **1971**, *4*, 65–73. [[CrossRef](#)]
37. Janke, R.H.; Haufe, G.; Würthwein, E.-U.; Borcken, J.H. Racemization barriers of helicenes: A computational study. *J. Am. Chem. Soc.* **1996**, *118*, 6031–6035. [[CrossRef](#)]
38. Groen, M.B.; Wynberg, H. Optical properties of some heterohelicenes. Absolute configuration. *J. Am. Chem. Soc.* **1971**, *93*, 2968–2974. [[CrossRef](#)]

39. Fujikawa, T.; Segawa, Y.; Itami, K. Synthesis, structures, and properties of π -extended double helicene: A combination of planar and nonplanar π -systems. *J. Am. Chem. Soc.* **2015**, *137*, 7763–7768. [[CrossRef](#)] [[PubMed](#)]
40. Liu, X.; Yu, P.; Xu, L.; Yang, J.; Shi, J.; Wang, Z.; Cheng, Y.; Wang, H. Synthesis for the mesomer and racemate of thiophene-based double helicene under irradiation. *J. Org. Chem.* **2013**, *78*, 6316–6321. [[CrossRef](#)] [[PubMed](#)]
41. Newman, M.S.; Wise, R.M. The synthesis and resolution of 1,12-dimethylbenzo[c]phenanthrene-5-acetic acid. *J. Am. Chem. Soc.* **1956**, *78*, 450–454. [[CrossRef](#)]
42. Martin, R.H. The Helicenes. *Angew. Chem. Int. Ed.* **1974**, *13*, 649–660. [[CrossRef](#)]
43. McCarthy, M.; Guiry, P.J. Axially chiral bidentate ligands in asymmetric catalysis. *Tetrahedron* **2001**, *57*, 3809–3844. [[CrossRef](#)]
44. Chen, Y.; Yekta, S.; YudiA, K. Modified BINOL ligands in asymmetric catalysis. *Chem. Rev.* **2003**, *103*, 3155–3212. [[CrossRef](#)] [[PubMed](#)]
45. Berthod, M.; Mignani, G.; Woodward, G.; Marc Lemaire, M. Modified BINAP: The how and the why. *Chem. Rev.* **2005**, *105*, 1801–1836. [[CrossRef](#)] [[PubMed](#)]
46. Hassine, B.B.; Gorsane, M.; Pecher, J.; Martin, R.H. Diastereoselective sodium borohydride reductions of (*dl*) α -keto esters. *Bull. Soc. Chim. Belg.* **1985**, *94*, 597–603. [[CrossRef](#)]
47. Hassine, B.B.; Gorsane, M.; Geerts-Evrard, F.; Pecher, J.; Martin, R.H.; Castelet, D. Payne syntheses and enantioselective syntheses of epoxides from (*E*)-stilbene and α -methylstyrene. *Bull. Soc. Chim. Belg.* **1986**, *95*, 557–566. [[CrossRef](#)]
48. Hassine, B.B.; Gorsane, M.; Pecher, J.; Martin, R.H. Potential asymmetric syntheses via the ene reaction. *Bull. Soc. Chim. Belg.* **1987**, *96*, 801–808.
49. Hassine, B.B.; Gorsane, M.; Pecher, J.; Martin, R.H. Asymmetric syntheses and potential asymmetric synthesis of α -amino alcohols: Hydroxyamination of olefins by the Sharpless method. *Bull. Soc. Chim. Belg.* **1985**, *94*, 759–769. [[CrossRef](#)]
50. Hassine, B.B.; Gorsane, M.; Pecher, J.; Martin, R.H. Atrolactic synthesis in the evaluation of the efficiency of inducers of asymmetric synthesis. *Bull. Soc. Chim. Belg.* **1986**, *95*, 547–556.
51. Yamamoto, K.; Shimizu, T.; Igawa, K.; Tomooka, K.; Hirai, G.; Suemune, H.; Usui, K. Rational design and synthesis of [5]helicene-derived phosphine ligands and their application in Pd-catalyzed asymmetric reactions. *Sci. Rep.* **2016**, *6*, 36211. [[CrossRef](#)] [[PubMed](#)]
52. Tsujihara, T.; Inada-Nozaki, N.; Takehara, T.; Zhou, D.-Y.; Suzuki, T.; Kawano, T. Nickel-catalyzed construction of chiral 1-[6]helicenols and application in the synthesis of [6]helicene-based phosphinite ligands. *Eur. J. Org. Chem.* **2016**, *2016*, 4948–4952. [[CrossRef](#)]
53. Reetz, M.T.; Sostmann, S. Kinetic resolution in Pd-catalyzed allylic substitution using the helical PHelix ligand. *J. Organomet. Chem.* **2000**, *603*, 105–109. [[CrossRef](#)]
54. Reetz, M.T.; Sostmann, S. First enantioselective catalysis using a helical diphosphane. *Tetrahedron Lett.* **1997**, *38*, 3211–3214. [[CrossRef](#)]
55. Nakano, D.; Yamaguchi, M. Enantioselective hydrogenation of itaconate using rhodium bihelicene phosphite complex. Matched/mismatched phenomena between helical and axial chirality. *Tetrahedron Lett.* **2003**, *44*, 4969–4971. [[CrossRef](#)]
56. Yavari, K.; Aillard, P.; Zhang, Y.; Nuter, F.; Retailleau, P.; Voituriez, A.; Marinetti, A. Helicenes with embedded phosphole units in enantioselective gold catalysis. *Angew. Chem. Int. Ed.* **2014**, *53*, 861–865. [[CrossRef](#)] [[PubMed](#)]
57. Aillard, P.; Voituriez, A.; Dova, D.; Cauteruccio, S.; Licandro, E.; Marinetti, A. Phosphathiahelicenes: Synthesis and uses in enantioselective gold catalysis. *Chem. Eur. J.* **2014**, *20*, 12373–12376. [[CrossRef](#)] [[PubMed](#)]
58. Cauteruccio, S.; Dova, D.; Benaglia, M.; Genoni, A.; Orlandi, M.; Licandro, E. Synthesis, characterisation, and organocatalytic activity of chiral tetrathiahelicene diphosphine oxides. *Eur. J. Org. Chem.* **2014**, *2014*, 2694–2702. [[CrossRef](#)]
59. Šamal, M.; Mísek, J.; Stara, I.G.; Stary, I. Organocatalysis with azahelicenes: The first use of helically chiral pyridine-based catalysts in the asymmetric acyl transfer reaction. *Collect. Czechoslov. Chem. Commun.* **2009**, *74*, 1151–1159. [[CrossRef](#)]

60. Misek, J.; Těplý, F.; Stara, I.G.; Tichý, M.; Saman, D.; Cisarova, I.; Vojtisek, P.; Stary, I. A straightforward route to helically chiral N-heteroaromatic compounds: Practical synthesis of racemic 1,14-diaza[5]helicene and optically pure 1- and 2-aza[6]helicenes. *Angew. Chem. Int. Ed.* **2008**, *47*, 3188–3191. [[CrossRef](#)] [[PubMed](#)]
61. Crittall, M.R.; Rzepa, H.S.; Carbery, D.R. Design, synthesis, and evaluation of a heliceneoidal DMAP Lewis base catalyst. *Org. Lett.* **2011**, *13*, 1250–1253. [[CrossRef](#)] [[PubMed](#)]
62. Ruble, J.C.; Latham, H.A.; Fu, G.C. Effective kinetic resolution of secondary alcohols with a planar–chiral analogue of 4-(Dimethylamino)pyridine. Use of the Fe(C₅Ph₅) group in asymmetric catalysis. *J. Am. Chem. Soc.* **1997**, *119*, 1492–1493. [[CrossRef](#)]
63. Ruble, J.C.; Tweddell, J.; Fu, G.C. Kinetic resolution of arylalkylcarbinols catalyzed by a planar–chiral derivative of DMAP: A new benchmark for nonenzymatic acylation. *J. Org. Chem.* **1998**, *63*, 2794–2795. [[CrossRef](#)]
64. Spivey, A.C.; Fekner, T.; Spey, S.E. Axially chiral analogues of 4-(Dimethylamino)pyridine: Novel catalysts for nonenzymatic enantioselective acylations. *J. Org. Chem.* **2000**, *65*, 3154–3159. [[CrossRef](#)] [[PubMed](#)]
65. Chen, J.; Takenaka, N. Helical chiral pyridine N-oxides: A new family of asymmetric catalysts. *Chem. Eur. J.* **2009**, *15*, 7268–7276. [[CrossRef](#)] [[PubMed](#)]
66. Narcis, M.J.; Takenaka, N. Helical–chiral small molecules in asymmetric catalysis. *Eur. J. Org. Chem.* **2014**, *2014*, 21–34. [[CrossRef](#)]
67. Takenaka, N.; Sarangthem, R.S.; Captain, B. Helical chiral pyridine N-oxides: A new family of asymmetric catalysts. *Angew. Chem. Int. Ed.* **2008**, *47*, 9708–9710. [[CrossRef](#)] [[PubMed](#)]
68. Chen, J.; Captain, B.; Takenaka, N. Helical chiral 2,20-bipyridine N-monoxides as catalysts in the enantioselective propargylation of aldehydes with allenyltrichlorosilane. *Org. Lett.* **2011**, *13*, 1654–1657. [[CrossRef](#)] [[PubMed](#)]
69. Lu, T.; Zhu, R.; An, Y.; Wheeler, S.E. Origin of enantioselectivity in the propargylation of aromatic aldehydes catalyzed by helical N-oxides. *J. Am. Chem. Soc.* **2012**, *134*, 3095–3102. [[CrossRef](#)] [[PubMed](#)]
70. Takenaka, N.; Chen, J.; Captain, B.; Sarangthem, R.S.; Chandrakumar, A. Helical chiral 2-aminopyridinium ions: A new class of hydrogen bond donor catalysts. *J. Am. Chem. Soc.* **2010**, *132*, 4536–4537. [[CrossRef](#)] [[PubMed](#)]
71. Narcis, M.J.; Sprague, D.J.; Captain, B.; Takenaka, N. Enantio- and periselective nitroalkene Diels–Alder reaction. *Org. Biomol. Chem.* **2012**, *10*, 9134–9136. [[CrossRef](#)] [[PubMed](#)]
72. Sato, I.; Yamashima, R.; Kadowaki, K.; Yamamoto, J.; Shibata, T.; Soai, K. Asymmetric induction by helical hydrocarbons: [6]- and [5]helicenes. *Angew. Chem. Int. Ed.* **2001**, *40*, 1096–1098. [[CrossRef](#)]
73. Kawasaki, T.; Suzuki, K.; Licandro, E.; Bossi, A.; Maiorana, S.; Soai, K. Enantioselective synthesis induced by tetrathia-[7]-helicenes in conjunction with asymmetric autocatalysis. *Tetrahedron Asymmetry* **2006**, *17*, 2050–2053. [[CrossRef](#)]
74. Dreher, S.D.; Katz, T.J.; Lam, K.-C.; Rheingold, A.L. Application of the Russig–Laatsch reaction to synthesize a bis[5]helicene chiral pocket for asymmetric catalysis. *J. Org. Chem.* **2000**, *65*, 815–822. [[CrossRef](#)]
75. Amemiya, R.; Yamaguchi, M. Chiral recognition in noncovalent bonding interactions between helicenes: Right-handed helix favors right-handed helix over left-handed helix. *Org. Biomol. Chem.* **2008**, *6*, 26–35. [[CrossRef](#)] [[PubMed](#)]
76. Okubo, H.; Yamaguchi, M.; Kabuto, C. Macrocyclic amides consisting of helical chiral 1,12-dimethylbenzo[c]phenanthrene-5,8-dicarboxylate. *J. Org. Chem.* **1998**, *63*, 9500–9509. [[CrossRef](#)]
77. Reetz, M.T.; Sostmann, S. 2,15-Dihydroxy-hexahelicene (HELIXOL): Synthesis and use as an enantioselective fluorescent sensor. *Tetrahedron* **2001**, *57*, 2515–2520. [[CrossRef](#)]
78. Nakazaki, M.; Yamamoto, K.; Ikeda, T.; Kitsuki, T.; Okamoto, Y. Synthesis and chiral recognition of novel crown ethers incorporating helicene chiral centres. *J. Chem. Soc. Chem. Commun.* **1983**, *0*, 787–788. [[CrossRef](#)]
79. Yamamoto, K.; Ikeda, T.; Kitsuki, T.; Okamoto, Y.; Chikamatsu, H.; Nakazaki, M. Synthesis and chiral recognition of optically active crown ethers incorporating a helicene moiety as the chiral centre. *J. Chem. Soc. Perkin Trans. 1* **1990**, *0*, 271–276. [[CrossRef](#)]
80. Pandey, A.D.; Mohammed, H.; Pissurlenkar, R.R.S.; Karnik, A.V. Size-induced chiral discrimination switching by (S)-(-)-2(α-hydroxyethyl)benzimidazole-derived azacrowns. *ChemPlusChem* **2015**, *80*, 475–479. [[CrossRef](#)]
81. Weix, D.J.; Dreher, S.D.; Katz, T.J. [5]HELOL phosphite: A helically grooved sensor of remote chirality. *J. Am. Chem. Soc.* **2000**, *122*, 10027–10032. [[CrossRef](#)]

82. Wang, D.Z.; Katz, T.J. A [5]HELOL analogue that senses remote chirality in alcohols, phenols, amines, and carboxylic acids. *J. Org. Chem.* **2005**, *70*, 8497–8502. [[CrossRef](#)] [[PubMed](#)]
83. Schweinfurth, D.; Zalibera, M.; Kathan, M.; Shen, C.; Mazzolini, M.; Trapp, N.; Crassous, J.; Gescheidt, G.; Diederich, F. Helicene quinones: Redox-triggered chiroptical switching and chiral recognition of the semiquinone radical anion lithium salt by electron nuclear double resonance spectroscopy. *J. Am. Chem. Soc.* **2014**, *136*, 13045–13052. [[CrossRef](#)] [[PubMed](#)]
84. Hasan, M.; Khose, V.N.; Mori, T.; Borovkov, V.; Karnik, A.V. Sui generis helicene-based supramolecular chirogenic system: Enantioselective sensing, solvent control, and application in chiral group transfer reaction. *ACS Omega* **2017**, *2*, 592–598. [[CrossRef](#)]
85. Hasan, M.; Pandey, A.D.; Khose, V.N.; Mirgane, N.A.; Karnik, A.V. Sterically congested chiral 7,8-dioxo[6]helicene and Its dihydro analogues: Synthesis, regioselective functionalization, and unexpected domino Prins reaction. *Eur. J. Org. Chem.* **2015**, *2015*, 3702–3712. [[CrossRef](#)]
86. Hasan, M.; Khose, V.N.; Pandey, A.D.; Borovkov, V.; Karnik, A.V. Tailor-made supramolecular chirogenic system based on Cs-symmetric rigid organophosphoric acid host and amino alcohols: Mechanistic studies, bulkiness effect, and chirality sensing. *Org. Lett.* **2016**, *18*, 440–443. [[CrossRef](#)] [[PubMed](#)]
87. Anger, E.; Iida, H.; Yamaguchi, T.; Hayashi, K.; Kumano, D.; Crassous, J.; Vanthuyne, N.; Roussel, C.; Yashima, E. Synthesis and chiral recognition ability of helical polyacetylenes bearing helicene pendants. *Polym. Chem.* **2014**, *5*, 4909–4914. [[CrossRef](#)]
88. An, Z.; Yamaguchi, M. Chiral recognition in aggregation of gold nanoparticles grafted with helicenes. *Chem. Commun.* **2012**, *48*, 7383–7385. [[CrossRef](#)] [[PubMed](#)]
89. Ichinose, W.; Miyagawa, M.; An, Z.; Yamaguchi, M. Optical resolution of aromatic alcohols using silica nanoparticles grafted with helicene. *Org. Lett.* **2012**, *14*, 3123–3125. [[CrossRef](#)] [[PubMed](#)]
90. Miyagawa, M.; Ichinose, W.; Yamaguchi, M. Equilibrium shift in solution: Molecular shape recognition and precipitation of a synthetic double helix using helicene-grafted silica nanoparticles. *Chem. Eur. J.* **2014**, *20*, 1272–1278. [[CrossRef](#)] [[PubMed](#)]
91. Yamada, K.; Ishii, R.; Nakagawa, H.; Kawazura, H. Inclusion of Trithia[5]heterohelicene by various serum albumins. An effective probe for chiral discrimination. *Chem. Pharm. Bull.* **1997**, *45*, 936–938. [[CrossRef](#)] [[PubMed](#)]
92. Nakagawa, H.; Kobori, Y.; Yamada, K. Spontaneous chirality conversion of [5]thiaheterohelicene in charge-transfer complexes in SDS micelles. *Chirality* **2001**, *13*, 722–726. [[CrossRef](#)] [[PubMed](#)]
93. Nakagawa, H.; Gomi, K.; Yamada, K. Chiral recognition of thiaheterohelicenes by alkyl b-D-pyranoside micelles. Influence of extension of helix. *Chem. Pharm. Bull.* **2001**, *49*, 49–53. [[CrossRef](#)] [[PubMed](#)]
94. Nakagawa, H.; Kobori, Y.; Yoshida, M.; Yamada, K. Chiral recognition by single bilayered phosphatidylcholine vesicles using [5]thiaheterohelicene as a probe. *Chem. Commun.* **2001**, *0*, 2692–2693. [[CrossRef](#)]
95. Nakagawa, H.; Yoshida, M.; Kobori, Y.; Yamada, K. Study of chiral recognition of bilayered phosphatidylcholine vesicles using a helicene probe: Characteristic function of cholesterol. *Chirality* **2003**, *15*, 703–708. [[CrossRef](#)] [[PubMed](#)]
96. Nakagawa, H.; Yamada, K. Difference in chiral recognition of gel and liquid-crystalline phases of phosphatidylcholine vesicles as determined by circular dichroism spectroscopy. *Chem. Pharm. Bull.* **2005**, *53*, 52–55. [[CrossRef](#)] [[PubMed](#)]
97. Tanaka, K.; Osuga, H.; Suzuki, H.; Shogase, Y.; Kitahara, Y. Synthesis, enzymic resolution and enantiomeric enhancement of bis(hydroxymethyl)[7]thiaheterohelicenes. *J. Chem. Soc. Perkin Trans. 1* **1998**, *0*, 935–940. [[CrossRef](#)]
98. Xu, Y.; Zhang, Y.X.; Sugiyama, H.; Umamo, T.; Osuga, H.; Tanaka, K. (P)-Helicene displays chiral selection in binding to Z-DNA. *J. Am. Chem. Soc.* **2004**, *126*, 6566–6567. [[CrossRef](#)] [[PubMed](#)]
99. Tanaka, K.; Osuga, H.; Kitahara, Y. Elongation and contraction of molecular springs. Synthesis, structures, and properties of bridged [7]thiaheterohelicenes. *J. Org. Chem.* **2002**, *67*, 1795–1801. [[CrossRef](#)] [[PubMed](#)]
100. Shinohara, K.; Sannohe, Y.; Kaieda, S.; Tanaka, K.; Osuga, H.; Tahara, H.; Xu, Y.; Kawase, T.; Bando, T.; Sugiyama, H. A chiral wedge molecule inhibits telomerase activity. *J. Am. Chem. Soc.* **2010**, *132*, 3778–3782. [[CrossRef](#)] [[PubMed](#)]
101. Tsuji, G.; Kawakami, K.; Sasaki, S. Enantioselective binding of chiral 1,14-dimethyl[5]helicene–spermine ligands with B- and Z-DNA. *Bioorg. Med. Chem.* **2013**, *21*, 6063–6068. [[CrossRef](#)] [[PubMed](#)]

102. Kel, O.; Frstenberg, A.; Mehanna, N.; Nicolas, C.; Laleu, B.; Hammanson, M.; Albinsson, B.; Lacour, J.; Vauthey, E. Chiral selectivity in the binding of [4]helicene derivatives to double-stranded DNA. *Chem. Eur. J.* **2013**, *19*, 7173–7180. [[CrossRef](#)] [[PubMed](#)]
103. Huang, Q.; Jiang, L.; Liang, W.; Gui, J.; Xu, D.; Wu, W.; Nakai, Y.; Nishijima, M.; Fukuhara, G.; Mori, T.; et al. Inherently chiral azonia[6]helicene-modified β -cyclodextrin: Synthesis, characterization, and chirality sensing of underivatized amino acids in water. *J. Org. Chem.* **2016**, *81*, 3430–3434. [[CrossRef](#)] [[PubMed](#)]
104. Okubo, H.; Nakano, D.; Anzai, S.; Yamaguchi, M. Synthesis of symmetrical polynitrohelicenes and their chiral recognition in the charge transfer complexation. *J. Org. Chem.* **2001**, *66*, 557–563. [[CrossRef](#)] [[PubMed](#)]
105. Murguly, E.; McDonald, R.; Branda, N.R. Chiral discrimination in hydrogen-bonded [7]helicenes. *Org. Lett.* **2000**, *2*, 3169–3172. [[CrossRef](#)] [[PubMed](#)]
106. Mikes, F.; Boshart, G.; Gil-Av, E. Resolution of optical isomers by high-performance liquid chromatography, using coated and bonded chiral charge-transfer complexing agents as stationary phases. *J. Chromatogr. A* **1976**, *122*, 205–221. [[CrossRef](#)]
107. Thongpanchang, T.; Paruch, K.; Katz, T.J.; Rheingold, A.R.; Lam, K.-C.; Liable-Sands, L. Why (1S)-camphanates are excellent resolving agents for helicen-1-ols and why they can be used to analyze absolute configurations. *J. Org. Chem.* **2000**, *65*, 1850–1856. [[CrossRef](#)] [[PubMed](#)]
108. Bucinskas, A.; Waghray, D.; Bagdziunas, G.; Thomas, J.; Grazulevicius, J.V.; Dehaen, W. Synthesis, functionalization, and optical properties of chiral carbazole-based diaza[6]helicenes. *J. Org. Chem.* **2015**, *80*, 2521–2528. [[CrossRef](#)] [[PubMed](#)]
109. Waghray, D.; Bagdziunas, G.; Jacobs, J.; Meervelt, L.V.; Grazulevicius, J.V.; Dehaen, W. Diastereoselective strategies towards thia[n]helicenes. *Chem. Eur. J.* **2015**, *21*, 18791–18798. [[CrossRef](#)] [[PubMed](#)]
110. Nakano, K.; Hidehira, Y.; Takahashi, K.; Hiyama, T.; Nozaki, K. Stereospecific synthesis of hetero[7]helicenes by Pd-catalyzed double N-arylation and intramolecular O-arylation. *Angew. Chem. Int. Ed.* **2005**, *44*, 7136–7138. [[CrossRef](#)] [[PubMed](#)]
111. Sako, M.; Takeuchi, Y.; Tsujihara, T.; Kodera, J.; Kawano, T.; Takizawa, S.; Sasai, T. Efficient enantioselective synthesis of oxahelicenes using redox/acid cooperative catalysts. *J. Am. Chem. Soc.* **2016**, *138*, 11481–11484. [[CrossRef](#)] [[PubMed](#)]
112. Šámal, M.; Chercheja, S.; Rybáček, J.; Chocholoušová, J.V.; Vacek, J.; Bednárová, L.; Šaman, D.; Stará, I.G.; Starý, I. An ultimate stereocontrol in symmetric synthesis of optically pure fully aromatic helicenes. *J. Am. Chem. Soc.* **2015**, *137*, 8469–8474. [[CrossRef](#)] [[PubMed](#)]
113. Barroso, J.; Cabellos, J.L.; Pan, S.; Murillo, F.; Zarate, X.; Fernandez-Herrera, M.A.; Merino, G. Revisiting the racemization mechanism of helicenes. *Chem. Commun.* **2018**, *54*, 188–191. [[CrossRef](#)] [[PubMed](#)]



© 2017 by the authors. Licensee MDPI, Basel, Switzerland. This article is an open access article distributed under the terms and conditions of the Creative Commons Attribution (CC BY) license (<http://creativecommons.org/licenses/by/4.0/>).

Review

Chiral Buckybowl Molecules

Kuppusamy Kanagaraj ^{1,†}, Kangjie Lin ^{1,†}, Wanhua Wu ¹, Guowei Gao ¹, Zhihui Zhong ²,
Dan Su ² and Cheng Yang ^{1,*}

¹ Key Laboratory of Green Chemistry & Technology, College of Chemistry, Sichuan University, Chengdu 610064, China; kanagaraj195@gmail.com (K.K.); kangjie_lin@outlook.com (K.L.); wuwanhua.510@163.com (W.W.); gaoguowei@scu.edu.cn (G.G.)

² State Key Laboratory of Biotherapy, West China Medical Center, Sichuan University, Chengdu 610064, China; zhihui.zhong@hcbiomed.com (Z.Z.); sudan.lab@hotmail.com (D.S.)

* Correspondence: yangchengyc@scu.edu.cn; Tel.: +86-28-8541-6298

† These authors contributed equally to this paper.

Received: 27 July 2017; Accepted: 21 August 2017; Published: 30 August 2017

Abstract: Buckybowls are polynuclear aromatic hydrocarbons that have a curved aromatic surface and are considered fragments of buckminsterfullerenes. The curved aromatic surface led to the loss of planar symmetry of the normal aromatic plane and may cause unique inherent chirality, so-called bowl chirality, which it is possible to thermally racemize through a bowl-to-bowl inversion process. In this short review, we summarize the studies concerning the special field of bowl chirality, focusing on recent practical aspects of attaining diastereo/enantioenriched chiral buckybowls through asymmetric synthesis, chiral optical resolution, selective chiral metal complexation, and chiral assembly formation.

Keywords: buckybowl; corannulene; sumanene; bowl chirality; bowl inversion; asymmetric synthesis; chiral resolution

1. Introduction

Studies on the physical and chemical characteristics of buckybowls have attracted significant interest owing to their direct structural correlation with fullerenes and potential applications in the realm of material science (Figure 1) [1–3]. Corannulene **1** and sumanene **2**, two prototypical buckybowls, are both highly curved π -conjugated aromatic molecules representing the substructures of fullerene. The smallest C_{3v} -symmetric fragment **2** comprises a central six-membered ring surrounded by three five- and three six-membered rings fused in an alternating fashion (Figure 1), whereas the smallest C_5 -symmetric fragment **1** contains a central five-membered ring surrounded by five six-membered rings (Figure 1). Regioselective allocation of the five- or six-membered ring subunits around the centroid pentagon or hexagon, respectively, gave the curved bowl-shaped structures. Certain buckybowls are inherently chiral and difficult to separate from the racemates due to their rapid bowl inversion [4]. Controlling the bowl chirality of these π -conjugates and obtaining enantioenriched buckybowls are challenging tasks for chemists, while buckybowls application in chiral materials is highly promising [5–14]. Further extension of the π -conjugation of these chiral enantioenriched buckybowls leads to homochiral carbon nanotubes, and these chiral carbon materials create new perspectives in chiral catalysis, chiral sensing, chiral separation sciences, etc. [15–27]. A better understanding of bowl chirality will help researchers find a good way to control the chiral self-assembly of carbon nanotubes (CNTs) or fullerenes, which have already exhibited exciting potential as next-generation functional materials [28–38].

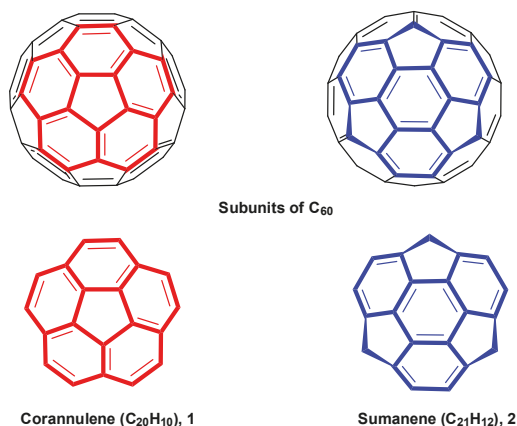


Figure 1. Chemical structures and bowl-shaped fragments of **1** (left) and **2** (right) as rim hydrogenated subunits of spherical buckminsterfullerene C_{60} .

While several buckybowl-related reviews have been published in recent years [6,39–44], most of them focused on the synthetic strategy and derivation method. Only a few publications involve the stereochemistry or chirality of the buckybowls. In this short review, we summarize recent progress on the stereochemistry of buckybowls and their derivatives. It covers recent developments in the asymmetric synthesis and optical resolution of buckybowls from their racemates, and application of the enantioenriched buckybowls in the chiral aggregate formation and homochiral CNT syntheses [45,46]. These structurally well-defined single-chiral CNTs exploit truly exciting applications ranging from space elevator to armchair quantum wire and bio-related applications [47]. Chiral buckybowls that possess a stable concave or convex shape are suitable for the construction of chiral molecular recognition sites [48]. They may also coordinate metals by virtue of their electron-rich/-deficient properties and thus have the potential for enantioselective organocatalysis [49,50]. Chiral buckybowls, acting as chiral building blocks, can also be used for constructing helical assemblies and preparing homochiral crystalline organic materials.

2. Classification of Bowl Chirality

Bowl-shaped carbon-based π -conjugated aromatic compounds, so-called “buckybowls”, are the partial structure of fullerenes or CNTs (Figure 1). These three-dimensional (3D) curved π -electron systems may possess inherent chirality and present many similarities to chiral fullerenes and CNTs, which is often defined as “bowl chirality” for convenience. The bowl-shaped polyaromatic hydrocarbon chiral buckybowl molecules can be broadly classified into three categories (Figure 2) based on the origin of their chirality. The conjugated bowl structure itself possesses the chirality, such as π -extended buckybowls, e.g., hemifullerene **3**; bowl chirality caused by introduction of one or more substituents on the rim of the buckybowl, e.g., trimethylsumanene **4**; and bowl chirality originated from the introduction of heteroatom into the π -bowl carbon skeleton, e.g., triazasumanene **5**.

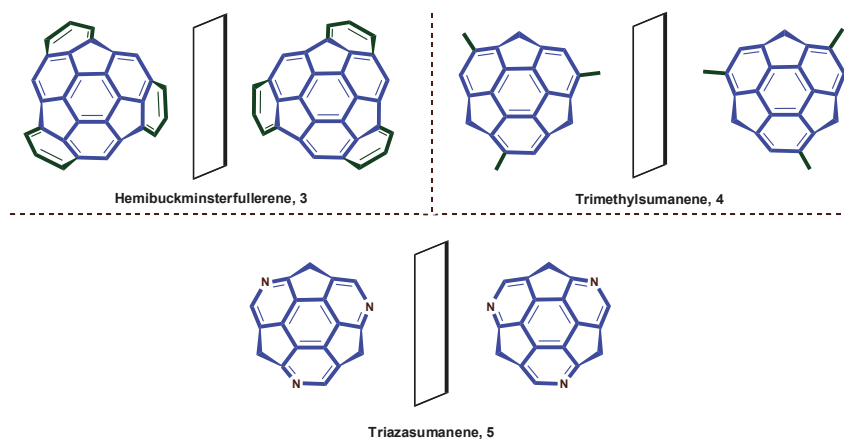


Figure 2. Classification of chiral buckybowl molecules.

Unlike common aromatic compounds, which often have a symmetry plane along the aromatic ring, buckybowls lose the cross-ring symmetry plane due to the curved shape. Unsubstituted buckybowls **1** and **2** are not chiral due to the presence of the reflection symmetry with respect to the mirror planes containing the rotational axis to show C_{5v} and C_{3v} symmetry, respectively. Introducing the addends may break the reflection symmetry to cause chirality, and alter their properties, such as bowl-to-bowl inversion [12–22], chirality [12,17,19,23], bowl depth [14,19,20], crystal structure [19,24,25], molecular recognition [2,26,27,51] and supramolecular assembly [3,28–30,52,53] behavior, metal complexation [23,31–36], electronic conductivity [19,37,38], and so on. Although the chirality is an important element in three-dimensional curved π -electron systems, thus far there have been no reports of the enantioselective synthetic control of the bowl chirality.

3. Stereodescriptor System of Buckybowls

Until now, the absolute configuration of bowl chirality of chiral buckybowl molecules was followed by two independent stereodescriptor systems: The stereodescriptor *C* or *A* based on fullerene nomenclature [17,54] and the another stereodescriptor *P* or *M* based on the Cahn–Ingold–Prelog (CIP) sequence rule [32]. The numbering system of fullerenes follows in general a helical numbering path, starting from the lowest set of numbers for substituents. To assign a descriptor in the chiral fullerene system, the viewer looks from the outside of the fullerene cage at the polygon to start the numbering and trace the path of numbering C(1)–C(6) (Figure 3a) [54]. The chirality of buckybowls is assigned in the same way, and a viewer looks from the convex face and traces the path of numbering from atom C(1) to C(6) (Figure 3b) [17]. If the numbering path describes a clockwise direction/travel, the configuration of the chiral bowl is designated as *C*. In contrast, if the path describes a counterclockwise direction/travel, the configuration of the chiral bowl is designated as *A*.

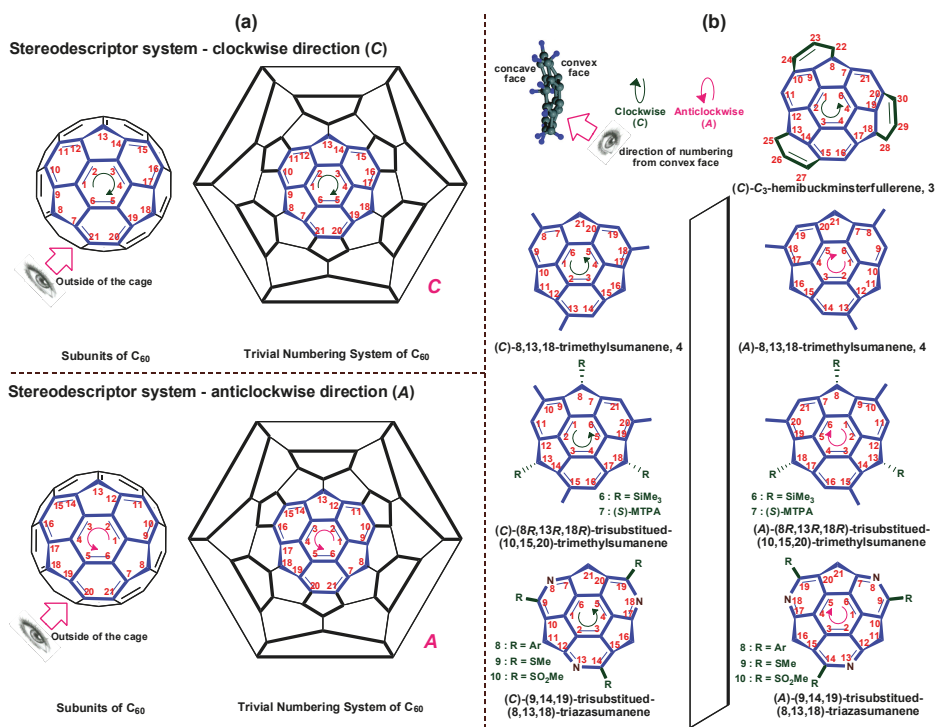


Figure 3. (a) Three-dimensional diagram of C_{60} with the subunit of sumanene including enantiomeric travel numbering schemes and the related stereodescriptor systems C and A; (b) The stereodescriptor system of some C_3 symmetric chiral buckybowls.

Another stereodescriptor system *P* or *M* for chiral buckybowls uses the CIP sequence rule [32]. Based on the CIP priority rule [55], the “non-fusion peripheral atoms” of buckybowl molecules are compared, and one atom with the highest CIP priority is chosen as the first priority (point of origin, ①, Figure 4) [17,18]. Furthermore, for the next highest CIP priority atom ② versus ①, compare the two neighboring rim atoms attached to this original point, and subsequent atoms attached thereto. For a viewer looking from the concave face of the buckybowl molecule, i.e., looking “into” the cavity of the bowl, the path of CIP priority numbering is from the original point atom to the neighboring atom with higher priority (①→②). If the path of CIP priority numbering direction describes clockwise travel, the configuration of the chiral bowl is designated as *P*. Otherwise, if the path of CIP priority numbering travels in a counterclockwise direction, the descriptor is *M*. The numbering to specify the positions of substituents follows the nomenclature of fused ring systems.

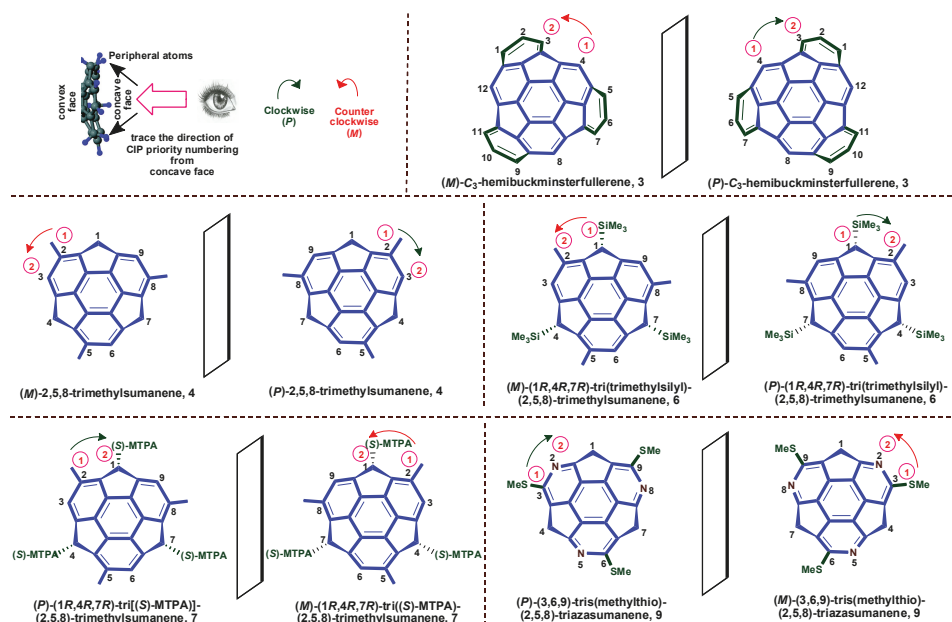


Figure 4. The *P* and *M* stereodescriptor system for some C₃ symmetric chiral buckybowl molecules based on the CIP priority rule.

4. Bowl Inversion/Racemization of Chiral Buckybowls

A unique property of buckybowls lies in that these molecules can thermally flip their curvature in solution via bowl-to-bowl inversion or concave–convex transition. During the bowl inversion process, the inherent bowl chirality inverts; this process is also called racemization (Figure 5a) [12,17–19]. The nonpolar polyaromatic small bowl molecules, like **1** and **2** can thermally flip through a planar transition state and the required energy to cross this transition barrier is defined as bowl inversion energy (ΔE) (Figure 5b) [20]. In the solid state, buckybowl molecules exist in a stack structure and show excellent physical properties, such as electron conductivity [24].

The thermally driven bowl-to-bowl inversion is of interest to basic science and can find various applications in functional materials for sensors, chemical machines, or ferroelectric memories. The lifetime of enantiopure chiral buckybowls is controlled by the bowl inversion energy (ΔE). The enantiopure chiral buckybowls are expected to contribute to a variety of applications such as asymmetric molecular recognition, homochiral crystal organic materials, chiral self-assembly, and chiral organometallic catalysis [6,7,9].

The introduction of substituents or heteroatoms in the carbon skeleton of buckybowls changes the bowl inversion energy within the range of 20–40 kcal/mol, and therefore could change the lifetimes of chiral buckybowls considerably. Furthermore, the nature, position, number of substituents, and stereoelectronic effects also significantly influence the bowl shape, depth (*x*), lifetime of keeping chirality, electron-deficient/-rich nature, and other physicochemical properties [56]. The bowl-inversion energy of corannulene derivatives was first determined by Scott and co-workers [13]. The interesting dynamic behavior of various buckybowl molecules has been extensively studied by Scott [57], Siegel [14,16], Hirao [15,35], Sakurai [12,17–20], and others. In particular, Sakurai and co-workers studied the effect of the substituent R at the benzylic position of sumanene **11**, which possesses two different conformers, *endo*-R and *exo*-R, differing in the direction of the aromatic bowl shape, concave or convex (Figures 6 and 7) [56].

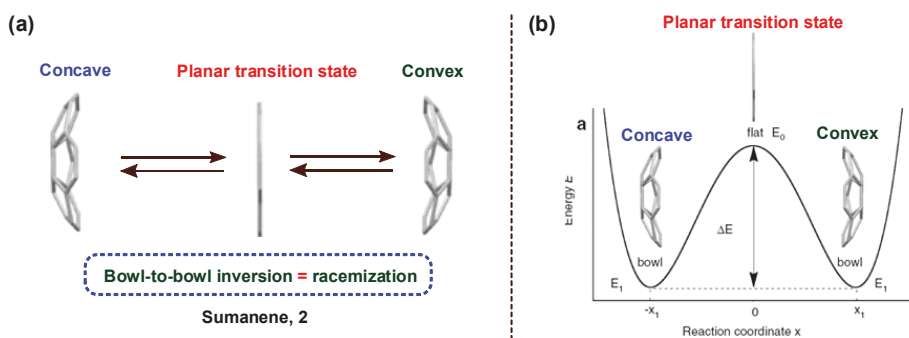


Figure 5. (a) Racemization of chiral 2 through bowl-to-bowl inversion/racemization; (b) the double-well potential energy profile. Reprinted from [20]. © 2014 Pure & Applied Chemistry.

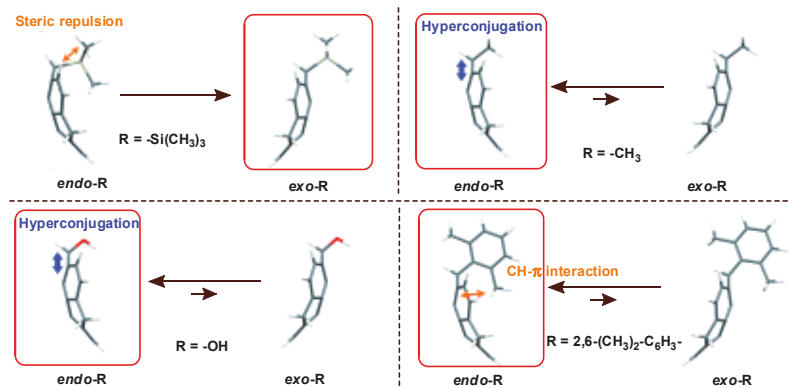


Figure 6. The *endo-R* and *exo-R* conformers of monosubstituted-sumanene 11 as determined by DFT calculations and the involved stereoelectronic effects. Reprinted from [56]. © 2013 Wiley-VCH Verlag GmbH & Co. KGaA, Weinheim.

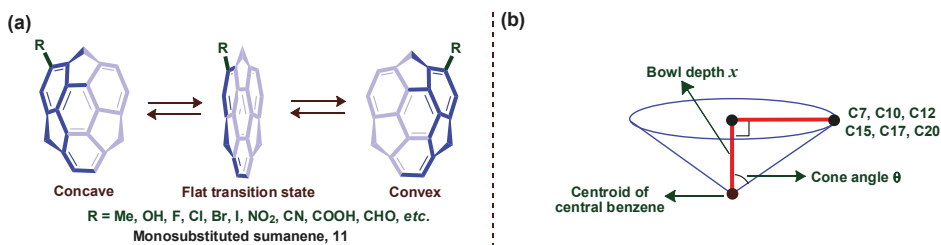


Figure 7. (a) Monosubstituted sumanene derivatives 11; (b) Its graphical representation bowl depth and cone angle.

Introduction of substituents will influence the geometries/conformations of buckybowl and bowl inversion energies as well. The effect of substituents in corannulene has been studied by Siegel and co-workers [14,16]. They demonstrated that introducing the acyclic substituents in corannulene usually decreases the bowl depth and increases the bowl inversion energy. Based on the results of the experimental and theoretical study, they proposed a quantitative equation for bowl inversion energy,

which relates the bowl depth to the bowl inversion energy (Figure 7) [14,16]. Steric and electronic factors of substituents also affect the bowl structure and bowl inversion energy of sumanene. Recently, Sakurai and co-workers found that sumanene **2** attached with a mono-iodo substituent induces a slightly deeper bowl depth and a higher bowl inversion energy compared with other sumanene derivatives because of its steric effect, whereas the electronic effects caused by formyl and nitro substituents induced a shallower bowl depth and a lower bowl inversion energy [20].

Siegel and co-workers studied the bowl-to-bowl inversion of corannulene **1** and ethylcorannulene derivatives mediated by extended tetracationic cyclophane (Figure 8) [22,30]. This synthetic host forms a supramolecular complex with **1** and ethylcorannulene via induced fit, and the bowl-to-bowl inversion process was accelerated by a factor of 10 at room temperature. Upon host–guest complexation, the transition state of the guest is stabilized through the stereoelectronic reorganization of the host, which switched from a strained conformation to an energetically favored conformation. Further, the experimental and DFT calculations for bowl-to-bowl inversion process of the host–guest complexation of **1** demonstrates the decrease of bowl-to-bowl inversion energy barrier of corannulene (Figure 8).

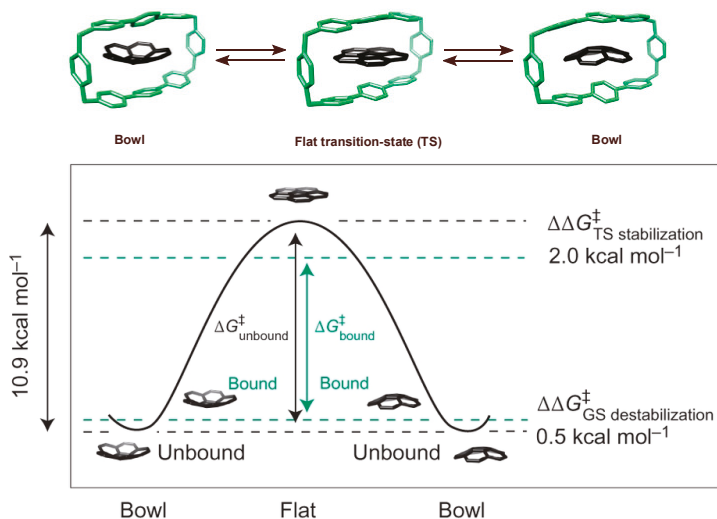


Figure 8. Comparison of energy profile of bowl-to-bowl inversion of corannulene **1** (black) and tetracationic cyclophane: **1**, complex (green) in Me₂CO; absolute contributions of ground-state (GS) destabilization (0.5 kcal mol^{−1}) and transition-state (TS) stabilization (2.0 kcal mol^{−1}) to the overall energy-barrier decrease ($\Delta\Delta G^{\ddagger}_{\text{catalysis}}$) of the bowl-to-bowl inversion process of **1** inside the tetracationic cyclophane calculated by DFT (B97D/Def2-TZVPP). Reprinted from [22]. © 2014 Nature Publishing Group.

5. Heterobuckybowls

Doping of heteroatoms to the carbon frameworks of bowl-shaped aromatic compounds drastically modulates their geometrical structure and physical and chemical properties. After the successful synthesis of corannulene and sumanene derivatives, researchers began to try to synthesize heteroatom-doped bucky bowl molecules, so-called “heterobuckybowls”. The introduction of heteroatoms into the carbon skeleton is expected to yield altered electronic properties of basic carbon skeleton buckybowls, especially electron-deficient or -rich in nature. Notably, the substitution of a hetero atom in its carbon skeleton also causes the geometrical change, especially the depth of the bowl. As a result of the change in depth of the bowl, the activation energy for the bowl-to-bowl inversion energy is also altered. The higher the bowl inversion energy is, the more stable the chiral conformer will be. Several heterobuckybowls have been reported in the literature, some of them chiral (Figure 9) [12,58–66].

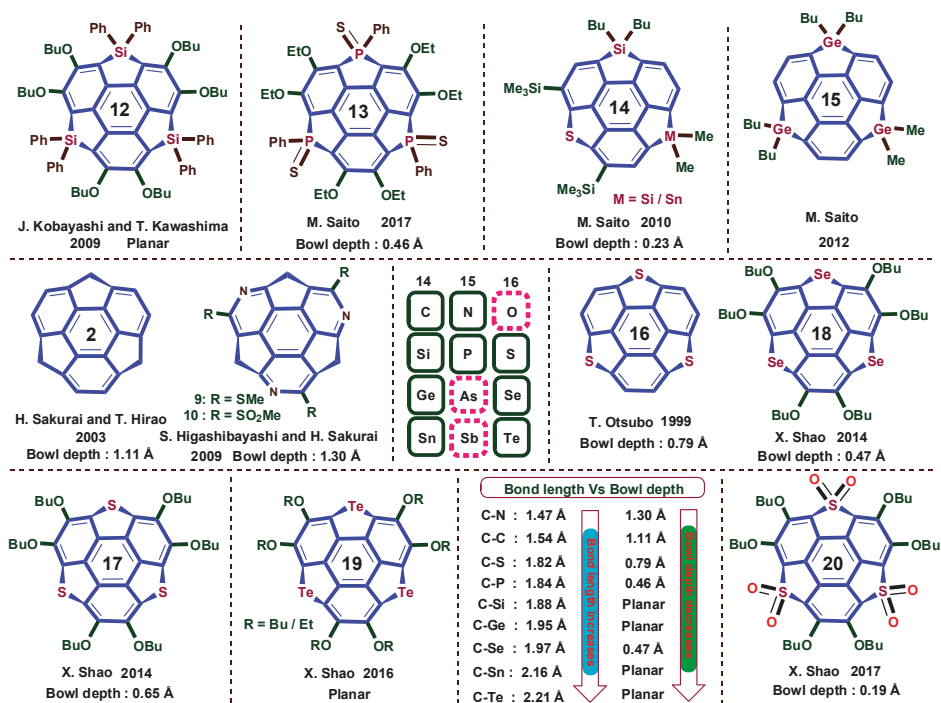


Figure 9. Heterobuckybowls with their bowl depth.

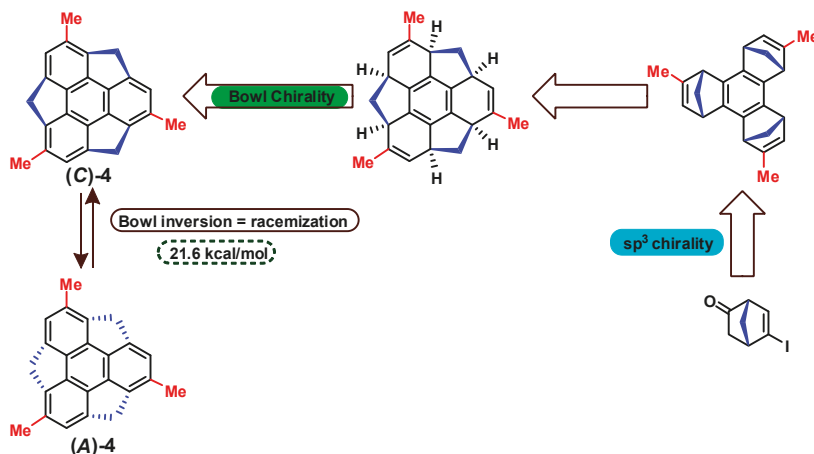
The heteroatoms embedded in the reported heterobuckybowls are mainly the group 14, 15, and 16 elements, such as nitrogen (second row), silicon, phosphorus and sulfur (third row), germanium and selenium (fourth row), and tin and tellurium (fifth row) (Figure 9). Introduction of heteroatoms in the periphery of buckybowls usually resulted in a decrease of the bowl depth of heterobuckybowls, because the bond lengths of carbon–heteroatom increased with the atomic size (Figure 9). The bowl depths of trithiasumanene **16** (0.79 Å) and triselenasumanene **18** (0.47 Å) [64] have a shallower bowl depth than that of normal sumanene **2** (1.11 Å) [24]. Trisilicasumanene **12** [59,63] and tritellurasumanene **19** have a plane structure, whereas triazasumanene **10** has a deeper bowl depth of 1.30 Å because the C–N bond length (1.47 Å) is shorter than the C–C bond length (1.54 Å) [12]. The high reactivity of nitrogen facilitates the formation of the highly strained triazasumanene derivative with higher bowl-to-bowl inversion energy. More recently, Saito and co-workers prepared a triphosphasumanene trisulfide **13** derivative with a large dipole moment (12.0 D) [67]. The bowl depth of *syn*-isomer **13** is 0.46 Å, which is identical to triselenasumanene **18** (0.47 Å) [64] and shallower than sumanene [24], whereas the *anti*-isomer of triphosphasumanene trisulfide **13** exists in an almost plane structure [67].

6. Asymmetric Synthesis of Buckybowl and Azabuckybowl

Synthesis of buckybowls was a highly challenging task for chemists. The first synthesis of the pristine corannulene was accomplished in 1966 by applying a long synthetic route [68]. The synthetic investigation was postponed until Scott et al. [69] and Siegel et al. [70] reinitiated the synthesis of corannulene with a succinct synthetic route by using the flash vacuum pyrolysis (FVP) method in the early 1990s. In the FVP method, the planar π -conjugated precursors are directly converted into buckybowls under high temperature to yield a racemic mixture [71]. Many buckybowls were thus synthesized using this FVP method, whereas FVP method was unsuccessful for the synthesis of **2** [72]. In 1996, Siegel and co-workers

developed the first solution phase synthesis of **1** [73]. Adopting this simple and short solution phase strategy, another pristine bucky bowl **2** was obtained by Sakurai and co-workers [74].

In 2008, Sakurai and co-workers reported the first asymmetric synthesis of trimethylsumanene **4** using stepwise conversion strategy under milder reaction conditions [17]. The synthetic strategy is described in Scheme 1.



Scheme 1. Strategy for the asymmetric synthesis of chiral (C)-trimethylsumanene **4**.

In this strategy, chiral norbornene possessing stereogenic carbon center was used as the precursor, which was converted into planar nonconjugated bowl by Pd catalyzed *syn*-selective cyclotrimerization [75,76], and the *sp*³ chirality was thus transmitted to the bowl chirality of **4**. The key concern of this strategy is the rate of racemization, which is directly correlated to the inversion barrier of buckybowl. Many buckybowl have a low bowl-to-bowl inversion barrier at room temperature and are unable to separate their enantiomers. For example, most corannulene derivatives are not able to enantiomerically isolate because of their bowl inversion energy of ca. 11.5 kcal/mol (bowl-to-bowl-inversion is >20,000 times per second at room temperature) [14]. In contrast, the bowl inversion energy of **2** and **4** is around 20.3 kcal/mol (one time per 143 s) [15,19] and 21.6 kcal/mol [19], respectively. Since the half-life of the bowl inversion of **4** are 2 h at 0 °C and 23 min at 20 °C [17], the isolation of an enantiomer would be possible if the last aromatization step is carried out at a low temperature.

Thus, the aromatization step, converting the nonconjugated bowl into a conjugated bowl, was carried out using excess DDQ in a very short reaction time (1 min) at 0 °C, and the resulting (C)-**4** quickly purified at <−20 °C. The isolated (C)-**4** was stored at −80 °C. The chirality of (C)-**4** was analyzed by the circular dichroism (CD) spectra at −40 °C, which show two positive Cotton effect curves at 247 nm and 284 nm, respectively (Figure 10a). In contrast, the intensity of CD signals gradually decreased at 10 °C (Figure 10b), indicating the racemization of (C)-**4** through bowl inversion. The experimentally observed bowl inversion energy is 21.6 kcal/mol, which is close to the calculated value (21 kcal/mol). The chiral (C)-**4** was converted into (C)-**7** (Scheme 2) using (*S*)-MTPA as a derivatization reagent [17]. The bowl inversion energy barrier of (C)-**7** is further increased and the *de* values can be determined using NMR or HPLC analysis.

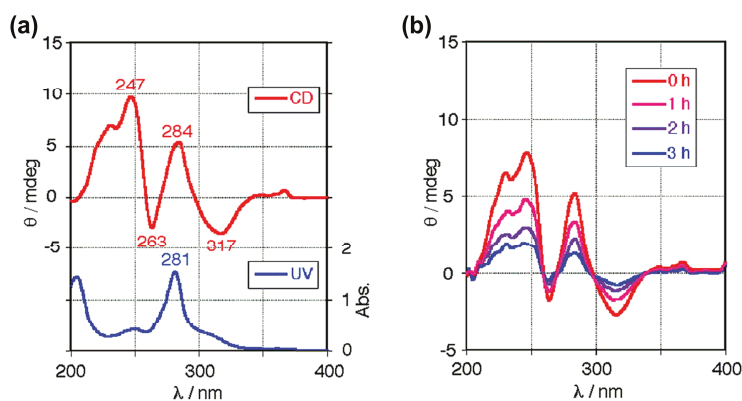
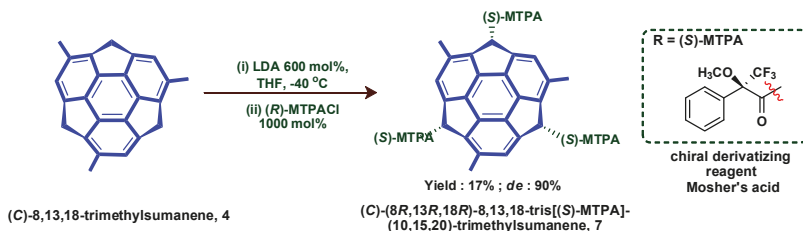


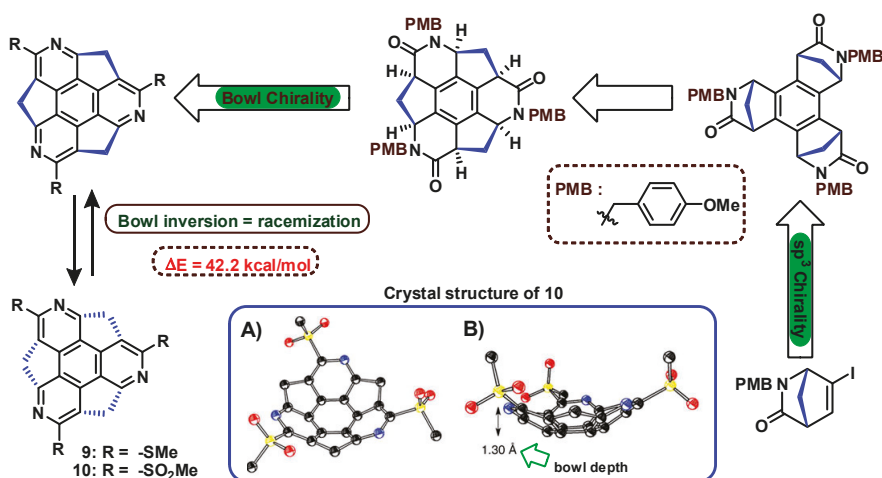
Figure 10. (a) CD spectra of (C)-4 in CH₃CN at $-40\text{ }^{\circ}\text{C}$ (red line) and UV spectra of (C)-4 in CH₃CN at room temperature (blue line); (b) Decay of CD spectra of (C)-4 in CH₃CN at $10\text{ }^{\circ}\text{C}$ for 3 h. Reprinted from [17]. © 2008 American Chemical Society.



Scheme 2. Derivatization of (C)-4 using chiral derivatizing reagent for the determination of *ee*.

It has been proven that the bowl inversion energy of buckybowls increased with bowl depth [14]. Theoretical studies suggested that doping of nitrogen will lead to deeper and curved bowl depth compared to the all-carbon counterparts [77]. Sakurai and co-workers reported the first chiral nitrogen-doped buckybowl (Scheme 3) [12]. Pure chiral (C)-(–)- and (A)-(+)-tris(methylthio)triazasumanene **9** was synthesized from corresponding enantiopure nonconjugated simple precursors, which was further converted into corresponding chiral sulfone derivative **10** by oxidation using *meta*-chloroperoxybenzoic acid (*m*-CPBA). From the single crystal analysis, the bowl depth of compound **10** is 1.30 Å, which is deeper than that of **2** (1.11 Å), indicating a higher bowl inversion barrier than the pristine **2**. The bowl inversion energy of triazasumanene is calculated to be 39.9 kcal/mol by DFT method at the B3LYP/6-311 + G(d,p) level. In contrast, the calculated values for **2** and **4** are 18.3 and 19.2 kcal/mol, respectively. This means that chiral triazasumanene **10** takes 1.1 billion years to racemize at $20\text{ }^{\circ}\text{C}$.

Both chiral derivatives of **9** and **10** exhibit the opposite Cotton effect curves (Figure 11), which are a mirror image of the corresponding enantiomers. The CD spectra of **9** and **10** demonstrated the existence of bowl chirality and remained intensive even after a week, indicative of a chiral memory effect. To measure the rate constant and bowl inversion energy of **9**, a racemization experiment was carried out at 488 K and analyzed by chiral HPLC. The racemization rate and energy of **9** were determined to be $1.24 \times 10^{-6}\text{ s}^{-1}$ (488 K) and 42.2 kcal/mol, respectively [12].



Scheme 3. Strategy for the asymmetric synthesis of chiral triazasumanene **9** and **10**; Insert: X-ray crystal ORTEP drawing structure of **10**; all hydrogen atoms omitted for clarity: (A) top view (with thermal ellipsoids set at 50% probability); (B) side view with bowl depth. Reprinted from [12]. © 2012 Nature Publishing Group.

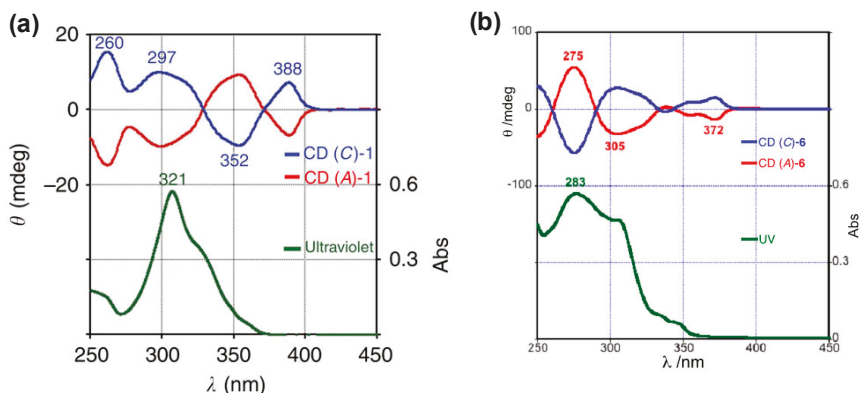


Figure 11. CD and ultraviolet/visible spectra of (a) compound **9** in CH₂Cl₂ solution (1.2 × 10⁻⁵ M). The blue line and red line are CD spectra of (C)-(-)-**9** and (A)-(+)-**9**, respectively; (b) Compound **10** in CH₂Cl₂ (5.0 × 10⁻⁵ M). The green line is an ultraviolet/visible spectrum. Reprinted from [12]. © 2012 Nature Publishing Group.

The above-discussed solution phase enantioselective synthesis of trimethylsumanene **4** and triazasumanene **9** and **10** represents a useful and versatile strategy for the construction of other homochiral curved π -electron systems from non-conjugated precursors. The chiral transmission from sp³ stereogenic chirality to bowl chirality creates a new dimension for chiral-controlled 3D carbon materials like fullerene and CNTs.

7. Chiral Resolution of Buckybowls

The optical resolution of racemic chiral buckybowls has also been accomplished using derivatization method [13,71,78–81]. Derivatization at the outer rim of the buckybowl results in

a deeper bowl with high bowl inversion energy and makes it resolvable from its racemates using chiral HPLC [12,17,18]. The purity of enantio-enriched chiral buckybowl and its bowl chirality is mainly analyzed using CD spectroscopy, NMR, and chiral HPLC methods [82–87].

As shown above, **2** has less bowl inversion energy than **4**, and it undergoes much slower racemization at 0 °C ($t_{1/2} = 2$ h) [17]. Based on this, Sakurai et al. reported the first asymmetric synthesis of chiral **4** [17], and the enantiomeric excess (*ee*) of **4** is determined by measuring the $^1\text{H-NMR}$ spectrum of **7**, which was derivatized from **4** using Mosher's acid chloride (Scheme 2) [17,18]. Upon introducing stereogenic centers at the sp^3 carbons at the benzylic positions, it became more stable and could be stored for a long time. The enantioselectivity of **6** was determined to be 89% *ee*, which matches the $^1\text{H-NMR}$ analysis of chiral derivatized compound **4** (90% *ee*). The chiral (*A*)-**6** buckybowl was eluted first with a retention time (t_R) of 38 min and another chiral buckybowl (*C*)-**6** was eluted later with a retention time of 42 min (Figure 12a). The separated enantiomers of buckybowl **6** were analyzed using CD spectroscopy, which showed the mirror image Cotton effect curves generated from its inherent bowl chirality (Figure 12b).

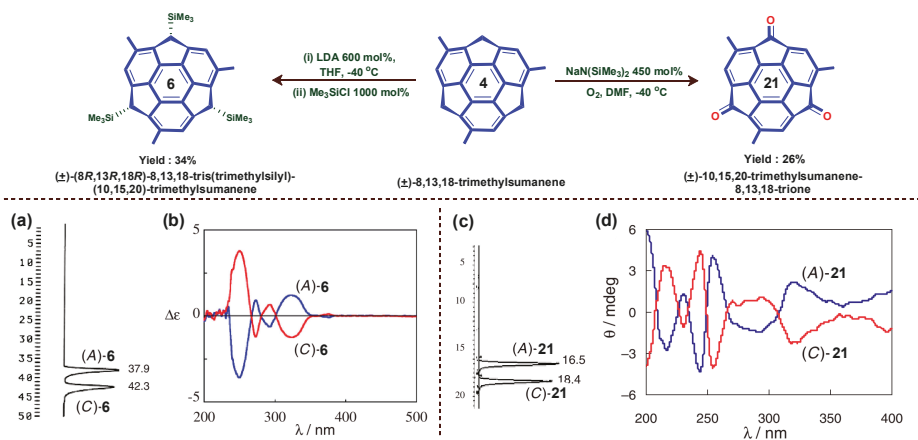


Figure 12. Synthesis of racemic (\pm)-**6** and (\pm)-**21** derivatives from racemic (\pm)-**4**. (a) Optical resolution of (\pm)-**6** by chiral HPLC (DAICEL CHIRALPAK IA, 2-propanol, retention time (t_R); 38 min for (*A*)-**6**, 42 min for (*C*)-**6**); (b) CD spectra of each enantiomers **6** in CHCl_3 ; (c) Optical resolution of (\pm)-**21** by chiral HPLC (DAICEL CHIRALPAK IA, hexane/2-propanol = 60/40, 9 °C, retention time (t_R); 17 min for (*A*)-**21**, 18 min for (*C*)-**21**); (d) CD spectra of enantioenriched **21** in CH_3CN at 27 °C. Blue line: CD spectra of (*A*)-**6** and (*A*)-**21**, respectively. Red line: CD spectra of (*C*)-**6** and (*C*)-**21**, respectively. Reprinted from [18]. © 2010 The Chemical Society of Japan.

Racemic (\pm)-**21** was prepared by aerobic oxidation of racemic (\pm)-**4** (Figure 12) [18]. The estimated bowl inversion energy of **21** was 23.5 kcal/mol, which corresponds to ca. 44 h half-life at 10 °C. Racemic (\pm)-**21** was optically resolved using a chiral HPLC (Figure 12c). The absolute configuration of each enantiomer was assigned based on the CD spectrum of the enantioenriched (*C*)-**21** prepared from (*C*)-**4**. The bowl chirality of the optically resolved enantioenriched buckybowl (*A*)- and (*C*)-**21** was analyzed using CD spectroscopy, which is shown in Figure 12d. In addition, the bowl inversion barrier of enantio-riched **21** was estimated to be 23.4 and 23.3 kcal/mol in CH_3CN and CH_2Cl_2 , respectively, by measuring the time-dependent decay of the intensity of CD spectra at 255 nm at 30 °C [18]. These results led to the elucidation of the substituent effect and the correlation between bowl structure and bowl inversion energy [19].

Azasumanene **10** had a deeper bowl depth (1.30 Å) than **2** (1.10 Å) and showed extremely stable bowl chirality ($t_{1/2} = 54$ billion years at 20 °C) because of its high bowl inversion energy

($\Delta E = 42.2$ kcal/mol) [12]. Similarly, C_3 symmetric chiral **8** was prepared by a Pd-catalyzed cross-coupling reaction between chiral **9** and (*p*-trifluoromethyl)phenyl boronic acid (Figure 13) [88]. The chirality of the obtained **8** was confirmed by chiral HPLC at 25 °C using a Daicel Chiralpak® IA column (Figure 13a,b). The CD and UV spectra were measured in a CH_2Cl_2 solution of enantioenriched **8** derivatives (Figure 13c), which shows the CD signals of the mirror image, indicating that the compounds are of opposite bowl chirality.

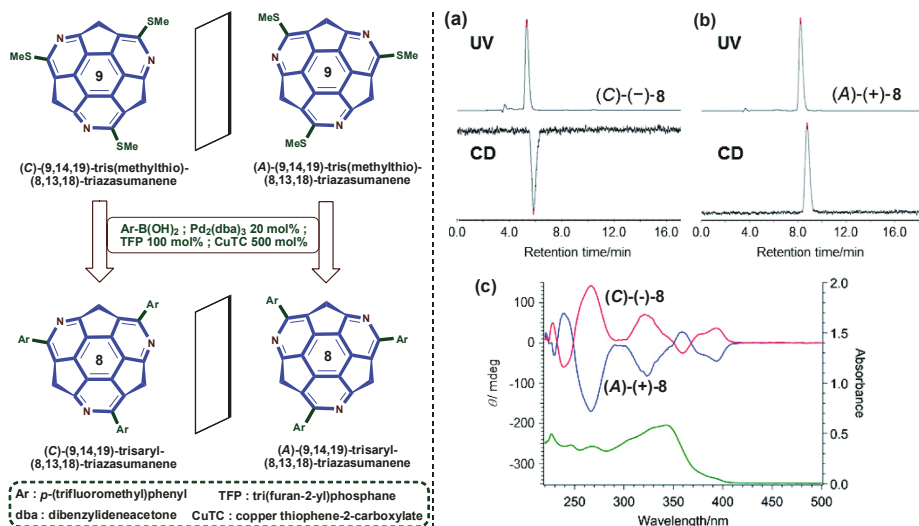


Figure 13. Strategy for the asymmetric synthesis of chiral **8** from chiral **9**: (a) HPLC chart of (C)-(-)-**8**; $t_R = 5.31$ min (UV) and 5.84 min (CD); (b) HPLC chart of (A)-(+)-**8**; $t_R = 8.21$ min (UV) and 8.76 min (CD). HPLC analysis was performed at 25 °C on a Daicel Chiralpak® IA column with hexane/ $\text{CH}_2\text{Cl}_2 = 50/50$. Flow rate: 1 mL/min, detector wavelength: UV, 254 nm; CD, 270 nm; (c) CD and UV spectra of compound **8** in CH_2Cl_2 solution (1.5×10^{-5} M). Blue and red lines: CD spectra of (A)-(+)-**8** and (C)-(-)-**8**, respectively. Green line: UV spectrum of **8**. Reprinted from [88]. © 2017 The Chemical Society of Japan.

Recently, Yang and co-workers prepared azonia[6]helicene tethered with supramolecular host β -cyclodextrin, and used a chirality sensing probe for underivatized amino acids in water [89–94]. Indeed, tethered azonia[6]helicene acts as a conformationally robust chiral auxiliary to improve the chiral recognition ability of native cyclodextrins. Scott and co-workers successfully synthesized the first corannulene-[*n*]helicenes hybrids **22–25** by combining two classical nonplanar conjugated systems: the chiral bowl-shaped π -system, corannulene, and the helically chiral helicene (Figure 14). These compounds show unique molecular dynamics in their enantiomerization processes, including inversion motions of both the bowl and the helix [95].

Helix inversion renders *P* and *M* isomers, while corannulene bowl inversion results in concave and convex isomers, so it is predicted to have four isomers (convex-*P*, concave-*P*, convex-*M*, and concave-*M*) in equilibrium. Among the different conformers of corannulene-[*n*]helicenes, the conformer with a terminal helicene ring facing the convex surface of the bowl is more stable than the terminal ring facing the concave bowl surface, as the two forms display different degrees of steric congestion. For **22** and **23**, the energy barriers for bowl-to-bowl inversions were calculated to be 10.6 kcal/mol and 10.1 kcal/mol, respectively, and the helix inversions were 20.9 kcal/mol and 34.6 kcal/mol, respectively.

The enantiomers of corannulene-[*n*]helicenes hybrid were successfully resolved using a chiral-stationary-phase HPLC. The kinetics of thermal racemization of obtained conformers with

the *ee* of >99% was studied under different temperature, and the helix inversion barrier value of $\Delta G^\ddagger = 33.5$ kcal/mol obtained experimentally is in consensus with the calculated one (34.6 kcal/mol) (Figure 14b). This hybrid system indicates that the chirality mainly arises from the rigid [6]helicene unit, and the non-rigid corannulene unit undergoes a rapid bowl-to-bowl inversion under ambient conditions.

The authors also synthesized **24** and **25** to study the different magnetic shielding effects of the convex and concave faces. The results show that the ring-current effect from the concave face of corannulene led to $^1\text{H-NMR}$ signal upfield shifts of 2 ppm to 5 ppm. However, the *t*-Bu group of **24** is shifted upfield by only 0.65 ppm compared to the *t*-Bu group in **25**, which is away from the convex face. This comparison demonstrates that the magnetic shielding of the concave face is much greater than that of the convex face. Similarly, various stereodynamic (non-rigid/fluctuating) systems **26–29** based on a corannulene bowl that possesses more than one stereogenic unit were synthesized and their selected diastereomeric conformers were studied via bowl-to-bowl inversion (Figure 14c) [57,96–98].

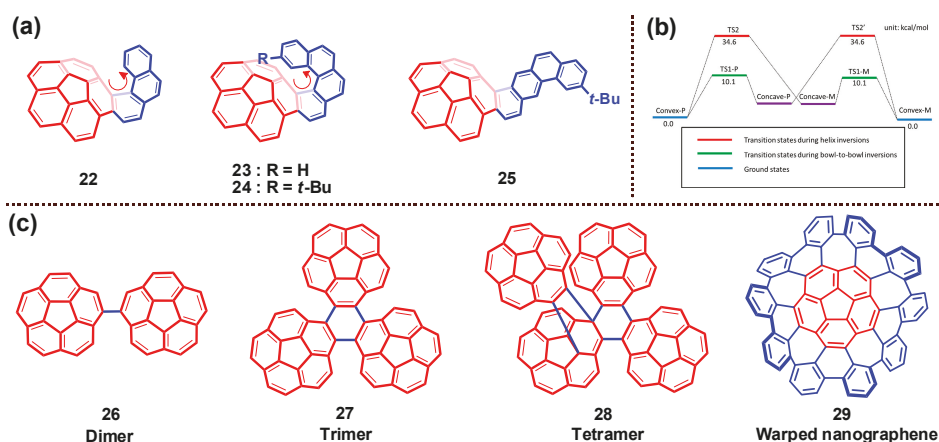


Figure 14. (a) Chemical structure of different chiral corannulene-[*n*]helicenes **22–25**; (b) Theoretical study of interconversion pathways of **23**. Relative Gibbs free energies (ΔG) were calculated at the B3LYP/6-31G(d) level at 298.15 K; (c) Structures of multiple corannulene derivatives **26–29**. (b) is reprinted from [95]. © 2016 American Chemical Society.

The enantiopure or enriched chiral buckybowls could be obtained by asymmetric synthesis or optical resolution of racemates using chiral HPLC. The enantiopure buckybowls with inherent chirality are expected to be applicable not only for asymmetric molecular recognition, novel chiral organic materials creation [15,24,39,99], and chiral ligands for transition metals, but also for precursors of chiral fullerenes and CNTs in chemical synthesis. Methods and approaches that control the bowl chirality can potentially be applied to the related chiral fullerenes and CNTs as well.

8. Chiral Metal Complexes of Buckybowls

In general, metals binding to π -conjugated compounds can be represented by the symbol η^n (*n* is the number of coordinating atoms). Fullerene and CNT and their derivatives form a coordination complex with various metal ion through their π -surfaces to form *exo*- as well as *endo*-hedral complexes, which have been used as a potential material in various fields such as molecular electronics and magnetic resonance imaging studies [100–102]. Interestingly, π -curved conjugated fragment **1** (bowl depth = 0.87 Å) preferentially coordinates with various metal ions in the convex surface in the η^1 , η^2 , and η^6 modes [23,31,32,39,103–106]. Some corannulene derivatives form concave as well as convex face η^6 -coordination complexes with ruthenium(II) [31,39,104]. Similarly, another C_{3v} symmetric,

curved π -conjugated bowl, **2**, forms coordination complexes through the η^1 , η^2 , η^4 , η^5 , and η^6 modes with limited transition metal ions [107].

In 2007, Hirao and co-workers reported the first selective concave-binding of CpFe^+ ($\text{Cp} = \text{C}_5\text{H}_5$) to **2** (Figure 15) [33]. The metalation of **2** was carried out in solvent-free conditions using ferrocene at 120 °C. Under the ligand exchange method with excesses of CpFe^+ , the monometalated concave complex **30** was selectively afforded with a η^6 coordination (Figure 15a). In order to study the substituent effect, a methyl group was introduced into the cyclopentadiene ring, resulting in the concave selective complex **31** (Figure 15b). The bowl depth of **2** was not affected upon selective concave complexation of CpFe^+ (1.07–1.13 Å), whereas in MeCpFe^+ complexation the coordinatized side is flattened to 0.98 Å and the noncoordinated side was not affected (1.13 Å) (Figure 15a,b). Introduction of a chiral substituent *sec*-Bu to the Cp ring causes the target compound **32** as chiral (Figure 15c). The peaks of H_a split in $^1\text{H-NMR}$ due to the presence of a chiral *sec*-butyl group. Meanwhile, the concave-selective complexation was confirmed by the split of $\text{H}_{b\text{endo}}$. Furthermore, the chirality of complex **32** was proved by CD spectral analysis, which shows positive CD peaks at 272, 303, and 517 nm, respectively [34].

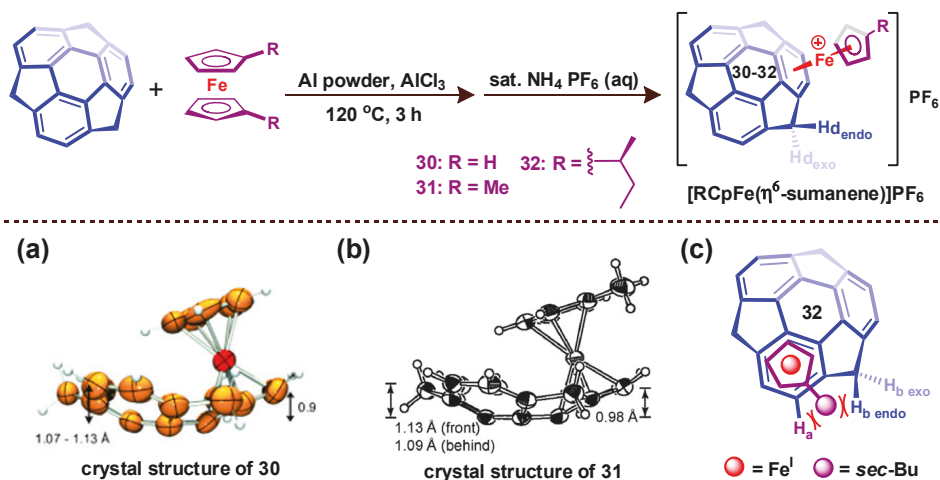


Figure 15. Synthetic strategy for the concave selective coordination complex formation of $[\text{RCpFe}(\text{sumanene})]\text{PF}_6$. (a) Crystal structure of the cation of **30** with thermal ellipsoids set at 50% probability; side view with bowl depth; (b) Crystal structure of the cation of **31** with thermal ellipsoids set at 40% probability (the PF_6 ion and acetone are omitted for clarity), side view with bowl depth; (c) Schematic illustration of chiral concave-face selective coordination of sumanene. (a) is reprinted from [33], © 2007 Wiley-VCH Verlag GmbH & Co. KGaA, Weinheim; (b) is reprinted from [34], © 2009 Wiley-VCH Verlag GmbH & Co. KGaA, Weinheim.

Four years later, the first chiral selective convex-face complex based on pentasubstituted C_5 -symmetric bowl corannulene was reported by Siegel and co-workers [36]. Four kinds of compounds were synthesized to investigate the effect of different substituents in bicyclo[2.2.1]hepta-2,5-diene (nbd) and corannulene derivatives ($\text{R} = \text{H}, \text{Me}$ and *t*-Bu). The crystal structure of **34** is given in Figure 16a. From the stereochemical analysis, **35** and **36** were predicted to have diastereomers **35a/35b** pair and **36a/36b** pair, respectively, arising from the rotation of chiral nbd ligand (Figure 16b). The complex is more likely to yield a static form with the steric repulsion between nbd ligand and corannulene. The calculated energy gaps between **35a/35b** pair and **36a/36b** pair are 1.88 kcal/mol and 3.54 kcal/mol, respectively. However, **35a/35b** was observed with a ratio of 2.5:1, while only **36a** was detected in the latter pair. These phenomena confirmed the hypothesis that the complex tends to exist in the static form with the steric hindrance.

The Cotton effects of **33** and **36** were observed in the CD spectra and confirmed the steric repulsion hypothesis. The distinct bathochromic shift of **33** and **36** compared to the free chiral nbd ligand was ascribed to the electron transfer from nbd ligand to the corannulene. This kind of curved π -bowl chiral complexation has the potential to function as a catalyst in asymmetrical organometallic chemistry and promote the understanding of selective π -bowl coordination.

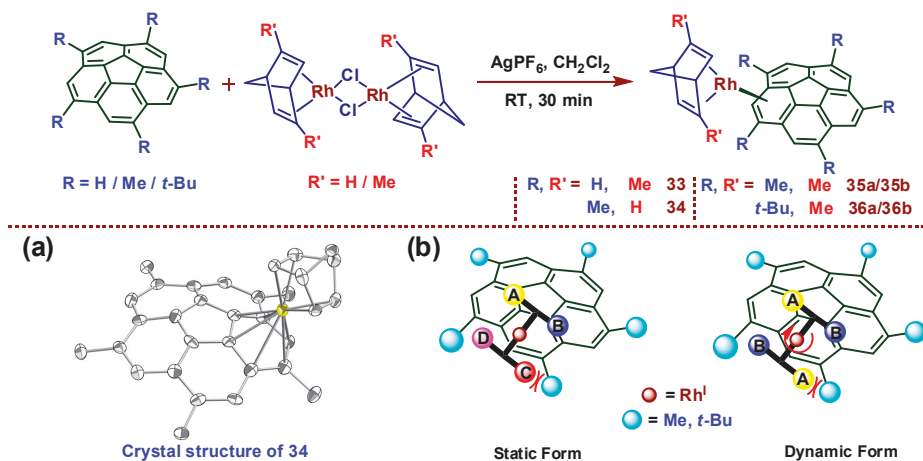


Figure 16. Synthesis route of selective C_5 -symmetric corannulene-based convex-face complexes **33–36**: (a) X-ray crystal structure of **34**; (b) schematic illustration of diastereomers due to steric repulsion from rotation of the fragment. (a) is reprinted from [36], © 2011 Wiley-VCH Verlag GmbH & Co. KGaA, Weinheim.

9. Chiral Assembly of Buckybowls

Generally, various cyclic systems have inherent chirality because of their conformational stability and rigidity, which make them useful as chiroptical sensing probes [108–110]. Their preorganized binding sites can recognize optically active molecular species selectively via noncovalent interactions and gave a conformationally stable chiral organic structures. Furthermore, essential molecular chiral components amplify to form 3D supramolecularly assembled architectures and oriented nanoscale assemblies [111,112]. The nanoscale chirality of these 3D chiral supramolecular assemblies has potential application in functional soft materials.

Curved π -conjugated buckybowl corannulenes mainly form noncolumnar structures through a $CH-\pi$ interaction rather than a $\pi-\pi$ stacking interaction [28–30]. C_5 -Symmetric corannulene undergoes rapid bowl-to-bowl inversion/racemization at ambient or even low temperatures, and is unable to resolve into their enantiomers. Aida and co-workers reported a C_5 -symmetric decasubstituted liquid crystalline (LC) corannulene derivative tethered with thioalkyl-amide-tribranched paraffinic side chains that forms self-assembled hexagonal columnar LC structures [3]. The nonpolar corannulene derivative can align homeotropically to the electrode surface with an applied electric field, and the alignment of corannulene was memorized for a long time. Hydrogen bond formation among the amide groups plays a key role in the formation of LC.

In order to resolve their enantiomers, the substituents were appended at the outer rim of corannulene viz. thioalkyl chains and amide groups (Figure 17A) [21]. C_5 -symmetric corannulene-based chiral initiators and monomers carrying amide-appended thioalkyl side chains were synthesized from 1,3,5,7,9-pentachlorocorannulene according to methods analogous to those reported by Scott and co-workers [113]. The amide derivatives form a unimolecular closed cage

through “intramolecular” H-bonding interactions, which represents the first unimolecular host that is responsive to the chiral hydrocarbon solvent and obeys the majority rule in a chiral environment.

Non-amide derivative **37** does not show chiroptical activity even in chiral limonene, and no CD signal could be seen for **38_R** despite a chiral center in the side chain, whereas amide derivative **40M** showed chiroptical activity in the presence of chiral limonene. Compounds **41M_R** and **41M_S**, in which amide linkers at the periphery of corannulene are attached to a chiral side chain, show chiroptical activity even in the achiral solvents. The computational simulation studies suggested that the formed stereoisomeric unimolecular closed cages exist in four equilibrated structures (Figure 17B). These amide derivatives form four kinds of “intramolecular” closed cages, and its cyclic amide H-bonded networks take clockwise and anticlockwise geometries. The corannulene bowl chirality axis and the direction of the intramolecular H-bonding (C=O···H-N) network rotate in the same clockwise or anticlockwise directions (denoted as AA and CC); **39_{AA}** and **39_{CC}** structures are more stable and energetically favored than different directions (denoted as AC and CA; **39_{AC}** and **39_{CA}**).

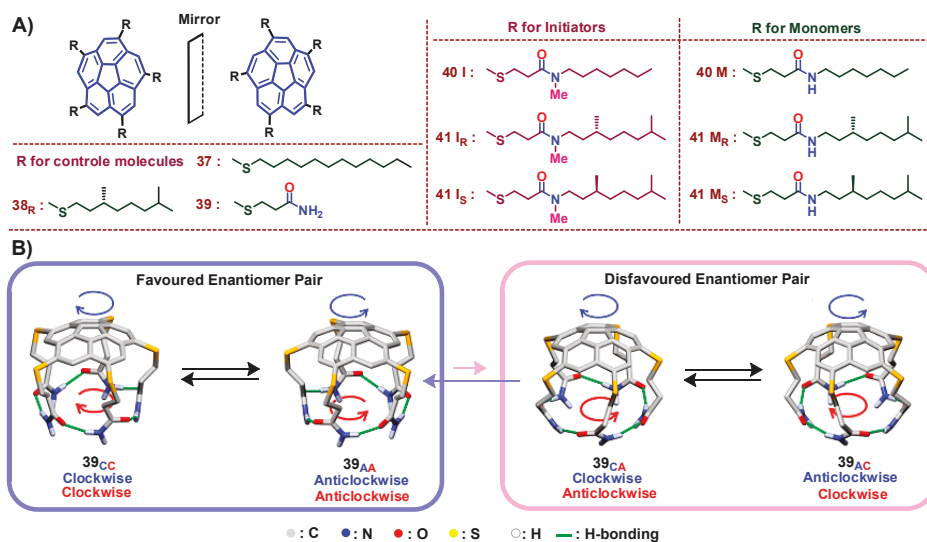


Figure 17. (A) Chemical structures of C₅-symmetric corannulene derivatives **37–41** bearing chiral or achiral side chains; (B) Schematic representations of the bowl inversion equilibrium using simplified molecular model **39** for C₅-symmetric corannulenes carrying thioalkyl side chains featuring intramolecularly H-bonded amide units. Blue- and red-colored arc-shaped arrows represent the directions of H→SR and H-bonded N-H→O=C arrays, respectively, along the corannulene periphery. Subscripts C and A for **39** denote the clockwise and anticlockwise directions (tentatively defined), respectively. Four possible stereoisomers were energy minimized at the SCS-MP2/def2-TZVPP//DFT-D3-TPSS/defTZVP level. (B) is reprinted from [21]. © 2014 American Chemical Society.

The compound **40M** exhibited opposite Cotton effect curves in chiral solvents (*S*)-limonene and (*R*)-limonene, respectively. Likewise, chiral **41M_R**/**41M_S** showed chiroptical activity even in an achiral solvent such as methylcyclohexane, displaying mutually mirror-imaged CD spectra (Figure 18a). However, upon addition of a protonic solvent like ethanol, which is known to deteriorate the H-bonding, the **41M_R**/**41M_S** became CD-silent due to the breaking of the intramolecular H-bonding network. In methylcyclohexane, the CD spectral change of **40M** was monitored in a wide temperature range from -40 to 40 °C. When the temperature is lowered to -40 °C, the %*de* of **40M** is increased to 45%. At 20 °C, %*de* of **41M_R** is enhanced to 80% when (*R*)-limonene was used as the solvent, whereas

41M_R becomes CD-silent when (*S*)-limonene is used as the solvent (Figure 18b). A similar trend is followed by **41M_S** (Figure 18b), which indicates that the chiral side-chain of **40M** could cooperate with the chiral solvent, either positively or negatively, in desymmetrizing the bowl inversion equilibrium of the corannulene core. A sigmoidal signal was observed in the CD spectra which demonstrated that the majority rule works in the unimolecular system [21].

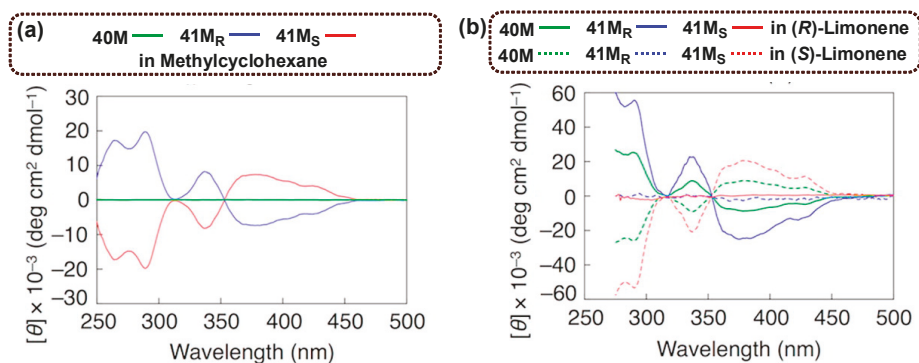


Figure 18. Circular dichroism (CD) spectra at 20 °C of **40M** (green), **41M_R** (blue), and **41M_S** (red) (20 μM) in (a) methylcyclohexane and (b) (*R*)- (solid curves) and (*S*)-limonene (dashed curves). Reprinted from [21]. © 2014 American Chemical Society.

Inspired by the metastable property of corannulene derivative **40M**, Aida and co-workers came up with an ingenious strategy to achieve the first example of chiral chain-growth supramolecular polymerization [8]. To break the intramolecular H-bonding network of **40M**, they replaced the H atom connected in N with a methyl group and used **40I** as an initiator of supramolecular polymerization. The carbonyl group of the initiator can function as an H-bonding acceptor, thus attacking the monomer via H-bonding. Subsequently, the self-opening monomer can act as an initiator using its own free C=O, resulting in an oligomer **I-[M]₂** with the free C=O end capped as well (Figure 19). As the oligomer elongates, the first chain-growth supramolecular polymerization is realized. Surprisingly, the chiral chain-growth polymerization can also be achieved via chiral initiator **41I_R**/**41I_S**. When chiral initiator **41I_S** was added with racemic monomers **41M_R** and **41M_S**, chiral helical assemblies were achieved from the analysis of size-exclusion chromatography (SEC), meaning that only **41M_S** can polymerize. As a result, chiral resolution of **41M_R** and **41M_S** was also realized successfully in the same way [8].

Differing from the classical chiral assembly formation in a macroscopic organic system, chiral microscopic assemblies of buckybowl hemifullerene at the surface of inorganic crystal were achieved by Fasel and co-workers [114]. They discovered how chiral bowl-shape hemifullerenes, derivatives of sumanene (Figure 20A), restructure on the copper surface atoms into chiral structures such as chiral nanowires and chiral islands. Unlike other researchers using polar molecules with carbonyl groups as chiral surface modifiers [115,116], Fasel et al. [114] turned their attention to metal-aromatic coordination bonds and found hemifullerenes suitable to induce chirality on a copper surface. Surprisingly, *M* enantiomers of hemifullerenes align along the [334] direction, creating R kinks, while *P* counterparts align along the $[\bar{3}\bar{3}\bar{4}]$ direction, forming S kinks, which differs from the previously reported arrangement of C₆₀/corannulene along the Cu[110] direction [2]. This phenomenon is observed via scanning tunneling microscopy (STM) at 50 K and X-ray photoelectron diffraction (XPD) at room temperature. The optimized adsorption configuration was simulated by DFT, revealing that the creation of chiral kink creation can be explained by a three-point contact model, which is three η¹-coordinated Cu–C bonds at this point.

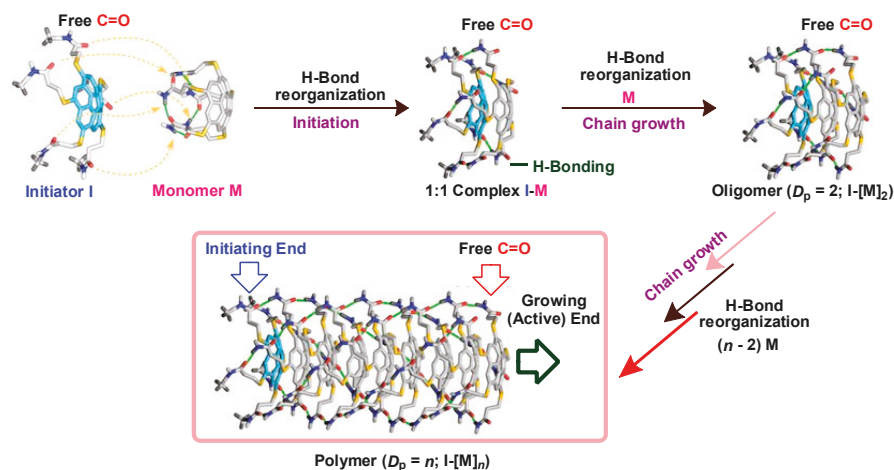


Figure 19. Schematic representations of the chiral chain-growth supramolecular polymerization of chiral pentasubstituted corannulene derivative. Reprinted from [8]. © 2015 Science American Association for the Advancement of Science (AAAS).

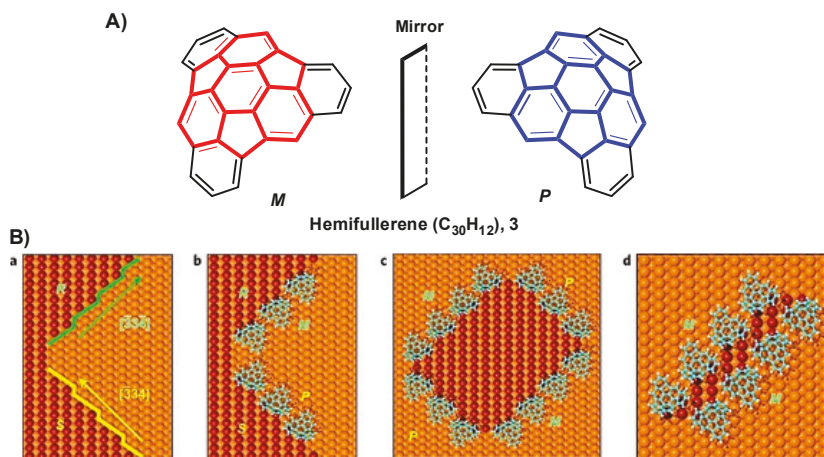


Figure 20. (A) Chemical structure of hemifullerene 3 enantiomers; (B) a. Structural model of the observed step edge with alternating $[\bar{3}\bar{3}4]$ and $[334]$ segments and the formation of chiral kink sites; b. structural model of R kinks decorated by M enantiomers and S kinks decorated by P enantiomers; c. structural model of a chiral island stabilized by hemifullerene enantiomers; d. structural model of a chiral Cu nanowire stabilized by M-hemifullerene along the $[\bar{3}\bar{3}4]$ direction. Reprinted from [114]. © 2010 Nature Publishing Group.

Furthermore, the chiral island and nanowire (Figure 20B) were found to form with different alignments of hemifullerenes. The results indicate the emergence of a chiral shape on Cu surface is of great importance to help investigate the elementary mechanism of chiral recognition or induction occurring on an achiral crystal surface. Unfortunately, efforts to separate the enantiomers adsorbed on the Cu surface were not successful [114].

Tethering the various alkyl chains with different length, number, substitution position, and nature of chiral carbons to the outer rim π -conjugated buckybowls is an effective way to tune the

chiral assembly formation, the function of the system and their soft materialization. Extension of π -conjugation through the outer rim of the corannulene provided a single chiral CNT [114].

10. Conclusions and Outlook

In conclusion, this review summarizes the recent progress of studies on the bowl chirality, focusing on the two kinds of buckybowl compounds, corannulenes and sumanenes. These buckybowls possess curved aromatic rings, and introducing substituents on their aromatic periphery results in the loss of planar symmetry to generate a unique kind of chirality, so-called bowl chirality. The curved aromatic surface is possibly flipped, and such a bowl-to-bowl inversion causes switching of the bowl chirality. The size and shape of the substituents, a doped heteroatom in the aromatic bowl, and introducing a metal complex on the surface of buckybowls will significantly influence the bowl-to-bowl inversion energy as well as the racemization rate. Enantio-/diastereo- pure/enriched chiral buckybowls could be obtained by chiral resolution or chiral synthesis. The introduction of a chiral chain to the rim of the buckybowl dominated the asymmetric synthesis of chiral buckybowls. Sumanene **2** usually has higher bowl-to-bowl inversion energy than corannulene **1**, and asymmetric synthesis of chiral trimethylsumanene **4** and triazasumanene **9** and **10** has been realized using chiral non-conjugated precursors. The selective chiral assemblies of buckybowls with unique chemical and electronic properties may contribute to the development of the field of electronic devices and energy storage. In addition, the synthesis of homochiral CNTs continuously attracts scientists and chiral buckybowls may open up new opportunities in this area. The chiral assemblies of buckybowls are attractive, in relation to topics such as chiral amplification, chiral induction, and chiral memory. There is no doubt that the study of chiral buckybowls is still immature yet highly promising; further investigation will provide more insight into this particular area and lead to applications in various fields such as materials, electronics, and photonics.

Acknowledgments: We acknowledge the National Natural Science Foundation of China (Nos. 21572142, 21402129, 21372165, 31370735, and 21321061), the National Key Research and Development Program of China (grant No. 2017YFA0505900), and the State Key Laboratory of Fine Chemicals (KF 1508) and Sichuan Province Science Foundation for Youths (No. 2015JQ0029) for financial support.

Author Contributions: Kuppusamy Kanagaraj, Kangjie Lin, Wanhua Wu, Guowei Gao, Zhihui Zhong, Dan Su and Cheng Yang collected and analyzed the references and data and wrote the paper.

Conflicts of Interest: The authors declare no conflict of interest.

References

- Shi, K.; Lei, T.; Wang, X.-Y.; Wang, J.-Y.; Pei, J. A bowl-shaped molecule for organic field-effect transistors: Crystal engineering and charge transport switching by oxygen doping. *Chem. Sci.* **2014**, *5*, 1041–1045. [[CrossRef](#)]
- Xiao, W.; Passerone, D.; Ruffieux, P.; Ait-Mansour, K.; Gröning, O.; Tosatti, E.; Siegel, J.S.; Fasel, R. C60/corannulene on Cu(110): A surface-supported bistable buckybowl-buckyball host-guest system. *J. Am. Chem. Soc.* **2008**, *130*, 4767–4771. [[CrossRef](#)] [[PubMed](#)]
- Miyajima, D.; Tashiro, K.; Araoka, F.; Takezoe, H.; Kim, J.; Kato, K.; Takata, M.; Aida, T. Liquid crystalline corannulene responsive to electric field. *J. Am. Chem. Soc.* **2009**, *131*, 44–45. [[CrossRef](#)] [[PubMed](#)]
- Lovas, F.J.; McMahon, R.J.; Grabow, J.-U.; Schnell, M.; Mack, J.; Scott, L.T.; Kuczkowski, R.L. Interstellar chemistry: A strategy for detecting polycyclic aromatic hydrocarbons in space. *J. Am. Chem. Soc.* **2005**, *127*, 4345–4349. [[CrossRef](#)] [[PubMed](#)]
- Zhang, L.; Qin, L.; Wang, X.; Cao, H.; Liu, M. Supramolecular chirality in self-assembled soft materials: Regulation of chiral nanostructures and chiral functions. *Adv. Mater.* **2014**, *26*, 6959–6964. [[CrossRef](#)] [[PubMed](#)]
- Li, X.; Kang, F.; Inagaki, M. Buckybowls: Corannulene and its derivatives. *Small* **2016**, *12*, 3206–3223. [[CrossRef](#)] [[PubMed](#)]
- Amaya, T.; Hirao, T. Chemistry of sumanene. *Chem. Rec.* **2015**, *15*, 310–321. [[CrossRef](#)] [[PubMed](#)]

8. Kang, J.; Miyajima, D.; Mori, T.; Inoue, Y.; Itoh, Y.; Aida, T. A rational strategy for the realization of chain-growth supramolecular polymerization. *Science* **2015**, *347*, 646–651. [[CrossRef](#)] [[PubMed](#)]
9. Higashibayashi, S.; Sakurai, H. Synthesis of sumanene and related buckybowls. *Chem. Lett.* **2011**, *40*, 122–128. [[CrossRef](#)]
10. Scott, L.T.; Jackson, E.A.; Zhang, Q.; Steinberg, B.D.; Bancu, M.; Li, B. A short, rigid, structurally pure carbon nanotube by stepwise chemical synthesis. *J. Am. Chem. Soc.* **2012**, *134*, 107–110. [[CrossRef](#)] [[PubMed](#)]
11. Hembury, G.A.; Borovkov, V.V.; Inoue, Y. Chirality-sensing supramolecular systems. *Chem. Rev.* **2008**, *108*, 1–73. [[CrossRef](#)] [[PubMed](#)]
12. Tan, Q.; Higashibayashi, S.; Karanjit, S.; Sakurai, H. Enantioselective synthesis of a chiral nitrogen-doped buckybowl. *Nat. Commun.* **2012**, *3*, 891. [[CrossRef](#)] [[PubMed](#)]
13. Scott, L.T.; Hashemi, M.M.; Bratcher, M.S. Corannulene bowl-to-bowl inversion is rapid at room temperature. *J. Am. Chem. Soc.* **1992**, *114*, 1920–1921. [[CrossRef](#)]
14. Seiders, T.J.; Baldrige, K.K.; Grube, G.H.; Siegel, J.S. Structure/energy correlation of bowl depth and inversion barrier in corannulene derivatives: Combined experimental and quantum mechanical analysis. *J. Am. Chem. Soc.* **2001**, *123*, 517–525. [[CrossRef](#)] [[PubMed](#)]
15. Amaya, T.; Sakane, H.; Muneishi, T.; Hirao, T. Bowl-to-bowl inversion of sumanene derivatives. *Chem. Commun.* **2008**, 765–767. [[CrossRef](#)]
16. Hayama, T.; Baldrige, K.K.; Wu, Y.-T.; Linden, A.; Siegel, J.S. Steric isotope effects gauged by the bowl-inversion barrier in selectively deuterated pentaarylcorannulenes. *J. Am. Chem. Soc.* **2008**, *130*, 1583–1591. [[CrossRef](#)] [[PubMed](#)]
17. Higashibayashi, S.; Sakurai, H. Asymmetric synthesis of a chiral buckybowl, trimethylsumanene. *J. Am. Chem. Soc.* **2008**, *130*, 8592–8593. [[CrossRef](#)] [[PubMed](#)]
18. Tsuruoka, R.; Higashibayashi, S.; Ishikawa, T.; Toyota, S.; Sakurai, H. Optical resolution of chiral buckybowls by chiral HPLC. *Chem. Lett.* **2010**, *39*, 646–647. [[CrossRef](#)]
19. Higashibayashi, S.; Tsuruoka, R.; Soujanya, Y.; Purushotham, U.; Sastry, G.N.; Seki, S.; Ishikawa, T.; Toyota, S.; Sakurai, H. Trimethylsumanene: Enantioselective synthesis, substituent effect on bowl structure, inversion energy, and electron conductivity. *Bull. Chem. Soc. Jpn.* **2012**, *85*, 450–467. [[CrossRef](#)]
20. Shrestha, B.B.; Karanjit, S.; Higashibayashi, S.; Sakurai, H. Correlation between bowl-inversion energy and bowl depth in substituted sumanenes. *Pure Appl. Chem.* **2014**, *86*, 747–753. [[CrossRef](#)]
21. Kang, J.; Miyajima, D.; Itoh, Y.; Mori, T.; Tanaka, H.; Yamauchi, M.; Inoue, Y.; Harada, S.; Aida, T. C₅-symmetric chiral corannulenes: Desymmetrization of bowl inversion equilibrium via “intramolecular” hydrogen-bonding network. *J. Am. Chem. Soc.* **2014**, *136*, 10640–10644. [[CrossRef](#)] [[PubMed](#)]
22. Juriček, M.; Strutt, N.L.; Barnes, J.C.; Butterfield, A.M.; Dale, E.J.; Baldrige, K.K.; Stoddart, J.F.; Siegel, J.S. Induced-fit catalysis of corannulene bowl-to-bowl inversion. *Nat. Chem.* **2014**, *6*, 222–228. [[CrossRef](#)] [[PubMed](#)]
23. Seiders, T.J.; Baldrige, K.K.; O'Connor, J.M.; Siegel, J.S. Hexahapto metal coordination to curved polyaromatic hydrocarbon surfaces: The first transition metal corannulene complex. *J. Am. Chem. Soc.* **1997**, *119*, 4781–4782. [[CrossRef](#)]
24. Sakurai, H.; Daiko, T.; Sakane, H.; Amaya, T.; Hirao, T. Structural elucidation of sumanene and generation of its benzylic anions. *J. Am. Chem. Soc.* **2005**, *127*, 11580–11581. [[CrossRef](#)] [[PubMed](#)]
25. Shrestha, B.B.; Morita, Y.; Kojima, T.; Kawano, M.; Higashibayashi, S.; Sakurai, H. Eclipsed columnar packing in crystal structure of sumanenetrione. *Chem. Lett.* **2014**, *43*, 1294–1296. [[CrossRef](#)]
26. Sygula, A.; Yanney, M.; Henry, W.P.; Fronczek, F.R.; Zabula, A.V.; Petrukhina, M.A. Inclusion complexes and solvates of buckycatcher, a versatile molecular host with two corannulene pincers. *Cryst. Growth Des.* **2014**, *14*, 2633–2639. [[CrossRef](#)]
27. Yamada, M.; Ohkubo, K.; Shionoya, M.; Fukuzumi, S. Photoinduced electron transfer in a charge-transfer complex formed between corannulene and li+@C60 by concave–convex π – π interactions. *J. Am. Chem. Soc.* **2014**, *136*, 13240–13248. [[CrossRef](#)] [[PubMed](#)]
28. Merz, L.; Parschau, M.; Zoppi, L.; Baldrige, K.K.; Siegel, J.S.; Ernst, K.-H. Reversible phase transitions in a buckybowl monolayer. *Angew. Chem. Int. Ed.* **2009**, *48*, 1966–1969. [[CrossRef](#)] [[PubMed](#)]
29. Bauert, T.; Merz, L.; Bändera, D.; Parschau, M.; Siegel, J.S.; Ernst, K.-H. Building 2d crystals from 5-fold-symmetric molecules. *J. Am. Chem. Soc.* **2009**, *131*, 3460–3461. [[CrossRef](#)] [[PubMed](#)]

30. Liu, Y.-M.; Xia, D.; Li, B.-W.; Zhang, Q.-Y.; Sakurai, T.; Tan, Y.-Z.; Seki, S.; Xie, S.-Y.; Zheng, L.-S. Functional sulfur-doped buckybowls and their concave–convex supramolecular assembly with fullerenes. *Angew. Chem. Int. Ed.* **2016**, *55*, 13047–13051. [[CrossRef](#)] [[PubMed](#)]
31. Vecchi, P.A.; Alvarez, C.M.; Ellern, A.; Angelici, R.J.; Sygula, A.; Sygula, R.; Rabideau, P.W. Synthesis and structure of a dimetallated buckybowl: Coordination of one {cp*ru}⁺ unit to each side of corannulene. *Angew. Chem. Int. Ed.* **2004**, *43*, 4497–4500. [[CrossRef](#)] [[PubMed](#)]
32. Petrukhina, M.A.; Andreini, K.W.; Peng, L.; Scott, L.T. Hemibuckminsterfullerene C₃₀H₁₂: X-ray crystal structures of the parent hydrocarbon and of the two-dimensional organometallic network ([Rh₂(O₂CCF₃)₄]₃(C₃₀H₁₂)). *Angew. Chem. Int. Ed.* **2004**, *43*, 5477–5481. [[CrossRef](#)] [[PubMed](#)]
33. Amaya, T.; Sakane, H.; Hirao, T. A concave-bound cpfe complex of sumanene as a metal in a π -bowl. *Angew. Chem. Int. Ed.* **2007**, *46*, 8376–8379. [[CrossRef](#)] [[PubMed](#)]
34. Sakane, H.; Amaya, T.; Moriuchi, T.; Hirao, T. A chiral concave-bound cyclopentadienyl iron complex of sumanene. *Angew. Chem. Int. Ed.* **2009**, *48*, 1640–1643. [[CrossRef](#)] [[PubMed](#)]
35. Amaya, T.; Wang, W.-Z.; Sakane, H.; Moriuchi, T.; Hirao, T. A dynamically inverting π -bowl complex. *Angew. Chem. Int. Ed.* **2010**, *49*, 403–406. [[CrossRef](#)] [[PubMed](#)]
36. Bandera, D.; Baldrige, K.K.; Linden, A.; Dorta, R.; Siegel, J.S. Stereoselective coordination of C₅-symmetric corannulene derivatives with an enantiomerically pure [rhi(nbd*)] metal complex. *Angew. Chem. Int. Ed.* **2011**, *50*, 865–867. [[CrossRef](#)] [[PubMed](#)]
37. Amaya, T.; Seki, S.; Moriuchi, T.; Nakamoto, K.; Nakata, T.; Sakane, H.; Saeki, A.; Tagawa, S.; Hirao, T. Anisotropic electron transport properties in sumanene crystal. *J. Am. Chem. Soc.* **2009**, *131*, 408–409. [[CrossRef](#)] [[PubMed](#)]
38. Schmidt, B.M.; Seki, S.; Topolinski, B.; Ohkubo, K.; Fukuzumi, S.; Sakurai, H.; Lentz, D. Electronic properties of trifluoromethylated corannulenes. *Angew. Chem. Int. Ed.* **2012**, *51*, 11385–11388. [[CrossRef](#)] [[PubMed](#)]
39. Wu, Y.-T.; Siegel, J.S. Aromatic molecular-bowl hydrocarbons: Synthetic derivatives, their structures, and physical properties. *Chem. Rev.* **2006**, *106*, 4843–4867. [[CrossRef](#)] [[PubMed](#)]
40. Tsefrikas, V.M.; Scott, L.T. Geodesic polyarenes by flash vacuum pyrolysis. *Chem. Rev.* **2006**, *106*, 4868–4884. [[CrossRef](#)] [[PubMed](#)]
41. Amaya, T.; Hirao, T. A molecular bowl sumanene. *Chem. Commun.* **2011**, *47*, 10524–10535. [[CrossRef](#)] [[PubMed](#)]
42. Sygula, A. Chemistry on a half-shell: Synthesis and derivatization of buckybowls. *Eur. J. Org. Chem.* **2011**, *2011*, 1611–1625. [[CrossRef](#)]
43. Filatov, A.S.; Petrukhina, M.A. Probing the binding sites and coordination limits of buckybowls in a solvent-free environment: Experimental and theoretical assessment. *Coord. Chem. Rev.* **2010**, *254*, 2234–2246. [[CrossRef](#)]
44. Zoppi, L.; Martin-Samos, L.; Baldrige, K.K. Structure–property relationships of curved aromatic materials from first principles. *Acc. Chem. Res.* **2014**, *47*, 3310–3320. [[CrossRef](#)] [[PubMed](#)]
45. Sanchez-Valencia, J.R.; Dienel, T.; Groning, O.; Shorubalko, I.; Mueller, A.; Jansen, M.; Amsharov, K.; Ruffieux, P.; Fasel, R. Controlled synthesis of single-chirality carbon nanotubes. *Nature* **2014**, *512*, 61–64. [[CrossRef](#)] [[PubMed](#)]
46. Sekiguchi, R.; Kudo, S.; Kawakami, J.; Sakai, A.; Ikeda, H.; Nakamura, H.; Ohta, K.; Ito, S. Preparation of a cyclic polyphenylene array for a chiral-type carbon nanotube segment. *Bull. Chem. Soc. Jpn.* **2016**, *89*, 1260–1275. [[CrossRef](#)]
47. Liu, B.; Wu, F.; Gui, H.; Zheng, M.; Zhou, C. Chirality-controlled synthesis and applications of single-wall carbon nanotubes. *ACS Nano* **2017**, *11*, 31–53. [[CrossRef](#)] [[PubMed](#)]
48. Brandt, J.R.; Salerno, F.; Fuchter, M.J. The added value of small-molecule chirality in technological applications. *Nat. Rev. Chem.* **2017**, *1*, 0045. [[CrossRef](#)]
49. Yang, C.; Inoue, Y. Supramolecular photochirogenesis. *Chem. Soc. Rev.* **2014**, *43*, 4123–4143. [[CrossRef](#)] [[PubMed](#)]
50. Yang, C.; Ke, C.; Liang, W.; Fukuhara, G.; Mori, T.; Liu, Y.; Inoue, Y. Dual supramolecular photochirogenesis: Ultimate stereocontrol of photocyclodimerization by a chiral scaffold and confining host. *J. Am. Chem. Soc.* **2011**, *133*, 13786–13789. [[CrossRef](#)] [[PubMed](#)]
51. Fan, C.; Wu, W.; Chruma, J.J.; Zhao, J.; Yang, C. Enhanced triplet-triplet energy transfer and upconversion fluorescence through host-guest complexation. *J. Am. Chem. Soc.* **2016**, *138*, 15405. [[CrossRef](#)] [[PubMed](#)]

52. Xiao, C.; Zhao, W.-Y.; Zhou, D.-Y.; Huang, Y.; Tao, Y.; Wu, W.-H.; Yang, C. Recent advance of photochromic diarylethenes-containing supramolecular systems. *Chin. Chem. Lett.* **2015**, *26*, 817–824. [[CrossRef](#)]
53. Yang, C. Recent progress in supramolecular chiral photochemistry. *Chin. Chem. Lett.* **2013**, *24*, 437–441. [[CrossRef](#)]
54. Thilgen, C.; Diederich, F. Structural aspects of fullerene chemistry a journey through fullerene chirality. *Chem. Rev.* **2006**, *106*, 5049–5135. [[CrossRef](#)] [[PubMed](#)]
55. Cahn, R.S.; Ingold, C.; Prelog, V. Specification of molecular chirality. *Angew. Chem. Int. Ed.* **1966**, *5*, 385–415. [[CrossRef](#)]
56. Higashibayashi, S.; Onogi, S.; Srivastava, H.K.; Sastry, G.N.; Wu, Y.-T.; Sakurai, H. Stereoelectronic effect of curved aromatic structures: Favoring the unexpected endo conformation of benzylic-substituted sumanene. *Angew. Chem. Int. Ed.* **2013**, *52*, 7314–7316. [[CrossRef](#)] [[PubMed](#)]
57. Eisenberg, D.; Filatov, A.S.; Jackson, E.A.; Rabinovitz, M.; Petrukina, M.A.; Scott, L.T.; Shenhar, R. Biorannuleny: Stereochemistry of a C₄₀H₁₈ biaryl composed of two chiral bowls. *J. Org. Chem.* **2008**, *73*, 6073–6078. [[CrossRef](#)] [[PubMed](#)]
58. Imamura, K.; Takimiya, K.; Otsubo, T.; Aso, Y. Triphenyleno[1,12-bcd:4,5-b[prime or minute]c[prime or minute]d[prime or minute]:8,9-b[double prime]c[double prime]d[double prime]]trithiophene: The first bowl-shaped heteroaromatic. *Chem. Commun.* **1999**, 1859–1860. [[CrossRef](#)]
59. Furukawa, S.; Kobayashi, J.; Kawashima, T. Development of a sila-friedel-crafts reaction and its application to the synthesis of dibenzosilole derivatives. *J. Am. Chem. Soc.* **2009**, *131*, 14192–14193. [[CrossRef](#)] [[PubMed](#)]
60. Furukawa, S.; Kobayashi, J.; Kawashima, T. Application of the sila-friedel-crafts reaction to the synthesis of [small pi]-extended silole derivatives and their properties. *Dalton Trans.* **2010**, *39*, 9329–9336. [[CrossRef](#)] [[PubMed](#)]
61. Saito, M.; Tanikawa, T.; Tajima, T.; Guo, J.D.; Nagase, S. Synthesis and structures of heterasumanenes having different heteroatom functionalities. *Tetrahedron Lett.* **2010**, *51*, 672–675. [[CrossRef](#)]
62. Tanikawa, T.; Saito, M.; Guo, J.D.; Nagase, S. Synthesis, structures and optical properties of trisilasumanene and its related compounds. *Org. Biomol. Chem.* **2011**, *9*, 1731–1735. [[CrossRef](#)] [[PubMed](#)]
63. Tanikawa, T.; Saito, M.; Guo, J.D.; Nagase, S.; Minoura, M. Synthesis, structures, and optical properties of heterasumanenes containing group 14 elements and their related compounds. *Eur. J. Org. Chem.* **2012**, *2012*, 7135–7142. [[CrossRef](#)]
64. Li, X.; Zhu, Y.; Shao, J.; Wang, B.; Zhang, S.; Shao, Y.; Jin, X.; Yao, X.; Fang, R.; Shao, X. Non-pyrolytic, large-scale synthesis of trichalcogenasumanene: A two-step approach. *Angew. Chem. Int. Ed.* **2014**, *53*, 535–538. [[CrossRef](#)] [[PubMed](#)]
65. Wang, S.; Li, X.; Hou, X.; Sun, Y.; Shao, X. Tritellurasumanene: Ultrasound assisted one-pot synthesis and extended valence adducts with bromine. *Chem. Commun.* **2016**, *52*, 14486–14489. [[CrossRef](#)] [[PubMed](#)]
66. Hou, X.; Zhu, Y.; Qin, Y.; Chen, L.; Li, X.; Zhang, H.-L.; Xu, W.; Zhu, D.; Shao, X. Tris(s,s-dioxide)-trithiasumanene: Strong fluorescence and cocrystal with 1,2,6,7,10,11-hexabutoxytriphenylene. *Chem. Commun.* **2017**, *53*, 1546–1549. [[CrossRef](#)] [[PubMed](#)]
67. Furukawa, S.; Suda, Y.; Kobayashi, J.; Kawashima, T.; Tada, T.; Fujii, S.; Kiguchi, M.; Saito, M. Triphosphasumanene trisulfide: High out-of-plane anisotropy and janus-type π -surfaces. *J. Am. Chem. Soc.* **2017**, *139*, 5787–5792. [[CrossRef](#)] [[PubMed](#)]
68. Barth, W.E.; Lawton, R.G. Dibenzo[ghi,mno]fluoranthene. *J. Am. Chem. Soc.* **1966**, *88*, 380–381. [[CrossRef](#)]
69. Scott, L.T.; Hashemi, M.M.; Meyer, D.T.; Warren, H.B. Corannulene. A convenient new synthesis. *J. Am. Chem. Soc.* **1991**, *113*, 7082–7084. [[CrossRef](#)]
70. Borchardt, A.; Fuchicello, A.; Kilway, K.V.; Baldrige, K.K.; Siegel, J.S. Synthesis and dynamics of the corannulene nucleus. *J. Am. Chem. Soc.* **1992**, *114*, 1921–1923. [[CrossRef](#)]
71. Abdourazak, A.H.; Marcinow, Z.; Sygula, A.; Sygula, R.; Rabideau, P.W. Buckybowls 2. Toward the total synthesis of buckminsterfullerene (C₆₀): Benz[5,6]-as-indaceno[3,2,1,8,7-mnopqr]indeno[4,3,2,1-cdef]chrysene. *J. Am. Chem. Soc.* **1995**, *117*, 6410–6411. [[CrossRef](#)]
72. Mehta, G.; Shahk, S.R.; Ravikumarc, K. Towards the design of tricyclopenta [def, jkl, pqr] triphenylene ('sumanene'): A 'bowl-shaped' hydrocarbon featuring a structural motif present in C₆₀(buckminsterfullerene). *J. Chem. Soc. Chem. Commun.* **1993**, 1006–1008. [[CrossRef](#)]
73. Seiders, T.J.; Baldrige, K.K.; Siegel, J.S. Synthesis and characterization of the first corannulene cyclophane. *J. Am. Chem. Soc.* **1996**, *118*, 2754–2755. [[CrossRef](#)]

74. Sakurai, H.; Daiko, T.; Hirao, T. A synthesis of sumanene, a fullerene fragment. *Science* **2003**, *301*, 1878. [[CrossRef](#)] [[PubMed](#)]
75. Higashibayashi, S.; Sakurai, H. Synthesis of an enantiopure syn-benzocyclotrimer through regio-selective cyclotrimerization of a halonorbornene derivative under palladium nanocluster conditions. *Chem. Lett.* **2007**, *36*, 18–19. [[CrossRef](#)]
76. Reza, A.F.G.M.; Higashibayashi, S.; Sakurai, H. Preparation of C₃-symmetric homochiral syn-trisnorbornabenzene through regioselective cyclotrimerization of enantiopure iodonorbornenes. *Chem. Asian J.* **2009**, *4*, 1329–1337. [[CrossRef](#)] [[PubMed](#)]
77. Priyakumar, U.D.; Sastry, G.N. Heterobuckybowls: A theoretical study on the structure, bowl-to-bowl inversion barrier, bond length alternation, structure-inversion barrier relationship, stability, and synthetic feasibility. *J. Org. Chem.* **2001**, *66*, 6523–6530. [[CrossRef](#)] [[PubMed](#)]
78. Hagen, S.; Bratcher, M.S.; Erickson, M.S.; Zimmermann, G.; Scott, L.T. Novel syntheses of three C₃₀H₁₂ bowl-shaped polycyclic aromatic hydrocarbons. *Angew. Chem. Int. Ed.* **1997**, *36*, 406–408. [[CrossRef](#)]
79. Amaya, T.; Nakata, T.; Hirao, T. Synthesis of highly strained π -bowls from sumanene. *J. Am. Chem. Soc.* **2009**, *131*, 10810–10811. [[CrossRef](#)] [[PubMed](#)]
80. Tsefrikas, V.M.; Arns, S.; Merner, P.M.; Warford, C.C.; Merner, B.L.; Scott, L.T.; Bodwell, G.J. Benzo[a]aceorannulene: Surprising formation of a new bowl-shaped aromatic hydrocarbon from an attempted synthesis of 1,2-diazadibenzo[d,m]corannulene. *Org. Lett.* **2006**, *8*, 5195–5198. [[CrossRef](#)] [[PubMed](#)]
81. Wu, Y.-T.; Hayama, T.; Baldrige, K.K.; Linden, A.; Siegel, J.S. Synthesis of fluoranthenes and indenocorannulenes: Elucidation of chiral stereoisomers on the basis of static molecular bowls. *J. Am. Chem. Soc.* **2006**, *128*, 6870–6884. [[CrossRef](#)] [[PubMed](#)]
82. Rickhaus, M.; Mayor, M.; Juricek, M. Chirality in curved polyaromatic systems. *Chem. Soc. Rev.* **2017**, *46*, 1643–1660. [[CrossRef](#)] [[PubMed](#)]
83. Suárez, M.; Branda, N.; Lehn, J.-M.; Decian, A.; Fischer, J. Supramolecular chirality: Chiral hydrogen-bonded supermolecules from achiral molecular components. *Helv. Chim. Acta* **1998**, *81*, 1–13. [[CrossRef](#)]
84. Dalla Cort, A.; Mandolini, L.; Pasquini, C.; Schiaffino, L. “Inherent chirality” and curvature. *New J. Chem.* **2004**, *28*, 1198–1199. [[CrossRef](#)]
85. Szumna, A. Inherently chiral concave molecules—from synthesis to applications. *Chem. Soc. Rev.* **2010**, *39*, 4274–4285. [[CrossRef](#)] [[PubMed](#)]
86. Supramolecular chirality. In *Topics in Current Chemistry*; Crego-Calama, M.; Reinhoudt, D.N., Eds.; Springer: Berlin/Heidelberg, Germany, 2006; Volume 265, p. 312.
87. Yao, J.; Wu, W.; Liang, W.; Feng, Y.; Zhou, D.; Chruma, J.J.; Fukuhara, G.; Mori, T.; Inoue, Y.; Yang, C. Temperature-driven planar chirality switching of a pillar[5]arene-based molecular universal joint. *Angew. Chem. Int. Ed.* **2017**, *56*, 6869–6873. [[CrossRef](#)] [[PubMed](#)]
88. Kaewmati, P.; Tan, Q.; Higashibayashi, S.; Yakiyama, Y.; Sakurai, H. Synthesis of triaryltriazasumanenes. *Chem. Lett.* **2017**, *46*, 146–148. [[CrossRef](#)]
89. Huang, Q.; Jiang, L.; Liang, W.; Gui, J.; Xu, D.; Wu, W.; Nakai, Y.; Nishijima, M.; Fukuhara, G.; Mori, T.; et al. Inherently chiral azonia[6]helicene-modified β -cyclodextrin: Synthesis, characterization, and chirality sensing of underivatized amino acids in water. *J. Org. Chem.* **2016**, *81*, 3430–3434. [[CrossRef](#)] [[PubMed](#)]
90. Yan, Z.; Huang, Q.; Liang, W.; Yu, X.; Zhou, D.; Wu, W.; Chruma, J.J.; Yang, C. Enantiodifferentiation in the photoisomerization of (z,z)-1,3-cyclooctadiene in the cavity of γ -cyclodextrin-curcubit[6]uril-wheeled [4]rotaxanes with an encapsulated photosensitizer. *Org. Lett.* **2017**, *19*, 898–901. [[CrossRef](#)] [[PubMed](#)]
91. Gui, J.-C.; Yan, Z.-Q.; Peng, Y.; Yi, J.-G.; Zhou, D.-Y.; Su, D.; Zhong, Z.-H.; Gao, G.-W.; Wu, W.-H.; Yang, C. Enhanced head-to-head photodimers in the photocyclodimerization of anthracenecarboxylic acid with a cationic pillar [6] arene. *Chin. Chem. Lett.* **2016**, *27*, 1017–1021. [[CrossRef](#)]
92. Yao, J.; Yan, Z.; Ji, J.; Wu, W.; Yang, C.; Nishijima, M.; Fukuhara, G.; Mori, T.; Inoue, Y. Ammonia-driven chirality inversion and enhancement in enantiodifferentiating photocyclodimerization of 2-anthracenecarboxylate mediated by diguanidino- γ -cyclodextrin. *J. Am. Chem. Soc.* **2014**, *136*, 6916–6919. [[CrossRef](#)] [[PubMed](#)]
93. Liang, W.; Yang, C.; Nishijima, M.; Fukuhara, G.; Mori, T.; Mele, A.; Castiglione, F.; Caldera, F.; Trotta, F.; Inoue, Y. Cyclodextrin nanosponge-sensitized enantiodifferentiating photoisomerization of cyclooctene and 1,3-cyclooctadiene. *Beilstein J. Org. Chem.* **2012**, *8*, 1305–1311. [[CrossRef](#)] [[PubMed](#)]

94. Wang, Q.; Yang, C.; Ke, C.; Fukuhara, G.; Mori, T.; Liu, Y.; Inoue, Y. Wavelength-controlled supramolecular photocyclodimerization of anthracenecarboxylate mediated by γ -cyclodextrins. *Chem. Commun.* **2011**, *47*, 6849–6851. [[CrossRef](#)] [[PubMed](#)]
95. Fujikawa, T.; Preda, D.V.; Segawa, Y.; Itami, K.; Scott, L.T. Corannulene–helicene hybrids: Chiral π -systems comprising both bowl and helical motifs. *Org. Lett.* **2016**, *18*, 3992–3995. [[CrossRef](#)] [[PubMed](#)]
96. Yanney, M.; Fronczek, F.R.; Sygula, A. Corannulene subunit acts as a diene in a cycloaddition reaction: Synthesis of C80H32 corannulyne tetramer. *Org. Lett.* **2012**, *14*, 4942–4945. [[CrossRef](#)] [[PubMed](#)]
97. Yanney, M.; Fronczek, F.R.; Henry, W.P.; Beard, D.J.; Sygula, A. Cyclotrimerization of corannulyne: Steric hindrance tunes the inversion barriers of corannulene bowls. *Eur. J. Org. Chem.* **2011**, *2011*, 6636–6639. [[CrossRef](#)]
98. Kawasumi, K.; Zhang, Q.; Segawa, Y.; Scott, L.T.; Itami, K. A grossly warped nanographene and the consequences of multiple odd-membered-ring defects. *Nat. Chem.* **2013**, *5*, 739–744. [[CrossRef](#)] [[PubMed](#)]
99. Amaya, T.; Mori, K.; Wu, H.-L.; Ishida, S.; Nakamura, J.-I.; Murata, K.; Hirao, T. Synthesis and characterization of [small pi]-extended bowl-shaped [small pi]-conjugated molecules. *Chem. Commun.* **2007**, 1902–1904. [[CrossRef](#)]
100. Chen, R.; Lu, R.-Q.; Shi, P.-C.; Cao, X.-Y. Corannulene derivatives for organic electronics: From molecular engineering to applications. *Chin. Chem. Lett.* **2016**, *27*, 1175–1183. [[CrossRef](#)]
101. Kobayashi, S.-i.; Mori, S.; Iida, S.; Ando, H.; Takenobu, T.; Taguchi, Y.; Fujiwara, A.; Taninaka, A.; Shinohara, H.; Iwasa, Y. Conductivity and field effect transistor of la2@C80 metallofullerene. *J. Am. Chem. Soc.* **2003**, *125*, 8116–8117. [[CrossRef](#)] [[PubMed](#)]
102. Kato, H.; Kanazawa, Y.; Okumura, M.; Taninaka, A.; Yokawa, T.; Shinohara, H. Lanthanoid endohedral metallofullerenols for MRI contrast agents. *J. Am. Chem. Soc.* **2003**, *125*, 4391–4397. [[CrossRef](#)] [[PubMed](#)]
103. Petrukhina, M.A.; Scott, L.T. Coordination chemistry of buckybowls: From corannulene to a hemifullerene. *Dalton Trans.* **2005**, 2969–2975. [[CrossRef](#)] [[PubMed](#)]
104. Vecchi, P.A.; Alvarez, C.M.; Ellern, A.; Angelici, R.J.; Sygula, A.; Sygula, R.; Rabideau, P.W. Flattening of a curved-surface buckybowl (corannulene) by η_6 coordination to $[cp^*Ru]^+$. *Organometallics* **2005**, *24*, 4543–4552. [[CrossRef](#)]
105. Zhu, B.; Ellern, A.; Sygula, A.; Sygula, R.; Angelici, R.J. η_6 -Coordination of the curved carbon surface of corannulene (C20H10) to $(\eta_6\text{-arene})M^{2+}$ ($M = Ru, Os$). *Organometallics* **2007**, *26*, 1721–1728. [[CrossRef](#)]
106. Zabala, A.V.; Spisak, S.N.; Filatov, A.S.; Rogachev, A.Y.; Clerac, R.; Petrukhina, M.A. Supramolecular trap for a transient corannulene trianion. *Chem. Sci.* **2016**, *7*, 1954–1961. [[CrossRef](#)]
107. Kameno, Y.; Ikeda, A.; Nakao, Y.; Sato, H.; Sakaki, S. Theoretical study of $M(PH_3)_2$ complexes of C60, corannulene (C20H10), and sumanene (C21H12) ($M = Pd$ or Pt). Unexpectedly large binding energy of $M(PH_3)_2(C60)$. *J. Phys. Chem. A* **2005**, *109*, 8055–8063. [[CrossRef](#)] [[PubMed](#)]
108. Agnes, M.; Nitti, A.; Vander Griend, D.A.; Dondi, D.; Merli, D.; Pasini, D. A chiroptical molecular sensor for ferrocene. *Chem. Commun.* **2016**, *52*, 11492–11495. [[CrossRef](#)] [[PubMed](#)]
109. Caricato, M.; Leza, N.J.; Roy, K.; Dondi, D.; Gattuso, G.; Shimizu, L.S.; Vander Griend, D.A.; Pasini, D. A chiroptical probe for sensing metal ions in water. *Eur. J. Org. Chem.* **2013**, *2013*, 6078–6083. [[CrossRef](#)]
110. Caricato, M.; Coluccini, C.; Dondi, D.; Vander Griend, D.A.; Pasini, D. Nesting complexation of C60 with large, rigid d2 symmetrical macrocycles. *Org. Biomol. Chem.* **2010**, *8*, 3272–3280. [[CrossRef](#)] [[PubMed](#)]
111. Caricato, M.; Sharma, A.K.; Coluccini, C.; Pasini, D. Nanostructuring with chirality: Binaphthyl-based synthons for the production of functional oriented nanomaterials. *Nanoscale* **2014**, *6*, 7165–7174. [[CrossRef](#)] [[PubMed](#)]
112. Nitti, A.; Pacini, A.; Pasini, D. Chiral nanotubes. *Nanomaterials* **2017**, *7*, 167. [[CrossRef](#)] [[PubMed](#)]
113. Bancu, M.; Rai, A.K.; Cheng, P.; Gilardi, R.D.; Scott, L.T. Corannulene polysulfides: Molecular bowls with multiple arms and flaps. *Synlett* **2004**, *2004*, 173–176.
114. Xiao, W.; Ernst, K.-H.; Palotas, K.; Zhang, Y.; Bruyer, E.; Peng, L.; Greber, T.; Hofer, W.A.; Scott, L.T.; Fasel, R. Microscopic origin of chiral shape induction in achiral crystals. *Nat. Chem.* **2016**, *8*, 326–330. [[CrossRef](#)] [[PubMed](#)]
115. Schunack, M.; Lægsgaard, E.; Stensgaard, I.; Johannsen, I.; Besenbacher, F. A chiral metal surface. *Angew. Chem. Int. Ed.* **2001**, *40*, 2623–2626. [[CrossRef](#)]
116. Karageorgaki, C.; Ernst, K.-H. A metal surface with chiral memory. *Chem. Commun.* **2014**, *50*, 1814–1816. [[CrossRef](#)] [[PubMed](#)]



Article

The Asymmetry is Derived from Mechanical Interlocking of Achiral Axle and Achiral Ring Components –Syntheses and Properties of Optically Pure [2]Rotaxanes–

Keiji Hirose ^{1,*}, Masaya Ukimi ¹, Shota Ueda ¹, Chie Onoda ¹, Ryohei Kano ¹, Kyosuke Tsuda ¹, Yuko Hinohara ¹ and Yoshito Tobe ²

¹ Graduate School of Engineering Science, Osaka University, 1-3 Machikaneyama, Toyonaka, Osaka 560-8531, Japan; ukimim@supra.chem.es.osaka-u.ac.jp (M.U.); uedas@supra.chem.es.osaka-u.ac.jp (S.U.); onodat@supra.chem.es.osaka-u.ac.jp (C.O.); kanor@supra.chem.es.osaka-u.ac.jp (R.K.); tsudak@supra.chem.es.osaka-u.ac.jp (K.T.); hinoharay@supra.chem.es.osaka-u.ac.jp (Y.H.)

² The Institute of Scientific and Industrial Research, Osaka University, 8-1 Mihogaoka, Ibaraki, Osaka 567-0047, Japan; tobe@chem.es.osaka-u.ac.jp

* Correspondence: hirose@chem.es.osaka-u.ac.jp; Tel.: +81-6-6850-6228

Received: 25 November 2017; Accepted: 27 December 2017; Published: 9 January 2018

Abstract: Rotaxanes consisting of achiral axle and achiral ring components can possess supramolecular chirality due to their unique geometrical architectures. To synthesize such chiral rotaxanes, we adapted a prerotaxane method based on aminolysis of a metacyclophane type prerotaxane that had planar chirality, which is composed of an achiral stopper unit and a crown ether type ring component. The prerotaxanes were well resolved using chiral HPLC into a pair of enantiomerically pure prerotaxanes, which were transferred into corresponding chiral rotaxanes, respectively. Obtained chiral rotaxanes were revealed to have considerable enantioselectivity.

Keywords: mechanical chirality; mecanostereochemistry; supramolecular chirality; rotaxane; aminolysis

1. Introduction

The discoveries of a crown ether and a very stable complex formation with a metal cation by C. J. Pedersen [1] in 1967, following neologisms of the “Host-guest chemistry” by D. J. Cram [2], and that of the “Supramolecular chemistry” by J. M. Lehn [3], showed the importance of interaction between molecules, were tremendously influential and initiated a huge amount of researches. Nobel prize of chemistry was awarded to these researchers in 1987. Many crops from this field of chemistry were industrialized such as ion sensors, ion selective membranes, and electrodes [4–9], which were contributed by ion recognition initiated by C. J. Pedersen and chiral selectors for chromatography [10–15] initiated by the contribution of D. J. Cram’s chirality recognition technology [16,17]. Research topics such as chiral shift reagents for the determination of enantiomeric excess of chiral substance [18], besides the reagents for the determination of absolute configuration [19,20], chiral indicators [19,21–24], and rapid chirality detection method using chiral hosts by means of mass spectrometry [25,26], as well as other well established methods [27–29] have long fascinated many researchers.

In the late 1980s, fabrications of molecular assemblies using inter- and/or intramolecular interactions of molecular components came under the spotlight. Typical examples are the syntheses of catenanes, rotaxanes, and molecular knots [30]. The emergence and excellent development of supramolecular methods make the syntheses of supramolecules much more effective, with a higher

chemical yield [31–35] than before [36]. Covalent methods [37], which were not thought to be versatile for the synthesis of interlocked molecules, were also well developed [38,39]. One of the applications in this field of chemistry is to make the smallest machines at molecular level using fabrications of molecular components. The Nobel prize in chemistry was awarded to three researchers working in this field: J.-P. Sauvage [40], Sir J. F. Stoddart [41], and B. L. Feringa [42] in 2016.

Chiral interlocked molecules provide unique three-dimensional, valuable-binding circumstances capable of chirality recognition of guests. However, the application of interlocked hosts for chirality recognition has been largely overlooked, especially the recognition by hosts with mechanical chirality. A rotaxane has a mechanically interlocked architecture consisting of a dumbbell-shaped axle component that is threaded through a ring component. Rotaxanes consisting of achiral axle components that have $C_{\infty v}$ symmetry and achiral ring components that have C_s symmetry can be chiral, caused by their geometrically specific architectures. In Figure 1, an enantiomeric pair of rotaxanes with the specific chirality composed of a $C_{\infty v}$ axle and a C_s ring components is shown. Rotaxanes with the specific chirality can be expected as new molecular platforms [43–45] for asymmetric catalysts, chiral sensors [27–29], etc. However, it is difficult to synthesize such rotaxanes as optically pure forms [46]. In order to synthesize such rotaxanes with the rotaxane-specific chirality in an optically pure form, we applied our prerotaxane method [39], in which a rotaxane can be synthesized via backside attack of a stopper unit to a prerotaxane with planar chirality composed of an achiral stopper unit and a C_s ring component (Scheme 1). In order to investigate binding properties of the rotaxanes that have a mechanically interlocked chirality as host compounds, precise evaluation of the enantioselective complexation ability of the rotaxanes with chiral guests were carried out.

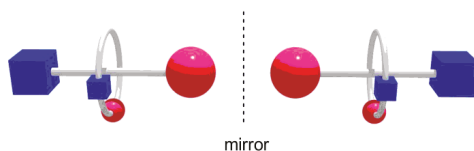
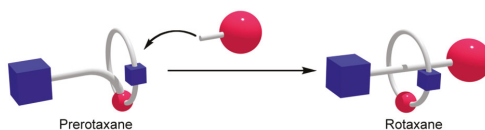


Figure 1. Rotaxane specific chirality by a combination of $C_{\infty v}$ axle component and C_s ring component.



Scheme 1. Key step of our rotaxane synthesis of covalent method via S_N2 reaction with a prerotaxane with planar chirality and stopper unit.

2. Materials and Methods

Compound **1** prepared using hydroquinone mono-methoxymethyl ether as starting material according to previously reported procedures [47–49] was used. All other compounds and reagents were obtained from commercial suppliers and used as received. CH_2Cl_2 and THF were dried by a Glass Contour solvent purification system prior to use. Melting points were measured with a hot-stage apparatus equipped with a thermometer. 1H NMR spectra were recorded with a JEOL GSX-270, a Varian Mercury 300, or a JEOL AL-400 spectrometer for solutions in $CDCl_3$ or C_6D_6 with $SiMe_4$ as an internal standard and J values given in Hz. ^{13}C NMR spectra were recorded at 75.5 MHz with a JEOL GSX-270 spectrometer, and chloroform (δ C 77.0) was used as a chemical shift reference. Multiplicities for 1H NMR spectra are as follows: singlet (s), doublet (d), triplet (t), quartet (q), and multiplet (m). Multiplicities for ^{13}C NMR spectra are as follows: primary (1°), secondary (2°), tertiary (3°), and quaternary (4°). IR spectra were measured on a JASCO FT/IR-410 spectrophotometer. Circular dichroism spectra were measured using a JASCO J-805 spectropolarimeter,

and θ values are given in units of mdeg. MS spectra were recorded with a JEOL JMS-700 spectrometer. Preparative GPLC was performed with JAI LC-908 on JAIGEL 1H and 2H columns with CHCl_3 as a solvent. Elemental analyses were carried out by using a Perkin–Elmer 2400II analyser. Analytical thin layer chromatography (TLC) was performed using precoated silica gel plates (Merck Kieselgel 60 F254). Preparative column chromatography was carried out using Fuji Silysia BW-300 silica gel (SiO_2 ; 0.038–0.075 mm) with the indicated solvents, which were mixed *v/v* as specified.

2-1 Synthetic Procedures and Characterization of Racemic Prerotaxanes (rac)-3

Into a solution of **1** (98.9 mg, 142 μmol) in dry THF (3.5 mL) and KO^tBu (55.6 mg, 495 μmol), 3,5-dinitrobenzoyl chloride (131 mg, 568 μmol) was added with stirring under a nitrogen atmosphere. After 2 h stirring at room temperature, the solvent was evaporated under reduced pressure. The residue was extracted with chloroform. The organic layer was washed with brine. After being dried over anhydrous MgSO_4 , the solvent was removed under reduced pressure. The residue was purified by preparative GPLC to give (rac)-**3** (74.8 mg, 84.4 μmol , 60%) as an orange powder: ^1H NMR (400 MHz, CDCl_3 , 30 $^\circ\text{C}$) δ 9.02 (d, 2H, $J = 1.9$ Hz), 8.86 (d, 1H, $J = 2.5$ Hz), 8.81 (t, 1H, $J = 1.9$ Hz), 8.58 (dd, 1H, $J = 2.5$, 8.8 Hz), 8.28 (d, 1H, $J = 2.5$ Hz), 8.16 (d, 1H, $J = 2.5$ Hz), 7.85 (d, 1H, $J = 8.8$ Hz), 7.45 (d, 2H, $J = 8.5$ Hz), 7.18–7.30 (m, 2H), 7.09 (s, 1H), 6.85 (s, 1H), 5.45 (d, 1H, $J = 12$ Hz), 5.15 (d, 1H, $J = 12$ Hz), 4.83 (d, 1H, $J = 13$ Hz), 4.70 (d, 1H, $J = 13$ Hz), 4.08–4.18 (m, 2H), 3.92 (t, 2H, $J = 4.2$ Hz), 3.48–3.78 (m, 16H); ^{13}C NMR (100 MHz, CDCl_3 , 30 $^\circ\text{C}$) δ 159.9 (4 $^\circ$), 151.2 (4 $^\circ$), 150.3 (4 $^\circ$), 148.9 (4 $^\circ$), 148.7 (4 $^\circ$), 147.84 (4 $^\circ$), 147.77 (4 $^\circ$), 146.5 (4 $^\circ$), 134.2 (4 $^\circ$), 131.3 (4 $^\circ$), 129.5 (3 $^\circ$), 129.2 (4 $^\circ$), 128.5 (4 $^\circ$), 127.9 (3 $^\circ$), 126.4 (3 $^\circ$), 126.0 (3 $^\circ$), 125.9 (3 $^\circ$), 125.1 (3 $^\circ$), 124.8 (3 $^\circ$), 124.4 (3 $^\circ$), 122.0 (3 $^\circ$), 120.19 (3 $^\circ$), 122.16 (3 $^\circ$), 109.2 (3 $^\circ$), 107.7 (3 $^\circ$), 71.3 (2 $^\circ$), 71.0 (2 $^\circ$), 70.8 (2 $^\circ$), 70.71 (2 $^\circ$), 70.65 (2 $^\circ$), 70.6 (2 $^\circ$), 70.1 (2 $^\circ$), 69.4 (2 $^\circ$), 69.0 (2 $^\circ$), 68.5 (2 $^\circ$), 67.7 (2 $^\circ$); IR (KBr) 3093, 2922, 2866, 1770, 1543, 1345, 1261, 1137, 1114, 920, 717 cm^{-1} ; HRMS (FAB) m/z calcd for $\text{C}_{41}\text{H}_{39}\text{N}_6\text{O}_{17}$ ($[\text{M} + \text{H}^+]$): 887.2372, found: 887.2379.

2-2 Characterization of Resolved Prerotaxane **3**_{1st}

3_{1st}: m.p. 88.8–90.1 $^\circ\text{C}$; ^1H NMR (400 MHz, CDCl_3 , 30 $^\circ\text{C}$) δ 9.02 (d, 2H, $J = 1.9$ Hz), 8.86 (d, 1H, $J = 2.5$ Hz), 8.81 (t, 1H, $J = 1.9$ Hz), 8.58 (dd, 1H, $J = 2.5$, 8.8 Hz), 8.28 (d, 1H, $J = 2.5$ Hz), 8.16 (d, 1H, $J = 2.5$ Hz), 7.85 (d, 1H, $J = 8.8$ Hz), 7.45 (d, 2H, $J = 8.5$ Hz), 7.18–7.30 (m, 2H), 7.09 (s, 1H), 6.85 (s, 1H), 5.45 (d, 1H, $J = 12$ Hz), 5.15 (d, 1H, $J = 12$ Hz), 4.83 (d, 1H, $J = 13$ Hz), 4.70 (d, 1H, $J = 13$ Hz), 4.08–4.18 (m, 2H), 3.92 (t, 2H, $J = 4.2$ Hz), 3.48–3.78 (m, 16H); ^{13}C NMR (100 MHz, CDCl_3 , 30 $^\circ\text{C}$) δ 160.0 (4 $^\circ$), 151.3 (4 $^\circ$), 150.4 (4 $^\circ$), 149.0 (4 $^\circ$), 148.8 (4 $^\circ$), 147.94 (4 $^\circ$), 147.89 (4 $^\circ$), 146.6 (4 $^\circ$), 134.2 (4 $^\circ$), 131.4 (4 $^\circ$), 129.6 (3 $^\circ$), 129.2 (4 $^\circ$), 128.6 (4 $^\circ$), 128.0 (3 $^\circ$), 126.5 (3 $^\circ$), 126.1 (3 $^\circ$), 126.0 (3 $^\circ$), 125.2 (3 $^\circ$), 124.9 (3 $^\circ$), 124.5 (3 $^\circ$), 122.1 (3 $^\circ$), 120.29 (3 $^\circ$), 120.25 (3 $^\circ$), 109.2 (3 $^\circ$), 107.7 (3 $^\circ$), 71.3 (2 $^\circ$), 71.0 (2 $^\circ$), 70.77 (2 $^\circ$), 70.75 (2 $^\circ$), 70.73 (2 $^\circ$), 70.66 (2 $^\circ$), 70.63 (2 $^\circ$), 70.1 (2 $^\circ$), 69.5 (2 $^\circ$), 69.0 (2 $^\circ$), 68.5 (2 $^\circ$), 67.7 (2 $^\circ$) (1 tertiary carbon and 1 quaternary carbon could not be seen); IR (KBr) 3101, 2869, 1752, 1543, 1344, 1261, 1137, 1114, 922, 717 cm^{-1} ; UV/Vis (CHCl_3 , 22 $^\circ\text{C}$) λ_{max} (log ϵ) 342 (4.3); MS (LDI) m/z 909.3 ($[\text{M} + \text{Na}^+]$). HRMS (ESI) m/z Calcd for $\text{C}_{41}\text{H}_{38}\text{N}_6\text{NaO}_{17}$: 909.2191, Found: 909.2200 ($[\text{M} + \text{Na}^+]$). Anal. Calcd for $\text{C}_{41}\text{H}_{38}\text{N}_6\text{O}_{17}$: C, 55.53; H, 4.32; N, 9.48. Found: C, 55.25; H, 4.22; N, 9.35.

2-3 Characterization of Resolved Prerotaxane **3**_{2nd}

3_{2nd}: m.p. 88.9–90.0 $^\circ\text{C}$; ^1H NMR (400 MHz, CDCl_3 , 30 $^\circ\text{C}$) δ 9.02 (d, 2H, $J = 1.9$ Hz), 8.86 (d, 1H, $J = 2.5$ Hz), 8.81 (t, 1H, $J = 1.9$ Hz), 8.58 (dd, 1H, $J = 2.5$, 8.8 Hz), 8.28 (d, 1H, $J = 2.5$ Hz), 8.16 (d, 1H, $J = 2.5$ Hz), 7.85 (d, 1H, $J = 8.8$ Hz), 7.45 (d, 2H, $J = 8.5$ Hz), 7.18–7.30 (m, 2H), 7.09 (s, 1H), 6.85 (s, 1H), 5.45 (d, 1H, $J = 12$ Hz), 5.15 (d, 1H, $J = 12$ Hz), 4.83 (d, 1H, $J = 13$ Hz), 4.70 (d, 1H, $J = 13$ Hz), 4.08–4.18 (m, 2H), 3.92 (t, 2H, $J = 4.2$ Hz), 3.48–3.78 (m, 16H); ^{13}C NMR (100 MHz, CDCl_3 , 30 $^\circ\text{C}$) δ 160.0, 151.3, 150.4, 149.0, 148.8, 147.94, 147.89, 146.6, 134.2, 131.4, 129.6, 129.2, 128.6, 128.0, 126.5, 126.1, 126.0, 125.2, 124.9, 124.5, 122.1, 120.3, 109.2, 107.7, 71.3, 71.1, 70.79, 70.77, 70.74, 70.69, 70.64, 70.2, 69.5, 69.0, 68.5, 67.8 (2 carbons couldn't be seen); IR (KBr) 3101, 2870, 1752, 1543, 1345, 1261, 1138, 1114, 922, 718 cm^{-1} ; MS (LDI) m/z 909.2 ($[\text{M} + \text{Na}^+]$). HRMS (ESI) m/z Calcd for $\text{C}_{41}\text{H}_{38}\text{N}_6\text{NaO}_{17}$: 909.2191, Found: 909.2185 ($[\text{M} + \text{Na}^+]$). Anal. Calcd for $\text{C}_{41}\text{H}_{38}\text{N}_6\text{O}_{17}$: C, 55.53; H, 4.32; N, 9.48. Found: C, 55.70; H, 4.46; N, 9.35.

2-4 Synthetic Procedures and Characterization of Rotaxanes 5_{1st}

Into a solution of **3**_{1st} (2.99 mg, 3.37 μ mol) in C₆D₆ (660 μ L), 3,5-bis(trifluoromethyl)benzylamine **4** (1.63 mg, 6.71 μ mol) in C₆D₆ (22 μ L) was added. The aminolysis was monitored by ¹H NMR (270 MHz) at 30 °C. After the reaction was completed, the solvent was removed under reduced pressure. The residue was purified by preparative GLPC. Following precipitation from CH₂Cl₂ and hexane afforded **5**_{1st} (2.93 mg, 2.59 μ mol, 77%) as an orange solid. m.p. 115.1–116.8 °C; ¹H NMR (270 MHz, C₆D₆, 30 °C) δ 8.69 (d, 2H, *J* = 1.7 Hz), 8.40 (t, 1H, *J* = 1.7 Hz), 8.27–8.24 (m, 1H), 8.20 (s, 2H), 8.07 (d, 1H, *J* = 2.2 Hz), 8.05 (d, 1H, *J* = 2.4 Hz), 7.66 (s, 1H), 7.62 (dd, 1H, *J* = 8.3, 2.4 Hz), 7.60 (d, 1H, *J* = 2.4 Hz), 7.37 (d, 1H, *J* = 9.0 Hz), 7.45–7.33 (m, 4H), 6.96 (s, 1H), 6.03 (s, 1H), 5.34 (dd, 1H, *J* = 16.2, 8.0 Hz), 5.20 (d, 1H, *J* = 8.8 Hz), 4.89 (dd, 1H, *J* = 16.2, 2.3 Hz), 4.71 (d, 1H, *J* = 10.6 Hz), 4.37 (d, 1H, *J* = 9.1 Hz), 3.78 (d, 1H, *J* = 10.6 Hz), 3.61–2.91 (m, 16H), 2.69 (t, 2H, *J* = 10.2 Hz), 2.43 (d, 1H, *J* = 10.7 Hz), 2.12 (t, 1H, *J* = 10.1 Hz); ¹³C NMR (100 MHz, CDCl₃, 30 °C) δ 163.0 (4°), 160.2 (4°), 148.7 (4°), 147.6 (4°), 147.4 (4°), 147.2 (4°), 146.8 (4°), 146.0 (4°), 140.7 (4°), 137.2 (4°), 132.0 (3°), 130.3 (3°), 130.2 (q, *J*_{CF} = 33 Hz, 4°), 128.9 (4°), 128.4 (4°), 127.8 (3°), 127.65 (3°), 127.59 (4°), 126.5 (3°), 125.6 (3°), 124.92 (4°), 124.90 (3°), 124.86 (3°), 124.7 (3°), 122.1 (4°), 120.4 (q, *J*_{CF} = 4.4 Hz, 3°), 120.0 (3°), 119.8 (3°), 119.7 (3°), 107.3 (3°), 105.8 (3°), 71.20 (2°), 71.15 (2°), 70.9 (2°), 70.6 (2°), 70.5 (2°), 70.4 (2°), 70.2 (2°), 70.1 (2°), 69.8 (2°), 69.4 (2°), 67.6 (2°), 65.1 (2°), 43.7 (2°) (2 tertiary carbon and 3 quaternary carbon could not be seen); IR (KBr) 3346, 3096, 2880, 1601, 1540, 1345, 1278, 1130, 850 cm⁻¹; UV/Vis (CHCl₃, 20 °C) λ _{max} (log ϵ) 390 (4.3); MS (MALDI) *m/z* 1152.4 ([M + Na⁺]); HRMS (FAB) *m/z* Calcd for C₅₁H₄₅F₆N₇O₁₇: 1130.2854, Found: 1130.2885 ([M + H⁺]).

2-5 Synthetic Procedures and Characterization of Rotaxanes 5_{2nd}

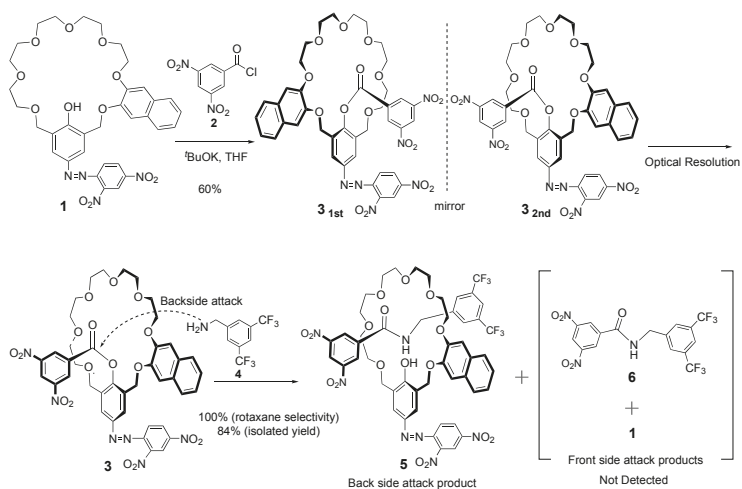
Into a solution of **3**_{2nd} (3.15 mg, 3.54 μ mol) in C₆D₆ (660 μ L), amine **4** (1.72 mg, 7.07 μ mol) in C₆D₆ (22 μ L) was added. The aminolysis was monitored by ¹H NMR (270 MHz) at 30 °C. After the reaction was completed, the solvent was removed under reduced pressure. The residue was purified by preparative GLPC. Following precipitation from CH₂Cl₂ and hexane afforded **5**_{2nd} (3.35 mg, 2.96 μ mol, 84%) as an orange solid. m.p. 115.2–116.7 °C; ¹H NMR (400 MHz, C₆D₆, 30 °C) δ 8.69 (d, 2H, *J* = 1.7 Hz), 8.40 (t, 1H, *J* = 1.7 Hz), 8.26–8.25 (m, 1H), 8.20 (s, 2H), 8.07 (d, 1H, *J* = 2.0 Hz), 8.05 (d, 1H, *J* = 2.5 Hz), 7.66 (s, 1H), 7.62 (dd, 1H, *J* = 8.3, 2.4 Hz), 7.60 (d, 1H, *J* = 2.4 Hz), 7.37 (d, 1H, *J* = 9.0 Hz), 7.45–7.33 (m, 4H), 6.96 (s, 1H), 6.03 (s, 1H), 5.34 (dd, 1H, *J* = 16.2, 8.0 Hz), 5.20 (d, 1H, *J* = 9.5 Hz), 4.89 (dd, 1H, *J* = 14.3, 2.3 Hz), 4.71 (d, 1H, *J* = 10.3 Hz), 4.37 (d, 1H, *J* = 9.5 Hz), 3.79 (d, 1H, *J* = 10.5 Hz), 3.60–2.91 (m, 16H), 2.68 (t, 2H, *J* = 10.2 Hz), 2.43 (d, 1H, *J* = 10.7 Hz), 2.13 (t, 1H, *J* = 10.1 Hz); ¹³C NMR (100 MHz, CDCl₃, 30 °C) δ 163.0, 160.2, 148.7, 147.6, 147.4, 147.2, 146.8, 146.0, 140.7, 137.2, 132.0, 130.3, 130.2 (q, *J*_{CF} = 33 Hz), 128.9, 128.4, 127.8, 127.65, 127.59, 126.5, 125.6, 124.92, 124.90, 124.86, 124.7, 122.1, 120.4 (q, *J*_{CF} = 4.4 Hz), 120.0, 119.8, 119.7, 107.3, 105.8, 71.20, 71.15, 70.9, 70.6, 70.5, 70.4, 70.2, 70.1, 69.8, 69.4, 67.6, 65.1, 43.7 (2 tertiary carbon and 3 quaternary carbon could not be seen); IR (KBr) 3351, 3101, 2880, 1601, 1540, 1345, 1278, 1131, 850 cm⁻¹; MS (MALDI) *m/z* 1152.3 ([M + Na⁺]); HRMS (FAB) *m/z* Calcd for C₅₁H₄₅F₆N₇O₁₇: 1130.2854, Found: 1130.2852 ([M + H⁺]).

3. Results and Discussion

We planned to synthesize rotaxanes **5** and the enantiomer as target chiral rotaxanes by way of prerotaxanes **3** with planar chirality followed by aminolysis with bulky amine **4** as shown in Scheme 2. This versatile covalent method to synthesize rotaxane consists of two steps: first, esterification of a phenolic crown ether with an acid chloride; second, aminolysis with an amine compound having a bulky group.

Prerotaxanes **3** were prepared from a phenolic pseudo-crown ether **1** and a 3,5-dinitrobenzoyl chloride in the presence of KO^tBu in THF. Optical resolution of obtained racemic prerotaxane (rac)-**3** was performed by preparative chiral HPLC on Daicel CHIRALFLASH IA. Chromatograms of (rac)-**3**, resolved **3**_{1st}, and **3**_{2nd} were shown in Figure 2. (rac)-**3** was well resolved into **3**_{1st} and **3**_{2nd}. In Figure 3, CD (a) and UV-visible (b) spectra of **3**_{1st} and **3**_{2nd} are shown. The CD spectra of **3**_{1st} and **3**_{2nd} are mirror

images each other. In general, chirality that appeared in mechanically interlocked systems is attractive due to its unique structure having large and flexible asymmetric field owing to the high mobility of the components. However, the determination of the absolute configuration is therefore difficult when applying chromophore sector rules on CD spectral data [50,51]. Because absolute structures of these enantiomers **3** were not determined in this stage, resolved prerotaxanes were denoted as **3**_{1st} and **3**_{2nd} according to the eluted order in this condition.



Scheme 2. Synthetic scheme of **5** via aminolysis of prerotaxane **3**.

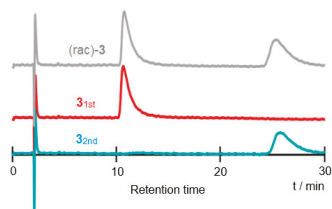


Figure 2. HPLC chromatogram of prerotaxane (rac)-**3**, and resolved **3**_{1st} and **3**_{2nd}, detected by UV at 330 nm. (Conditions; Column: DAICEL CHIRALPAK IA (10 mm ϕ \times 250 mm); mobile phase: hexane/dichloromethane = 50/50; flow rate = 1.0 mL/min; temperature: 30 $^{\circ}\text{C}$).

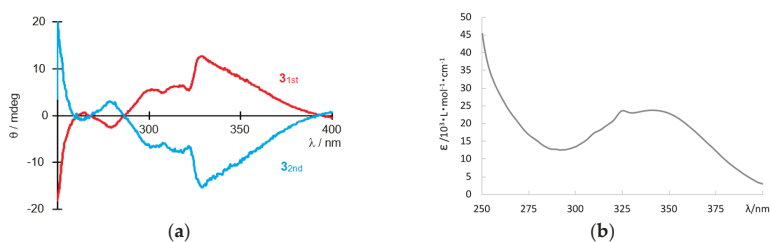


Figure 3. (a) Circular dichroism spectra of enantiomerically pure prerotaxanes **3**_{1st} (red) and **3**_{2nd} (blue) in CHCl_3 at room temperature ($[\text{3}_{1\text{st}}] = 65.9 \mu\text{M}$, $[\text{3}_{2\text{nd}}] = 76.1 \mu\text{M}$, cell length = 1.0 cm); (b) UV-visible spectrum of **3**_{2nd} under same condition.

For preparation of optically pure rotaxane **5**, aminolyses of corresponding enantiomeric pure prerotaxanes **3** were carried out. A mixture of a prerotaxane **3** and amine **4** in benzene was stirred at room temperature. Because the aminolysis proceeds via the nucleophilic attack of amino group of **4** from the backside of the crown ether ring of prerotaxanes **3** as shown with dotted arrow in Scheme 2, the corresponding rotaxanes **5** were afforded from a pair of enantiomerically pure prerotaxanes **3**, respectively. The reactions of the resolved prerotaxanes **3**_{1st} and **3**_{2nd} with amine **4** proceeded quantitatively in C₆D₆ to give corresponding rotaxanes **5**_{1st} and **5**_{2nd}, respectively. The residue after removal of the solvent in the reaction mixture was subjected to GLPC and/or column chromatography on silica gel to give rotaxane **5**_{1st} and **5**_{2nd} without producing any dumbbell compound **6** and crown ether **1**. The efficiency of the reaction was easily monitored by ¹H NMR. The aminolysis by the backside attack of amine **4** took place selectively. ¹H NMR spectra of a reaction mixture of aminolysis of **3** are shown in Figure 4. H^A signal of prerotaxane **3** (H^A(**3**)) at 9.02 ppm decreased with increasing H^A signal of rotaxane **5** (H^A(**5**)) at 8.69 ppm without producing any ring compound **1**, e.g., H^a and H^b signals at 5.02 and 4.60 ppm were not observed. Reaction proceeded fast (t_{1/2}: 20 min) and selectively (rotaxane selectivity: >99%). Actually, **5** was obtained in high isolated yield (84%).

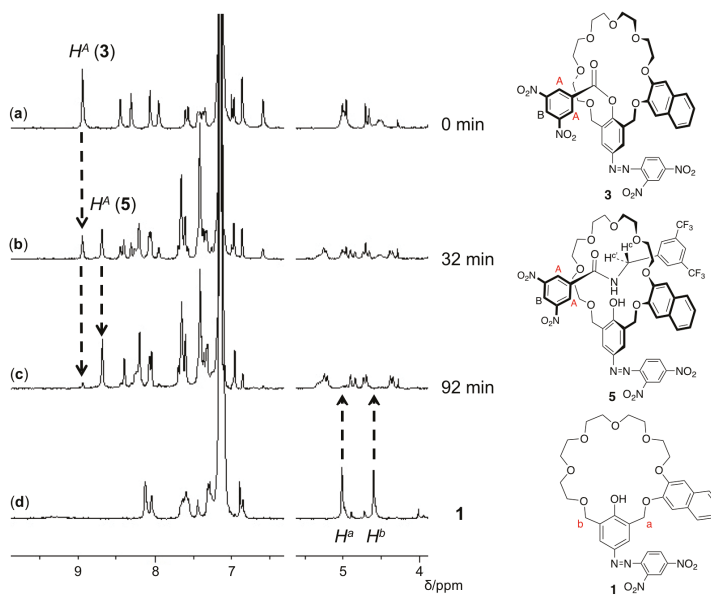


Figure 4. ¹H NMR (270 MHz, C₆D₆) spectra of (a) reaction mixture at 0 min (prerotaxane **3**_{2nd}), (b) 32 min, (c) 92 min, and (d) ring **1** for reference. The descriptors refer to the signals representing rotaxane (H^A(**5**)), dumbbell (H^A(**6**)), and ring1 (H^a and H^b) protons are shown in Scheme 1.

The structures of rotaxanes **5** were characterized by spectral data. ¹H NMR spectra of rotaxane **5** and the corresponding dumbbell **6** are shown in Figure 5. Significant downfield shift of the signal of the amide proton NH of the axle in rotaxanes **5** was observed relative to the corresponding signal of dumbbell **6** (δ 6.83 to 8.25), indicating the formation of hydrogen bonding between the amide hydrogen with the oxygen atoms of the crown ether moiety of **5**. Two singlets assigned to the benzylic protons H^a and H^b of the crown ether became double double-doublets (H^a, H^{a'}, H^b, and H^{b'}), evidencing that the ring components are threaded and interlocked by the dumbbell component **6** with different stoppers. More importantly, signals of homotopic methylene protons H^c on the axle component became multiplet, because the methylene protons H^c became diastereotopic in the chiral circumstance

of the rotaxane structure-specific chirality generated by interlocking with C₃ ring component as shown in Figure 5.

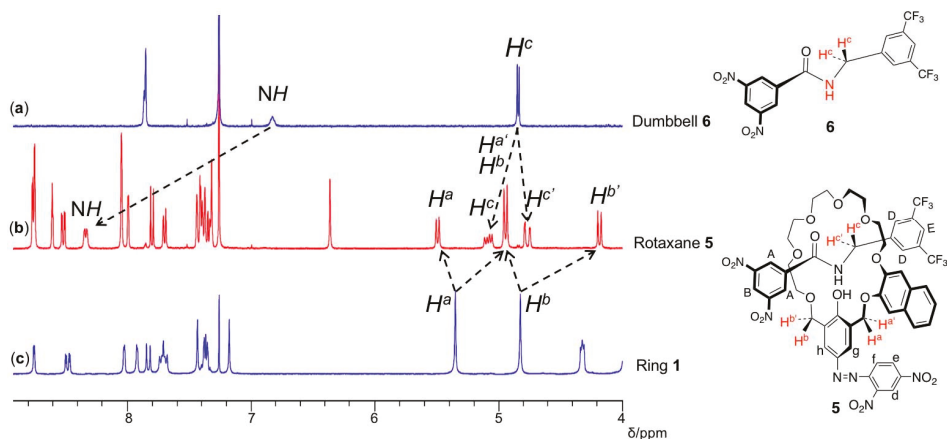


Figure 5. ¹H NMR spectra of dumbbell 6 (a), chiral rotaxane 5 (b), and ring 1 (c) in CDCl₃ at 30 °C (400 MHz).

HPLC Chromatograms on Daicel CHIRALPAK IA shown in Figure 6 with the mirror images of the CD spectra shown in Figure 7a evidenced that obtained 5_{1st} and 5_{2nd} are pure enantiomers.

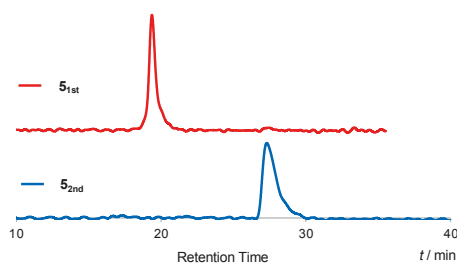


Figure 6. HPLC chromatograms of rotaxanes 5_{1st} (red), 5_{2nd} (blue) detected by UV at 254 nm. (Column: CHIRALPAK IA (4.6 mm ϕ \times 150 mm); mobile phase: hexane/dichloromethane /trifluoroacetic acid = 80/20/0.1; flow rate = 0.8 mL/min; temperature: 30 °C).

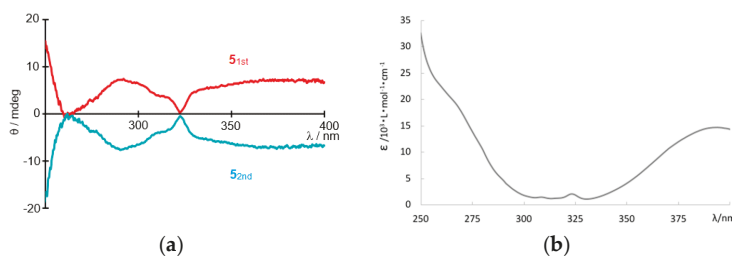


Figure 7. (a) Circular dichroism spectra of enantiomerically pure rotaxanes 5_{1st} (red) and 5_{2nd} (blue) in CHCl₃ at room temperature ($[5_{1st}] = 90.7 \mu\text{M}$, $[5_{2nd}] = 94.6 \mu\text{M}$, cell length = 1.0 cm); (b) Uv-visible spectrum of 5_{2nd} under same condition.

In order to evaluate the enantioselective complexation ability of the rotaxane, titration experiments of rotaxane **5**_{2nd} with (*R*)-phenylglycinol (PGO) and (*S*)-PGO were carried out. Because chiral host molecules with 2,4-dinitrophenylazophenol moiety produce ammonium phenolate salts in complexation with PGO accompanying large spectral change in UV-visible region with clear color change [22], there is a considerable chemical shift change of ¹H NMR signals assigned to the aromatic protons at low magnetic field.

As shown in Figure 8, spectral and color changes of CHCl₃ solution of **5**_{2nd} and (*R*)-PGO were observed. This observation shows that the extent of color change is clear enough as a sensor for naked eyes, and that the obtained rough extent of binding constant was around 100 L mol⁻¹. Then, ¹H NMR titration was revealed to be suitable for precise evaluation [52,53] of complexation ability of host **5** with PGO. The ¹H NMR titration was carried out with **5**_{2nd} and enantiomeric pair of amines (*S*)- and (*R*)-PGO in chloroform. Experimental details are filed in Supplementary Materials and Appendixs A–D. As shown in Table 1, the determined binding constants of **5**_{2nd} were $(8.47 \pm 0.40) \times 10^1$ L mol⁻¹ for (*S*)-PGO and $(1.25 \pm 0.03) \times 10^2$ L mol⁻¹ for (*R*)-PGO, respectively. The ratio of binding constants K_R/K_S was 1.48. Generally speaking, as perspectives with the ratio of binding constant, it is not enough for application as chirality indicator [19,53], but is promising for application as a chiral selector of a stationary phase for a chiral chromatography [54].

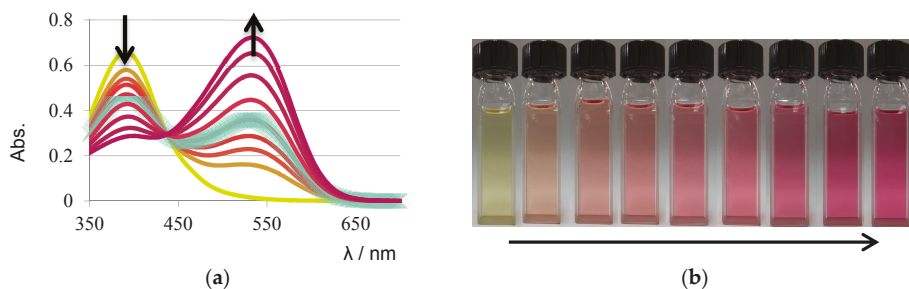


Figure 8. UV-Vis spectral and color changes of rotaxane **5**_{2nd} with (*R*)-PGO in CHCl₃: (a) UV-Vis spectra and (b) corresponding pictures: rotaxane **5** (41.5 μM) ((a) yellow line and (b) yellow solution) and same solutions containing different (*R*)-PGO concentration 899 μM, 1.35, 1.87, 2.62, 3.75, 5.99, 8.99, and 12.7 mM in order shown by arrows at 17 °C.

Table 1. Binding constants of **5**_{2nd} for PGO obtained by ¹H NMR titration experiments.

| Guests | $K/L \text{ mol}^{-1}$ | K_R/K_S |
|------------------|-------------------------------|-----------|
| (<i>R</i>)-PGO | $(1.25 \pm 0.03) \times 10^2$ | 1.48 |
| (<i>S</i>)-PGO | $(8.47 \pm 0.40) \times 10^1$ | |

In CDCl₃ at 30 °C, 400 MHz.

4. Conclusions

We developed an efficient method of rotaxane synthesis based on an aminolysis of a prerotaxane, which proceeded with excellent selectivities and chemical yields. We also found that the rotaxane with mechanical chirality has complexation ability against chiral amine PGO, with high enough enantioselectivity to be applied as a chiral selector of the chiral stationary phase for chiral chromatography.

Supplementary Materials: The followings are available online at www.mdpi.com/2073-8994/10/1/20/s1, Table S1: Tabulated ^1H NMR titration data of Rotaxane $5_{2\text{nd}}$ with (R)-PGO in CDCl_3 at 30°C , Figure S1: ^1H NMR titration curve for the complexation of Rotaxane $5_{2\text{nd}}$ with (R)-PGO at 30°C , Table S2: Tabulated ^1H NMR titration data of Rotaxane $5_{2\text{nd}}$ with (S)-PGO in CDCl_3 at 30°C , Figure S2. ^1H NMR titration curve for the complexation of Rotaxane $5_{2\text{nd}}$ with (S)-PGO at 30°C .

Acknowledgments: This work was partly supported by a Grant-in-Aid for Scientific Research from the Ministry of Education, Culture, Sports, Science, and Technology of Japan.

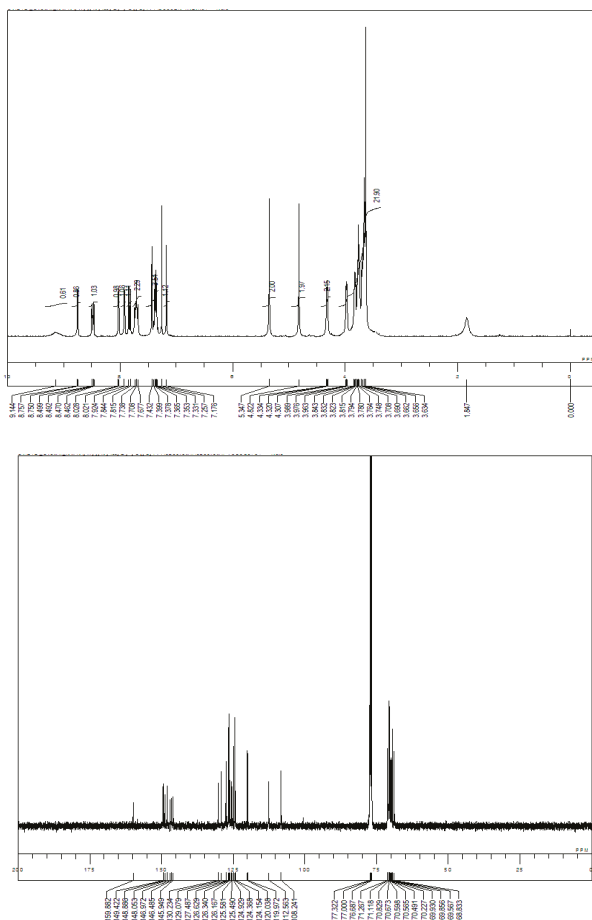
Author Contributions: Keiji Hirose conceived and designed the experiments; Masaya Ukimi, Shota Ueda, Chie Onoda, Ryohei Kano, Kyosuke Tsuda and Yuko Hinohara performed the experiments; Yoshito Tobe contributed for scientific guide; Masaya Ukimi, Shota Ueda, and Ryohei Kano analyzed the data; Keiji Hirose, Masaya Ukimi and Chie Onoda wrote the paper.

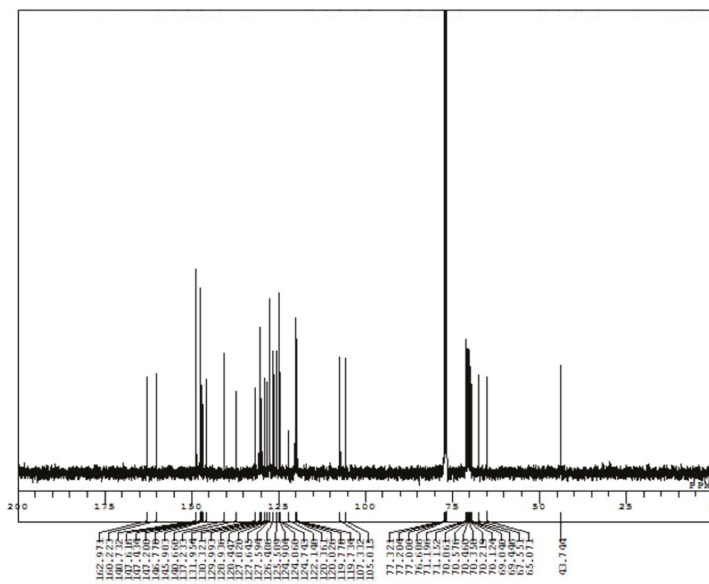
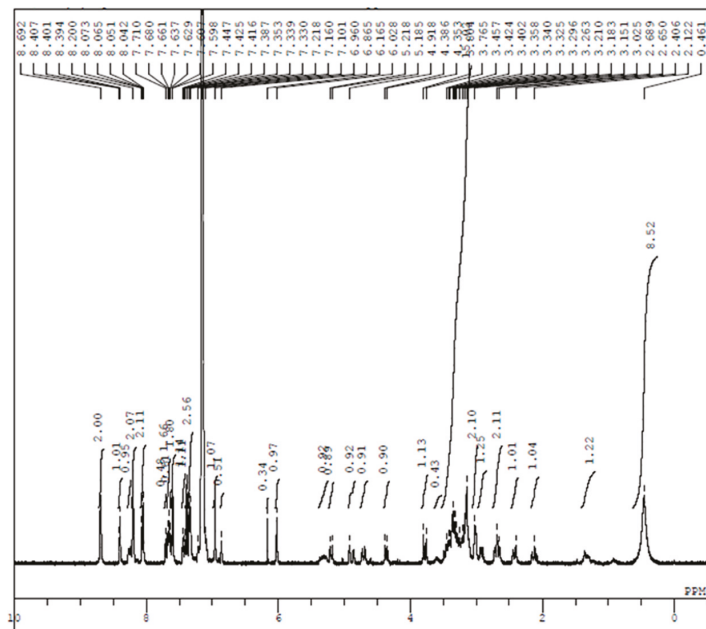
Conflicts of Interest: The authors declare no conflict of interest. The founding sponsors had no role in the design of the study; in the collection, analyses, or interpretation of data; in the writing of the manuscript, and in the decision to publish the results.

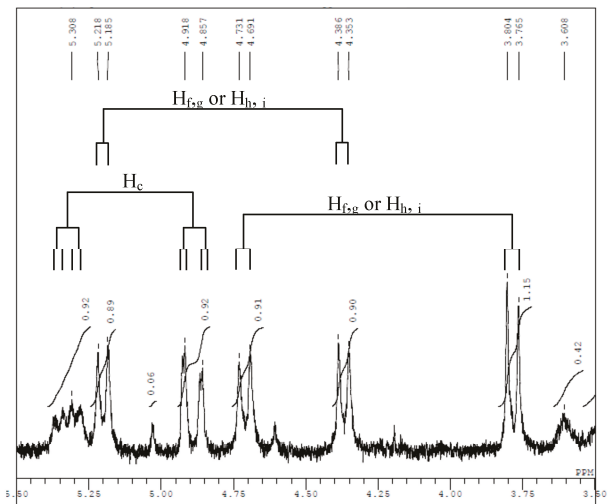
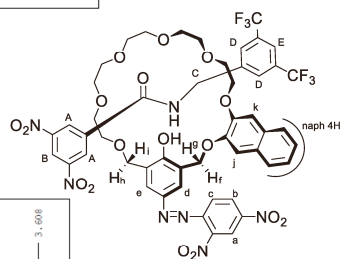
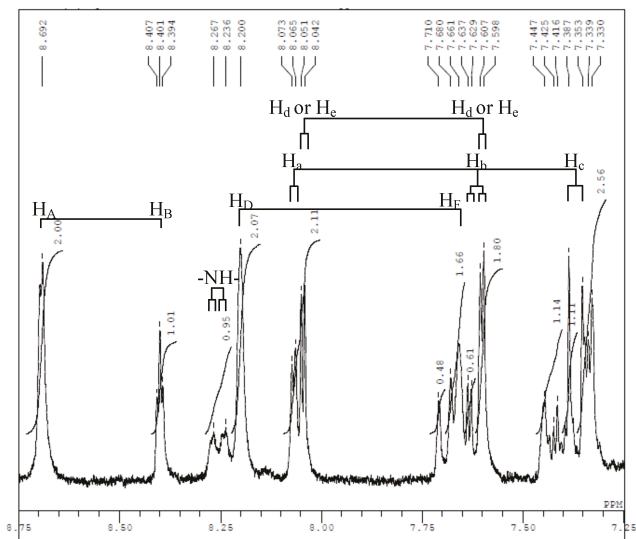
Appendix A. General

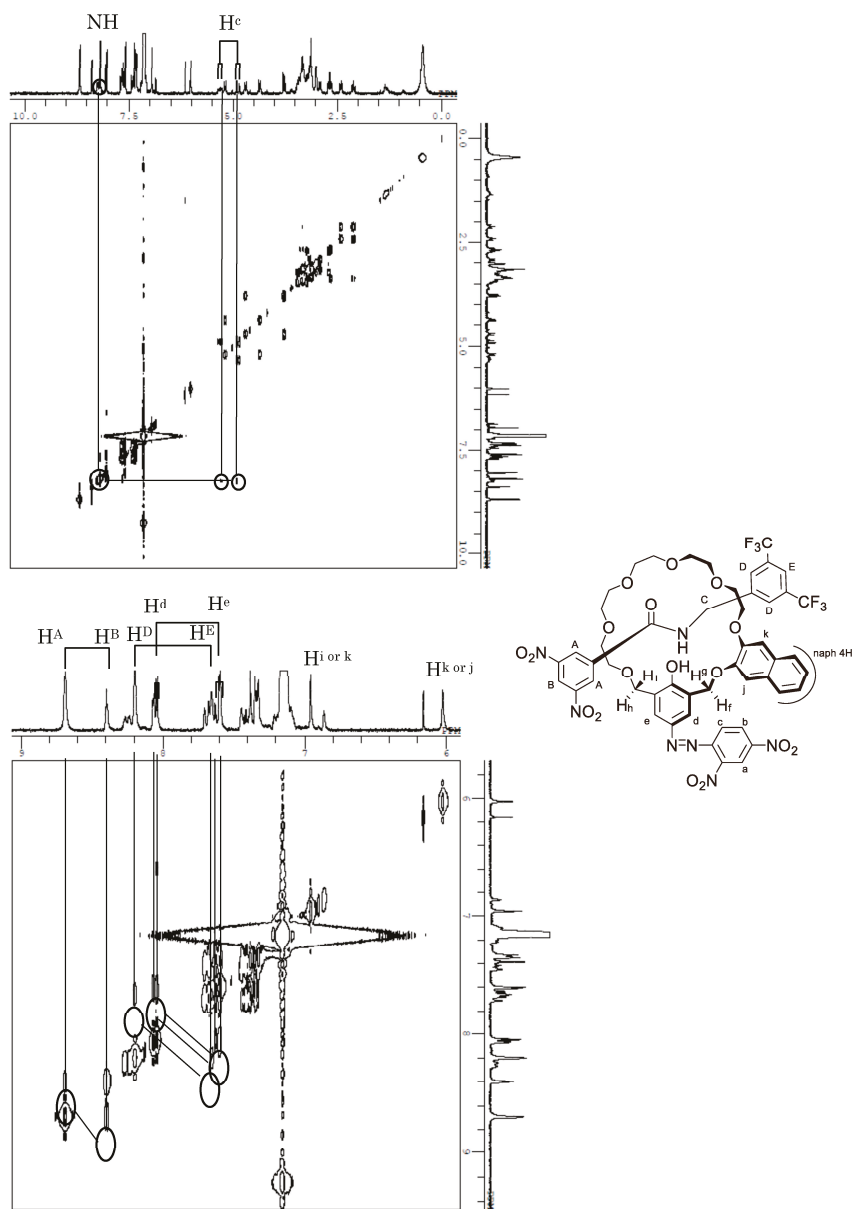
^1H NMR and ^{13}C NMR charts are filed here. Details of each chart are mentioned in Materials and Methods.

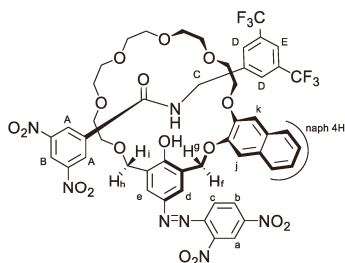
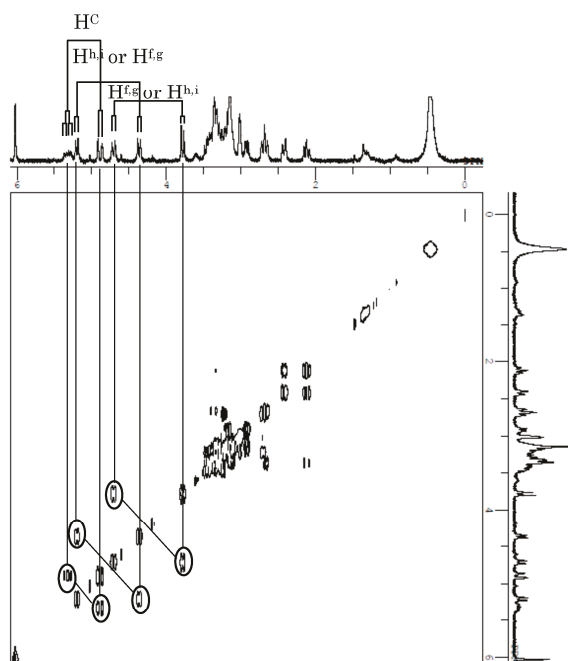
Appendix B. ^1H -and ^{13}C -NMR Spectra of Ring 1



Appendix D. ^1H - and ^{13}C -NMR Spectra of Rotaxanes 5







References and Note

1. Pedersen, C.J. The discovery of crown ethers. *Science* **1988**, *241*, 536–540. [[CrossRef](#)] [[PubMed](#)]
2. Cram, D.J. The design of molecular hosts, guests, and their complexes. *J. Incl. Phenom.* **1988**, *6*, 397–413. [[CrossRef](#)]
3. Lehn, J.M. Supramolecular chemistry—Scope and perspectives molecules, supermolecules, and molecular devices. *Angew. Chem. Int. Ed.* **1988**, *27*, 89–112. [[CrossRef](#)]
4. Takagi, M.; Nakamura, H. Analytical application of functionalized crown ether-metal complexes. *J. Coord. Chem.* **1986**, *15*, 53–82. [[CrossRef](#)]
5. Nakashima, K.; Nagaoka, Y.; Nakatsuji, S.I.; Kaneda, T.; Tanigawa, I.; Hirose, K.; Misumi, S.; Akiyama, S. Fluorescence reactions of “crowned” benzothiazolylphenols with alkali and alkaline earth metal ions and their analytical applications. *Bull. Chem. Soc. Jpn.* **1987**, *60*, 3219–3223. [[CrossRef](#)]
6. Desilva, A.P.; Gunaratne, H.Q.N.; Gunlaugsson, T.; Huxley, A.J.M.; Mccoy, C.P.; Rademacher, J.T.; Rice, T.E. Signaling recognition events with fluorescent sensors and switches. *Chem. Rev.* **1997**, *97*, 1515–1566. [[CrossRef](#)]
7. Hisamoto, H. Ion-selective optodes: Current developments and future prospects. *Trac-Trends Anal. Chem.* **1999**, *18*, 513–524. [[CrossRef](#)]

8. Stradiotto, N.R.; Yamanaka, H.; Zanoni, M.V.B. Electrochemical sensors: A powerful tool in analytical chemistry. *J. Braz. Chem. Soc.* **2003**, *14*, 159–173. [[CrossRef](#)]
9. Faridbod, F.; Ganjali, M.R.; Dinarvand, R.; Norouzi, P.; Riahi, S. Schiff's bases and crown ethers as supramolecular sensing materials in the construction of potentiometric membrane sensors. *Sensors* **2008**, *8*, 1645–1703. [[CrossRef](#)] [[PubMed](#)]
10. Sogah, G.D.Y.; Cram, D.J. Total chromatographic optical resolutions of alpha-amino acid and ester salts through chiral recognition by a host covalently bound to polystyrene resin. *J. Am. Chem. Soc.* **1976**, *98*, 3038–3041. [[PubMed](#)]
11. Machida, Y.; Nishi, H.; Nakamura, K.; Nakai, H.; Sato, T. Enantiomer separation of amino compounds by a novel chiral stationary phase derived from crown ether. *J. Chromatogr. A* **1998**, *805*, 85–92. [[CrossRef](#)]
12. Hyun, M.H.; Jin, J.S.; Lee, W.J. Liquid chromatographic resolution of racemic amino acids and their derivatives on a new chiral stationary phase based on crown ether. *J. Chromatogr. A* **1998**, *822*, 155–161. [[CrossRef](#)]
13. Maier, N.M.; Franco, P.; Lindner, W. Separation of enantiomers: Needs, challenges, perspectives. *J. Chromatogr. A* **2001**, *906*, 3–33. [[CrossRef](#)]
14. Hirose, K.; Nakamura, T.; Nishioka, R.; Ueshige, T.; Tobe, Y. Preparation and evaluation of novel chiral stationary phases covalently bound with chiral pseudo-18-crown-6 ethers. *Tetrahedron Lett.* **2003**, *44*, 1549–1551. [[CrossRef](#)]
15. Hirose, K.; Jin, Y.; Nakamura, T.; Nishioka, R.; Ueshige, T.; Tobe, Y. Chiral stationary phase covalently bound with a chiral pseudo-18-crown-6 ether for enantiomer separation of amino compounds using a normal mobile phase. *Chirality* **2005**, *17*, 142–148. [[CrossRef](#)] [[PubMed](#)]
16. Cram, D.J.; Cram, J.M. Design of complexes between synthetic hosts and organic guests. *Acc. Chem. Res.* **1978**, *11*, 8–14. [[CrossRef](#)]
17. Cram, D.J.; Trueblood, K.N. Concept, structure, and binding in complexation. *Top. Curr. Chem.* **1981**, *98*, 43–106.
18. Wenzel, T.J.; Freeman, B.E.; Sek, D.C.; Zopf, J.J.; Nakamura, T.; Jin, Y.; Hirose, K.; Tobe, Y. Chiral recognition in NMR spectroscopy using crown ethers and their Ytterbium(III) complexes. *Anal. Bioanal. Chem.* **2004**, *378*, 1536–1547. [[CrossRef](#)] [[PubMed](#)]
19. Kaneda, T.; Hirose, K.; Misumi, S. Chiral azophenolic acerands: Color indicator to judge the absolute configuration of chiral amines. *J. Am. Chem. Soc.* **1989**, *111*, 742–743. [[CrossRef](#)]
20. Hirose, K.; Goshima, Y.; Wakebe, T.; Tobe, Y.; Naemura, K. Supramolecular method for the determination of absolute configuration of chiral compounds: Theoretical derivatization and a demonstration for phenolic crown ether—2-amino-1-ethanol system. *Anal. Chem.* **2007**, *79*, 6295–6302. [[CrossRef](#)] [[PubMed](#)]
21. Kubo, Y.; Maeda, S.; Tokita, S.; Kubo, M. Colorimetric chiral recognition by a molecular sensor. *Nature* **1996**, *382*, 522–524. [[CrossRef](#)]
22. Naemura, K.; Takeuchi, S.; Hirose, K.; Tobe, Y.; Kaneda, T.; Sakata, Y. Preparation and enantiomer recognition behaviour of azophenolic crown ethers containing cis-cyclohexane-1,2-diol as the chiral centre. *J. Chem. Soc. Perkin Trans.* **1995**, 213–219. [[CrossRef](#)]
23. Van Delden, R.A.; Feringa, B.L. Color indicators of molecular chirality based on doped liquid crystals. *Angew. Chem. Int. Ed.* **2001**, *40*, 3198–3200. [[CrossRef](#)]
24. Kim, H.N.; Guo, Z.; Zhu, W.; Yoon, J.; Tian, H. Recent progress on polymer-based fluorescent and colorimetric chemosensors. *Chem. Soc. Rev.* **2011**, *40*, 79–93. [[CrossRef](#)] [[PubMed](#)]
25. Sawada, M.; Takai, Y.; Yamada, H.; Hirayama, S.; Kaneda, T.; Tanaka, T.; Kamada, K.; Mizooku, T.; Takeuchi, S.; Ueno, K.; et al. Chiral recognition in host-guest complexation determined by the enantiomer-labeled guest method using fast atom bombardment mass spectrometry. *J. Am. Chem. Soc.* **1995**, *117*, 7726–7736. [[CrossRef](#)]
26. Sawada, M.; Takai, Y.; Yamada, H.; Nishida, J.; Kaneda, T.; Arakawa, R.; Okamoto, M.; Hirose, K.; Tanaka, T.; Naemura, K. Chiral amino acid recognition detected by electrospray ionization (ESI) and fast atom bombardment (FAB) mass spectrometry (MS) coupled with the enantiomer labelled (EL) guest method. *J. Chem. Soc. Perkin Trans.* **1998**, *2*, 701–710. [[CrossRef](#)]
27. Finn, M.G. Emerging methods for the rapid determination of enantiomeric excess. *Chirality* **2002**, *14*, 534–540. [[CrossRef](#)] [[PubMed](#)]

28. Hembury, G.A.; Borovkov, V.V.; Inoue, Y. Chirality-sensing supramolecular systems. *Chem. Rev.* **2008**, *108*, 1–73. [[CrossRef](#)] [[PubMed](#)]
29. Jo, H.H.; Lin, C.-Y.; Anslyn, E.V. Rapid optical methods for enantiomeric excess analysis: From enantioselective indicator displacement assays to exciton-coupled circular dichroism. *Acc. Chem. Res.* **2014**, *47*, 2212–2221. [[CrossRef](#)] [[PubMed](#)]
30. Sauvage, J.P. Interlacing molecular threads on transition-metals: Catenands, catenates, and knots. *Acc. Chem. Res.* **1990**, *23*, 319–327. [[CrossRef](#)]
31. Blanco, M.J.; Jimenez, M.C.; Chambron, J.C.; Heitz, V.; Linke, M.; Sauvage, J.P. Rotaxanes as new architectures for photoinduced electron transfer and molecular motions. *Chem. Soc. Rev.* **1999**, *28*, 293–305. [[CrossRef](#)]
32. Kawasaki, H.; Kihara, N.; Takata, T. High yielding and practical synthesis of rotaxanes by acylative end-capping catalyzed by tributylphosphine. *Chem. Lett.* **1999**, *10*, 1015–1016. [[CrossRef](#)]
33. Schalley, C.A.; Weilandt, T.; Bruggemann, J.; Vögtle, F. Hydrogen-bond-mediated template synthesis of rotaxanes, catenanes, and knotanes. In *Templates in Chemistry I*; Springer: Berlin/Heidelberg, Germany, 2004; pp. 141–200. [[CrossRef](#)]
34. Arico, F.; Badjic, J.D.; Cantrill, S.J.; Flood, A.H.; Leung, K.C.F.; Liu, Y.; Stoddart, J.F. Templated synthesis of interlocked molecules. In *Templates in Chemistry II*; Springer: Berlin/Heidelberg, Germany, 2005; pp. 203–259.
35. Narita, M.; Yoon, I.; Aoyagi, M.; Goto, M.; Shimizu, T.; Asakawa, M. Transition metal(II)-salen and -salophen macrocyclic complexes for rotaxane formation: Syntheses and crystal structures. *Eur. J. Inorg. Chem.* **2007**, 4229–4237. [[CrossRef](#)]
36. Harrison, I.T.; Harrison, S. Synthesis of a stable complex of a macrocycle and a threaded chain. *J. Am. Chem. Soc.* **1967**, *89*, 5723–5724. [[CrossRef](#)]
37. Schill, G.; Zolzenko, H. Rotaxane compounds 1. *Liebigs Ann. Chem.* **1969**, *721*, 53–74. [[CrossRef](#)]
38. Hiratani, K.; Suga, J.; Nagawa, Y.; Houjou, H.; Tokuhisa, H.; Numata, M.; Watanabe, K. A new synthetic method for rotaxanes via tandem claisen rearrangement, diesterification, and aminolysis. *Tetrahedron Lett.* **2002**, *43*, 5747–5750. [[CrossRef](#)]
39. Hirose, K.; Nishihara, K.; Harada, N.; Nakamura, Y.; Masuda, D.; Araki, M.; Tobe, Y. Highly selective and high-yielding rotaxane synthesis via aminolysis of prerotaxanes consisting of a ring component and a stopper unit. *Org. Lett.* **2007**, *9*, 2969–2972. [[CrossRef](#)] [[PubMed](#)]
40. Sauvage, J.P. From chemical topology to molecular machines (nobel lecture). *Angew. Chem. Int. Ed.* **2017**, *56*, 11080–11093. [[CrossRef](#)] [[PubMed](#)]
41. Stoddart, J.F. Mechanically interlocked molecules (MIMS)-molecular shuttles, switches, and machines (nobel lecture). *Angew. Chem. Int. Ed.* **2017**, *56*, 11094–11125. [[CrossRef](#)] [[PubMed](#)]
42. Feringa, B.L. The art of building small: From molecular switches to motors (nobel lecture). *Angew. Chem. Int. Ed.* **2017**, *56*, 11059–11078. [[CrossRef](#)] [[PubMed](#)]
43. Bordoli, R.J.; Goldup, S.M. An efficient approach to mechanically planar chiral rotaxanes. *J. Am. Chem. Soc.* **2014**, *136*, 4817–4820. [[CrossRef](#)] [[PubMed](#)]
44. Goldup, S.M. Mechanical chirality a chiral catalyst with a ring to it. *Nat. Chem.* **2016**, *8*, 404–406. [[CrossRef](#)] [[PubMed](#)]
45. Nakazono, K.; Takata, T. Chiral interlocked molecule: Synthesis and function. *J. Synth. Organ. Chem. Jpn.* **2017**, *75*, 491–502. [[CrossRef](#)]
46. Bruns, C.J.; Stoddart, J.F.; Sauvage, J.-P.; Fujita, M. *The Nature of the Mechanical Bond: From Molecules to Machines*; Wiley: Hoboken, NJ, USA, 2017; pp. 471–554. ISBN 9781119044000.
47. Borsche, W. Ueber die beziehungen zwischen chinonhydrazonen und p-oxyazoverbindungen. (vierte abhandlung): Ueber die condensation von nitroderivaten des phenylhydrazins mit chinonen und chinonoximen der benzolreihe. *Liebigs Ann. Chem.* **1907**, *357*, 171–191. [[CrossRef](#)]
48. Naemura, K.; Asada, M.; Hirose, K.; Tobe, Y. Preparation and enantiomer recognition of chiral azophenolic crown ethers having three chiral barriers on each of the homotopic faces. *Tetrahedron Asymmetry* **1995**, *6*, 1873–1876. [[CrossRef](#)]
49. Naemura, K.; Takeuchi, S.; Sawada, M.; Ueno, K.; Hirose, K.; Tobe, Y.; Kaneda, T.; Sakata, Y. Synthesis of azophenolic crown ethers of cs symmetry incorporating cis-1-phenylcyclohexane-1,2-diol residues as a steric barrier and diastereotopic face selectivity in complexation of amines by their diastereotopic faces. *J. Chem. Soc. Perkin Trans.* **1995**, *1*, 1429–1435. [[CrossRef](#)]

50. Berova, N.; Di Bari, L.; Pescitelli, G. Application of electronic circular dichroism in configurational and conformational analysis of organic compounds. *Chem. Soc. Rev.* **2007**, *36*, 914–931. [[CrossRef](#)] [[PubMed](#)]
51. Stoncius, S.; Bagdziunas, G.; Malinauskiene, J.; Butkus, E. A study of planar chromophores in dichromophoric molecules by circular dichroism spectroscopy. *Chirality* **2008**, *20*, 337–343. [[CrossRef](#)] [[PubMed](#)]
52. Hirose, K. A practical guide for the determination of binding constants. *J. Incl. Phenom.* **2001**, *39*, 193–209. [[CrossRef](#)]
53. Hirose, K. Quantitative analysis of binding properties. In *Analytical Methods in Supramolecular Chemistry*; Schalley, C.A., Ed.; John Wiley & Sons: Weinheim, Germany, 2012; pp. 27–66, ISBN 9783527644131.
54. Requirements for an application to a chromatography: Resolution factor (α) for baseline separation (Resolution (R) > 1.25, 99.4% separation) through normal size column (Number of theoretical plates (N) = 5000) is around 1.10 (Retention factor ($k'2$) = 10) where ratio of binding constant corresponds to resolution factor (α) of HPLC separation on chiral column.



© 2018 by the authors. Licensee MDPI, Basel, Switzerland. This article is an open access article distributed under the terms and conditions of the Creative Commons Attribution (CC BY) license (<http://creativecommons.org/licenses/by/4.0/>).

MDPI
St. Alban-Anlage 66
4052 Basel
Switzerland
Tel. +41 61 683 77 34
Fax +41 61 302 89 18
www.mdpi.com

Symmetry Editorial Office
E-mail: symmetry@mdpi.com
www.mdpi.com/journal/symmetry



MDPI
St. Alban-Anlage 66
4052 Basel
Switzerland

Tel: +41 61 683 77 34
Fax: +41 61 302 89 18

www.mdpi.com



ISBN 978-3-0365-1017-0